SIMPLE MODELS FOR DRIFT ESTIMATES IN FRAMED STRUCTURES DURING NEAR-FIELD EARTHQUAKES

A THESIS SUBMITTED TO
THE GRADUATE SCHOOL OF NATURAL AND APPLIED SCIENCES
OF
MIDDLE EAST TECHNICAL UNIVERSITY

BY

BURCU ERDOĞAN

IN PARTIAL FULFILLMENT OF THE REQUIREMENTS
FOR
THE DEGREE OF MASTER OF SCIENCE
IN
CIVIL ENGINEERING

SEPTEMBER 2007

Approval of the thesis:

SIMPLE MODELS FOR DRIFT ESTIMATES IN FRAMED STRUCTURES DURING NEAR-FIELD EARTHQUAKES

submitted by **BURCU ERDOĞAN** in partial fulfillment of the requirements for the degree of **Master of Science in Civil Engineering Department, Middle East Technical University** by,

Prof. Dr. Canan Özgen _____
Dean, Graduate School of **Natural and Applied Sciences**

Prof. Dr. Güney Özcebe _____
Head of Department, **Civil Engineering**

Prof. Dr. Polat Gülkan _____
Supervisor, **Civil Engineering Dept., METU**

Examining Committee Members

Assoc. Prof. Dr. Ahmet Yakut _____
Civil Engineering Dept., METU

Prof. Dr. Polat Gülkan _____
Civil Engineering Dept., METU

Assoc. Prof. Dr. Sinan Akkar _____
Civil Engineering Dept., METU

Asst. Prof. Dr. Altuğ Erberik _____
Civil Engineering Dept., METU

Assoc. Prof. Dr. Murat Dicleli _____
Engineering Science Dept., METU

Date: 04.09.2007

I hereby declare that all information in this document has been obtained and presented in accordance with academic rules and ethical conduct. I also declare that, as required by these rules and conduct, I have fully cited and referenced all material and results that are not original to this work.

Name, Last name : Burcu ERDOĞAN

Signature :

ABSTRACT

SIMPLE MODELS FOR DRIFT ESTIMATES IN FRAMED STRUCTURES DURING NEAR-FIELD EARTHQUAKES

Erdoğan, Burcu
M.S., Department of Civil Engineering
Supervisor: Prof. Dr. Polat Gülkan

September 2007, 187 pages

Maximum interstory drift and the distribution of this drift along the height of the structure are the main causes of structural and nonstructural damage in frame type buildings subjected to earthquake ground motions. Estimation of maximum interstory drift ratio is a good measure of the local response of buildings. Recent earthquakes have revealed the susceptibility of the existing building stock to near-fault ground motions characterized by a large, long-duration velocity pulse. In order to find rational solutions for the destructive effects of near fault ground motions, it is necessary to determine drift demands of buildings. Practical, applicable and accurate methods that define the system behavior by means of some key parameters are needed to assess the building performances quickly instead of detailed modeling and calculations.

In this study, simple equations are proposed in order for the determination of the elastic interstory drift demand produced by near fault ground motions on regular and irregular steel frame structures. The proposed equations enable the

prediction of maximum elastic ground story drift ratio of shear frames and the maximum elastic ground story drift ratio and maximum elastic interstory drift ratio of steel moment resisting frames. In addition, the effects of beam to column stiffness ratio, soft story factor, stiffness distribution coefficient, beam-to-column capacity ratio, seismic force reduction factor, ratio of pulse period to fundamental period, regular story height and number of stories on elastic and inelastic interstory drift demands are investigated in detail. An equation for the ratio of maximum inelastic interstory drift ratio to maximum elastic interstory drift ratio developed for a representative case is also presented.

Keywords: maximum interstory drift demand, ground story drift demand, shear frame, steel moment resisting frame, elastic and inelastic response, near-fault ground motions

ÖZ

YAKIN ALAN DEPREMLERİ SIRASINDA ÇERÇEVE YAPILARDA OLUŞAN KAT ARASI YER DEĞİŞTİRMELERİN HESABI İÇİN BASİT MODELLER

Erdoğan, Burcu
Yüksek Lisans, İnşaat Mühendisliği Bölümü
Tez Yöneticisi: Prof. Dr. Polat Gülkan

Eylül 2007, 187 sayfa

Deprem yer hareketlerine maruz kalan binalardaki yapısal ve yapısal olmayan hasarların temel nedeni azami kat arası ötelenme miktarı ve kat arası ötelenme oranın bina yüksekliği boyunca dağılımıdır. Azami kat arası ötelenmesinin tahmini binaların lokal davranışları açısından önemli bir göstergedir.Yakın zamandaki depremler sonrasındaki gözlemler, binaların büyük genlikli ve uzun periyotlu hız pulsları ile karakterize edilen yakın alansal depremlere karşı hassasiyetlerini göstermektedir. Bu tarz depremlerin hasar verici etkilerine rasyonel çareler getirmek için binalardaki ötelenme taleplerinin bilinmesi gerekmektedir. Binaların performanslarının çabukça belirlenebilmesi için detaylı modelleme ve hesaplar yerine, sistemin davranışını bazı anahtar göstergelere bağlı olarak belirleyen pratik, doğru ve uygulanabilir basit yöntemlere ihtiyaç vardır. Bu çalışmada yakın kaynaklı hareketlerin düzenli ve düzensiz çelik

çerçeve yapılarda yarattığı kat ötelenme taleplerinin belirlenmesi için basit denklemler üretilmiştir. Çıkarılan denklemler, kayma çerçevelerinin azami elastik zemin kat ötelenmesinin ve moment taşıyan çelik çerçevelerin azami elastik zemin kat ve ara kat ötelenmelerinin tahmin edilmesine imkan sağlamaktadır. Ayrıca kiriş/kolon rijitlik oranının, "yumuşak" kat faktörünün, rijitlik dağılım faktörünün, kiriş/kolon kapasite oranının, sismik yük azaltma katsayısının, puls periyodunun temel titreşim periyoduna oranının, kat yüksekliğinin ve kat sayısının elastik ve elastik ötesi kat arası ötelenme talepleri üzerindeki etkileri detaylı olarak araştırılmıştır. Temsili bir örmeğin azami elastik ötesi kat arası ötelenmesinin azami elastik kat arası ötelenmesine oranı için denklem sunulmuştur.

Anahtar Kelimeler: azami kat arası ötelenme talebi, zemin kat ötelenme talebi, kayma çerçevesi, moment taşıyan çelik çerçeve, elastik ve elastik ötesi davranım, yakın alan depremleri

To My Family

ACKNOWLEDGMENTS

This study was conducted under the supervision of Prof. Dr. Polat Gülkan. I would like to express my sincere appreciation for the support, guidance and insights that he has provided me throughout the study.

I would like to express my deepest thanks and gratitude to Mehmet Selim Günay for his encouragements, productive comments and invaluable discussions throughout this study.

The scholarship provided by The Scientific and Technological Research Council of Turkey (TÜBİTAK) during the graduate study is highly acknowledged.

I would like to thank Barış Erdil and Yasemin Didem Aktaş. Their support and encouragement are priceless for me.

I want to thank my friends and colleagues at Structural Mechanics Laboratory for their help and friendship during my assistantship.

I would like to express my deepest appreciation to my parents and my brother -the most precious people in my life- for the support, friendship, love and understanding that they have provided for me throughout my life.

TABLE OF CONTENTS

ABSTRACT……iv
ÖZ……vi
ACKNOWLEDGMENTS……ix
TABLE OF CONTENTS……x
LIST OF TABLES……xiv
LIST OF FIGURES……xv
LIST OF SYMBOLS……xxi
CHAPTER
1. INTRODUCTION 1
1.1 STATEMENT OF THE PROBLEM 1
1.2 LITERATURE SURVEY 2
1.2.1 PAST STUDIES ON THE ESTIMATION OF ELASTIC AND INELASTIC DISPLACEMENT DEMAND 2
1.2.2 PAST STUDIES ON NEAR FAULT GROUND MOTIONS 5
1.3 OBJECT AND SCOPE 6
2. NEAR-FAULT GROUND MOTIONS AND ANALYTICAL MODELLING 8
2.1 GROUND MOTION RECORDS 8
2.2 CHARACTERISTICS OF NEAR-FAULT GROUND MOTIONS 9
2.2.1 FACTORS AFFECTING NEAR-FAULT GROUND MOTIONS 14
2.2.2 PULSE PERIOD 16
2.2.3 THE RATIO OF PGV TO PGA 18
2.3 EVALUATION OF PRESENT EARTHQUAKE CODES AND PROVISIONS IN TERMS OF NEAR FAULT RECORDS 20

2.4 BUILDING MODELS 21
2.5 ANALYTICAL MODELS 25
2.5.1 VALIDATION OF THE GENERIC FRAME MODEL 29
2.6 STRUCTURAL PROPERTIES AFFECTING DISPLACEMENT DEMAND 31
2.6.1 BEAM TO COLUMN STIFFNESS RATIO (ρ) 32
2.6.2 STIFFNESS DISTRIBUTION COEFFICIENT (λ) 36
2.6.3 BEAM TO COLUMN CAPACITY RATIO (Q) 38
2.6.4 SOFT STORY FACTOR (ψ) 40
2.6.5 REGULAR STORY HEIGHT (h_2) AND NUMBER OF STORIES (N) 41
3. ELASTIC MULTI-DEGREE-OF-FREEDOM ANALYSIS AND DERIVATION OF REGRESSION EQUATIONS 42
3.1 INTRODUCTION 42
3.2 EFFECTS OF NEAR-FAULT GROUND MOTIONS AND STRUCTURAL PROPERTIES ON THE RESPONSE OF ELASTIC MOMENT RESISTING FRAMES 43
3.2.1 EFFECTS OF PULSE PERIOD ON LATERAL DISPLACEMENT DEMAND 43
3.2.2 EFFECTS OF BEAM TO COLUMN STIFFNESS RATIO (ρ) ON LATERAL DISPLACEMENT DEMAND 50
3.2.3 EFFECTS OF STIFFNESS DISTRIBUTION COEFFICIENT (λ) ON LATERAL DISPLACEMENT DEMAND 54
3.2.4 EFFECTS OF SOFT STORY FACTOR (ψ) ON LATERAL DISPLACEMENT DEMAND 62
3.2.5 EFFECTS OF REGULAR STORY HEIGHT (h_2) AND NUMBER OF STORIES (N) ON LATERAL DISPLACEMENT DEMAND 66
3.3 ASSUMPTIONS EMPLOYED IN THE DERIVATION OF EQUATIONS 69
3.4 DERIVATION OF THE EQUATIONS FOR ESTIMATING LINEAR DEFORMATION DEMANDS OF FRAME SYSTEMS 69
3.4.1 MODIFICATION OF THE PROCEDURE PRENSENTED BY GÜLKAN AND AKKAR (2002) 69
3.4.2 MODIFICATION OF THE PROCEDURE PRENSENTED BY AKKAR ET AL. (2005) 74

3.5 SUMMING UP THIS CHAPTER 82

4. INELASTIC MULTI-DEGREE-OF-FREEDOM ANALYSIS 84

4.1 INTRODUCTION 84

4.2 INELASTIC MODELLING 85

4.3 DEFINITION OF INELASTIC DRIFT RATIO (C_Δ) 87

4.4 EFFECTS OF NEAR-FAULT GROUND MOTIONS AND STRUCTURAL PROPERTIES ON THE RESPONSE OF INELASTIC MOMENT RESISTING FRAMES 87

4.4.1 EFFECT OF BEAM TO COLUMN CAPACITY RATIO (Q) 88

4.4.2 EFFECTS OF SEISMIC FORCE REDUCTION FACTOR (q) 101

4.4.3 EFFECTS OF THE RATIO OF PULSE PERIOD TO FUNDAMENTAL PERIOD (T_P/T) 104

4.4.4 EFFECTS OF BEAM TO COLUMN STIFFNESS RATIO (ρ) 108

4.4.5 EFFECTS OF SOFT STORY FACTOR (ψ) 117

4.4.6 EFFECTS OF STIFFNESS DISTRIBUTION FACTOR (λ) 127

4.4.7 EFFECTS OF REGULAR STORY HEIGHT (h_2) 127

4.5 REPRESENTATIVE EQUATION FOR INELASTIC DRIFT RATIO 128

5. VERIFICATION 143

5.1 VERIFICATION OF THE PROPOSED EQUATIONS FOR THE ELASTIC GSDR AND MIDR 143

6. SUMMARY, CONCLUSIONS AND RECOMMENDATIONS FOR FUTURE STUDIES 173

6.1 SUMMARY 173

6.2 CONCLUSIONS 175

6.2.1 CONCLUSIONS CONCERNING EFFECTS OF NEAR SOURCE GROUND MOTIONS 175

6.2.2 CONCLUSIONS CONCERNING ELASTIC RESPONSE OF MULTI STORY FRAMES 175

6.2.3 CONCLUSIONS CONCERNING INELASTIC RESPONSE OF MULTI STORY FRAMES 177

6.3 SUGGESTED FUTURE RESEARCH 178

REFERENCES…………………………………………………………………..180

LIST OF TABLES

TABLES

Table 2.1: Ground Motion Database.....11
Table 2.2: Column Sections (Pre-Northridge Designs) for Los Angeles Model Buildings (Section designations correspond to standard AISC abbreviations.) 23
Table 2.3: Seismic masses for moment resisting frames 25
Table 2.4: Comparison of natural periods of the original frame and generic frame 30
Table 4.1: C_{Δ} values obtained from time history analyses.....131
Table 5.1: A/E statistics for $GSDR_{SH}$ 153
Table 5.2: A/E statistics for $GSDR_{MF}$ 162
Table 5.3: A/E statistics for $MIDR_{MF}$ 171

LIST OF FIGURES

FIGURES

Figure 2.1: Distribution of near-fault recordings 9
Figure 2.2: Typical acceleration, velocity, displacement, and pseudo-velocity of (a) far-fault (b) near-fault (fling-step) (c) near-fault (forward directivity) ground motion records……13
Figure 2.3: T_p and T_{p-v} for 1999 Kocaeli Earthquake Düzce Station 270º Comp...17
Figure 2.4: Correlation between T_p and T_{p-v} 17
Figure 2.5: Pulse period, magnitude and distance distribution of earthquakes classified by fault mechanism.....19
Figure 2.6: Plan and elevation views 22
Figure 2.7: Generic Frame Modeling.....27
Figure 2.8 : Comparison of fundamental mode shapes of OF and GF 30
Figure 2.9: Comparison of maximum interstory drift ratios and roof drift ratios of structures based on OF and GF.....31
Figure 2.10: Fundamental mode shapes of 20-story frames with uniform stiffness corresponding to different ρ values 34
Figure 2.11: Effect of ρ on lateral deformation 34
Figure 2.12: Deformation shapes of columns and beams when ρ equals to (a) zero and (b) infinity 35
Figure 2.13: The variation of ρ along the height of SAC MRFs with non-uniform stiffness and effect of constant ρ assumption on fundamental mode shape and interstory drift 36

Figure 2.14: Effects of linear stiffness distribution on mode shape and story drift 38
Figure 2.15: Moment directions at joint 39
Figure 3.1: T_p/T effect on GSDR 46
Figure 3.2: T_p/T effect on MIDR 47
Figure 3.3: Higher mode effect on GSDR 48
Figure 3.4: Higher mode effect on MIDR 49
Figure 3.5: Interstory drift profiles for 20, 9 and 3 story MRFs with different ρ values 52
Figure 3.6: First mode and mean interstory drift profiles for 20, 9 and 3 story MRFs with different ρ values 53
Figure 3.7: Fundamental mode shapes 54
Figure 3.8: Effect of λ on fundamental mode shapes of 20 Story MRFs 56
Figure 3.9: Effect of λ on fundamental mode shapes for 9 Story MRFs 57
Figure 3.10: Non-uniform stiffness distribution effect on lateral deformation demand of 20 story MRF 58
Figure 3.11: Non-uniform stiffness distribution effect on lateral deformation demand of 9 story MRF 59
Figure 3.12: First mode and mean interstory drift profiles obtained from elastic response history analyses of 20 story MRFs with different λ values 60
Figure 3.13 First mode and mean interstory drift profiles obtained from elastic response history analyses of 9 story MRFs with different λ values 61
Figure 3.14: Soft story effect on period 62
Figure 3.15: Soft story effect on the fundamental modal displacement 63
Figure 3.16 : First mode and mean interstory drift profiles obtained from elastic response history analyses of 9 story MRFs with different ψ values 64
Figure 3.17: Soft story effect on MIDR 65
Figure 3.18: Effects of story height on fundamental mode shape 66
Figure 3.19: Effect of story height on fundamental period 67
Figure 3.20 : Effect of story height on IDR 68
Figure 3.21: Variation in α with stiffness distribution coefficient and soft story factors 73

Figure 3.22 : Comparison of α values calculated from modal analysis and proposed equation 74
Figure 3.23: Comparison of γ_{MF} values calculated from modal analysis and the Equation (3.13) 76
Figure 3.24: Error of Equation (3.13) 77
Figure 3.25: Error of Equation (3.17) for regular frames 79
Figure 3.26: Error of Equation (3.17) for irregular frames 80
Figure 3.27: Comparison of γ_{MIDR} values calculated from analysis and Equation (3.18) 81
Figure 4.1: Failure mechanism of 9 story MRF 86
Figure 4.2: Effect of Q on base shear (N=20, h_2=3 m) 90
Figure 4.3: Effect of Q on base shear capacity (N=20, h_2=5 m) 91
Figure 4.4: Effect of Q on base shear capacity (N=9, h_2=3 m) 92
Figure 4.5: Effect of Q on base shear capacity (N=9, h_2=5 m) 93
Figure 4.6: Effect of Q on base shear capacity (N=3, h_2=3 m and 5 m) 94
Figure 4.7: Effect of Q on IDR (N=20, h_2=3 m) 95
Figure 4.8: Effect of Q on IDR (N=20, h_2=5 m) 96
Figure 4.9: Effect of Q on IDR (N=9, h_2=3 m) 97
Figure 4.10: Effect of Q on IDR (N=9, h_2=5 m) 98
Figure 4.11: Effect of Q on IDR (N=3, h_2=3 m) 99
Figure 4.12: Effect of Q on IDR (N=3, h_2=5 m) 100
Figure 4.13: Relationship between C_Δ and q (ρ=0.50) 102
Figure 4.14: Relationship between C_Δ and q (ρ=infinity) 103
Figure 4.15: Effect of T_p/T on the inelastic drift demand (N=20) 105
Figure 4.16: Effect of T_p/T on the inelastic drift demand (N=9) 106
Figure 4.17: Effect of T_p/T on the inelastic drift demand (N=3) 107
Figure 4.18: Comparison of ρ on the inelastic and elastic drift demands (N=20) 109
Figure 4.19: Comparison of ρ on the inelastic and elastic drift demands (N=9) 110
Figure 4.20: Comparison of ρ on the inelastic and elastic drift demands (N=3) 111
Figure 4.21: Effect of ρ on inelastic drift ratio (N=20, Q=0.40) 112
Figure 4.22: Effect of ρ on inelastic drift ratio (N=20, Q=1.2) 113

Figure 4.23: Effect of ρ on inelastic drift ratio (N=9, Q=0.40) 114
Figure 4.24: Effect of ρ on inelastic drift ratio (N=9, Q=1.2) 115
Figure 4.25: Effect of ρ on inelastic drift ratio (N=3) 116
Figure 4.26: Comparison of soft story effect on the inelastic and elastic drift demand (N=20, Q=0.40).....118
Figure 4.27: Comparison of soft story effect on the inelastic and elastic drift demand (N=20, Q=1.2).....119
Figure 4.28: Comparison of soft story effect on the inelastic and elastic drift demand (N=9, Q=0.40).....120
Figure 4.29: Comparison of soft story effect on the inelastic and elastic drift demand (N=9, Q=1.2).....121
Figure 4.30: Comparison of soft story effect on the inelastic and elastic drift demand (N=3, Q=0.40).....122
Figure 4.31: Comparison of soft story effect on the inelastic and elastic drift demand (N=3, Q=1.2).....123
Figure 4.32: Effect of soft story on inelastic drift ratio (N=20) 124
Figure 4.33: Effect of soft story on inelastic drift ratio (N=9) 125
Figure 4.34: Effect of soft story on inelastic drift ratio (N=3) 126
Figure 4.35: Comparison of stiffness distribution on the inelastic and elastic drift demand (N=20, Q=0.40).....132
Figure 4.36: Comparison of stiffness distribution on the inelastic and elastic drift demand (N=20, Q=1.2).....133
Figure 4.37: Comparison of stiffness distribution on the inelastic and elastic drift demand (N=9, Q=0.40).....134
Figure 4.38: Comparison of stiffness distribution on the inelastic and elastic drift demand (N=9, Q=1.2).....135
Figure 4.39: Effect of stiffness distribution on inelastic drift ratio (N=20 and 9, Q=0.40 and 1.2) 136
Figure 4.40: Comparison of regular story height effect on the inelastic and elastic drift demand (N=20, Q=0.40).....137

Figure 4.41: Comparison of regular story height effect on the inelastic and elastic drift demand (N=20, Q=1.2) 138
Figure 4.42: Comparison of regular story height effect on the inelastic and elastic drift demand (N=9, Q=0.40) 139
Figure 4.43: Comparison of regular story height effect on the inelastic and elastic drift demand (N=9, Q=1.2) 140
Figure 4.44: Effect of regular story height on inelastic drift ratio (N=20 and 9, Q=0.40 and 1.2) 141
Figure 4.45: Correlation between $(C_{\Delta})_{FORMULA}$ and $(C_{\Delta})_{ANALYSIS}$ 142
Figure 5.1: Comparison of approximate results with exact values of $GSDR_{SH}$ (N=20, h_2 =3 m) 146
Figure 5.2: Comparison of approximate results with exact values of $GSDR_{SH}$ (N=15, h_2 =3 m) 147
Figure 5.3: Comparison of approximate results with exact values of $GSDR_{SH}$ (N=12, h_2 =3 m) 148
Figure 5.4: Comparison of approximate results with exact values of $GSDR_{SH}$ (N=9, h_2 =3 m) 149
Figure 5.5: Comparison of approximate results with exact values of $GSDR_{SH}$ (N=7, h_2 =3 m) 150
Figure 5.6: Comparison of approximate results with exact values of $GSDR_{SH}$ (N=5, h_2 =3 m) 151
Figure 5.7: Comparison of approximate results with exact values of $GSDR_{SH}$ (N=3, h_2 =3 m) 152
Figure 5.8: Comparison of approximate results with exact values of $GSDR_{MF}$ (N=20, h_2 =3 m) 155
Figure 5.9: Comparison of approximate results with exact values of $GSDR_{MF}$ (N=15, h_2 =3 m) 156
Figure 5.10: Comparison of approximate results with exact values of $GSDR_{MF}$ (N=12, h_2 =3 m) 157

Figure 5.11: Comparison of approximate results with exact values of $GSDR_{MF}$ (N=9, h_2 =3 m) 158
Figure 5.12: Comparison of approximate results with exact values of $GSDR_{MF}$ (N=7, h_2 =3 m) 159
Figure 5.13: Comparison of approximate results with exact values of $GSDR_{MF}$ (N=5, h_2 =3 m) 160
Figure 5.14: Comparison of approximate results with exact values of $GSDR_{MF}$ (N=3, h_2 =3 m) 161
Figure 5.15: Comparison of approximate results with exact values of $MIDR_{MF}$ (N=20, h_2 =3 m) 164
Figure 5.16: Comparison of approximate results with exact values of $MIDR_{MF}$ (N=15, h_2 =3 m) 165
Figure 5.17: Comparison of approximate results with exact values of $MIDR_{MF}$ (N=12, h_2 =3 m) 166
Figure 5.18: Comparison of approximate results with exact values of $MIDR_{MF}$ (N=9, h_2 =3 m) 167
Figure 5.19: Comparison of approximate results with exact values of $MIDR_{MF}$ (N=7, h_2 =3 m) 168
Figure 5.20: Comparison of approximate results with exact values of $MIDR_{MF}$ (N=5, h_2 =3 m) 169
Figure 5.21: Comparison of approximate results with exact values of $MIDR_{MF}$ (N=3, h_2 =3 m) 170

LIST OF SYMBOLS

α	: modification factor for nonuniform shear frame
C_{Δ}	: inelastic drift ratio
D_1	: displacement of the MRF considering only the first mode
D_{all}	: displacement of the MRF considering all modes
$D_n(t)$	: the displacement response of the SDOF system
d	: closest site to fault rupture distance
E	: Young's modulus
$\underline{\phi}_n$	: the n^{th} mode shape vector
$\phi_{1,1}$	: the amplitude of the first mode vector in the ground story
$\phi_{1,1}^{MF}$	: the ground story drift of MRF in the first mode shapes
$\phi_{1,1}^{SH}$	: the ground story drift of shear frame in the first mode shapes
$\phi_{n,1}$	: the drift of n^{th} story in the first mode
$\phi_{n-1,1}$	: the drift of the story below n^{th} story in the first mode
Γ_n	: the modal participation factor of the n^{th} mode
Γ_1^{MF}	: the first mode participation factor of the MRF
Γ_1^{SH}	: the first mode participation factor of the shear frame
γ_{MF}	:modification factor for moment resisting frame GSDR
γ_{MIDR}	:modification factor for MIDR of uniform MRF
$\gamma_{MIDR}^{'}$	:modification factor for MIDR of nonuniform MRF
H_{Cij}	: height of the jth column in the ith floor
h_1	: ground story height
h_2	: regular story height

η : percentage of the higher mode

$\underline{\iota}$: the influence vector

I_b : moment of inertia of beam

I_c : moment of inertia of column

$I_{C_{GROUND}}$: moment of inertia of ground story column

$I_{C_{TOP}}$: moment of inertia of top story column

I_{Bij} : moment of inertia of the jth beam in the ith floor

I_{Cij} : moment of inertia of the jth column in the ith floor

$K_{spring,i}$: stiffness of the spring at the ith story

L_b : the length of beam

L_c : the length of column

L_{Bij} : length of the jth beam in the ith floor

L_{Cij} : length of the jth column at the ith story

λ : stiffness distribution coefficient

$\underline{m}$: the mass matrix of the system

M_w : moment magnitude

M_{Bij} : the moment capacity of the jth beam in the ith floor

$M_{Bij_{LEFT}}$: left moment at beam ij

$M_{Bij_{RIGHT}}$: right moment at beam ij

M_{Cij} : the moment capacity of the jth column in the ith floor

$M_{Cij_{BOTTOM}}$: bottom moment of the column ij

$M_{Cij_{TOP}}$: top moment of the column ij

$M_{Y_{ABOVE}}$: the moment capacity at the column end above floor level

$M_{Y_{BELOW}}$: the moment capacity at the column end below floor level

$M_{Y_{BEAM-LEFT}}$: left moment at beam

$M_{Y_{BEAM-RIGHT}}$: right moment at beam

N : number of stories

r : number of bays

ρ	: beam to column stiffness ratio
S_a	: spectral acceleration
S_d	: spectral displacement
Q	: beam to column capacity ratio
q	: seismic force reduction factor
$q_n(t)$	: the time variation of displacement in the n^{th} mode
$u_{1,1}$	: the ground story displacement in the first mode
T	: fundamental period
T_n	: fundamental period
T_p	: pulse period
$T_{p\text{-}v}$	: dominant pseudo-spectral velocity period
θ_i	: the nodal rotation at ith floor level
θ_{i+1}	: the nodal rotation at (i+1)th floor level
ψ	: soft story factor
W	: the weight of the system
V_y	: lateral yield strength of the system
Ω	: factor of inelastic drift ratio
ζ	: the viscous damping ratio
Z(n)	: sum of the inertia of the n'th story

CHAPTER 1

INTRODUCTION

1.1 STATEMENT OF THE PROBLEM

At the risk of generalizing, we can state that damage (structural as well as nonstructural) experienced in buildings as a result of earthquake ground motions are produced by lateral displacements. A major challenge for performance-based seismic engineering is to develop simple methods for the accurate estimation of these displacements. The estimation of seismic deformation demands for multi-degree-of-freedom structures has been the subject of many studies [3, 26]. In current practice, response history analysis and pushover analysis are used to estimate seismic demands. Response history analysis is the most accurate analysis type, but there are several problems associated with it. The first one is that it can be difficult to choose an appropriate earthquake ground motion record to use as the loading. The generation of site specific input includes many uncertainties. The second problem is that it is too computer intensive to be practical especially if inelastic analysis is performed [71]. On the other hand, there are some limitations and assumptions of pushover analysis which have been discussed by many researchers [20, 42]. Conventional pushover analysis is based on the approximation that fundamental mode controls the response even after the structure yields. Moreover, it estimates seismic demands well when the maximum displacements are accurately estimated by the Coefficient Method of FEMA-356

[15] or the Capacity-Spectrum Method of ATC-40 [7], but predictions are generally restricted to low-rise and medium-rise structures in which nonlinear behavior is distributed in prescribed ways throughout the height of the structure [17]. In order to conduct either response history analysis or pushover analysis, detailed modeling and computation efforts are needed. For rapid assessment and preliminary design purposes, the effort associated with detailed modeling and analysis is not feasible and a quick estimate of the system response is needed.

The response of structures to ground motions within the near-fault region of an earthquake is currently of great interest [4, 5, 28, 32, 37, 45,]. It is observed that the response of frames to near fault ground motions is not well understood. The inelastic displacement demands caused by near fault records may be significantly larger than those estimated with displacement prediction techniques commonly used for far-fault records. This is a result of pulse type character within near fault ground motion. The damaging effects of this type of ground motion have been recognized during many worldwide earthquakes (e.g. 1992 Erzincan, 1994 Northridge, and 1995 Kobe, 1999 Düzce). There exists a need to improve current design procedures to overcome the destructive effect of near fault ground motions in the design process for structures located near an earthquake fault. Much more research and data are needed in order to understand all important aspects of the near fault ground motions and the improvement of current design procedures considering this type of ground motions.

1.2 LITERATURE SURVEY

1.2.1 PAST STUDIES ON THE ESTIMATION OF ELASTIC AND INELASTIC DISPLACEMENT DEMAND

During the preliminary design stage of a building or the evaluation of existing buildings, approximate methods can be useful in providing required lateral deformations. However, these methods must be simple and provide reasonably

good results. Researchers have used simplified models of buildings that take into account only flexural or shear type deformations. For instance, Montes and Rosenblueth [51] utilized flexural beams to estimate overturning moment and shear demands along the height of chimneys. Westergaard [70], Jennings and Newmark [36] used a shear beam model to estimate lateral deformations. In 1997, Iwan proposed the drift demand spectrum, which is a measure of earthquake demand based on the propagation of shear waves in a uniform cantilever shear beam. It was suggested as an alternative to the response spectrum for expressing the seismic demand of near fault ground motions that are characterized by long-period velocity pulses. Kim and Collins [39] applied the concept of drift spectrum to develop uniform hazard drift demand spectra for a site near Los Angeles. Kim and Collins [40] indicated that the computed interstory drift using Iwan's model did not return to zero as time approached infinity for ground motions including a permanent ground displacement at the end of the record. They stated that the drift response should converge to zero after the ground motion because the drift demand spectrum proposed by Iwan is based on linear elastic shear beam model. Later, Chopra and Chintanapakdee [18] used shear beam model and showed that drift spectra could be computed using conventional modal analysis techniques. Moreover, Gülkan and Akkar [26] used the first mode shear beam deformation pattern to generate a simpler replacement for drift spectrum.

Utilization of only shear beams or flexural beams do not provide sufficient models for certain types of buildings. There are many types of frames for which these two models are not suitable. For example, maximum interstory drift of shear beam model occurs at the ground story, which is not true for general frame behavior. Therefore, a simplified model that consists of a combination of a flexural cantilever beam and a shear cantilever beam was studied by Khan and Sbarounis [38], Rosman [58], Heidebrecht and Stafford Smith [29], Fajfar and Strojnik [22], Miranda [46], Zalka [73], Miranda and Reyes [49], Potzta and Kollár [53], Akkar et al. [3] and Miranda and Akkar [48]. Heidebrecht and Stafford Smith [29] derived the differential equation that expresses the response of a model with uniform lateral stiffness and closed form solutions for lateral displacements. Using

these closed form solutions Miranda [46] proposed a procedure that estimates elastic and inelastic maximum interstory drift ratio in buildings responding in the fundamental mode and having uniform stiffness throughout the structure. Miranda and Reyes [49] improved the method proposed by Miranda [46] by adding the effect of nonuniform lateral stiffness distribution on lateral displacement demand. Akkar et al. [3] modified the procedure by Gülkan and Akkar [26] in order to estimate the ground story and maximum interstory drift ratios of regular moment resisting frames deforming in the elastic range. The proposed drift expression of Akkar et al. [3] includes the beam to column stiffness ratio that determines the joint rotation in structural systems by means of the beam and column flexural stiffness contributions at the story level. Miranda and Akkar [48] proposed generalized interstory drift spectrum to obtain estimates of interstory drift demands in buildings by using the continuum model that consists of a flexural cantilever beam and shear cantilever beam.

There is significant research effort to estimate maximum global inelastic displacement demands without performing detailed nonlinear analyses because the maximum displacement is utilized as a structural response parameter for evaluating the inelastic deformation of structures. While a single number falls short of describing the displacement performance of a building, it is still useful as an indicator of whether a design is likely to be revised at an early stage. The displacement coefficient method in FEMA-356 [15] is based on the amplification of the maximum displacement of a linear elastic SDOF system by a series of coefficients in order to determine the maximum global inelastic displacement demand. The factor which relates the maximum inelastic and elastic displacements considers strength reduction factor, natural period and characteristic period of the response spectrum. Saiidi and Sozen [60], Fajfar and Fischinger [21], Qi and Moehle [55], Seneviratna and Krawinkler [61] and Miranda [46] have shown that the global inelastic response of many multi-degree-of-freedom structures can be estimated from the response of SDOF systems by utilizing appropriate modification factors. Another simplified inelastic procedure is the capacity spectrum method (CSM) in ATC-40 [7]. This method is based on equivalent

linearization, but involves a good many simplifying assumptions for the purpose of being useable. In the capacity spectrum method, the maximum displacement of a nonlinear SDOF system can be estimated from the maximum displacement of a linear SDOF system with lower lateral stiffness and higher damping coefficient (e.g. Rosenblueth and Herrera [57], Gülkan and Sözen [27], Iwan [33, 34]).

1.2.2 PAST STUDIES ON NEAR FAULT GROUND MOTIONS

The first strong seismological evidence about near fault ground motions is the explanation of intensity patterns observed in the 1952 Kern County earthquake by Benioff [9]. After the 1971 San Fernando earthquake, Mahin et al. [44] and Bertero et al. [11] stated that observed damage of buildings were caused by a severe pulse and this was a characteristic of near-fault ground motions. Anderson and Bertero [6] pointed out the importance of directivity effects associated with the direction of rupture propagation after the 1979 Imperial Valley earthquake. In addition, they showed the sensitivity of inelastic near-fault response to structure strength and to the ratio of the fundamental period of the structure to the period of a pulse contained in the near-fault record. Wald [69] studied the rupture models of the 1995 Kobe earthquake in order to explain long-period pulses that are indicative of rupture directivity effects.

The response of a continuous shear building to pulse-type ground motions was studied by Hall et al. [28]. They emphasized the damaging effects of near-fault ground motions and the inadequacy of current code provisions. As a measure of seismic demand for MDOF structures subjected to near-fault ground motions with pulse-type characteristics, Iwan [31] proposed the drift spectrum method based on a uniform elastic shear beam model. Somerville et al. [63] pointed out that the propagation of the fault rupture towards a site at a velocity close to the shear wave velocity causes most of the seismic energy from the rupture to arrive in a single large long-period pulse of motion that occurs at the beginning of the record. Moreover, Somerville [64] stated that the radiation pattern of the shear

dislocation on the fault causes large pulse of motion to be oriented in the direction perpendicular to the fault, causing the strike normal peak velocity to be larger than the strike parallel peak velocity. However, Akkar and Gülkan [26] studied the forward directivity effects of the 1999 Kocaeli and 1999 Düzce earthquakes and observed that the ground motion component with highest displacement demand was not always in the fault normal direction. These apparent contradictions notwithstanding, it is agreed in both the seismological and the earthquake engineering communities that at distances of perhaps up to 10 km to the causative fault rupture structural response may be affected by factors that are disregarded under traditional conditions.

1.3 OBJECT AND SCOPE

One of the aims of this study is the improvement of the equations that estimate maximum ground story displacement ratio of shear frames presented by Gülkan and Akkar [26] and maximum ground story drift ratio and interstory drift ratio of regular moment resisting frames presented by Akkar et al. [3]. The proposed equations modify these equations by including stiffness distribution coefficient, soft story factor, regular story height and number of stories. In addition, a representative equation is proposed for the ratio of maximum inelastic interstory drift ratio to maximum elastic interstory drift ratio.

Another objective of this study is to provide knowledge on the response of regular and irregular, elastic and inelastic frame structures in the near fault region. The effects of beam to column capacity ratio, seismic force reduction factor, the ratio of pulse period to fundamental period, beam to column stiffness ratio, soft story factor, stiffness distribution coefficient, regular story height and number of stories on elastic and inelastic drift demand are presented here.

For the purpose of demonstrating the statistical variations of systematically conducted response calculations a total of 90’480 elastic and 542’880 inelastic time history analyses were conducted in this study. 20-story, 9-story and 3-story

steel moment resisting frame buildings designed as part of the SAC steel project were analyzed under the effect of 58 near-fault pulse-type ground motions using generic “fishbone” models. All nonlinear static analyses and time history analyses are conducted by using the software DRAIN-2DX [54].

This thesis is composed of six main chapters. Contents of each chapter are summarized as follows:

Chapter 1 Statement of the problem and literature survey on estimation of elastic and inelastic displacement demands and fundamental features of near fault ground motions.

Chapter 2 Examination of fundamental properties of utilized near fault ground motion records. Information about building models and a generic fishbone frame model used in this study. Definition of different structural properties with controlling effects on structural response are investigated in this chapter.

Chapter 3 Investigation of the effects of near-fault ground motions and different structural properties on the response of elastic moment resisting frames. Modification of the equations proposed by Gülkan and Akkar [26] and Akkar et al. [3].

Chapter 4 Investigation of the effects of near-fault ground motions and different structural properties on the response of inelastic moment resisting frames. Derivation of the representative equation for inelastic drift ratio follows from this chapter.

Chapter 5 Verification of the proposed procedure.

Chapter 6 Summary, conclusions and further recommendations regarding the study are presented.

CHAPTER 2

NEAR-FAULT GROUND MOTIONS AND ANALYTICAL MODELLING

2.1 GROUND MOTION RECORDS

A set of 58 near-fault pulse-type ground motion records whose average shear wave velocity values in the upper 30 m range from 180 m/s to 750 m/s was used in this study. Records were downloaded from the PEER Strong Motion Database (http://peer.berkeley.edu/smcat/). The upper and lower limits of the moment magnitude and closest site-to-fault rupture distances for the ground motions are $6.0 \leq M_w \leq 7.6$ and $0.5 \text{ km} \leq d \leq 18.5 \text{ km}$, respectively. Records have peak ground accelerations (PGA) in the range of 0.09g to 0.97g and peak ground velocities (PGV) are in the range of 36 cm/s to 130 cm/s. Utilized near-fault ground motions are characterized by a large, long-period velocity pulse, and they are capable of causing severe structural damage. Ground motion data is taken from 10 different destructive earthquakes. The important features of these ground motions are listed in Table 2.1. Moment magnitudes of the earthquakes are plotted against the closest distances to the fault rupture in Figure 2.1. Fault types are also indicated in this graph. This is not a feature that has been taken into account explicitly in this study.

The damaging effects of ground motions with a pulse-like character have been recognized during many earthquakes, such as the 1992 Erzincan, 1994 Northridge, 1995 Kobe, 1999 Kocaeli, Düzce and Chi-Chi earthquakes. The need exists to refine current design procedures to counteract the destructive effect of this type of ground motions in the design process for structures located in the near-fault region. This is one of the motivating reasons for embarking on this study.

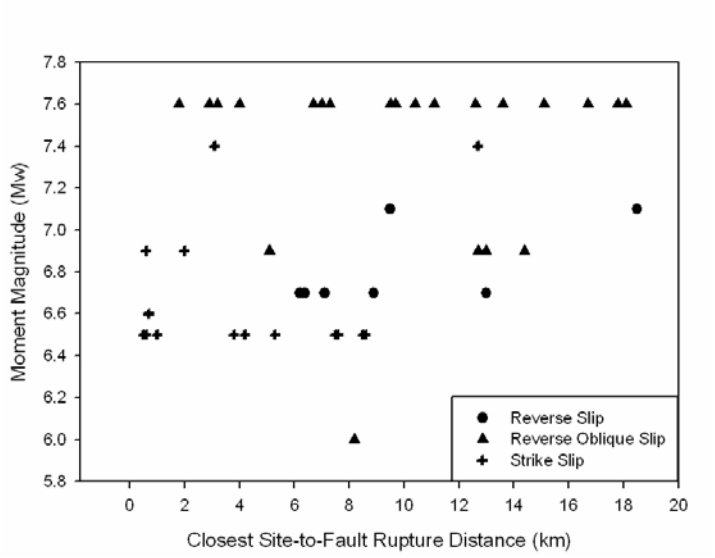

Figure 2.1: Distribution of near-fault recordings

2.2 CHARACTERISTICS OF NEAR-FAULT GROUND MOTIONS

The near-fault zone is assumed to be restricted to within a distance of about 20 km from the ruptured fault. The distance is typically much smaller than the source dimensions. Ground motions that occur near an active fault are significantly affected by the faulting mechanism, direction of rupture propagation relative to the site (forward directivity, backward directivity, neutral directivity), and the static

deformation of the ground surface associated with fling effects which is the source of long period motion.

Near-fault ground motions can be considerably different than those observed further away from the seismic source. Whereas distinctive differences in their respective acceleration time histories may not be obvious, examination of the velocity and displacement time series of these motions displays the special nature of the pulse like motion due to forward directivity or apparent tectonic deformation caused by fling step. The acceleration, velocity, and displacement histories of near-fault ground motions having forward directivity and fling step effects are compared to that of ordinary far fault motion in Figure 2.2. As shown in Figure 2.2 large, long period pulses are conspicuous for near fault ground motions (Chi-Chi and Kocaeli Earthquakes) whereas such pulses do not exist in far fault records, a typical example of which is the Kern Country Earthquake of 1952. Another distinctive difference is that there is a permanent displacement (fling step) in the displacement time series of the Chi-Chi Earthquake.

Table 2.1: Ground Motion Database

#	Earthquake	Country	Date	Station Name	Site Geology*	Mechanism	Component	Magnitude (Mw)	d** (km)	PGA** (g)	PGV** (cm/s)	Tp** (s)	Tp-v** (s)
1	Chi-Chi	Taiwan	20.09.1999	TCU087	stiff soil	Reverse - Oblique	NS	7.6	3.2	0.12	37	4.4	4.0
2	Chi-Chi	Taiwan	20.09.1999	TCU087	stiff soil	Reverse - Oblique	EW	7.6	3.2	0.13	41	9.5	8.0
3	Chi-Chi	Taiwan	20.09.1999	CHY080	rock	Reverse - Oblique	NS	7.6	7.0	0.90	102	1.4	1.0
4	Chi-Chi	Taiwan	20.09.1999	CHY080	rock	Reverse - Oblique	EW	7.6	7.0	0.97	108	0.9	0.9
5	Chi-Chi	Taiwan	20.09.1999	NSY	stiff soil	Reverse - Oblique	EW	7.6	9.7	0.14	48	8.1	8.0
6	Chi-Chi	Taiwan	20.09.1999	NSY	stiff soil	Reverse - Oblique	NS	7.6	9.7	0.13	42	3.7	4.6
7	Chi-Chi	Taiwan	20.09.1999	TCU128	stiff soil	Reverse - Oblique	NS	7.6	9.7	0.17	69	4.0	4.8
8	Chi-Chi	Taiwan	20.09.1999	TCU128	stiff soil	Reverse - Oblique	EW	7.6	9.7	0.14	73	7.8	7.5
9	Chi-Chi	Taiwan	20.09.1999	TCU057	stiff soil	Reverse - Oblique	NS	7.6	12.6	0.09	43	6.6	7.5
10	Chi-Chi	Taiwan	20.09.1999	TCU104	stiff soil	Reverse - Oblique	NS	7.6	13.6	0.09	47	6.4	5.5
11	Chi-Chi	Taiwan	20.09.1999	TCU102	rock	Reverse - Oblique	NS	7.6	1.8	0.17	77	2.8	2.4
12	Chi-Chi	Taiwan	20.09.1999	TCU101	rock	Reverse - Oblique	EW	7.6	2.9	0.20	68	7.6	8.5
13	Chi-Chi	Taiwan	20.09.1999	TCU103	Deep broad soil	Reverse - Oblique	EW	7.6	4.0	0.13	62	7.9	7.0
14	Chi-Chi	Taiwan	20.09.1999	TCU053	Deep broad soil	Reverse - Oblique	NS	7.6	6.7	0.14	41	6.6	6.0
15	Chi-Chi	Taiwan	20.09.1999	CHY028	rock	Reverse - Oblique	NS	7.6	7.3	0.82	67	0.8	0.9
16	Chi-Chi	Taiwan	20.09.1999	TCU060	Deep broad soil	Reverse - Oblique	EW	7.6	9.5	0.20	36	8.4	11.0
17	Chi-Chi	Taiwan	20.09.1999	TCU063	Deep broad soil	Reverse - Oblique	NS	7.6	10.4	0.13	73	5.2	3.4
18	Chi-Chi	Taiwan	20.09.1999	CHY101	Deep broad soil	Reverse - Oblique	NS	7.6	11.1	0.44	115	4.7	4.8
19	Chi-Chi	Taiwan	20.09.1999	CHY101	Deep broad soil	Reverse - Oblique	EW	7.6	11.1	0.35	71	3.4	3.2
20	Chi-Chi	Taiwan	20.09.1999	WGK	Deep broad soil	Reverse - Oblique	EW	7.6	11.1	0.33	69	3.3	3.2
21	Chi-Chi	Taiwan	20.09.1999	WGK	Deep broad soil	Reverse - Oblique	NS	7.6	11.1	0.48	74	4.5	4.8
22	Chi-Chi	Taiwan	20.09.1999	TCU064	Deep broad soil	Reverse - Oblique	NS	7.6	15.1	0.12	54	7.2	7.0
23	Chi-Chi	Taiwan	20.09.1999	TCU036	Deep broad soil	Reverse - Oblique	EW	7.6	16.7	0.14	60	5.8	4.2
24	Chi-Chi	Taiwan	20.09.1999	TCU059	Deep broad soil	Reverse - Oblique	EW	7.6	17.8	0.17	59	6.0	6.5
25	Chi-Chi	Taiwan	20.09.1999	CHY035	stiff soil	Reverse - Oblique	EW	7.6	18.1	0.25	46	1.3	1.4
26	Erzincan	Turkey	13.03.1992	Erzincan	Deep broad soil	Strike - Slip	NS	6.9	2.0	0.52	84	2.4	2.0
27	Kobe	Japan	16.01.1995	KJMA	stiff soil	Strike - Slip	90	6.9	0.6	0.60	74	1.4	0.8
28	Kobe	Japan	16.01.1995	KJMA	stiff soil	Strike - Slip	0	6.9	0.6	0.82	81	0.9	0.9
29	Kocaeli	Turkey	17.08.1999	Duzce	Deep broad soil	Strike - Slip	270	7.4	12.7	0.36	46	1.5	1.4
30	Kocaeli	Turkey	17.08.1999	Sakarya	stiff soil	Strike - Slip	90	7.4	3.1	0.38	80	3.1	6.5
31	Northridge	USA	17.01.1994	Newhall - W. Pico Canyon	stiff soil	Reverse	46	6.7	7.1	0.45	93	3.2	2.0
32	Northridge	USA	17.01.1994	Newhall - W. Pico Canyon	stiff soil	Reverse	316	6.7	7.1	0.33	67	1.9	1.8
33	Northridge	USA	17.01.1994	Slymar Converter	Deep broad soil	Reverse	52	6.7	6.2	0.61	117	2.5	2.6
34	Northridge	USA	17.01.1994	Sylmar - Olive View Med	Deep broad soil	Reverse	360	6.7	6.4	0.84	130	1.9	1.6
35	Northridge	USA	17.01.1994	Sepulveda VA	Deep broad soil	Reverse	270	6.7	8.9	0.75	85	0.8	0.8

Table 2.1: Ground Motion Database (Continued)

#	Earthquake	Country	Date	Station Name	Site Geology*	Mechanism	Component	Magnitude (Mw)	d** (km)	PGA** (g)	PGV** (cm/s)	Tp** (s)	Tp-v** (s)
36	Northridge	USA	17.01.1994	Canyon Country - W Lost Cany	Deep narrow soil	Reverse	270	6.7	13.0	0.48	45	0.7	0.7
37	Cape Mendocino	USA	25.04.1992	Rio Dell Overpass	Deep narrow soil	Reverse	270	7.1	18.5	0.39	44	1.2	1.3
38	Cape Mendocino	USA	25.04.1992	Petrolia	stiff soil	Reverse	90	7.1	9.5	0.66	90	0.7	0.7
39	Loma Prieta	USA	18.10.1989	Corralitos	rock	Reverse - Oblique	90	6.9	5.1	0.48	45	0.7	0.8
40	Loma Prieta	USA	18.10.1989	Saratoga - Aloha Ave	Deep broad soil	Reverse - Oblique	90	6.9	13.0	0.32	43	3.1	3.8
41	Loma Prieta	USA	18.10.1989	Gilroy Array #2	Deep broad soil	Reverse - Oblique	90	6.9	12.7	0.32	39	1.4	1.5
42	Loma Prieta	USA	18.10.1989	Gilroy Array #3	Deep broad soil	Reverse - Oblique	90	6.9	14.4	0.37	45	2.1	2.0
43	Superstition Hills	USA	24.11.1987	Parachute Test Site	Deep broad soil	Strike - Slip	225	6.6	0.7	0.45	112	2.2	1.9
44	N. Palm Springs	USA	08.07.1986	North Palm Springs	Deep broad soil	Reverse - Oblique	210	6.0	8.2	0.59	73	1.4	1.1
45	Imperial Valley	USA	06.06.1938	EC Meloland Overpass FF	Deep broad soil	Strike - Slip	270	6.5	0.5	0.30	91	3.1	3.0
46	Imperial Valley	USA	15.10.1979	El Centro Array #7	Deep broad soil	Strike - Slip	230	6.5	0.6	0.46	109	3.8	3.2
47	Imperial Valley	USA	15.10.1979	El Centro Array #5	Deep broad soil	Strike - Slip	230	6.5	1.0	0.38	91	3.9	3.4
48	Imperial Valley	USA	15.10.1979	El Centro Array #6	Deep broad soil	Strike - Slip	140	6.5	1.0	0.41	65	2.9	2.4
49	Imperial Valley	USA	15.10.1979	El Centro Array #6	Deep broad soil	Strike - Slip	230	6.5	1.0	0.44	110	3.9	3.4
50	Imperial Valley	USA	15.10.1979	El Centro Array #8	Deep broad soil	Strike - Slip	230	6.5	3.8	0.45	49	4.0	4.0
51	Imperial Valley	USA	15.10.1979	El Centro Array #4	Deep broad soil	Strike - Slip	230	6.5	4.2	0.36	77	4.3	4.0
52	Imperial Valley	USA	15.10.1979	El Centro Differential Array	Deep broad soil	Strike - Slip	270	6.5	5.3	0.35	71	4.5	2.6
53	Imperial Valley	USA	15.10.1979	Holtville Post Office	Deep broad soil	Strike - Slip	225	6.5	7.5	0.25	49	2.4	4.0
54	Imperial Valley	USA	15.10.1979	Holtville Post Office	Deep broad soil	Strike - Slip	315	6.5	7.5	0.22	50	3.7	3.4
55	Imperial Valley	USA	15.10.1979	EC County Center FF	Deep broad soil	Strike - Slip	92	6.5	7.6	0.23	69	3.3	3.2
56	Imperial Valley	USA	15.10.1979	Brawley Airport	Deep broad soil	Strike - Slip	225	6.5	8.5	0.16	36	3.4	3.0
57	Imperial Valley	USA	15.10.1979	El Centro Array #10	Deep broad soil	Strike - Slip	50	6.5	8.6	0.17	48	2.0	1.5
58	Imperial Valley	USA	15.10.1979	El Centro Array #10	Deep broad soil	Strike - Slip	320	6.5	8.6	0.22	41	3.9	3.8

* Site Geology = Rock: Instrument on rock (Vs > 600 m/sec) or < 5m of soil over rock
Stiff soil: Instrument on/in soil profile up to 20m thick overlying rock
Deep narrow soil: Instrument on/in soil profile at least 20m thick overlying rock, in a narrow canyon or valley no more than several km wide
Deep broad soil: Instrument on/in soil profile at least 20m thick overlying rock, in a broad valley

** d, PGA, PGV, T_p, and $T_{p\text{-}v}$: closest site to fault rupture distance, peak ground acceleration, peak ground velocity, pulse period and dominant pseudo-spectral velocity period, respectively

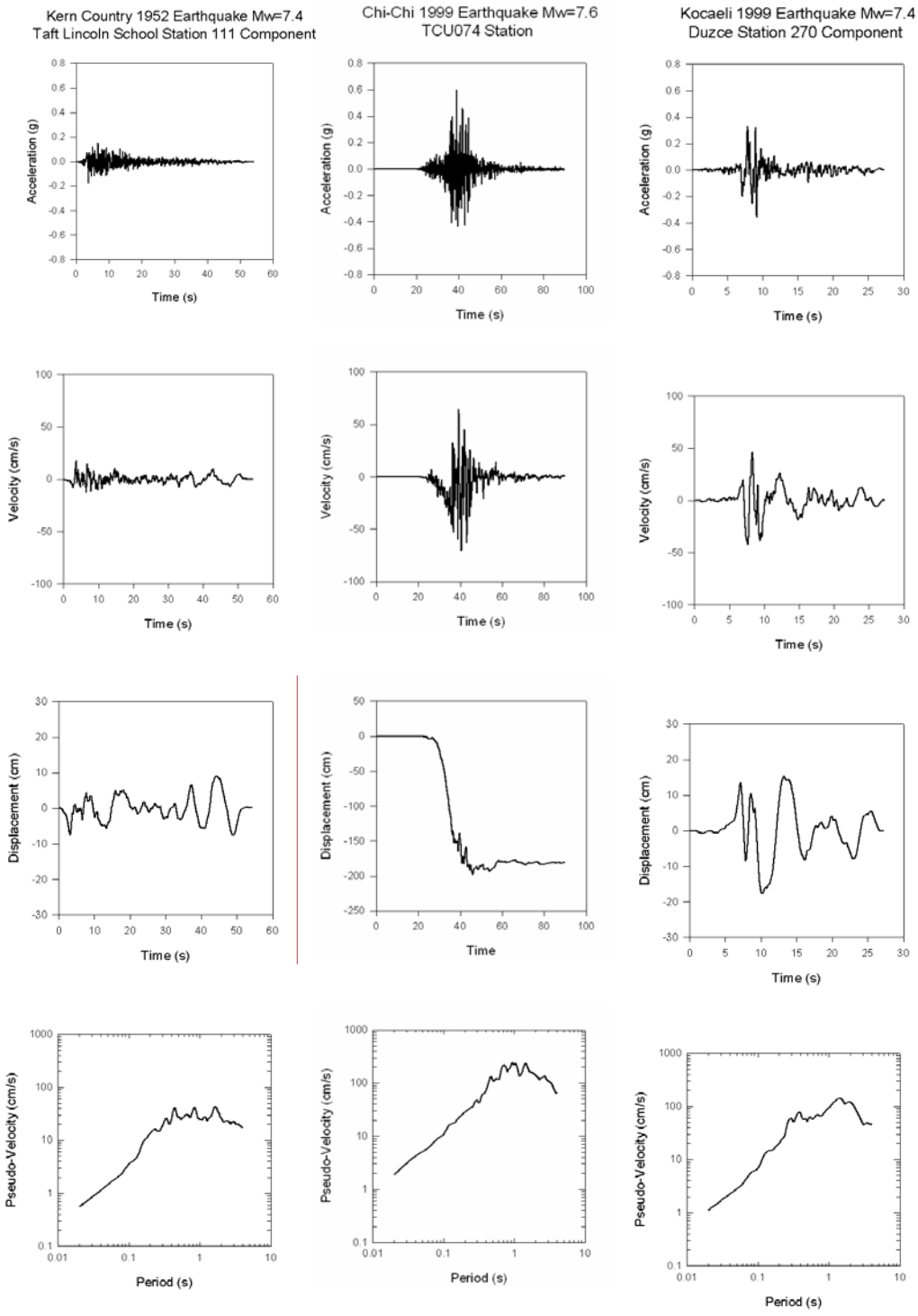

(a) (b) (c)

Figure 2.2: Typical acceleration, velocity, displacement, and pseudo-velocity of (a) far-fault (b) near-fault (fling-step) (c) near-fault (forward directivity) ground motion records

2.2.1 FACTORS AFFECTING NEAR-FAULT GROUND MOTIONS

One of the significant factors is the forward directivity effect. Forward directivity develops when the rupture front propagates toward the site and the direction of slip on the fault is aligned with the site. The effects of forward directivity are generated where the fault rupture propagates with a velocity close to the shear wave velocity. This is present in some but not all near fault rupture processes. Forward directivity conditions exist in both strike-slip and dip-slip faulting (including both reverse and normal faults). Even though forward directivity conditions are largest for sites near the end of the fault in strike-slip events, dip-slip faulting produces forward directivity effects on sites located in the up-dip projection of the fault plane. The propagation of the rupture toward a site at a velocity that is approximately equal to the shear wave velocity causes most of the seismic energy from the rupture to arrive in a single large pulse motion, which occurs at the beginning of the record. The radiation pattern of the shear dislocation around the fault causes this large velocity pulse of motion to be oriented in the direction perpendicular to the fault for strike-slip faulting [63]. The acceleration does not clearly exhibit the directivity effects because it is high frequency dominant. On the other hand, this does not imply that the acceleration time series do not convey forward directivity effects. The effect of directivity focusing is most pronounced on displacements, less on velocities, and least on acceleration [62]. Ground motions with forward directivity have large amplitude, long duration pulses that are best observed in the velocity or displacement time history traces (Figure 2.2).

Records may also exhibit backward directivity if a site is located at one end of the fault and rupture propagates away from the site. They are characterized by longer duration, lower amplitude ground motions, and do not have distinctive velocity pulses [64]. Unlike forward directivity, backward directivity effects are typically less severe. Neutral directivity occurs for sites located off to the side of the fault rupture surface when the rupture is neither predominantly towards nor away from the site [13].

Pulse type motion can also be generated by permanent ground displacement (fling step) due to tectonic deformation associated with rupture mechanism. Fling step affects the peak velocity and displacement of ground motions. Unlike forward directivity pulse which is bidirectional, fling step is characterized by a unidirectional large amplitude velocity pulse. Kalkan and Kunnath [37] observed that the forward and backward momentums are acquired during the initial and final phase of the forward directivity pulses and they result in higher displacement demands than fling step pulses. Fling type of motion contains only forward momentum [37]. While forward directivity occurs at sites located close to the fault but away from epicenter, fling step occurs at sites located near the fault rupture independent of the epicenter location. Fling step displacements occur in the direction of fault slip, and therefore are not coupled with rupture directivity [66]. Fling step arises in strike-slip faults in the strike parallel direction and in the strike-normal direction for dip-slip faults. However, forward directivity is polarized in the fault normal direction for strike-slip and dip-slip events [1].

Somerville has stated that the radiation pattern of shear dislocation around the fault causes the fault-normal component to be more severe than the fault-parallel component [64]. However, Akkar and Gülkan [26] have found out that the peak near fault motions are not necessarily in the fault normal direction. They have pointed out that the ground motion components in the maximum velocity directions generally have higher spectral drifts than the strike normal component for the near fault ground motion records taken from the 1999 Kocaeli and Düzce Earthquakes.

Near fault ground motions that contain large amplitude pulses in both velocity and displacement traces can cause high level of inter-story drift ratio in structural systems [35]. In addition, Hall et al. [28] state that the damage potential also depends on how much ground displacement occurs during these velocity pulses. The damage capacity of near fault earthquakes attracts great attention because of the complicated nature of these earthquakes and their impact on structural performance. In spite of the fact that the severe demands imposed by near fault ground motions have been recognized since 1957 [10], they have

received resumed attention after destructive earthquakes, such as the 1994 Northridge, 1999 Kocaeli and Düzce earthquakes.

2.2.2 PULSE PERIOD

The pulse period (T_p) is the duration of the largest amplitude pulse in the velocity time history of the ground motion. Starting and ending times of the pulse are either the zero crossing time or the time at which velocity is equal to 10 % of the peak velocity [66]. Krawinkler and Alavi [41] define the velocity pulse period ($T_{p\text{-}v}$) as the period corresponding to a global peak in the velocity response spectrum of the ground motion. The parameters T_p and $T_{p\text{-}v}$ are listed in Table 2.1.

Pulse periods and velocity pulse periods for 55 earthquakes are taken from Yazgan [72]. Pulse periods are measured from velocity traces of ground motions. Dominant velocity pulses are determined from the pseudo-velocity spectra of ground motions records. Figure 2.3 shows T_p and $T_{p\text{-}v}$ measurements for the Düzce 270º component of 1999 Kocaeli Earthquake.

The coincidence of T_p and $T_{p\text{-}v}$ indicates that the velocity pulse contains energy in a narrow period band [13]. The relation between T_p and $T_{p\text{-}v}$ is plotted in Figure 2.4. Mean and standard deviation of the ratio between T_p and $T_{p\text{-}v}$ are 1.07 and 0.23, respectively. Rodriguez-Marek [56] found a mean ratio of 0.84 and a standard deviation of 0.28.

Pulse period appears to be related to the magnitude (M_w) of the earthquakes and the closest distance from the rupture plane (d). Based on studies of the magnitude scaling of earthquake source parameters [64], it can be stated that the period of the pulse is magnitude dependent because it is related to the duration of slip at a point on the fault, which increases with magnitude. Somerville propounded that $\log_{10} T_p$ is a linear function of M_w, independent of distance [64]. Rodriguez-Marek [56], Alavi and Krawinkler [4] have proposed similar linear equations.

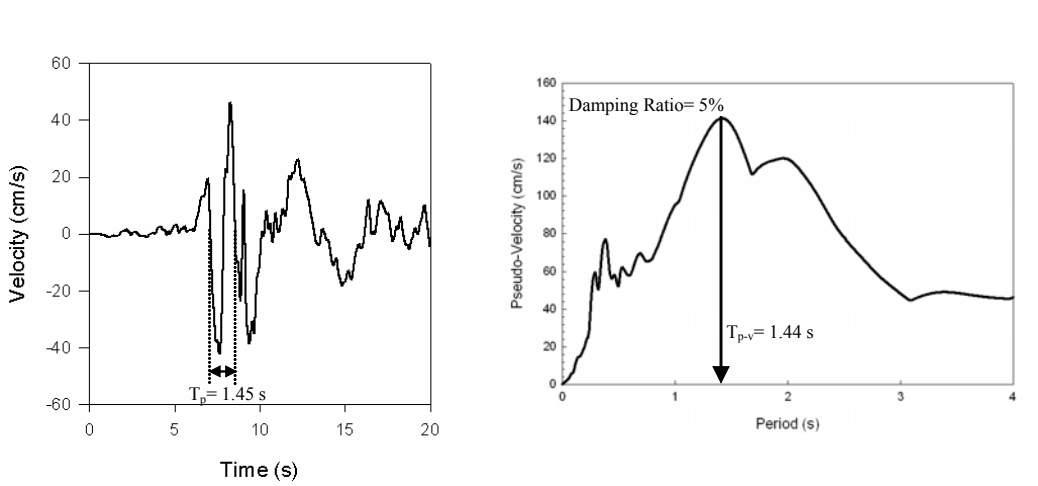

Figure 2.3: T_p and T_{p-v} for 1999 Kocaeli Earthquake Düzce Station 270º Comp.

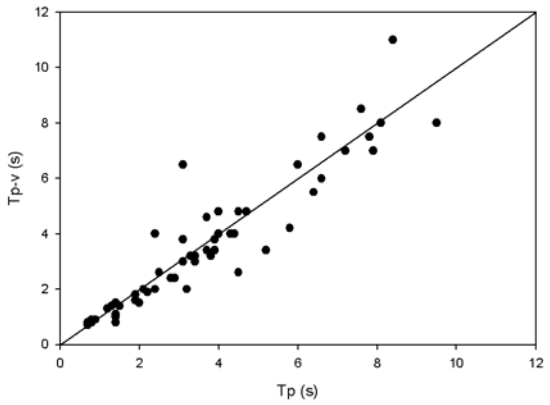

Figure 2.4: Correlation between T_p and T_{p-v}

Figure 2.5 shows the variation of pulse period with magnitude, closest site to fault rupture distance to fault, and fault mechanism. It is observed that large magnitude earthquakes have longer pulse periods. In addition, it can be stated that strike slip and reverse oblique slip events produce longer pulses than reverse slip events. No clear trend with respect to closest site to fault rupture distance is noticeable in this figure.

2.2.3 THE RATIO OF PGV TO PGA

Near fault ground motions with directivity effects tend to have high PGV/PGA ratio, which influences their response characteristics, because the ratio is dominated by the high PGV of the pulse. Moreover, higher PGV/PGA ratio results in wider acceleration-sensitive region in the response spectra. Malhotra [45] showed that a wide acceleration sensitive region reduces apparent flexibility of structures, contribution of higher modes, effectiveness of additional damping and increases base shear, interstory drifts, and ductility demand.

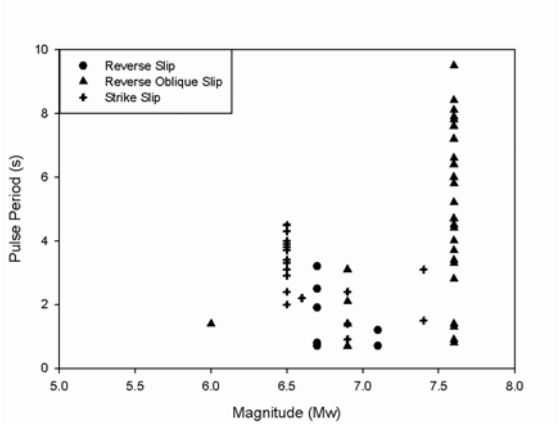

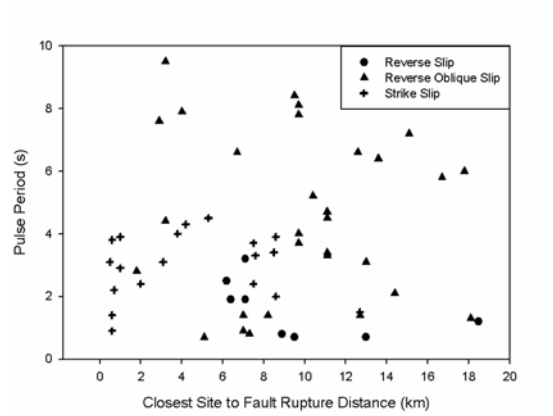

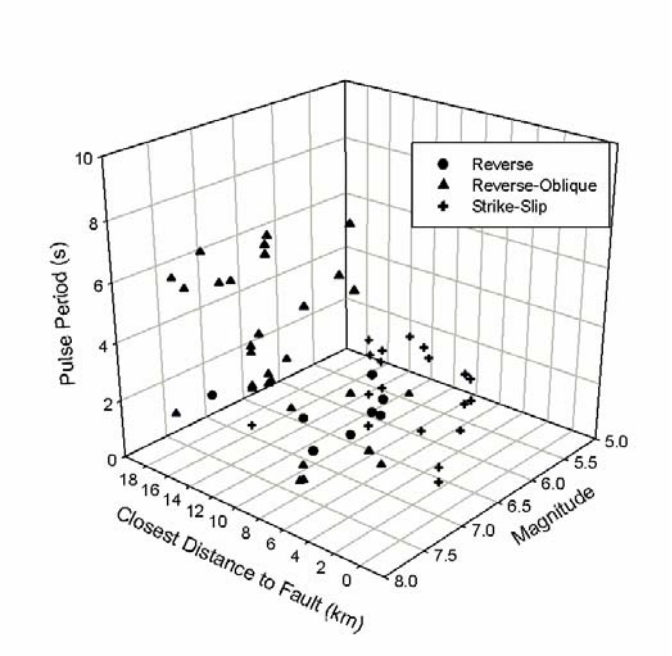

Figure 2.5: Pulse period, magnitude and distance distribution of earthquakes classified by fault mechanism

2.3 EVALUATION OF PRESENT EARTHQUAKE CODES AND PROVISIONS IN TERMS OF NEAR FAULT RECORDS

Recent earthquakes have revealed the susceptibility of the existing building stock to near-fault ground motions. Structures designed according to current procedures are vulnerable to the high amplitude, long period velocity pulse type ground motion in the near source region. The demands of these ground motions impose on frame structures are not adequately represented in present code design procedures. [4]. While code recommendations typically require much research and empirical support before becoming incorporated as general tools of design, a good understanding of the parameters that play a role in building response to near-source motions is desirable.

Iwan [32] demonstrated the failure of pushover methods to predict demands for pulse like near fault ground motions because they fail to account adequately for critical higher mode contributions. In addition, he also showed that in capacity spectrum method equivalent viscous damping fails for short period structures subjected to near fault ground motions.

Recent design codes and provisions, such as ATC-40 [7] and FEMA-356 [15], have taken into account near-fault effects by introducing source type and distance dependent near fault factors to amplify the elastic design spectrum. However, constant scaling of a fixed response spectrum cannot adequately describe near fault effects. For example, these codes do not pay any attention to the effect of pulse-like ground motions on the dynamic response of structure. P-delta effects may be an important concern for structures subjected to the large displacement pulses of near-fault ground motions, especially if inelastic interstory drifts become large and lead to increase the seismic response [25]. However, current design provisions do not take any measures to account for P-delta effects caused by near fault ground motions.

2.4 BUILDING MODELS

20-story, 9-story and 3-story steel moment resisting frame buildings designed as a part of the SAC steel project are used in this study. Selected buildings are pre-Northridge designs, and are used in this study as instruments to understand the features of response. Necessary information about SAC steel project is obtained from FEMA-355C [23]. The plan view and elevation views of the selected buildings are shown in Figure 2.6. One of the perimeter moment-resisting frames in the north-south direction is modeled as two-dimensional generic frame according to the procedure described in the following section. The original 20-story and 9-story SAC buildings have two and one basement floors, respectively. However, in this study, these stories are not modeled. Ground story heights (h_1=5.49 m) of the 20 and 9 story frames are approximately 40 % taller than the upper stories (h_2=3.96 m). 3 story SAC moment resisting frame story heights (h_2=3.96 m) are equal to each other. Column sections of the 20-story, 9-story and 3-story buildings are presented in Table 2.2. Beam to column stiffness ratio (ρ) and capacity ratio (Q) effects on maximum story drift ratio are the parameters to be investigated in this study, so models with different sectional properties of columns and girders changing according to ρ and Q are prepared. Column section yield stress is equal to 345 MPa.

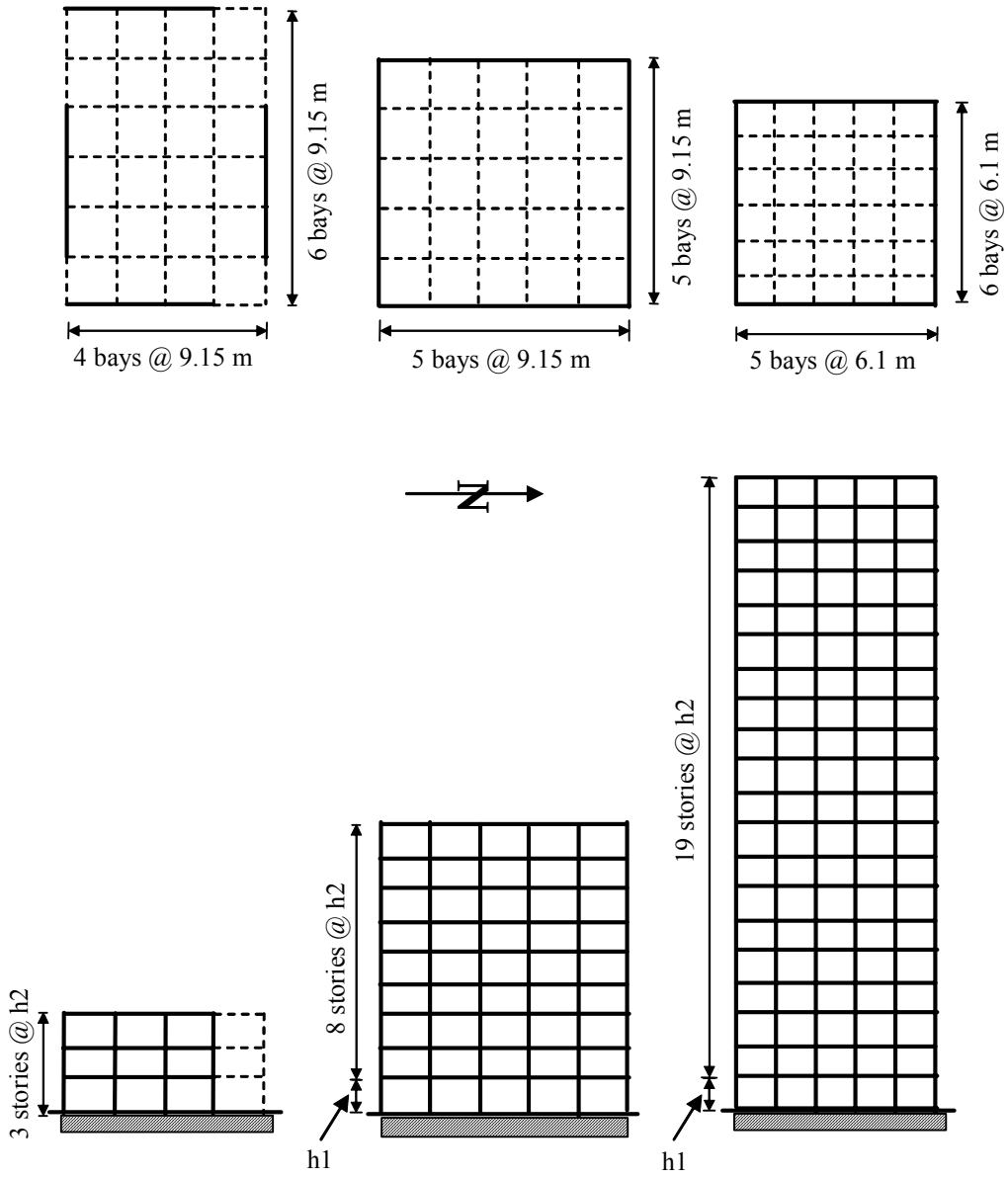

Figure 2.6: Plan and elevation views

Table 2.2: Column Sections (Pre-Northridge Designs) for Los Angeles Model Buildings (Section designations correspond to standard AISC abbreviations.)

3-Story

STORY/FLOOR	COLUMNS		GIRDER
	EXTERIOR	INTERIOR	
1/2	W14x257	W14x311	W33x118
2/3	W14x257	W14x311	W30x116
3/Roof	W14x257	W14x311	W24x68

9-Story

STORY/FLOOR	COLUMNS		GIRDER
	EXTERIOR	INTERIOR	
1/2	W14x370	W14x500	W36x160
2/3	W14x370	W14x500	W36x160
3/4	W14x370	W14x455	W36x135
4/5	W14x370	W14x455	W36x135
5/6	W14x283	W14x370	W36x135
6/7	W14x283	W14x370	W36x135
7/8	W14x257	W14x283	W30x99
8/9	W14x257	W14x283	W27x84
9/Roof	W14x233	W14x257	W24x68

20-Story

STORY/FLOOR	COLUMNS		GIRDER
	EXTERIOR	INTERIOR	
1/2	15x15x2.0	W24x335	W30x99
2/3	15x15x2.0	W24x335	W30x99
3/4	15x15x1.25	W24x335	W30x99
4/5	15x15x1.25	W24x335	W30x99
5/6	15x15x1.25	W24x335	W30x108
6/7	15x15x1.0	W24x229	W30x108

Table 2.2: Column Sections (Pre-Northridge Designs) for Los Angeles Model Buildings (Continued)

20-Story

STORY/FLOOR	COLUMNS		GIRDER
	EXTERIOR	INTERIOR	
7/8	15x15x1.0	W24x229	W30x108
8/9	15x15x1.0	W24x229	W30x108
9/10	15x15x1.0	W24x229	W30x108
10/11	15x15x1.0	W24x229	W30x108
11/12	15x15x1.0	W24x229	W30x99
12/13	15x15x1.0	W24x192	W30x99
13/14	15x15x1.0	W24x192	W30x99
14/15	15x15x1.0	W24x192	W30x99
15/16	15x15x0.75	W24x131	W30x99
16/17	15x15x0.75	W24x131	W30x99
17/18	15x15x0.75	W24x131	W27x84
18/19	15x15x0.75	W24x117	W27x84
19/20	15x15x0.75	W24x117	W24x62
20/Roof	15x15x0.75	W24x84	W21x50

FEMA 355C [23] gives the seismic mass of every story. As stated before, only one of the moment resisting frames oriented in the north-south direction is modeled and the presence of the gravity frames is ignored. Each story has two uniform moment resisting frames in this direction. During earthquake excitation seismic effects are transmitted to moment resisting frames. Therefore, half of the given seismic mass of the structure at each floor level is lumped at the floor levels of the generic frame. The seismic masses for the fishbone models are presented in Table 2.3. Justification for the “fishbone” model is provided in Section 2.5.

Table 2.3: Seismic masses for moment resisting frames

3-Story

STORY	MASS (kN.sec^2/m)
1~2	478
3	518

9-Story

STORY	MASS (kN.sec^2/m)
1	504
2~8	495
9	534

20-Story

STORY	MASS (kN.sec^2/m)
1	282
2~19	276
20	292

2.5 ANALYTICAL MODELS

Response of structural systems to ground motions is a complex process to estimate because many factors control the outcome. In this study, the effects of various parameters on the local deformation demands of moment resisting frames are investigated. A large number of frames are generated for an accurate investigation of structural features. The effort associated with detailed modeling and analysis is not feasible, because quick estimate of the system response is considered sufficient for purpose of this study. Therefore, a simplified process is needed to obtain quick and reasonable estimates of seismic demands. A generic fishbone frame model [51] is used for the simulation of earthquake responses of steel moment resisting frames. The relatively small number of degrees of freedom

for each generic model allows considering a large number of buildings and ground motions. Not only is nonlinear time history analysis of generic frame computationally less time consuming than that of original frame, but also similar responses are obtained. To avoid intrinsic complexity and additional computational effort required by detailed modeling, fishbone models, which can be very useful for structural performance assessment and for design, are used in this research. Generic frame model should have the same accuracy that can be attained by frame models with member-by-member representation.

Characteristics of gravity frames are different from those of the moment resisting frames. Therefore, these two frames cannot be joined into a single generic frame; instead they should be represented by two different generic models. Since earthquake response of moment resisting frames is of concern in this study, only moment resisting frames are modeled. The following assumptions are made:

I. All mass at a given floor level is concentrated at the column node of that floor level
II. Member yielding is represented by concentrated plastic hinges at member ends
III. All rotations at beam-to column connections are the same, and axial elongation and contraction of beams and columns is neglected

Each member is assumed to have the same cross section, and effects of floor slabs on beam stiffness and strength are neglected. At each floor all columns are combined to form one representative column and all beams are combined to form only one rotational spring, as shown in Figure 2.7. The end moment of a beam of the original frame is equal to

$$M_{Bij_{LEFT}} = M_{Bij_{RIGHT}} = K_{Bij}\theta_i \qquad K_{Bij} = \frac{6EI_{Bij}}{L_j} \tag{2.1}$$

$M_{Bij_{LEFT}}$, $M_{Bij_{RIGHT}}$ are left and right moments at beam ij; θ_i is the nodal rotation at ith floor level; E is Young's modulus; I_{Bij} is moment of inertia and L_{Bij} is length

of the jth beam in the ith floor. Using assumption (III), the spring stiffness that represents all beams at the ith floor level is expressed as

$$M'_{Bi} = K'_{Bi}\theta_i \qquad K'_{Bi} = 2\sum_{j=1}^{r} K_{Bij} \tag{2.2}$$

where r is the number of bays.

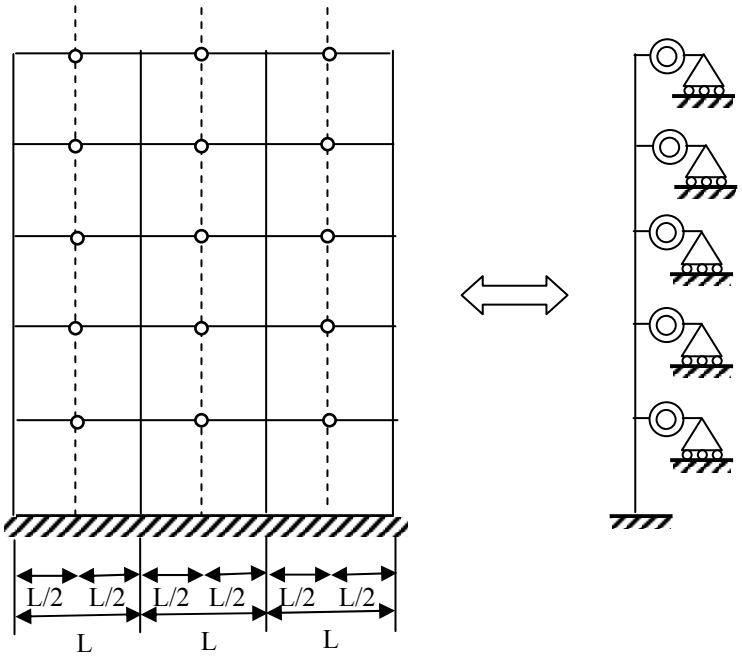

Figure 2.7: Generic Frame Modeling

Utilizing assumption (III), the bottom and top moment of column of the original frame are specified as

$$M_{Cij_{BOTTOM}} = K_{Cij}\theta_i \qquad K_{Cij} = \frac{6EI_{Cij}}{H_{Cij}} \tag{2.3}$$

$$M_{Cij_{TOP}} = K_{Cij}\theta_{i+1} \qquad K_{Cij} = \frac{6EI_{Cij}}{H_{Cij}} \tag{2.4}$$

Here $M_{Cij_{BOTTOM}}$, $M_{Cij_{TOP}}$ are bottom and top moments of the column ij; respectively. θ_i is the nodal rotation at ith floor level; θ_{i+1} is the nodal rotation at (i+1)th floor level, E is Young's modulus; I_{Cij} is moment of inertia and H_{Cij} is height of the jth column in the ith floor.

By means of assumption (III), stiffness of the i'th story representative column is stated as

$$M'_{Ci_{BOTTOM}} = K'_{Ci}\theta_i \qquad M'_{Ci_{TOP}} = K'_{Ci}\theta_{i+1} \qquad K'_{Ci} = \sum_{j=1}^{r+1} K_{Cij} \tag{2.5}$$

By using assumptions II and III, moment capacity of the spring and representative column are given in Equations (2.6) and (2.7), respectively. The spring moment capacity of generic model is taken to be the sum of moment capacities of all beam ends at the concerned floor level. Moment capacity of columns in generic frame equals to the sum of column capacities in the related story.

$$M'_{Bi} = 2\sum_{j=1}^{r} M_{Bij} \tag{2.6}$$

$$M'_{Ci} = \sum_{j=1}^{r+1} M_{Cij} \tag{2.7}$$

where M_{Bij} is the moment capacity of the jth beam in the ith floor. M_{Cij} is the moment capacity of the jth column in the ith floor. r is the number of bays.

2.5.1 VALIDATION OF THE GENERIC FRAME MODEL

Generic model should have the same accuracy that can be attained by original frame models with member-by-member representation. In order to verify the generic frame model, the perimeter moment resisting frames in the north-south direction of SAC 20-story, 9-story and 3-story (designed for pre-Northridge Los Angles) are modeled as fishbone and full-frame model. The validity of the proposed generic model is tested by comparing estimates of element deformation demands (elastic maximum interstory drift ratio and top story displacement ratio) and modal characteristics (mode shape and period) obtained using the simple fishbone model to estimates obtained using full frame. Table 2.4 summarizes the natural periods of the original frame (OF) and the generic frame (GF). The periods of the two models are very close. The difference is not greater than 1.3 per cent for the first natural periods, 0.8 per cent for second periods and 0.6 per cent for third periods. Moreover, the fundamental mode shapes of OF and GF are compared in Figure 2.8 and no major difference is observed. In fact, modal displacements are equal at each floor level.

Linear elastic time history analyses of the two models are conducted using 58 near fault ground motions. Rayleigh damping of 5 % for the first two modes is adopted in the analyses. The drift ratios computed using the original frame are designated as “exact” and the drift ratios found using the fishbone mode is referred as “approximate.” Maximum interstory drift ratios and maximum roof drift ratios of OF and GF are compared in Figure 2.9. The comparisons are presented as scatter diagrams which show the perfect correlation as the diagonal line. Correlation coefficients between exact and approximate results are very close to 1.0.

Table 2.4: Comparison of natural periods of the original frame and generic frame

20-story SAC MRF

	First Natural Period (sec)	Second Natural Period (sec)	Third Natural Period (sec)
Original Frame	3.465	1.232	0.745
Generic Frame	3.421	1.222	0.741

9-story SAC MRF

	First Natural Period (sec)	Second Natural Period (sec)	Third Natural Period (sec)
Original Frame	2.026	0.770	0.446
Generic Frame	2.018	0.776	0.444

3-story SAC MRF

	First Natural Period (sec)	Second Natural Period (sec)	Third Natural Period (sec)
Original Frame	1.008	0.327	0.172
Generic Frame	1.004	0.326	0.172

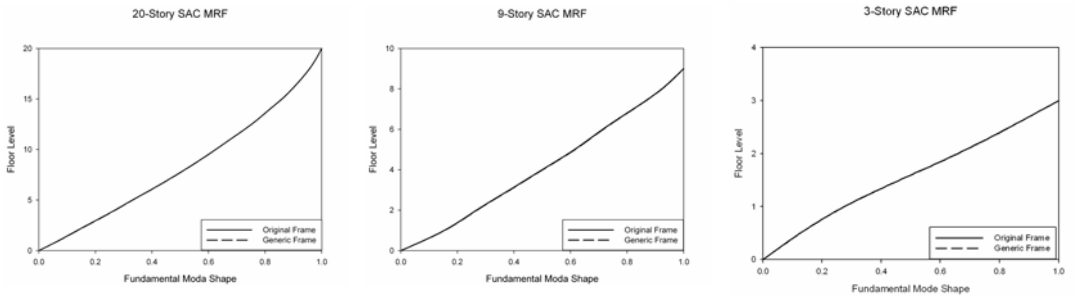

Figure 2.8 : Comparison of fundamental mode shapes of OF and GF

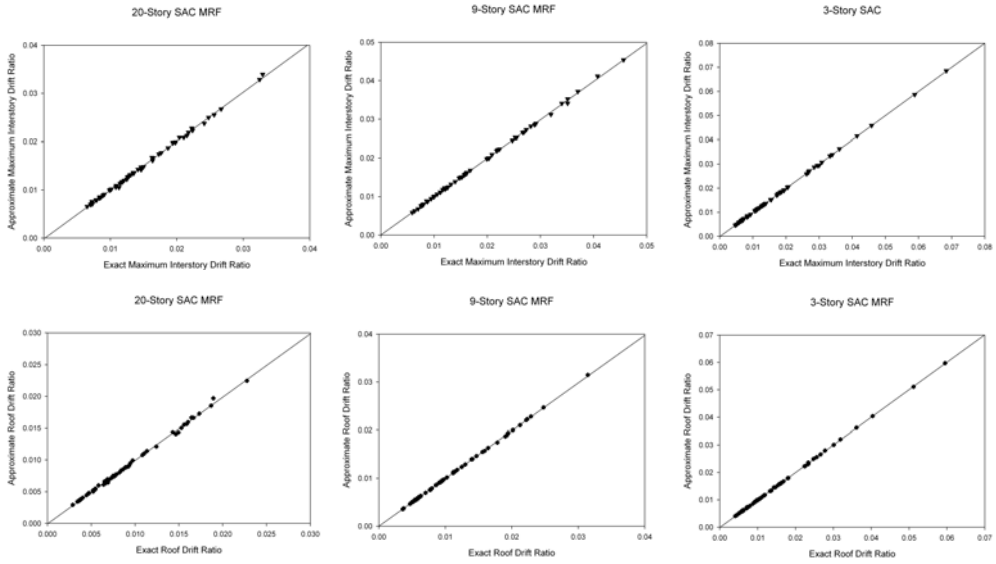

Figure 2.9: Comparison of maximum interstory drift ratios and roof drift ratios of structures based on OF and GF

It is found that the modal properties and response parameters obtained by using the fishbone model are very similar to those obtained by using original moment resisting frame. Utilization of generic models reduces computational and data management efforts substantially. Therefore, it can be concluded that the fishbone model is an effective instrument for performing extensive analyses involving systematic variations of many interrelated parameters.

2.6 STRUCTURAL PROPERTIES AFFECTING DISPLACEMENT DEMAND

In order to investigate the effects of different structural properties on structural response, a set of generic frames were generated. Beam to column stiffness ratio (ρ), stiffness distribution coefficient, beam to column capacity ratio (Q), ratio of the first story height to regular story height (soft story factor), regular story height and number of stories were varied to investigate response of characteristics of different frame systems.

2.6.1 BEAM TO COLUMN STIFFNESS RATIO (ρ)

Beam to column stiffness ratio (ρ), as noted by Blume [12], determines the joint rotation in structural systems by means of the beam and column flexural stiffness contributions at the story level. It is the ratio of sum of beam rigidities to column rigidities at the mid-height story. This parameter has an effect on the degree of participation of shear and lateral flexural deformations. The joint index, ρ, for beams and columns having the same modulus of elasticity is defined as follows

$$\rho = \frac{\sum_{beams}(I_b / L_b)}{\sum_{columns}(I_c / L_c)} \tag{2.8}$$

in which I_b and I_c are the moment of inertia of beams and columns, and L_b and L_c are the length of beams and columns at the story which is closest to the midheight of the building, respectively. Blume [12] points out that if the structural properties of beams or columns change at the mid-height story, values of two adjacent stories might be averaged.

The fundamental mode shapes corresponding to different ρ values for regular 20-story frames with uniform stiffness along the height are presented in Figure 2.10 and Figure 2.11. When ρ equals zero, the mode shape represents flexural behavior and the beams (I_b=0) do not impose any restraint to joint rotations, as shown Figure 2.12(a). Frame deforms like a vertical cantilever bending beam. When ρ equals infinity, the frame becomes a shear frame that deforms as shown in Figure 2.10 and Figure 2.11, in which beams (I_b=∞) are infinitely stiff and deformations occur only trough double curvature bending of columns as illustrated in Figure 2.12(b). Frames with an intermediate value of ρ display flexural and shear lateral deformations, where columns and beams deform with joint rotations.

Figure 2.11 show the influence of different ρ values on maximum interstory drift locations. When a frame behaves like a cantilever beam (ρ = 0) or a shear frame (ρ = ∞), maximum drift occurs at the top story or at the ground story, respectively. There is an abrupt change, when ρ increases from 0 to 0.125. Maximum drift shifts from upper stories to lower stories. As a result, it can be stated that beam to column stiffness ratio has a significant effect on lateral displacement demands in multistory moment resisting frames.

As stated before, ρ is defined as the ratio of beam to column stiffness at the story closest to the mid-height of the building. However, when each story is considered individually, it can be observed that ρ is not constant throughout the height of the buildings as shown in Figure 2.13. For instance, beam to column ratio of ground story is 24 % lower than mid-height ρ value for the 20 story SAC MRF. Fundamental mode shapes of the original frame (exact case) are compared with the fundamental mode shapes computed from frames which are modeled by using the mid-height beam to column stiffness ratios (approximate case). In the approximate models, original column sections are preserved and girder sections are modified in order to keep ρ constant. As illustrated in Figure 2.13, approximate case underestimates fundamental mode displacements for the 20 story frame, but leads to conservative displacements for the 9 and 3 story frames. The mid-height ρ value of the original 20 story frame is higher than the ρ value of the lower stories. When this value of ρ is distributed uniformly, maximum modal interstory drift is underestimated, because the stories from the ground story to the fifth story are made stiffer. The approximate method overestimates modal maximum interstory drift of the 9 and 3 story SAC MRFs, since the mid-height beam to column ratio is smaller than ρ of lower half of the frames.

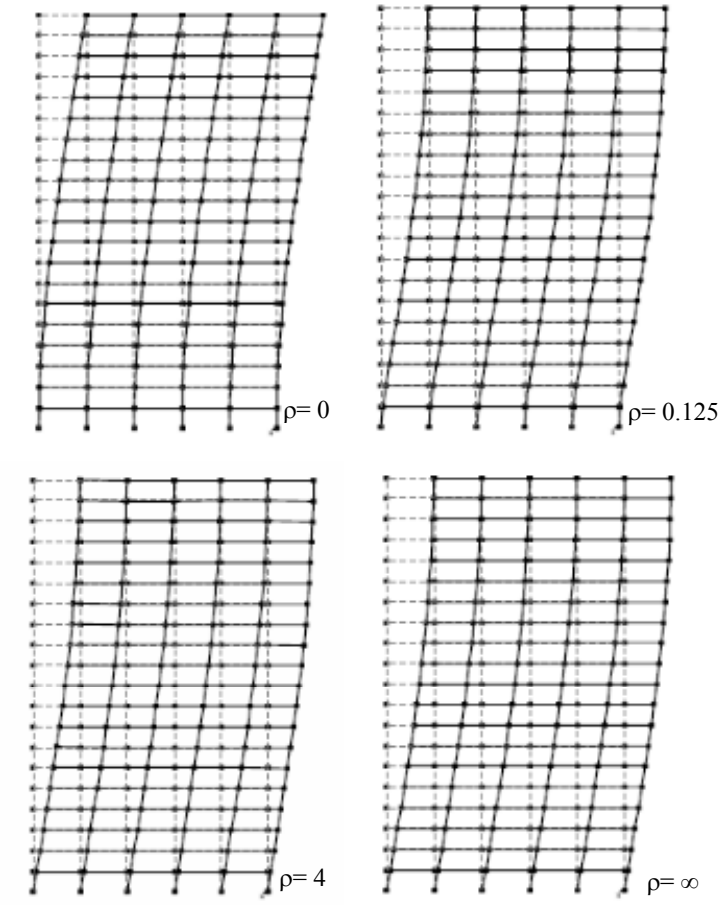

Figure 2.10: Fundamental mode shapes of 20-story frames with uniform stiffness corresponding to different ρ values

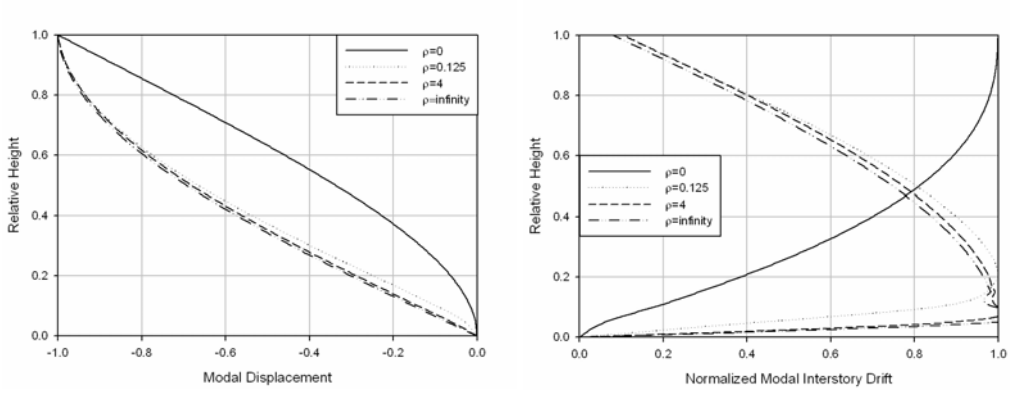

Figure 2.11: Effect of ρ on lateral deformation

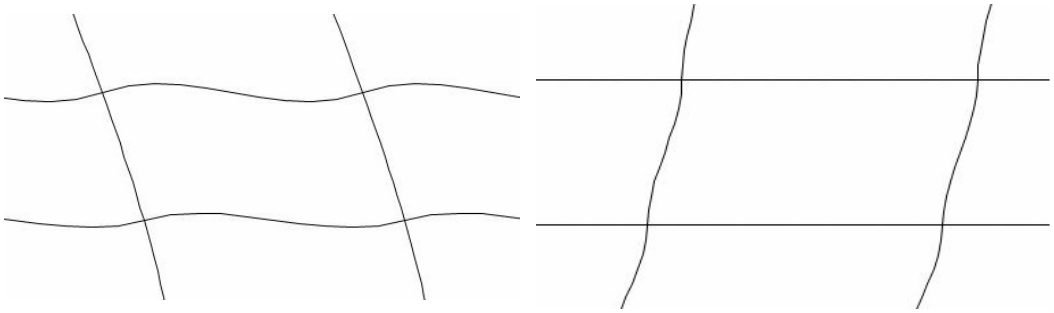

(a) (b)

Figure 2.12: Deformation shapes of columns and beams when ρ equals to (a) zero and (b) infinity

Differences may arise due to approximation of fundamental mode shape through a single ρ value by disregarding non-uniform ρ distribution. In order to eliminate these differences, the beam to column stiffness ratios are kept constant throughout the height in all analyses (ρ=0.25, 0.50, 1.0, 2.0, 4.0 and ∞). The column sections are not changed and girder sections are modified to obtain the required ρ value. Inertia of girder sections in the moment resisting frame and the stiffness of rotational springs in the fishbone model are calculated from Equations (2.9) and (2.10), respectively.

$$I_{Bij} = \frac{L_{Bij} \times \sum (I_{Cij} / L_{Cij})}{\#\,\text{of beams}} \times \rho \tag{2.9}$$

$$K_{spring,i} = 2\sum_{j=1}^{r} \frac{6EI_{Bij}}{L_{Bij}} \tag{2.10}$$

where L_{Bij} and I_{Bij} are length and inertia of the jth beam at the ith story, respectively. L_{Cij} and I_{Cij} are length and inertia of the jth column at the ith story. $K_{spring,i}$ is stiffness of the spring at the ith story. ρ is beam to column stiffness ratio.

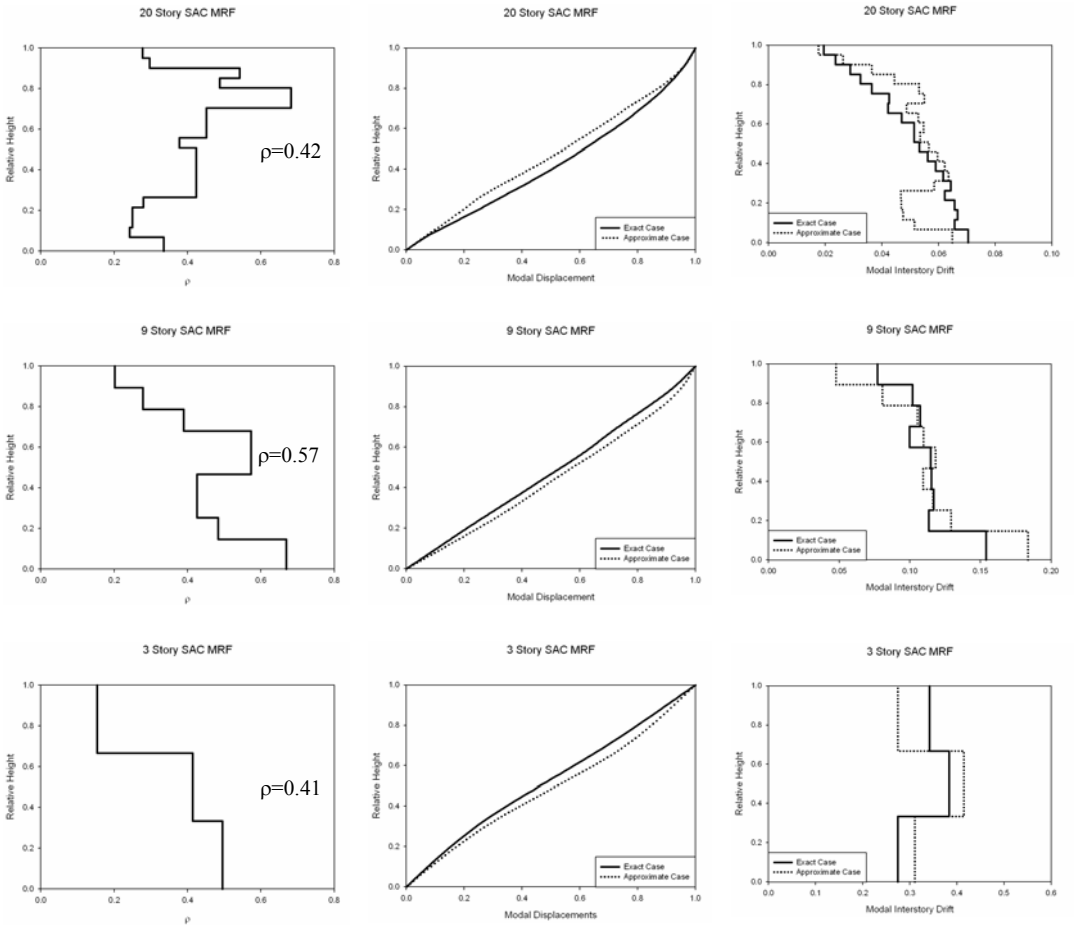

Figure 2.13: The variation of ρ along the height of SAC MRFs with non-uniform stiffness and effect of constant ρ assumption on fundamental mode shape and interstory drift

2.6.2 STIFFNESS DISTRIBUTION COEFFICIENT (λ)

Most of the studies are handled with frames composed of identical columns and girders at each story. Especially for high rise building this is not realistic, because stiffness is reduced from the lower part of the structure to the upper part of the structure. The presence of irregularity in a structure produces an increase in elastic and inelastic story drift. The effects of the reduction in stiffness along the

height must be reflected on lateral deformation demands in order to simulate real buildings. The following relationship is used for the stiffness distribution

$$Z(n) = \left(\sum_{j=1}^{r+1} I_{Cj_{GROUND}} \right) \left[1 - \frac{(\lambda - 1)}{\lambda (N-1)} (n-1) \right] \tag{2.11}$$

$$\text{where} \qquad \lambda = \frac{\sum_{j=1}^{r+1} I_{Cj_{GROUND}}}{\sum_{j=1}^{r+1} I_{Cj_{TOP}}} \tag{2.12}$$

Here λ = stiffness distribution coefficient, $I_{C_{GROUND}}$ =inertia of ground story column, $I_{C_{TOP}}$ =inertia of top story column and Z(n)=sum of the inertia of the n'th story columns, N = number of stories, r = number of the bays. Equation (2.11) represents a linear reduction of column stiffness along height. Figure 2.14 shows the effects of linear stiffness approach on the 20 and 9 story SAC MRFs. The non-uniform frames are modeled by using pertinent column sections described in FEMA-355C [23] and frames with linear stiffness distribution are simulated by reducing the lateral stiffness at the ground linearly to the top level. In both cases, girder sections are designed to attain constant ρ at each level (ρ = 0.42 for 20 story and ρ = 0.57 for 9 story). The values of λ are equal to 4.65 and 2.23 for 20 story and 9 story SAC MRF, respectively. These values are selected in particular, because they are the typical λ values of SAC moment resisting frames. The fundamental mode shape and maximum modal interstory drift are not affected much by linear stiffness reduction approach as presented in Figure 2.14. It is expected that low rise steel MRF buildings (e.g., N = 3) have uniform stiffness distribution; hence parameter λ is equal to 1. Six different values of λ (1.0, 2.0, 3.0, 4.0, 5.0 and 6.0) are used in the analyses of the 20 and 9 story generic frames.

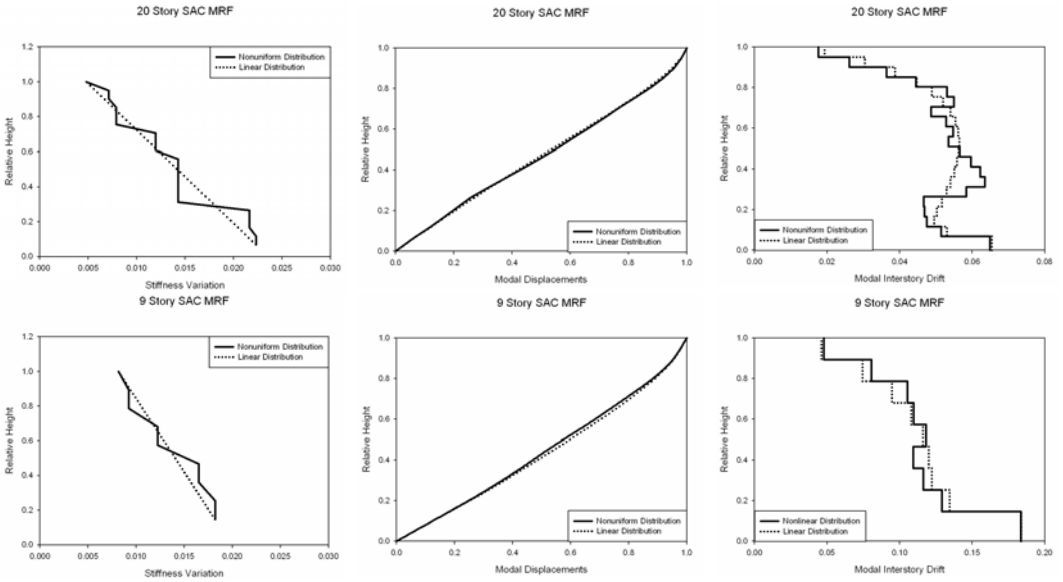

Figure 2.14: Effects of linear stiffness distribution on mode shape and story drift

2.6.3 BEAM TO COLUMN CAPACITY RATIO (Q)

The elasto-plastic moment curvature relation is used for inelastic behavior of structural systems. Beam to column capacity ratio (Q) is defined as the ratio of beam capacities to column capacities. The general form of Q is given by

$$Q = \frac{\sum_{j=1}^{r} (M_{Yj_{BEAM-LEFT}} + M_{Yj_{BEAM-RIGHT}})}{\sum_{j=1}^{r+1} (M_{Yj_{ABOVE}} + M_{Yj_{BELOW}})} \tag{2.13}$$

$M_{Y_{ABOVE}}$ and $M_{Y_{BELOW}}$ are the moment capacities at the column ends above and below floor level, respectively. $M_{Y_{BEAM-LEFT}}$ and $M_{Y_{BEAM-RIGHT}}$ are left and right moments at beams, respectively. The capacity ratio controls the inelastic behavior of structural systems by distributing the inelasticity to either beams or columns or both. An irregular distribution of strength is common in real building structures.

Linear stiffness reduction approach is applied to frames, capacity of columns and girders are also reduced linearly accordingly. Like stiffness variation, capacities of columns are unchanged and girder capacities are adjusted in order to obtain constant Q along the height of the structure. In steel frame systems the requirement of having stronger columns than beams is that the sum of yield moments of columns must be greater than the sum of yield moments of beams into beam-column joint [67]. This requirement is expressed by

$$(M_{ya} + M_{yb}) \geq (M_{yi} + M_{yj}) \tag{2.14}$$

M_{ya}, M_{yb}, M_{yj} and M_{yi} are shown in Figure 2.15. M_{ya} and M_{yb} are the yield moments at the column ends above and below floor level. M_{yj} and M_{yi} are positive or negative yield moment calculated at the right end of the beam on the left side of the joint and at the left end of the beam on the right side of the joint, respectively.

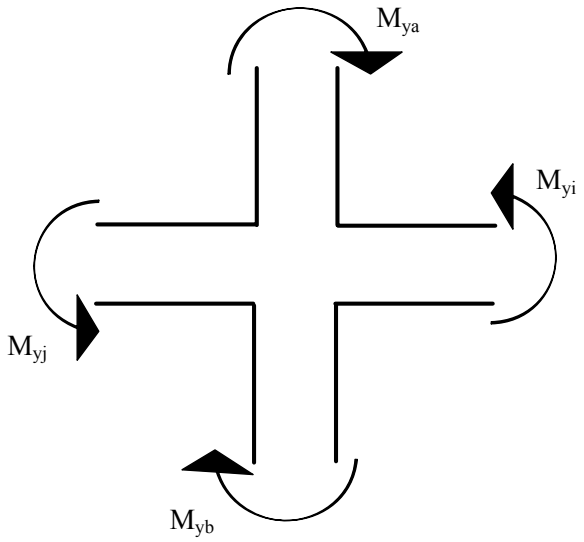

Figure 2.15: Moment directions at joint

A small value of Q indicates strong column-weak beam frame, which is mandatory for steel moment frames in seismic zones. A weak column leads to undesirable response such as column failures. If capacities of columns above and below the floor are accepted as identical, Q less than 0.75 for 3 story SAC MRF and 0.83 for 20 story and 9 story SAC MRFs satisfies strong column-weak beam condition. This Q factor provides important information about the inelasticity effects on displacement demand of building frames. Q values equal to 0.2, 0.4, 0.6, 0.8, 1.0 and 1.2 in the analyses to study systematically the effect of this variation.

2.6.4 SOFT STORY FACTOR (ψ)

The larger first story height with respect to the above stories leads to the formation of a soft story. Soft story forces the first story column to dissipate all energy and increases the deformation demand. It has been observed in many collapsed structures that deformation concentration takes place at a soft story under severe earthquake loading, which directly led to building failure. It is acceptable that if the structure exhibits a uniform interstory drift distribution when undergoing significant plasticity, the structure will undergo less damage. In order to investigate effect of soft story on lateral displacement demand, soft story factor (ψ) is applied during generation of frames. The soft story factor is equal to

$$\psi = \frac{h_1}{h_2} \tag{2.15}$$

where h_1 is the first story height and h_2 is regular story height. The values of ψ are allowed to vary from 1 to 1.8 with increments of 0.2.

2.6.5 REGULAR STORY HEIGHT (h_2) AND NUMBER OF STORIES (N)

The drift demand is strongly dependent on the number of stories (N). As building increases in height, the lateral displacement of the building due to wind or seismic loads becomes a primary concern. Excessive lateral displacements and interstory drifts may cause the failure of both structural and nonstructural members. Therefore, especially for irregular high rise buildings control of damage mechanism is important.

Most of the researchers have used frame models with constant story height. According to Lin et al. [43], the maximum roof displacement and yield displacement increase with story height. However, there is not enough information about the effects of regular story height on ground story displacement ratio and maximum interstory drift ratio. Therefore, one of the purposes of this study is to point out its effects on displacement demands.

In addition, the fundamental period of buildings depends on number of stories and the building height ($H=h_2*[N-1]+h_1$). Frames with high story height have longer fundamental period. Story heights of 3 m, 4 m, 5 m and 6 m are employed in the generation of fishbone models.

CHAPTER 3

ELASTIC MULTI-DEGREE-OF-FREEDOM ANALYSIS AND DERIVATION OF REGRESSION EQUATIONS

3.1 INTRODUCTION

Elastic response of multi-degree-of-freedom (MDOF) systems subjected to near-fault ground motions are analyzed in this chapter. Effects of different structural properties (beam to column stiffness ratio, stiffness distribution coefficient, soft story effect, regular story height and number of stories) on the structural response of linear MDOF systems are investigated. Moreover, the simple ground story drift estimation equation proposed by Gülkan and Akkar (2002) for shear frames and the maximum ground story and maximum interstory drift estimation equations proposed by Akkar et al. (2005) for moment resisting frames are modified by using the above-mentioned structural properties.

In this study, frames were analyzed by using DRAIN-2DX and NONLINPRO which is a Windows version of DRAIN-2DX [54]. In order to prepare the huge number of input files for modal analyses, elastic and inelastic response history analyses, special MATLAB and FORTRAN programs were prepared. Only flexural deformations of structural members are taken into account in this study. For response history analyses, proportional damping is taken as 5 percent of critical and it is kept constant for all the computations. The

proportionality constants are chosen to attain 5 percent of critical damping in the first and second modes. SPSS [65] is used for all of the regression analyses. Inelastic response results are described in Chapter 4. This survey is necessary to quantify the roles of key parameters that affect seismic response.

3.2 EFFECTS OF NEAR-FAULT GROUND MOTIONS AND STRUCTURAL PROPERTIES ON THE RESPONSE OF ELASTIC MOMENT RESISTING FRAMES

A total of 90'480 elastic time history analysis were conducted to investigate the effects of beam to column stiffness ratio (ρ), stiffness distribution coefficient (λ), soft story factor (ψ), regular story height (h_2) and number of stories (N) on elastic response of steel moment resisting frames subjected to 58 near fault ground motions. Furthermore, remarks about the effects of near-fault pulse-type ground motions on the response of elastic steel MRF are presented.

Damage in moment resisting frames is affected by two drift parameters: (a) the interstory drifts and (b) its distribution along the height of the structure [24]. Interstory drift ratio (IDR), defined as the lateral displacement difference between two consecutive stories normalized by the story height, ground story displacement ratio (GSDR), defined as the lateral drift of the ground story divided by the story height, and the maximum interstory drift ratio (MIDR), defined as the maximum of interstory story drift ratios along the height, are used to quantify the displacement demand parameters of MDOF structures to near-fault ground motions.

3.2.1 EFFECTS OF PULSE PERIOD ON LATERAL DISPLACEMENT DEMAND

High-velocity pulses can place severe inelastic demands on multistory structures [28]. Recent investigations have shown that demand depends on the ratio of pulse period (T_p) to fundamental period (T). Figure 3.1 and Figure 3.2

show the effect of T_p/T on GSDR and MIDR for 20 and 9 story regular MRF frames, respectively. Demands are amplified as the pulse period approaches the fundamental period of the structure and high displacement demands are observed near T_p/T =1.0. The maximum story demands are concentrated on the lower levels in the neighborhood of the ratio T_p/T =1.0, which indicates a primarily first mode response. When the pulse period approaches the second and third mode periods and the ratio is lower than 1.0, maximum interstory demands shift to the upper stories, which indicates the participation of higher modes. Hence, these distinct pulses can cause the response of taller buildings to have greater participation from the higher modes. According to Kalkan and Kunnath [37], higher mode effects are not obvious in the response to fling type motions, but they are clearly evident for forward directivity pulses when T_p/T is less than 0.8. Fling step displacement almost always causes the systems to respond primarily in the fundamental mode [37]. Equation 3.1 is considered as a possible criterion to evaluate the error caused by eliminating modes other than the first mode.

$$\eta = \frac{D_{all} - D_1}{D_{all}} \tag{3.1}$$

η is the percentage of the higher mode effect in the displacement demand parameter (D). D_1 and D_{all} are the displacement of the MRFs considering only the first and all modes of vibration, respectively. Figure 3.3 and Figure 3.4 show how the higher mode effect factor η varies with T_p/T for frames with different story heights (h_2). It can be seen that the percentage of higher mode effects increases with decreasing T_p/T which indicates the importance of higher modes in high rise frames and for T_p/T values less than 0.8. For T_p/T values greater than 1.0, higher mode effect on both GSDR and MIDR are almost always less than 20 percent.

Alavi and Krawinkler [5] studied the elastic and inelastic responses of frame structures subjected to near fault earthquakes. They showed that for structures with fundamental periods longer than the pulse period, distribution of

elastic story shear forces over the height are sensitive to the ratio of natural period of structure to the pulse duration. They have stated that short period structures are not affected as much by the long period velocity pulse. The maximum story ductility demands occur in the lower stories regardless of strength for short period structures ($T \leq Tp$) [5].

To sum up, response of structures to near fault ground motions is affected by the ratio of pulse period to fundamental period. For systems with $T_p/T < 1$, contributions of higher modes significantly affect the general response, while for systems with $T_p/T > 1$ fundamental mode is dominant in the overall response of structures. This is in confirmation of results from other investigations.

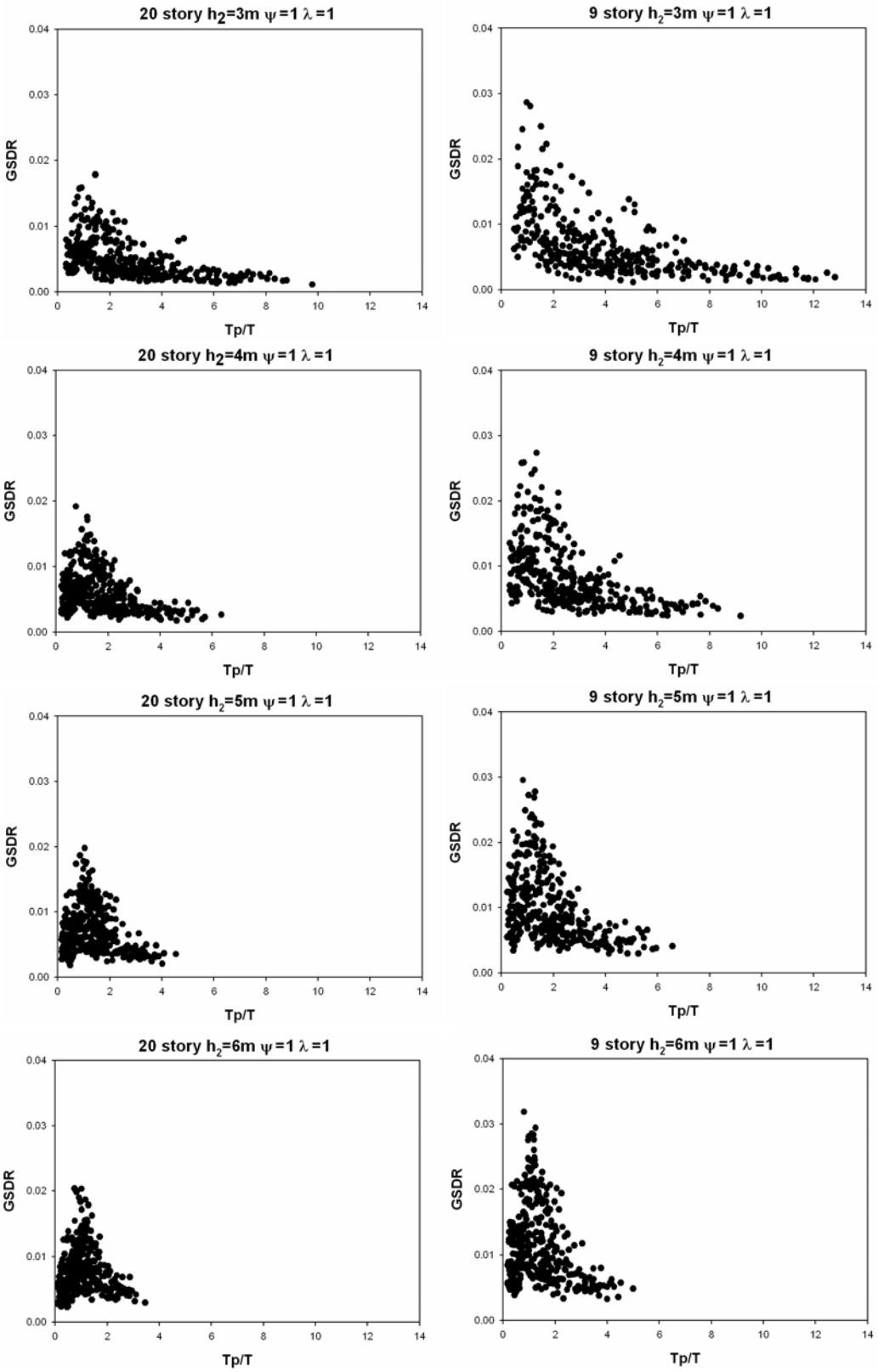

Figure 3.1: T_p/T effect on GSDR

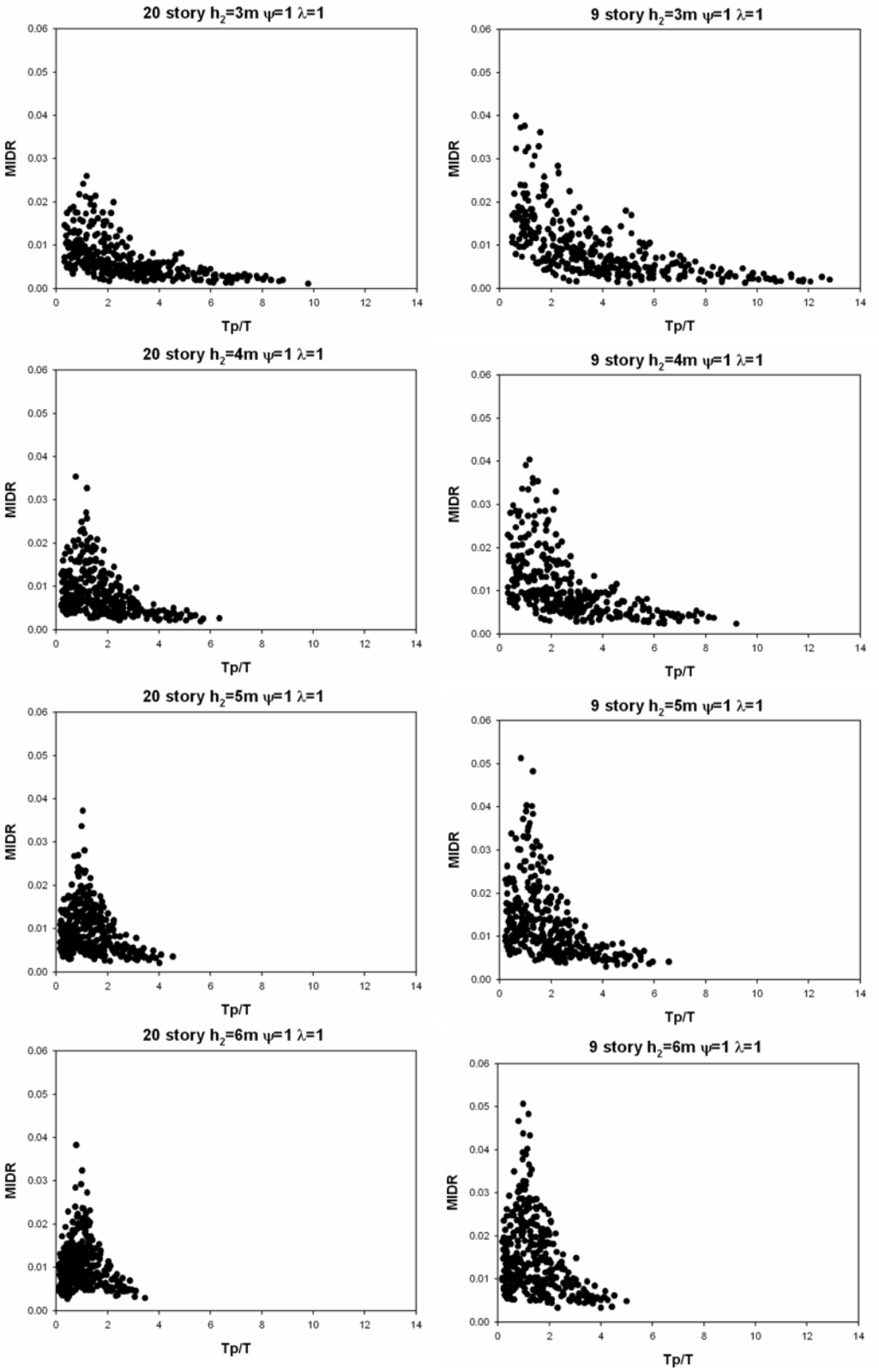

Figure 3.2: T_p/T effect on MIDR

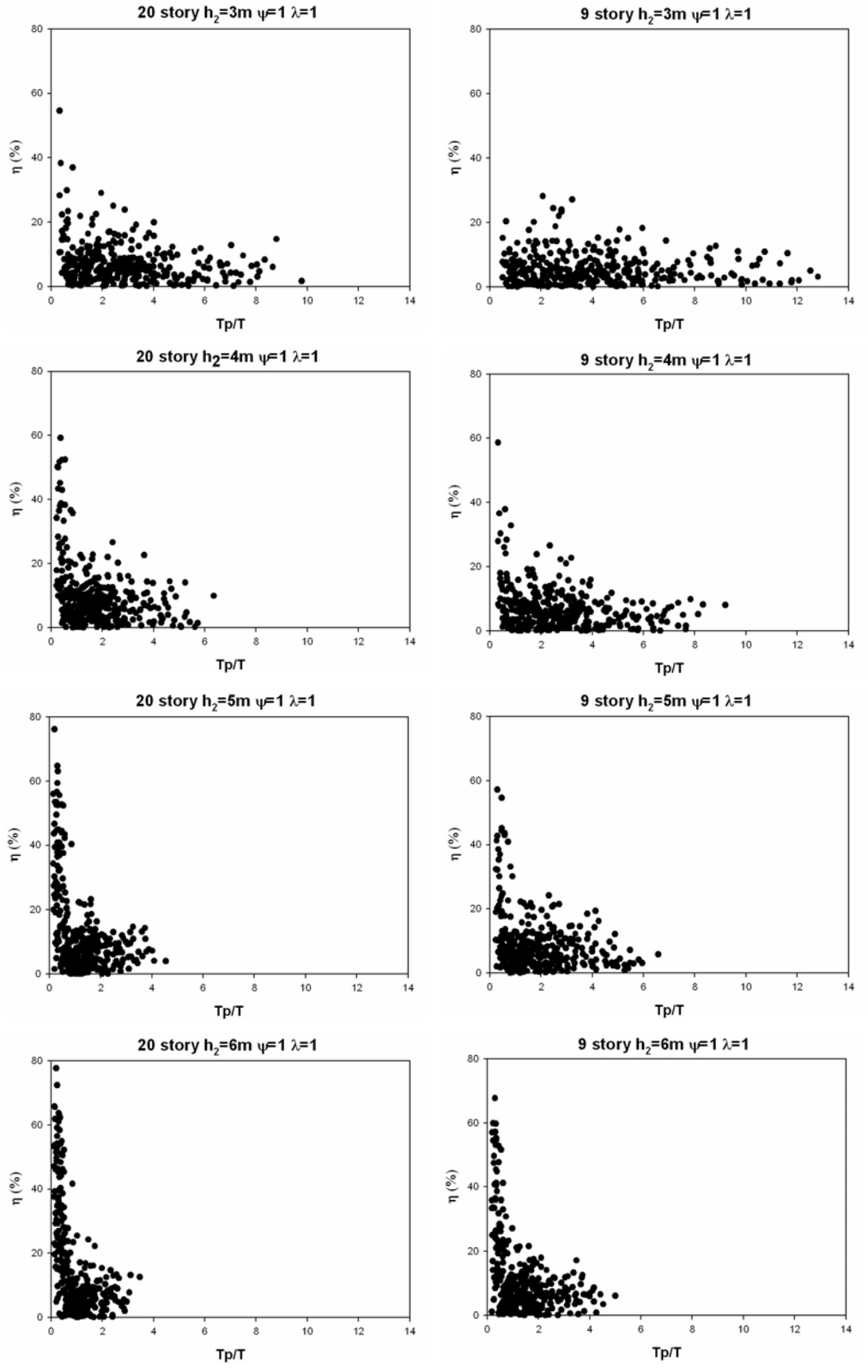

Figure 3.3: Higher mode effect on GSDR

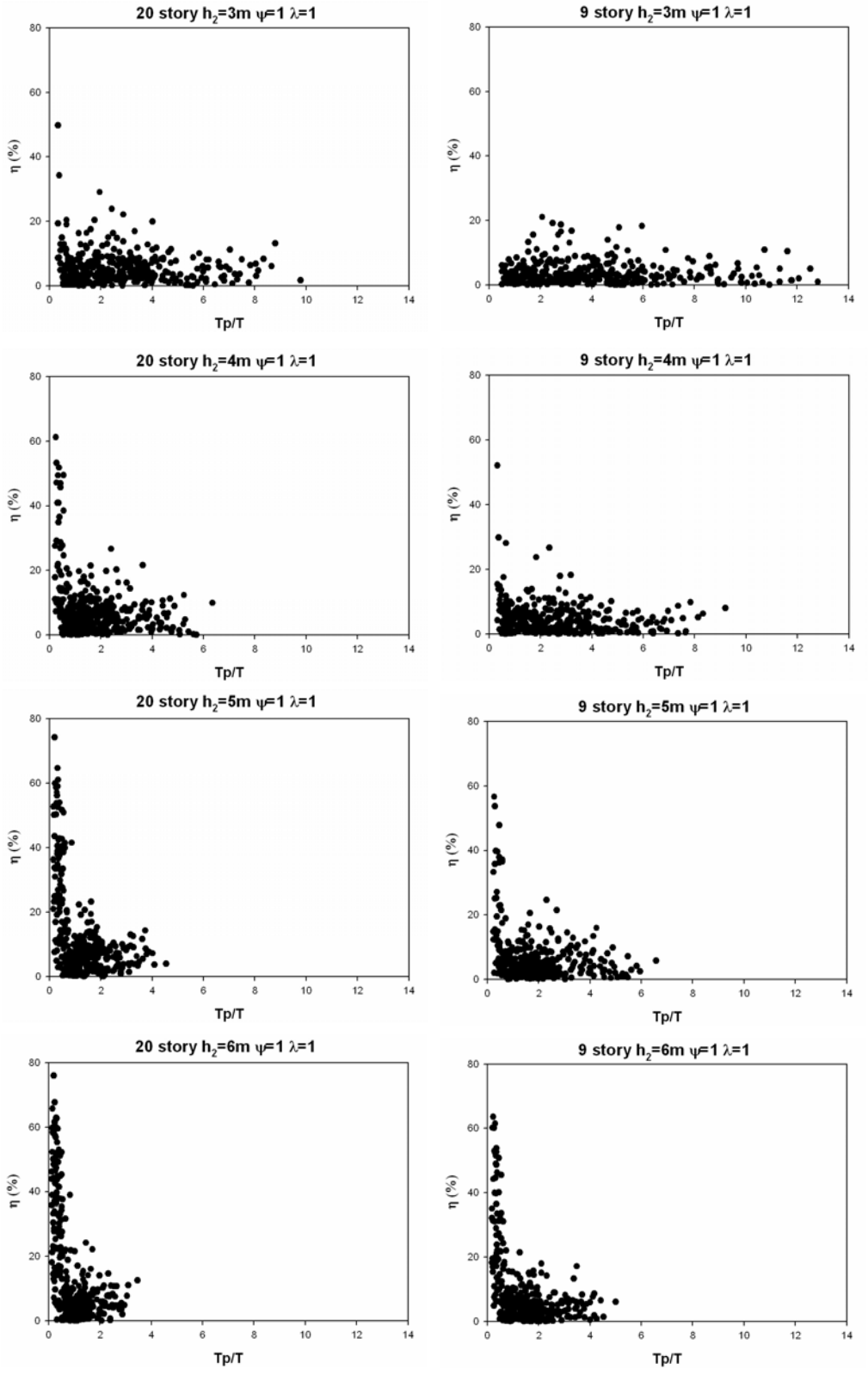

Figure 3.4: Higher mode effect on MIDR

3.2.2 EFFECTS OF BEAM TO COLUMN STIFFNESS RATIO (ρ) ON LATERAL DISPLACEMENT DEMAND

In order to examine the effects of ρ, interstory drift profiles obtained from elastic response history analyses are investigated. Figure 3.5 shows the mean, mean plus and minus one standard deviation of IDR profiles of 20, 9 and 3 story MRFs with different ρ values by using 58 near fault ground motions. While obtaining IDR values for a ground motion, maximum value of IDR of each story throughout the response is utilized. It is seen that maximum interstory drift location shifts from ground story to upper stories as ρ decreases. Moreover, standard deviation is larger for frames with small ρ values. When ρ goes to "infinity", maximum interstory drift occurs in the ground story. It is observed that interstory drifts computed for smaller ρ values are higher than those computed for greater ρ values.

In order to compare the fundamental mode response and elastic response history analysis results, normalized interstory drift profiles are utilized. Interstory drift ratios obtained from the first mode shape are divided by the maximum of these drift ratios and the mean of the maximum interstory drift ratio of each story calculated from elastic response history analyses is divided by the maximum of these mean values. Resulting normalized drift profiles are presented in Figure 3.6. Deviations from the fundamental mode shape are more pronounced for smaller ρ values and 20-story MRFs. Fundamental periods for these frames are very long and other modes contribute to the response. Since first mode response is dominant for 3 story MRFs, results between elastic response history analyses and first response are in good agreement as illustrated in Figure 3.6. Furthermore, it can be observed that there are no noticeable deviations in the ratio of MIDR to GSDR, maximum interstory drift location and its neighborhood stories for all frames. Since the maximum interstory drift ratio and ground story drift ratio are concerns of this study, utilization of only the first mode response does not lead to a significant error in estimating these deformation demands.

The effect of ρ (0.25, 0.50, 1.0, 2.0, 4.0 and "infinity") on fundamental mode shape is shown in Figure 3.7. It is observed that these ρ values result in frames where shear-type deformations control the lateral behavior. In fact, the smallest ρ value is inadequate to obtain flexural frame which deforms like a vertical cantilever beam. In addition, it can be stated that there are slight differences between mode shapes corresponding to different ρ values for 20 and 9 story MRFs.

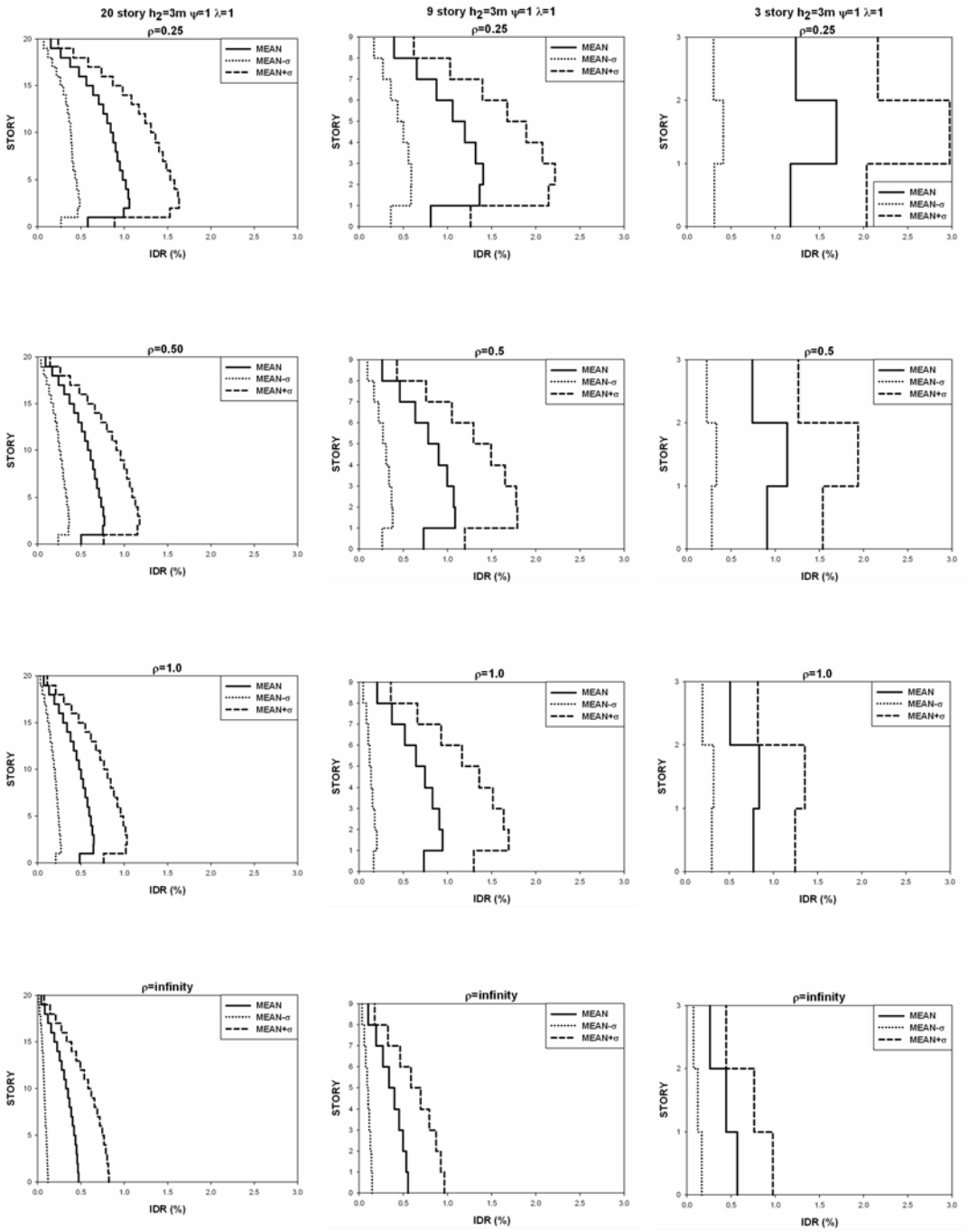

Figure 3.5: Interstory drift profiles for 20, 9 and 3 story MRFs with different ρ values

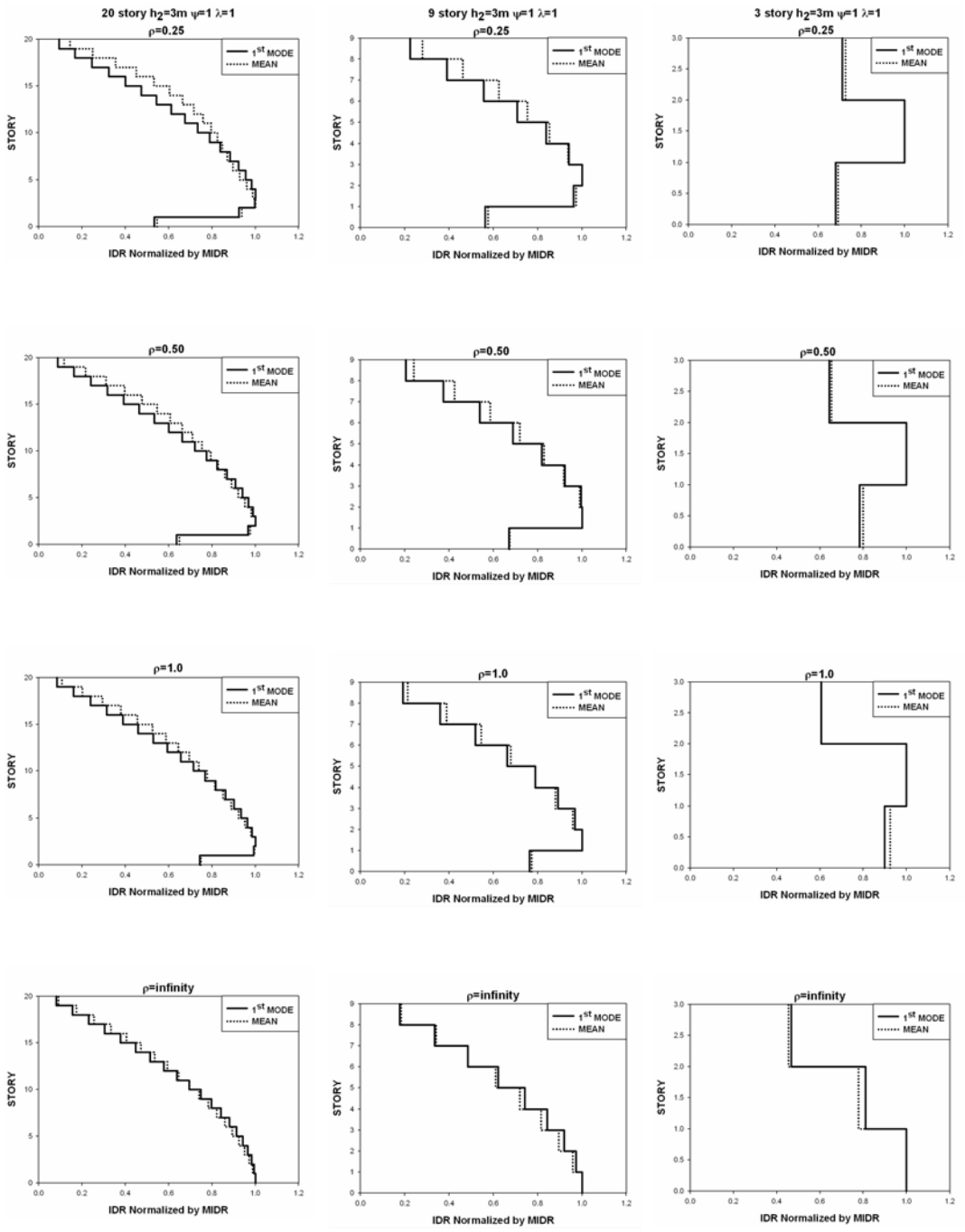

Figure 3.6: First mode and mean interstory drift profiles for 20, 9 and 3 story MRFs with different ρ values

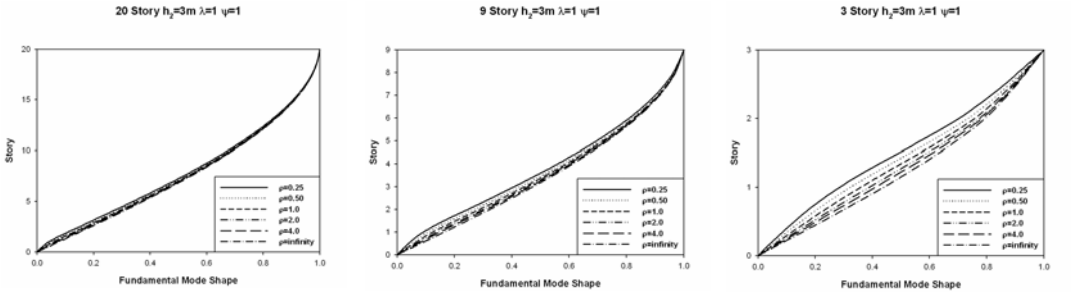

Figure 3.7: Fundamental mode shapes

3.2.3 EFFECTS OF STIFFNESS DISTRIBUTION COEFFICIENT (λ) ON LATERAL DISPLACEMENT DEMAND

In order to simulate the reduction in stiffness along the height, the parameter λ, defined as the ratio of the lateral stiffness at the top story of the structure to the lateral stiffness at the ground story of the structure, is changed from 1.0 to 6.0. In this study stiffness is reduced linearly along the height, as explained in Chapter 2. In general, low-rise buildings have uniform stiffness distribution; hence λ equals to 1. These frames do not conform to cantilever behavior, 20-story, 9-story and 3-story MRFs with ρ values of 0.0005 are formed to obtain non-uniform stiffness distribution effect on cantilever frames. As illustrated in Figure 3.8 and Figure 3.9, variation of stiffness distribution effect is more pronounced for shear frames (ρ=0.25, 0.50, 1.0, 2.0, 4.0 and infinity) than cantilever frames (ρ=0.0005). Moreover, shear frames with non-uniform stiffness (λ≠1) have similar fundamental mode shapes.

The beam to column stiffness ratio has an effect on the location of MIDR in uniform frames, such as upper portion or lower portion of the frame. However, when nonuniform stiffness is included, it is difficult to make a comment about maximum drift location without considering the stiffness distribution. For instance, Figure 3.10 and Figure 3.11 show the drift profiles for 20 and 9 story MRFs,

respectively. The ρ value which equals to 0.5 is selected deliberately since this value belongs to original SAC MRFs. Maximum drifts occur at 3rd and 2nd stories for regular (λ=1) 20 and 9 story MRFs, respectively. When the stiffness distribution factor is increased from 1 to 6, maximum drift location begins to move to upper part of the frames because lateral stiffness of upper stories is decreased relative to the lower stories with increasing λ. From Figure 3.10 and Figure 3.11, it can also be seen that MIDR increase with λ, whereas GSDR is not significantly affected.

Increase in stiffness distribution coefficient increases the period of the building and the contribution of higher modes. The differences between drift profiles in Figure 3.12 and Figure 3.13 are on account of higher mode effects, which affect structures to varying degrees depending on the number of stories and the frequency characteristics of the ground motion. In addition, it is observed that consideration of the fundamental mode would result in conservative drifts in the lower stories and relatively unsafe drifts in the upper stories when $\lambda \neq 1.0$. There are several near fault ground motions in which second mode displacement demand is higher than first mode displacement demand. Due to these ground motions the high deviations from fundamental modes arise in the analysis.

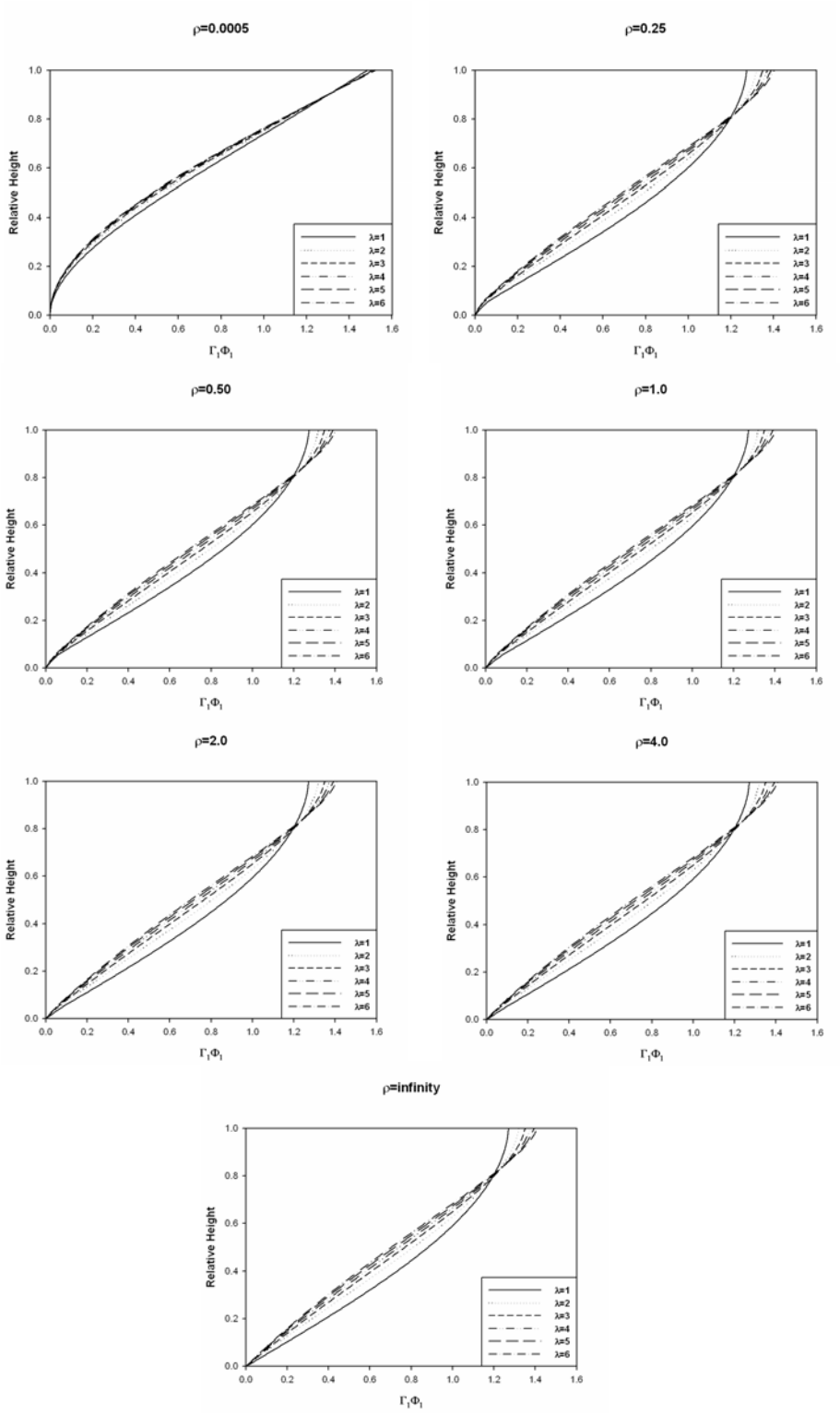

Figure 3.8: Effect of λ on fundamental mode shapes of 20 Story MRFs

9 STORY h_2=3m ψ=1.0

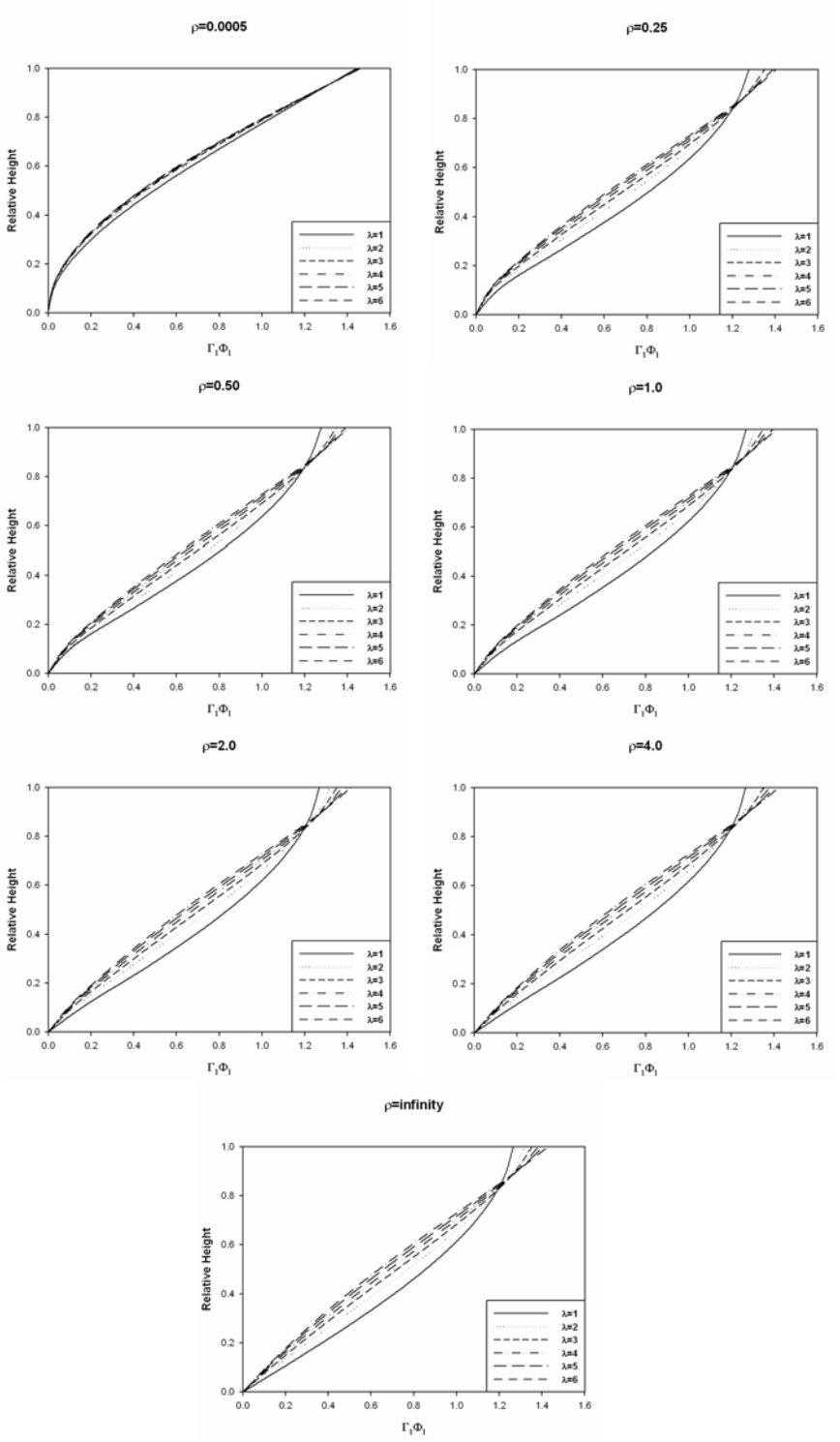

Figure 3.9: Effect of λ on fundamental mode shapes for 9 Story MRFs

20 STORY h_2=3m ρ=0.5 ψ=1.0

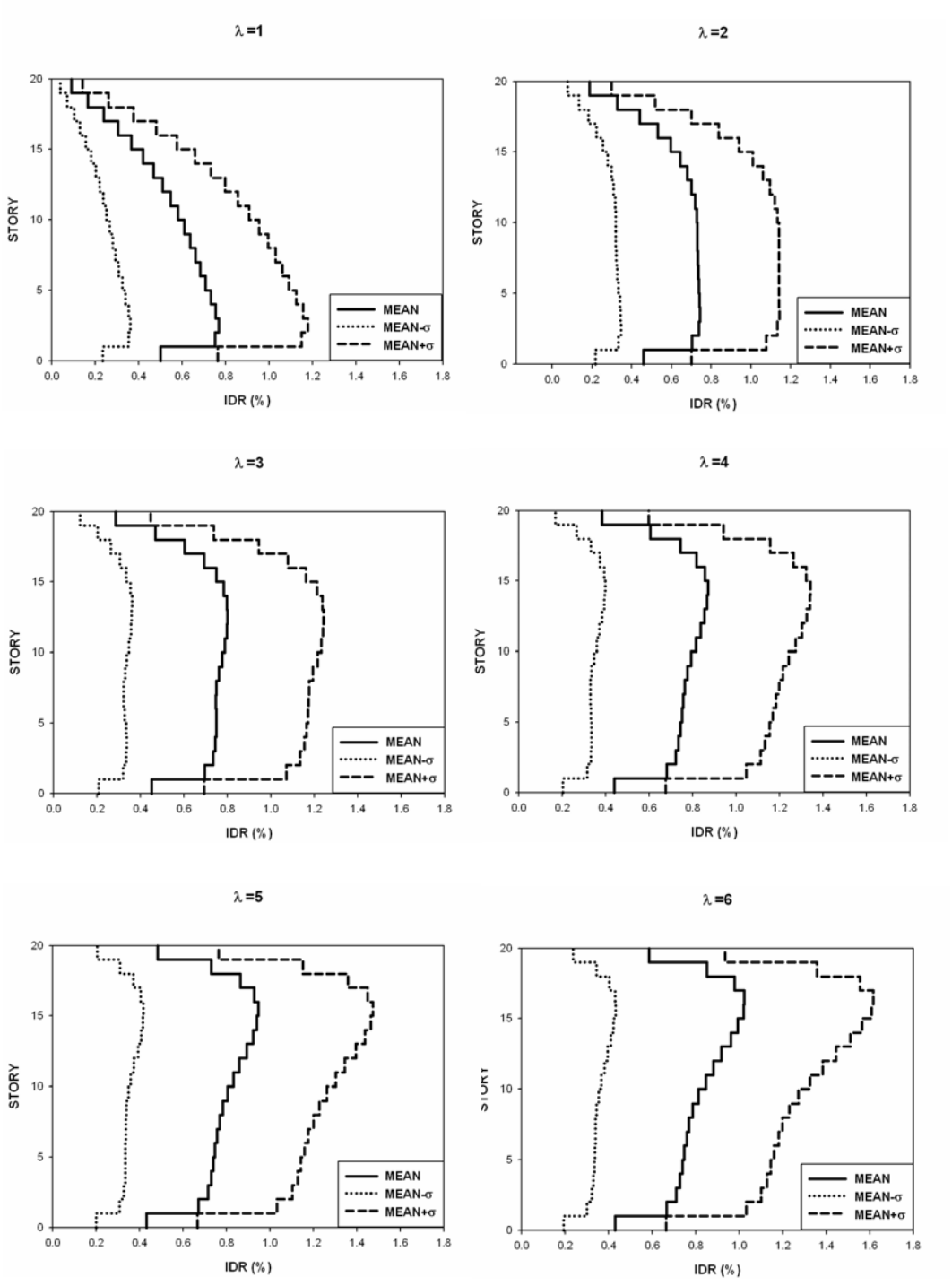

Figure 3.10: Non-uniform stiffness distribution effect on lateral deformation demand of 20 story MRF

9 STORY h_2=3m ρ=0.5 ψ=1.0

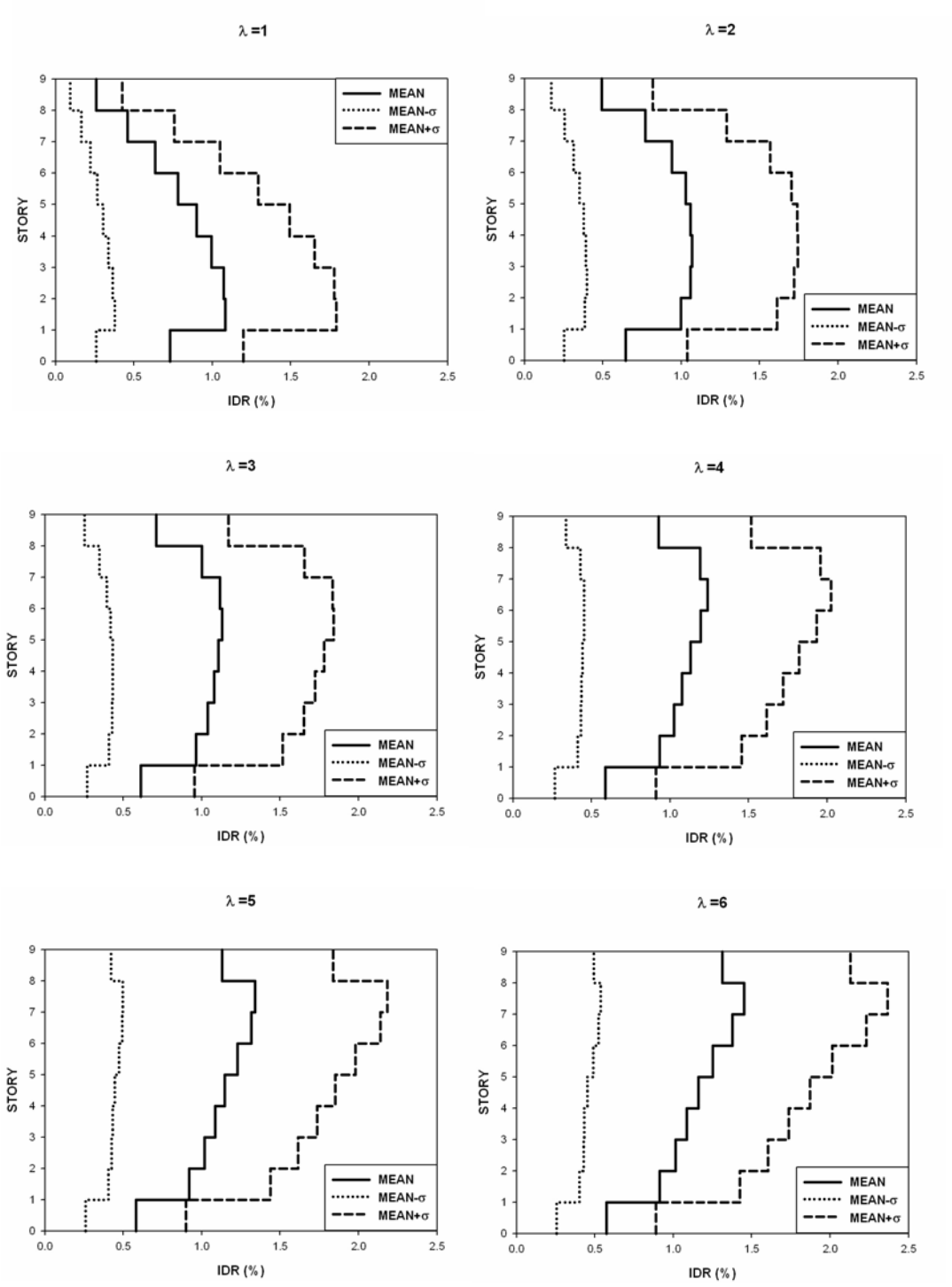

Figure 3.11: Non-uniform stiffness distribution effect on lateral deformation demand of 9 story MRF

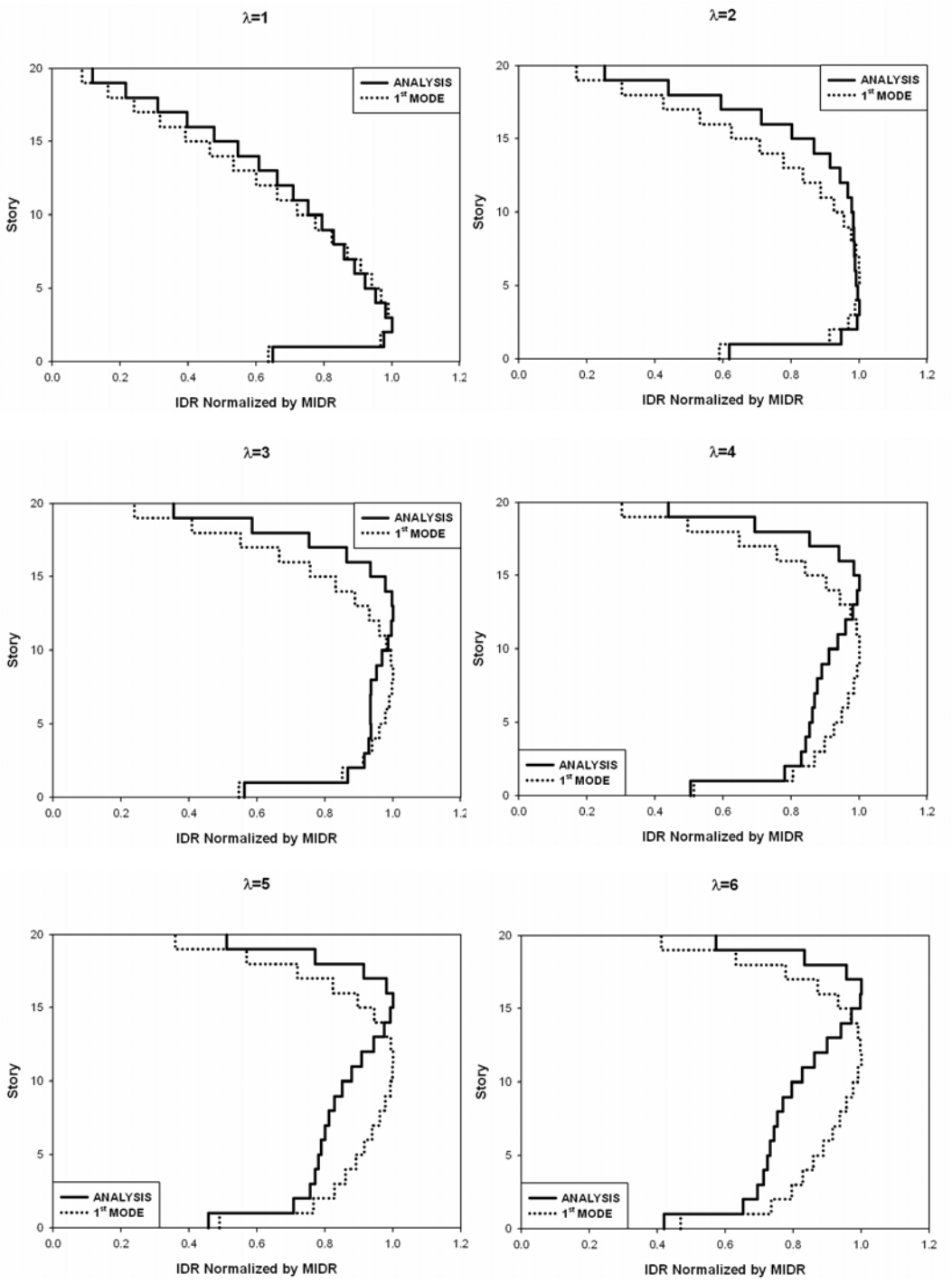

Figure 3.12: First mode and mean interstory drift profiles obtained from elastic response history analyses of 20 story MRFs with different λ values

9 STORY h_2=3m ρ=0.5 ψ=1.0

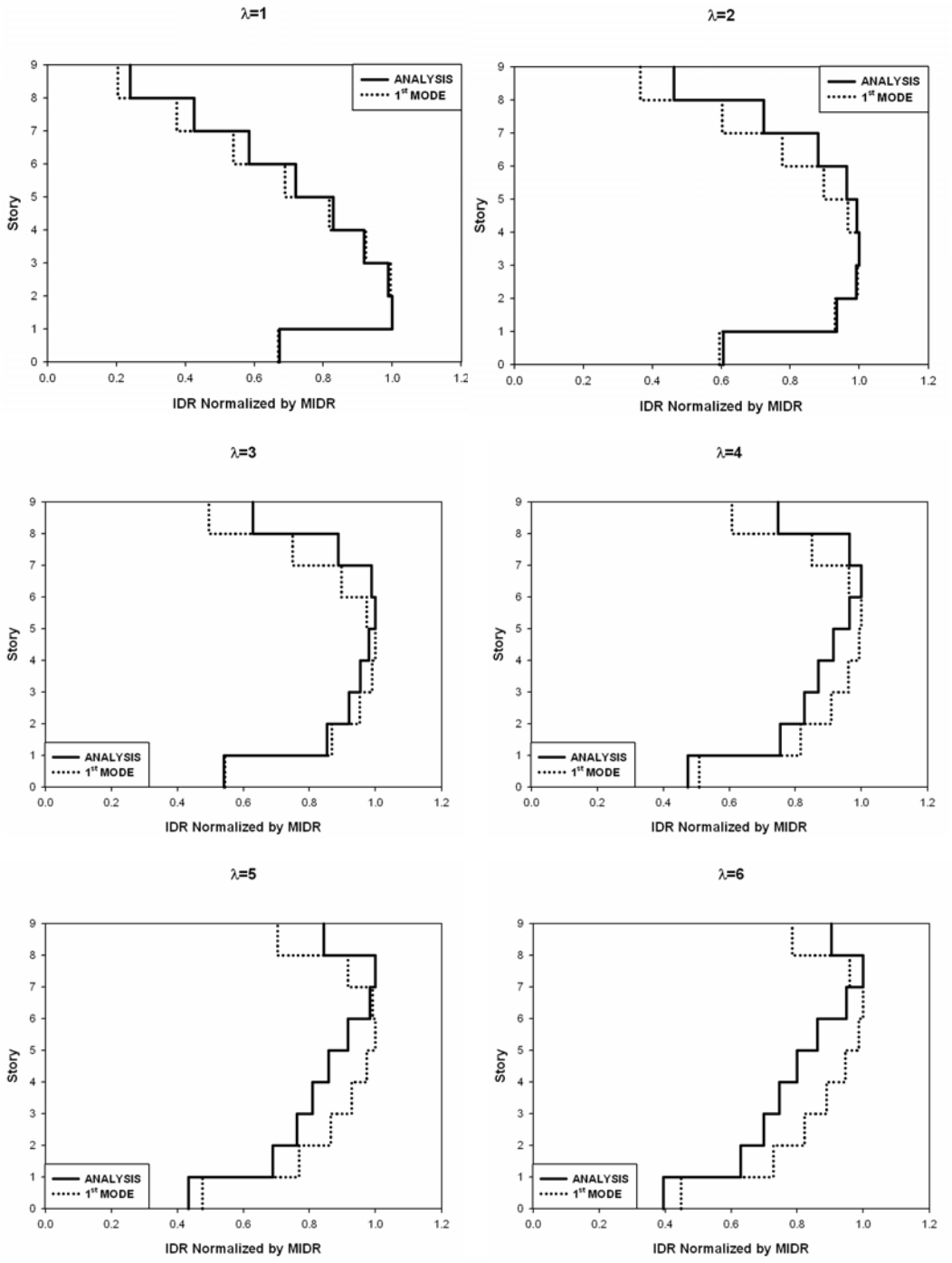

Figure 3.13 First mode and mean interstory drift profiles obtained from elastic response history analyses of 9 story MRFs with different λ values

3.2.4 EFFECTS OF SOFT STORY FACTOR (Ψ) ON LATERAL DISPLACEMENT DEMAND

Soft-story has been recognized as an unfavorable feature for building structures. The soft story factor (ψ) is defined as the ratio of the first story height to the regular story height. Here, ψ values of 1.0, 1.2, 1.4, 1.6 and 1.8 are employed in order to investigate the effects of this factor. Increase in ground story height reduces the lateral stiffness of this story. Due to the reduction in stiffness, the fundamental period of vibration for buildings with a soft story is increased as presented in Figure 3.14. The same trend is observed between period and soft story factor for 20, 9 and 3 story steel MRFs.

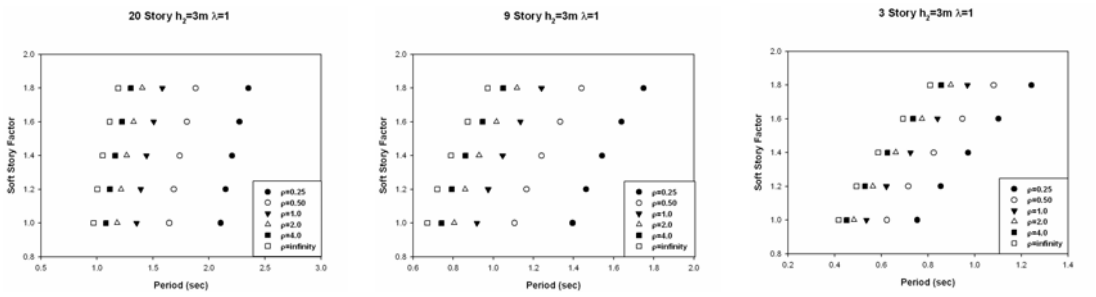

Figure 3.14: Soft story effect on period

Soft story affects high-rise frames more than low-rise frames. Figure 3.15 shows the effect of the presence of soft story with different values of ψ on the fundamental modal displacement. For example, for soft story factor 1.4 the first mode ground story displacement increases by 133%, 113% and 56% considering fundamental mode responses of regular 20, 9 and 3 story frames, respectively. Furthermore, as soft story factor increases, there is a rise in these percentages.

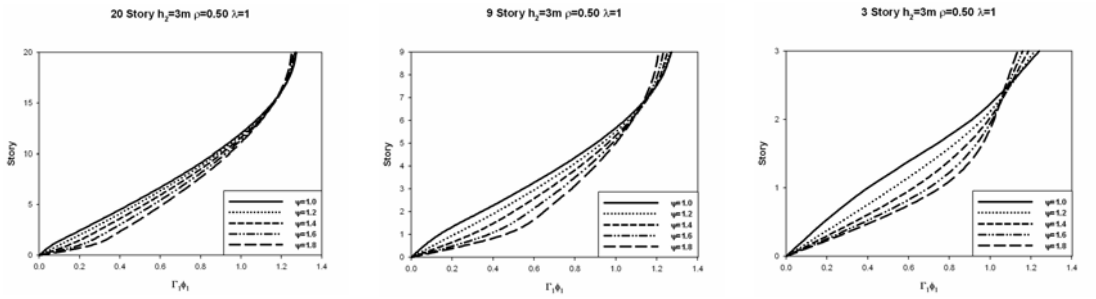

Figure 3.15: Soft story effect on the fundamental modal displacement

Comparison of normalized interstory drifts obtained from elastic response history analyses and first mode response corresponding to different soft story factors are presented in Figure 3.16. It can be seen that the profiles obtained from elastic response history analyses resemble a first mode pattern. Maximum interstory drift location can be accurately determined by using fundamental mode shape. MIDR migrates toward lower levels for MRFs with increasing ground story height as shown in Figure 3.16 and Figure 3.17. In addition, frames with high soft story factor have greater MIDR. A rise in ground story height also increases the interstory drift ratio of second story.

Observing the results of elastic response history analyses in Figure 3.17, it can be stated that the increase in the dispersion from the mean with increasing soft story factor is more pronounced in the 3 story MRFs than the high-rise frames. The deviation from MIDR of regular frame becomes greater as the ground story height increases.

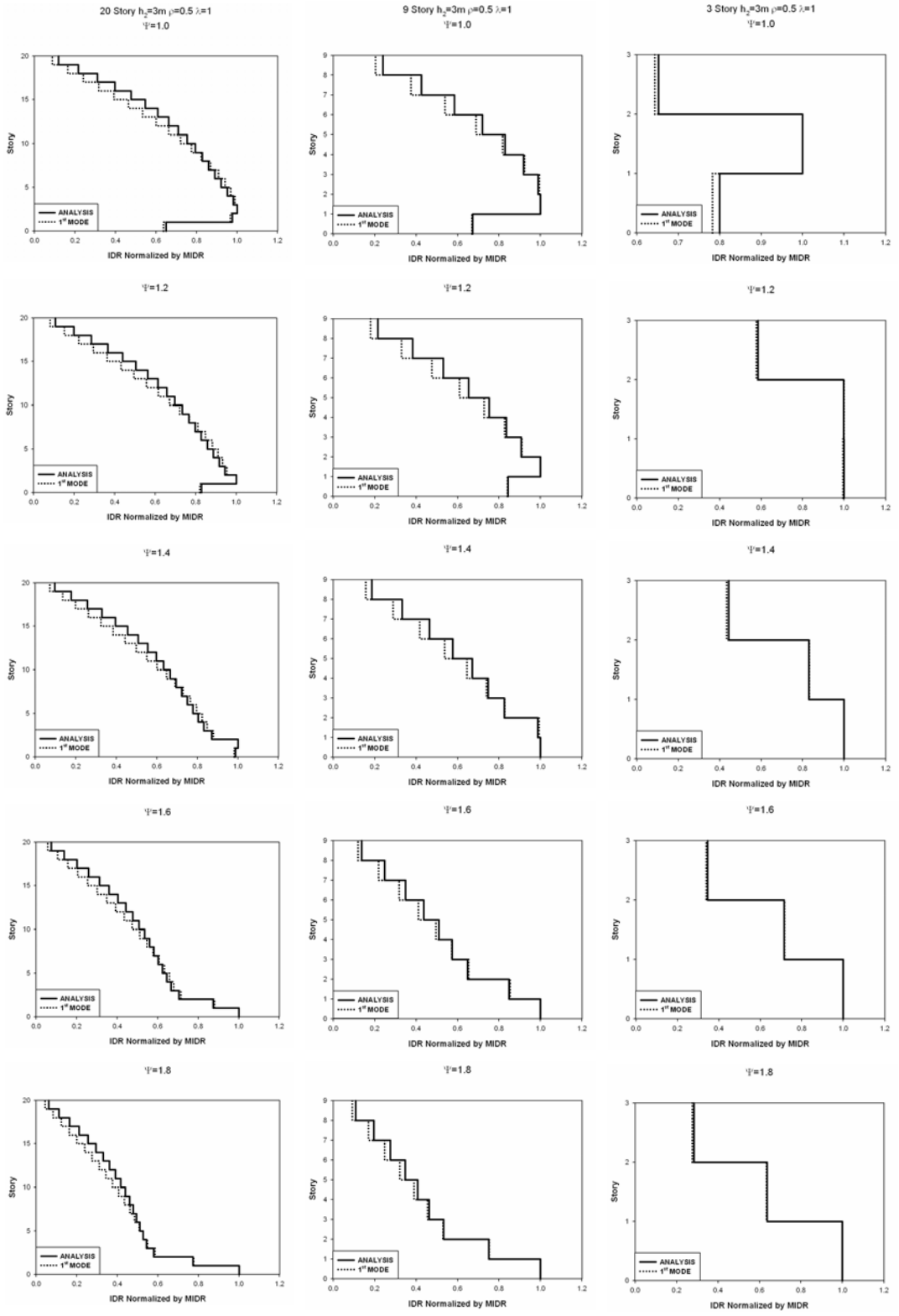

Figure 3.16 : First mode and mean interstory drift profiles obtained from elastic response history analyses of 9 story MRFs with different ψ values

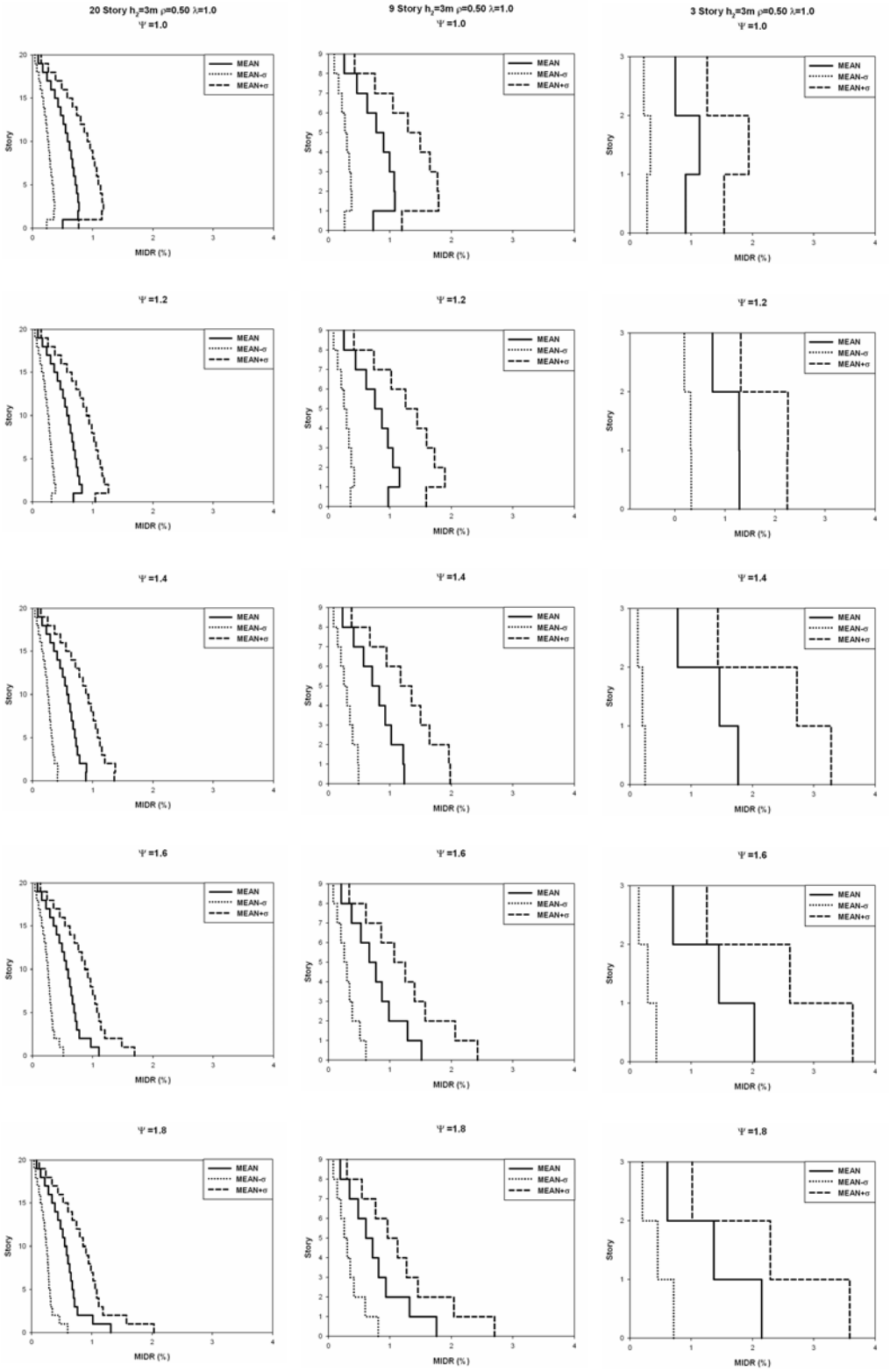

Figure 3.17: Soft story effect on MIDR

3.2.5 EFFECTS OF REGULAR STORY HEIGHT (h_2) AND NUMBER OF STORIES (N) ON LATERAL DISPLACEMENT DEMAND

In order to investigate regular story height (h_2) and number of stories (N), three different number of stories (N=20,9,3) with four different h_2 values (3m, 4m, 5m and 6m) are employed in the analysis. Changing story heights do not lead to any differences on mode shapes as presented in Figure 3.18. Changing the story height does not modify participation factors (Γ) and mode shapes of vibration (Φ) because stiffness of all stories decreases or increases by the same ratio. Therefore, stiffness matrix of the frame is multiplied with a scalar; hence mode shapes are not influenced by modification of regular story height.

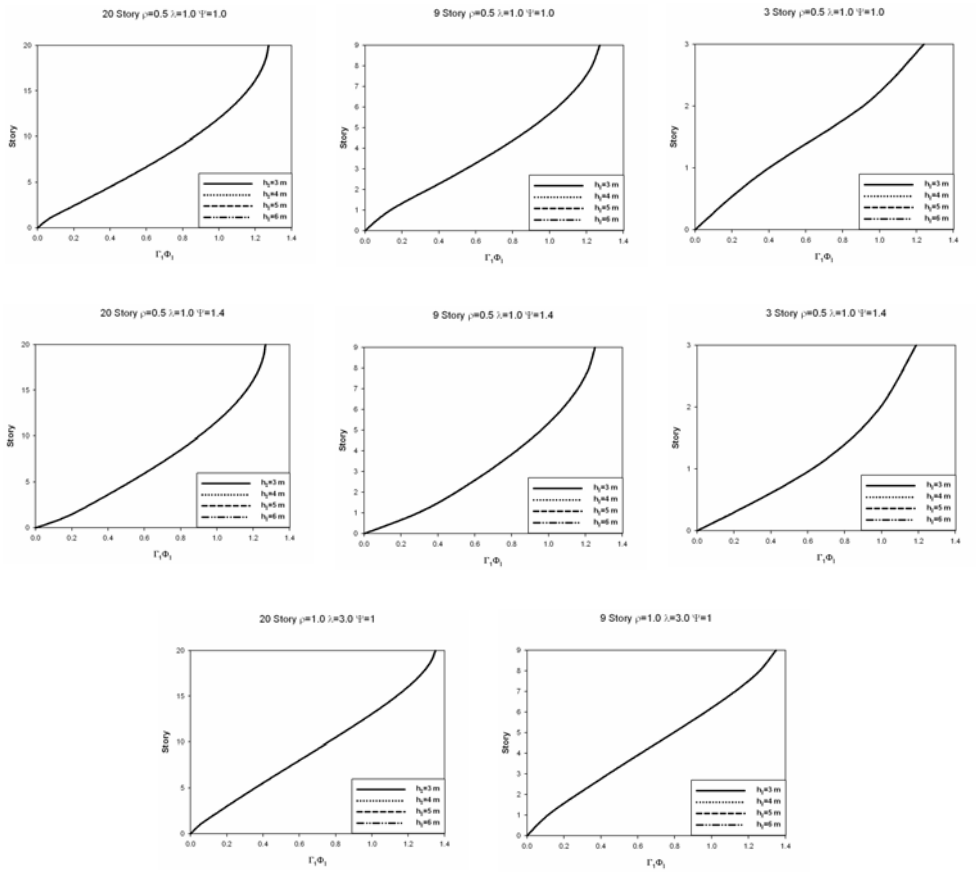

Figure 3.18: Effects of story height on fundamental mode shape

Generally, the empirical formulas used to predict fundamental period of a building are a function of height alone because the building height (number of stories) has been found to play the most important role in prediction of the period [30]. Increasing regular story height that means an increase in the total story height results in longer period frames as shown in Figure 3.19.

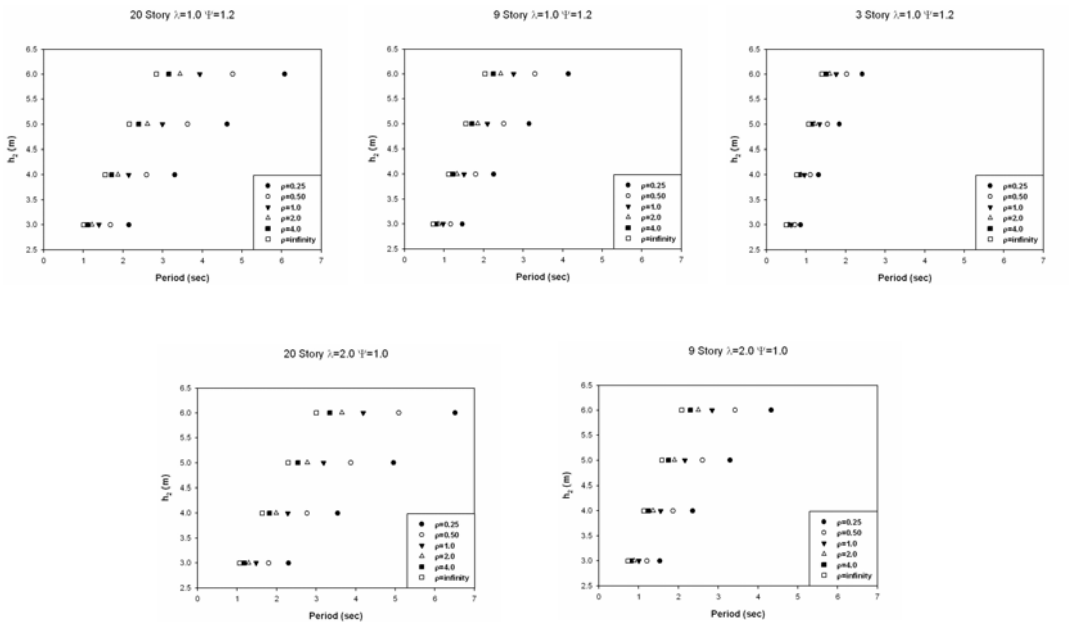

Figure 3.19: Effect of story height on fundamental period

Despite of the fact that story height change does not influence the fundamental mode shape, interstory drift ratio increases with story height as illustrated in Figure 3.20. This increase in interstory drift ratio is due to the increase in spectral displacement. As period increases with story height, spectral displacement increases. Since mode shape is not affected by the change in story height, interstory drift ratio is directly affected by spectral displacement. For instance, when story height is changed from 3 m to 6 m, maximum interstory drift ratio is increased by 55, 68 and 110 percent for 20-story, 9-story and 3-story MRF (ρ=0.5, λ=1.0, ψ=1.0), respectively. Also it can be stated that increase in spectral

displacement is higher than the increase in story height. Low rise frames are influenced by increase of story height more than high rise frames, since increase in spectral displacement corresponding to period increase is greater in low rise frames due to the spectral displacement shapes of ground motions. Whereas drift profiles are not affected by different story heights, magnitudes of IDR increase in all frames.

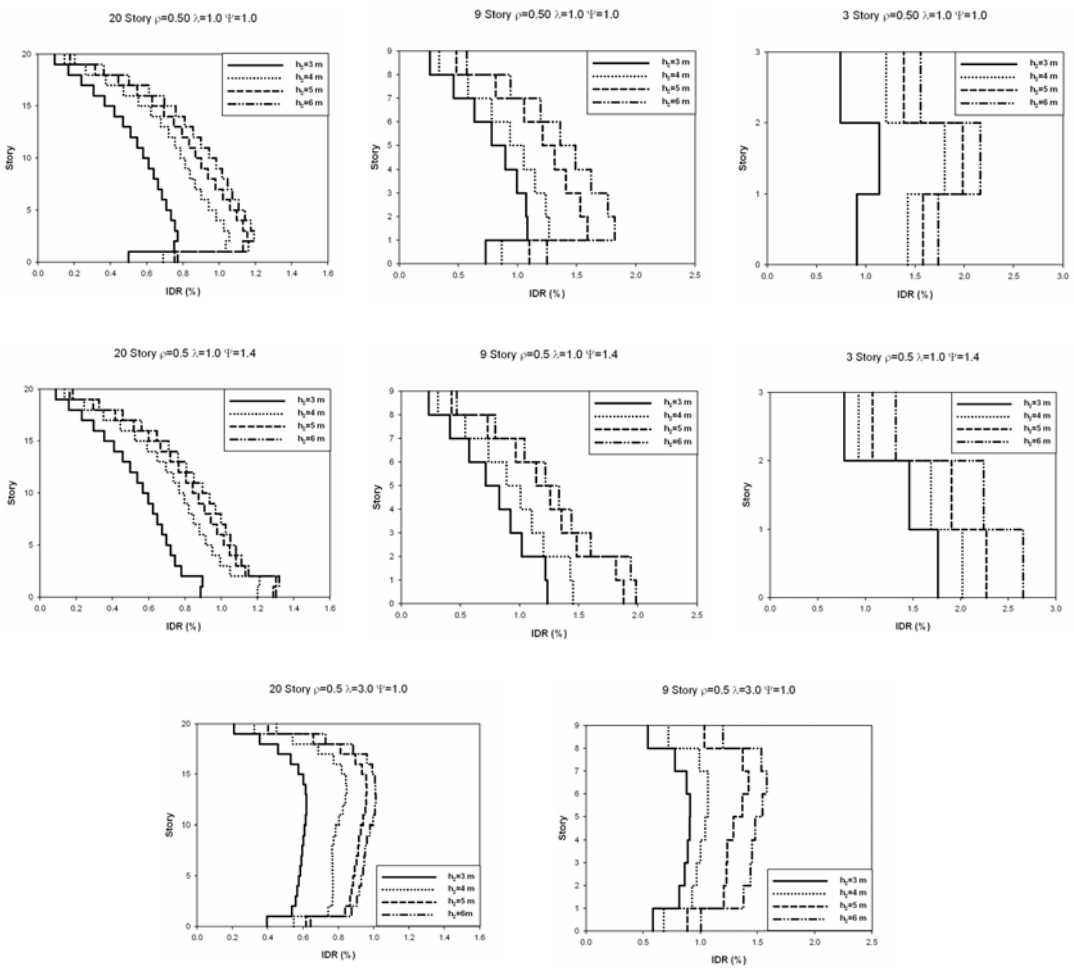

Figure 3.20 : Effect of story height on IDR

3.3 ASSUMPTIONS EMPLOYED IN THE DERIVATION OF EQUATIONS

- ✓ Assumptions related to generic frame model are accepted (Section 2.5).
- ✓ Fundamental mode response is assumed to be enough for estimating total response.
- ✓ Mass distribution in real SAC project is used and not modified during the analysis procedure.
- ✓ Other than the 20-story, 9-story and 3-story MRFs described in Chapter 2, a 15-story steel MRF is generated from 20-story SAC MRF by extracting the top five stories of this building. The 15 story model is used only in the modification of the equation of Gülkan and Akkar [26] as presented in the next section.

3.4 DERIVATION OF THE EQUATIONS FOR ESTIMATING LINEAR DEFORMATION DEMANDS OF FRAME SYSTEMS

One of the aims of this study is the improvement of the equations that estimate maximum ground story displacement ratio of shear frames presented by Gülkan and Akkar [26] and Akkar et al. [3] for maximum ground story drift ratio and interstory drift ratio of moment resisting frames. The proposed procedure modifies these methods by including stiffness distribution coefficient, soft story factor, regular story height and number of stories.

3.4.1 MODIFICATION OF THE PROCEDURE PRENSENTED BY GÜLKAN AND AKKAR (2002)

Gülkan and Akkar [26] derived an approximate equation, which utilized the fundamental mode response of a shear beam, for estimating the ground story drift ratios (GSDR) of shear frames with fundamental periods less than 2 s within an

error bound of $\pm 10\%$ under near fault ground motions. For a given ground motion, this expression for GSDR is given as

$$GSDR_{SH} = 1.27 \frac{S_d(T,\xi)}{h} \sin\left(\frac{\pi}{2N}\right) \tag{3.2}$$

where $S_d(T,\xi)$ is the displacement spectrum ordinate corresponding to the fundamental period T and the viscous damping ratio ζ, h is the height of the ground story column and N is the number of stories. Performance of Equation (3.2) is evaluated by Gülkan and Akkar [26] and it is found that Equation (3.2) provides acceptable accuracy for estimating the GSDR of shear frames.

Equation (3.2) is valid for the shear frames (ρ=infinity) that have columns with the same stiffness and height, and constant story masses. Hence, this formula can not be used for non-uniform shear frames and should be modified by considering non-uniform variables. Modification factor (α) can be written as follows

$$GSDR'_{SH} = \alpha \times 1.27 \frac{S_d(T,\xi)}{h} \sin\left(\frac{\pi}{2N}\right) \tag{3.3}$$

where $GSDR'_{SH}$ is the ground story drift ratio of nonuniform or uniform shear frame, T is the fundamental period of shear frame (uniform or nonuniform) and h is ground story height of shear frame (uniform or nonuniform). α should be 1.0 when shear frame is uniform. In order to find an expression for α principles of modal analysis are employed [16]. Displacement response of a linear elastic system ($\underline{u}$) can be expressed as

$$\underline{u}(t) = \sum_{n=1}^{N} \underline{\phi}_n q_n(t) \tag{3.4}$$

where N is the total number of modes, $\underline{\phi}_n$ is the nth mode shape vector and $q_n(t)$ represents the time variation of displacements in the nth mode. $q_n(t)$ can be represented with Equation (3.5).

$$q_n(t) = \Gamma_n D_n(t) \tag{3.5}$$

where $\Gamma_n = \dfrac{\phi_n^T m \iota}{\phi_n^T m \phi_n}$

where Γ_n is the modal participation factor of the nth mode, $D_n(t)$ is the displacement response of the SDOF system with period T_n and damping ξ_n, $\underline{m}$ is the mass matrix of the system and $\underline{\iota}$ is the influence vector. The contribution of the first mode to the ground story displacement is represented as

$$u_{1,1} = \Gamma_1 \phi_{1,1} D(t) \tag{3.6}$$

where $u_{1,1}$ is the ground story displacement in the first mode, Γ_1 is the first mode participation factor, $\phi_{1,1}$ is the amplitude of the first mode vector in the ground story and $D_1(t)$ is the displacement response of the SDOF system with period T_1 and damping ξ_1. The maximum absolute value u_{max} of the ground story displacement in the first mode is

$$u_{1,1_{max}} = \Gamma_1 \phi_{1,1} S_d \tag{3.7}$$

where S_d is the spectral displacement of the SDOF system with period T_1 and damping ξ_1.

Substituting Equation (3.7) in Equation (3.3) and rearranging, Equation (3.8) is obtained.

$$\alpha = \frac{(\Gamma_1 \phi_{1,1})_{SH}^{NU}}{(\Gamma_1 \phi_{1,1})_{SH}^{U}} \tag{3.8}$$

Here, $(\Gamma_1\phi_{1,1})_{SH}^{NU}$ and $(\Gamma_1\phi_{1,1})_{SH}^{U}$ are the fundamental mode shape of nonuniform shear frame and the fundamental mode shape of uniform shear frame at the ground story, respectively.

The ratio in Equation (3.8) is computed for all idealized frames used in the analysis. Since the variation of regular height does not change the fundamental mode shapes, α does not change with h_2. α is a function of stiffness distribution factor, soft story factor and number of stories as shown in Figure 3.21. A nonlinear regression analysis has been performed to find an expression for α, based on N, λ and ψ. The resulting equation is given as follows:

$$\alpha = \left[1 - 0.18\ln(\lambda)\right] \times \left[1 + 1.67N^{0.38}\ln(\psi)\right] \tag{3.9}$$

where λ is the non-uniform stiffness distribution coefficient, N is the number of stories and ψ is the soft story factor. Theoretically, α should equal to 1.0 for regular frames (λ=1.0 and ψ=1.0). It is seen that for λ=1.0 and ψ=1.0 Equation (3.9) is indeed equal to 1.0. Therefore, Equation (3.9) satisfies this requirement.

The α values calculated from modal analysis by using Equation (3.8) are compared with the α values found by using Equation (3.9) in Figure 3.22. $\alpha_{ANALYSIS}$ linearly relates to $\alpha_{FORMULA}$ with a correlation coefficient of 0.98. As a result, Equation (3.9) provides very accurate estimations of α.

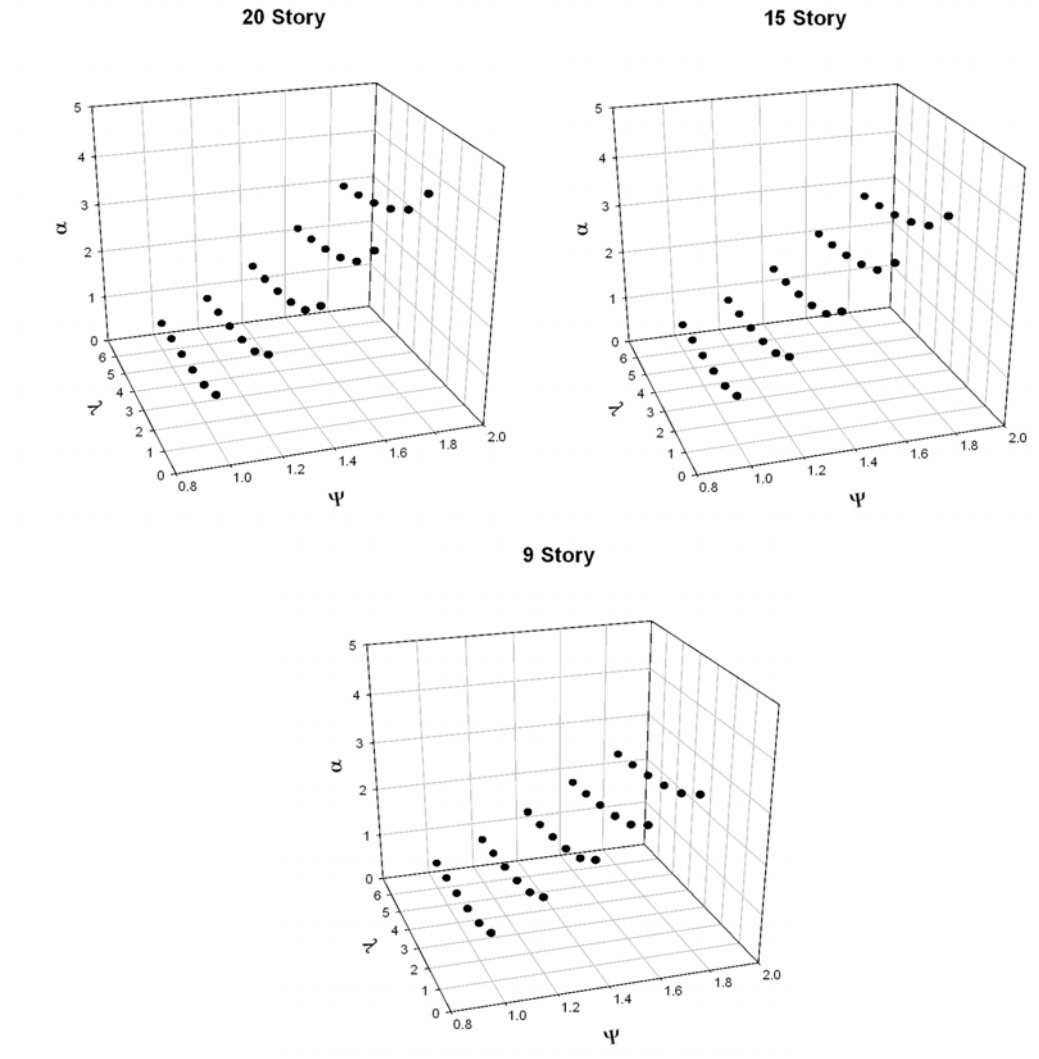

Figure 3.21: Variation in α with stiffness distribution coefficient and soft story factors

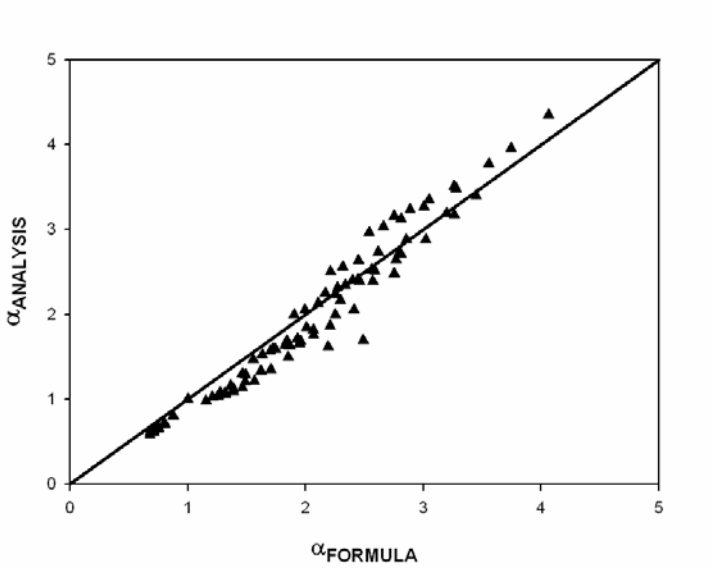

Figure 3.22 : Comparison of α values calculated from modal analysis and proposed equation

3.4.2 MODIFICATION OF THE PROCEDURE PRENSENTED BY AKKAR ET AL. (2005)

The procedure proposed by Akkar et al.[3] estimates the elastic GSDR and MIDR in regular frame-type structures by modifying the ground story drift equation presented by Gülkan and Akkar [26] for shear frames. The improved method utilizes beam-to-column stiffness ratio (ρ), proposed by Blume [12], to account for the general MRF behavior and modifies the local displacements demands computed in Equation (3.2). Details of the improvement procedure are taken from Yazgan [72].

Equation (3.2) is valid for frames having high ρ values and it gives inaccurate results for moment resisting frames having low ρ values. Therefore, this equation is modified by Akkar et al. [3] as follows

$$GSDR_{MF} = \gamma_{MF} GSDR_{SH} \tag{3.10}$$

$$MIDR_{MF} = \gamma_{MIDR} \gamma_{MF} GSDR_{SH} \tag{3.11}$$

where $GSDR_{MF}$ is the approximate ground story drift ratio for a general moment resisting frame, γ_{MF} is modification factor for correcting the shear frame ground story drift ratio to the general moment resisting frame GSDR, $MIDR_{MF}$ is the approximate maximum interstory drift ratio of the general moment frame and γ_{MIDR} is the conversion factor for modifying ground story drift ratio to maximum interstory drift ratio. γ_{MF} is formulated by Yazgan [72] as follows

$$\gamma_{MF} = \frac{\Gamma_1^{MF} \phi_{1,1}^{MF}}{\Gamma_1^{SH} \phi_{1,1}^{SH}} \tag{3.12}$$

where Γ_1^{MF} and Γ_1^{SH} are the first mode participation factors of the moment resisting frame and shear frame, respectively. $\phi_{1,1}^{MF}$ and $\phi_{1,1}^{SH}$ are the ground story drifts of MRF and shear frame in the first mode shapes. The following equation is found for γ_{MF}

$$\gamma_{MF} = c_1(\rho) + \frac{c_2(\rho)}{T_n} \tag{3.13}$$

where $c_1(\rho) = \frac{1}{1 + 0.35/\rho^{0.65}}$ and $c_2(\rho) = \frac{1}{8 + 25\rho^{0.4}}$

where T_n is the fundamental period and ρ is the beam-column stiffness ratio.

Equation (3.13) is derived for regular frames (i.e. constant height and stiffness throughout the height of the frame). Therefore, the validity of the equation is checked for irregular moment resisting frames in Figure 3.23. A strong correlation exists between γ_{MF} obtained from modal analysis and γ_{MF} calculated from Equation (3.13) with a correlation coefficient of 0.97.

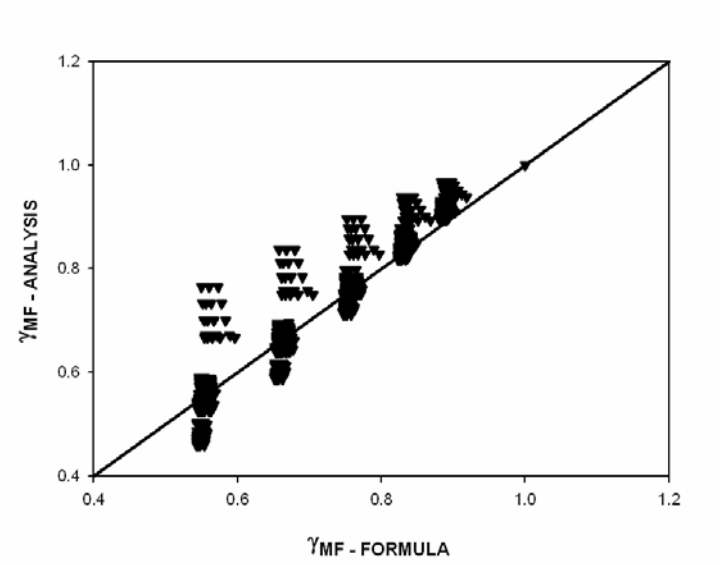

Figure 3.23: Comparison of γ_{MF} values calculated from modal analysis and the Equation (3.13)

From Equation (3.12) it is seen that regular story height does not have any effects on γ_{MF} since mode shapes and participation factors do not change with regular story height. In addition, it is observed that there are no significant effects of soft story factor and stiffness distribution coefficient on γ_{MF}. Another observation is that Equation (3.13) leads to acceptable errors that depend on number of stories. Figure 3.24 shows that Equation (3.13) overestimates and underestimates the response for 20 story and 3-story irregular MRFs, respectively. However, it estimates approximately required response for 9-story irregular MRFs. Mean and standard deviation of the errors considering all the frames are 1.0 and 0.059, respectively.

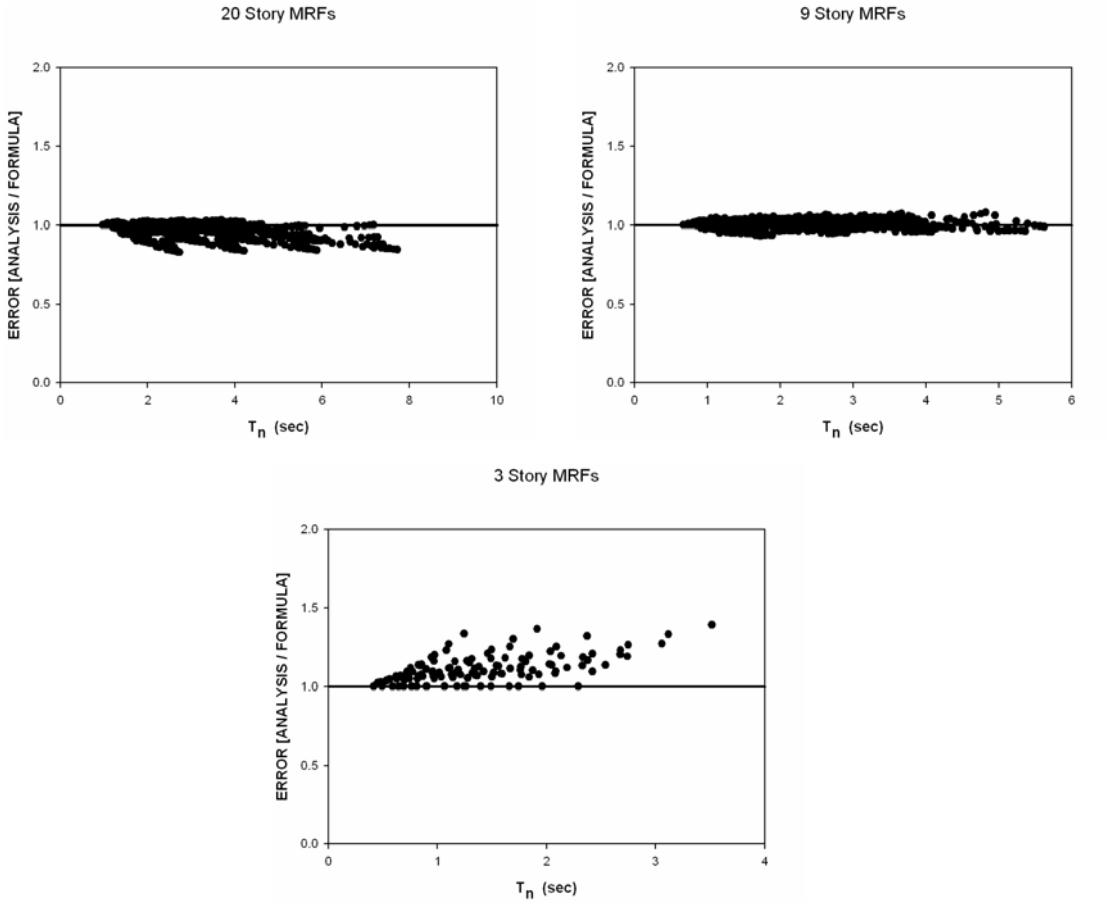

Figure 3.24: Error of Equation (3.13)

Yazgan [72] eliminates $\frac{S_d(T_1)^{MF}}{S_d(T_1)^{SH}}$ ratio in Equation (3.12), since masses are adjusted in order to obtain the same period for moment frame and shear frame. As a result, $S_d(T_1)$ for systems with the same period and damping is the same and γ_{MF} depends on only the first mode participation factors and the first mode shapes of the shear frame and moment frame. However, in this study masses remain constant as defined in SAC Steel Projects. Therefore, shear frame and moment resisting frame have different periods and $\frac{S_d(T_1)^{MF}}{S_d(T_1)^{SH}}$ ratio can not be eliminated in this study. This ratio is included as a multiplier to γ_{MF} given in Equation (3.13).

Then $GSDR'_{MF}$ (ground story drift ratio of uniform or nonuniform moment resisting frame) can be represented through Equation (3.14)

$$GSDR'_{MF} = 1.27 \cdot \frac{1}{h} \cdot \sin(\frac{\pi}{2N}) \cdot \gamma_{MF} \cdot \alpha \cdot S_d(T_1, \xi_1)^{MF} \tag{3.14}$$

Modal analysis results are used by Yazgan [72] in the development of the coefficient γ_{MIDR} in Equation (3.11). First mode contribution to the interstory displacement at the nth story, $\Delta_{1,n}$, is computed as follows

$$\Delta_{1,n} = \Gamma_1(\phi_{n,1} - \phi_{n-1,1})D_1(t) \tag{3.15}$$

where Γ_1 is the modal participation factor of the first mode, $\phi_{n,1}$ and $\phi_{n-1,1}$ are the drifts of nth story and the story below nth story in the first mode, respectively. In fact, γ_{MIDR} is the ratio of maximum interstory drift ratio to the ground story drift ratio. Considering the first mode response γ_{MIDR} is defined as

$$\gamma_{MIDR} = \frac{\max\left[\frac{\phi_{n,1} - \phi_{n-1,1}}{h}\right]}{\frac{\phi_{1,1}}{h_{GROUND}}} \tag{3.16}$$

where $\max\left[\frac{\phi_{n,1} - \phi_{n-1,1}}{h}\right]$ is the maximum interstory drift ratio in the fundamental mode and $\frac{\phi_{1,1}}{h_{GROUND}}$ is the ground story drift ratio in the fundamental mode. As a result of the regression analyses, γ_{MIDR} is expressed by Akkar et al. [3] as

$$\gamma_{MIDR} = e^{(c_3(\rho) - c_4(\rho)/T_n)} \tag{3.17}$$

where $c_3(\rho) = \dfrac{1}{2\rho + 1}$ and $c_4(\rho) = \dfrac{0.07}{\rho^{0.25}}$

The modification factor γ_{MIDR} equals to 1 for large ρ which provides the necessary limiting requirement for shear frames. Equation (3.17) is generated for frames with constant story height and cross-section throughout the height of the frame. In Figure 3.25, γ_{MIDR} values calculated from Equation (3.17) are compared with the modal analysis results for regular frames. It is seen that it gives fairly good estimates with an error limit of ± 4 percent. However, when this formula is utilized for irregular frames, it may provide inaccurate estimates. Figure 3.26 shows the scatter diagram of the error if Equation (3.17) is used for irregular moment resisting frames ($\psi \neq 1.0$ and $\lambda \neq 1.0$). An aim of this study is to improve Equation (3.17) in order to make use of the procedure proposed by Akkar et al. [3] for irregular frames.

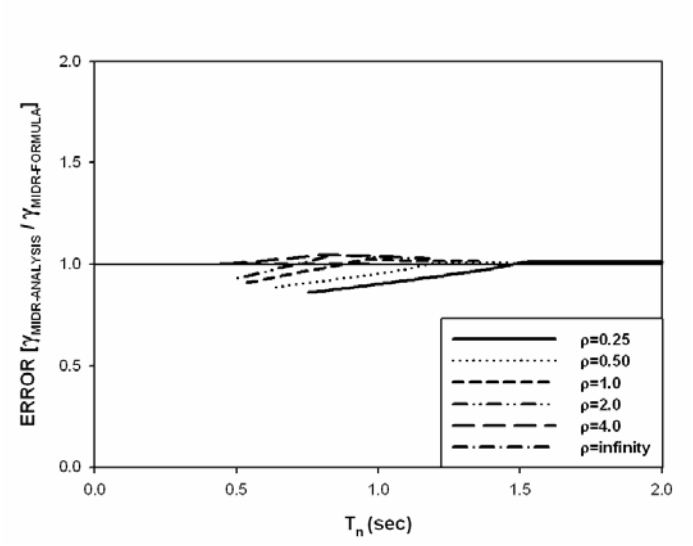

Figure 3.25: Error of Equation (3.17) for regular frames

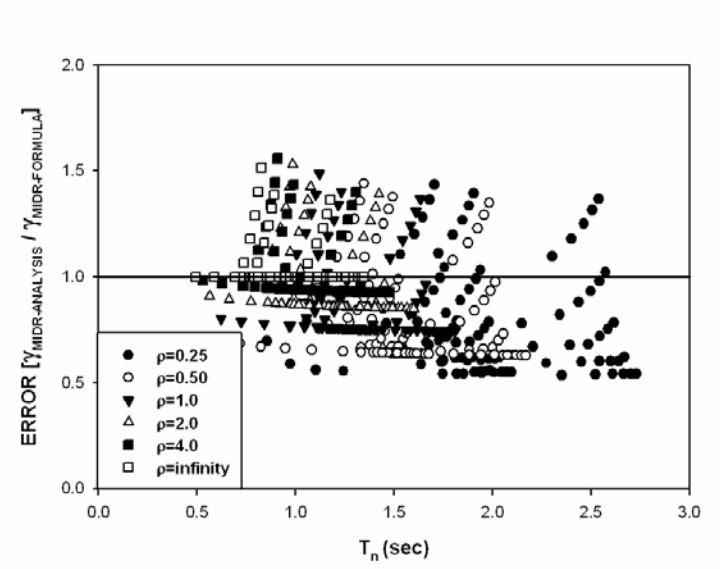

Figure 3.26: Error of Equation (3.17) for irregular frames

When regression analyses are performed for γ'_{MIDR} and the following improved equation is obtained:

$$\gamma'_{MIDR} = \max\left[\left\{a_{MIDR} \times b_{MIDR} \times \exp(c_{MIDR} - \frac{d_{MIDR}}{T_n})\right\} or\, 1\right] \tag{3.18}$$

where $a_{MIDR} = 1 + 0.1N^{0.32}\ln(\lambda)$ $\quad$ $b_{MIDR} = 1 - 1.36\ln(\psi)$

$$c_{MIDR} = \frac{1}{0.12N\rho + 1} \qquad d_{MIDR} = \frac{0.6N^{-0.58}}{\rho^{0.26}}$$

where a_{MIDR} and b_{MIDR} are correction factors for presence of non-uniform stiffness distribution and soft story, respectively. λ and ψ are stiffness distribution coefficient and soft story factor, respectively. ρ, T_n and N are the beam-to-column stiffness ratio, fundamental period and number of stories, respectively. γ'_{MIDR} does not depend on regular story height because the fundamental mode shapes are not

influenced by h_2. There are three boundary conditions for Equation (3.18). First boundary condition is that γ'_{MIDR} should be equal to 1.0 for $\rho = \infty$, because maximum interstory drift is always at the ground story in the first mode of shear frames. Second and third boundary conditions are that a_{MIDR} and b_{MIDR} should be equal to 1.0 for frames with λ=1.0 and ψ=1.0, respectively. It can be seen that these three limiting conditions are met in Equation (3.18). Figure 3.27 illustrates comparison of γ_{MIDR} calculated from modal analysis results with γ'_{MIDR} values calculated by using Equation (3.18). It can be seen that $\gamma_{MIDR(ANALYSIS)}$ appear to be linearly related to γ'_{MIDR} with a correlation coefficient of 0.99. As a result, Equation (3.18) provides good improvement in prediction of maximum interstory drift ratio of irregular buildings.

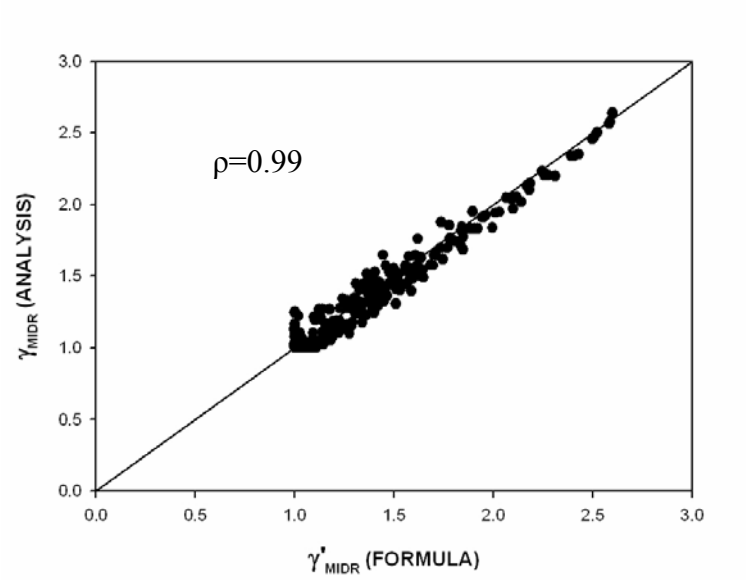

Figure 3.27: Comparison of γ_{MIDR} values calculated from analysis and Equation (3.18)

To sum up, the maximum interstory drift ratio of an irregular moment resisting frame can be calculated by using Equation (3.19).

$$MIDR'_{MF} = 1.27 \cdot \frac{1}{h} \cdot \sin(\frac{\pi}{2N}) \cdot \gamma_{MF} \cdot \alpha \cdot S_d(T_1, \xi_1)^{MF} \cdot \gamma'_{MIDR} \quad (3.19)$$

where $MIDR'_{MF}$ is the maximum interstory drift ratio, $S_d(T_1, \xi_1)^{MF}$ is the spectral displacement of an SDOF system with the first mode period and damping ratio of the moment resisting frame, h is the ground story height and N is the number of stories. γ'_{MIDR} is the coefficient that modifies ground story drift ratio to maximum interstory drift ratio calculated with Equation (3.18) and γ_{MF} is the factor that modifies GSDR of shear frame to GSDR of moment resisting frame expressed with Equation (3.13). α is the modification factor of $GSDR_{SH}$ for irregular shear frames and its formula is given in Equation (3.9). It should be noted that $GSDR'_{SH}$, γ_{MF} , γ'_{MIDR} and α are based on the first mode responses.

Error statistics associated with the estimates obtained from Equations (3.3), (3.14) and (3.19) will be evaluated in Chapter 5.

3.5 SUMMING UP THIS CHAPTER

Idealized multi-story frames contain many features that have an impact on how they are likely to respond to imposed ground motions. These are itemized below:

- beam to column stiffness ratio (ρ),
- stiffness distribution along the elevation (λ),
- soft story factor (ψ),
- regular story height (h_2)
- number of stories (N)

These have been identified and examined in detail in this chapter as regards the way they affect story drifts either at the base or along the height of the frame. The vast number of calculations of dynamic response allows a better insight on the relative importance of these structural parameters. Equations (3.3) and (3.18) should be considered as improved versions of similar expressions presented by Gülkan and Akkar [26] and Akkar et al. [3] for these non-uniform frames.

CHAPTER 4

INELASTIC MULTI-DEGREE-OF-FREEDOM ANALYSIS

4.1 INTRODUCTION

Recently introduced seismic displacement-based design criteria use displacements as demand parameters for the design, evaluation and rehabilitation of buildings. In order to utilize such criteria for preliminary design and rapid assessment simplified analysis procedures are required to estimate inelastic displacement demands of structures expected to behave in inelastic fashion.

The objective of this chapter is to investigate the effects of several structural parameters on the inelastic response of multi-degree-of-freedom (MDOF) systems subjected to near-fault ground motions and the ratio of maximum inelastic interstory drift to maximum elastic interstory drift. This exercise is expected to complement and expand observations of the previous chapter. The parameters that are considered are as follows:

(i) beam to column stiffness ratio (ρ),
(ii) stiffness distribution along the elevation (λ),
(iii) soft story factor (ψ),
(iv) the ratio of pulse period to fundamental period (T_p/T_n),
(v) beam to column capacity ratio (Q),
(vi) seismic force reduction factor (q),

(vii) regular story height (h_2) and
(viii) number of stories (N)

When all of these permutations are investigated 542,880 inelastic time history analyses must be conducted, which is unfeasible. Further, most structural systems would be expected to display properties that can not be captured by the range of the parameters that will be included in the following. The aim is to reflect any trends that may exist, rather than make categorical statements. As final product of this exercise an equation for the ratio of maximum inelastic interstory drift ratio to maximum elastic interstory drift ratio will be developed for a representative case is presented at the end of the chapter.

4.2 INELASTIC MODELLING

As stated in Chapter 2, the generic frame models consist of columns and springs placed at the story levels. In these generic frame models, lumped plasticity approach is utilized by assigning elastoplastic moment curvature relations to the column ends and the springs. Yielding takes place only in the plastic hinges. The hinge yield moments are specified to be the same at two column elements ends. In this study, the inelastic behavior of structural systems is controlled by beam to column capacity ratio (Q), defined as the ratio of beam capacities to column capacities. The expression of Q is given in Equation 2.13. In order to obtain constant Q along the height of the structure, capacities of columns are kept constant and girders capacities are adjusted. Figure 4.1 shows the plastic hinge location of 9 story MRFs for different Q values. When Q is equal to 0.2, the failure mechanism follows beam failure pattern that implies strong column-weak beam behavior and hinges occur at girders as shown in Figure 4.1(a). When Q equals to 1.2, the failure mechanism follows column failure pattern that implies weak column-strong beam behavior and hinges occur at column ends as shown in Figure 4.1(b).

(a) Q=0.20 (b) Q=1.20

Figure 4.1: Failure mechanism of 9 story MRF

4.3 DEFINITION OF INELASTIC DRIFT RATIO (C_Δ)

The inelastic drift ratios, C_Δ, is defined as the ratio of maximum inelastic interstory drift ratio, $MIDR_{INELASTIC}$, to the maximum elastic interstory drift ratio, $MIDR_{ELASTIC}$. Its values are computed for moment resisting frames having different structural properties experiencing different levels of inelastic deformation when subjected to 58 near fault ground motions. This ratio is expressed as

$$C_\Delta = \frac{MIDR_{INELASTIC}}{MIDR_{ELASTIC}} \tag{4.1}$$

The ratio defined in Equation (4.1) is used to modify elastic drift. C_Δ permits a rapid estimation of maximum inelastic drift demands from maximum elastic drift demands.

4.4 EFFECTS OF NEAR-FAULT GROUND MOTIONS AND STRUCTURAL PROPERTIES ON THE RESPONSE OF INELASTIC MOMENT RESISTING FRAMES

In this section, effects of beam to column capacity ratio, seismic force reduction factor, the ratio of pulse period to fundamental period, beam to column stiffness ratio, soft story factor, stiffness distribution coefficient, and regular story height on inelastic drift demand and inelastic drift ratio are presented separately for each parameter. Effect of number of stories is examined within the scope of the other parameters.

It is to be expected that very strong interference exists among these parameters to produce a given response quantity. Therefore a discriminating exercise should be conducted to isolate unequivocally the relative weight of each

parameter. This will be done in an ad-hoc fashion because the alternative requires studies that are outside of the present scope.

4.4.1 EFFECT OF BEAM TO COLUMN CAPACITY RATIO (Q)

Beam to column capacity ratio, defined as the ratio of beam capacities to column capacities at the joint, is varied in the range 0.2 - 1.2 at 0.2 increments. Increase in Q increases girder capacities, which results in an increase in the base shear capacity of the structure as shown in Figure 4.2 - 4.5. It is observed that varying Q does not affect base shear capacity of shear frames ($\rho=\infty$). This result is expected because in shear frames beam capacities can not affect the response because they serve only to prevent the rotation of joints. In addition, it is seen that base shear capacity remains constant after Q reaches a value which changes according to the properties of the frame. These Q values represent column yielding mechanisms. These figures show that beam to column stiffness ratio (ρ) and stiffness distribution coefficient (λ) do not have an effect on the value of Q for which column yielding mechanism starts. However, increase in soft story factor (ψ) and the regular story height decreases the value of Q after which column yielding mechanism is initiated. For example, in Figure 4.4 column mechanism occurs for Q values larger than 1.0, 0.8 and 0.6 for ψ values of 1.0, 1.2 and 1.6, respectively. Another observation is that increasing the ground story height, stiffness distribution coefficient and regular story height reduce base shear capacity. Base shear capacity is equal to the sum of the moments at bottom and top ends of the ground story column in the limit state divided by the length of the column. Therefore, base shear capacity reduces with increasing ground story height and regular story height if the two are correlated.

Figures from 4.7 to 4.12 show effects of Q on maximum inelastic interstory drift ratio profiles of moment resisting frames. Mean, mean plus standard deviation and mean minus standard deviation values obtained from 58 ground motions are plotted. It is observed that when capacity ratio is increased from 0.20 to 0.80,

maximum interstory drift ratio decreases and maximum drift ratio location does not change for 20 and 9 story frames. However; for these frames when Q is increased from 0.8 to 1.0 or 1.2, maximum interstory drift ratio increases and its location moves to lower stories as shown in Figure 4.7, 4.8, 4.9 and 4.10. This observation is consistent with Figures 4.2 to 4.5 where it can be seen that column yielding mechanism starts with Q equal to 1.0. Therefore, for beam yielding mechanisms increase in beam capacities reduces maximum interstory drifts, but the drifts increase when column yielding takes place. There is a small change between the maximum interstory drift profiles of Q=1.0 and Q=1.2 because in both cases yielding takes place in the columns, which results in similar drift profiles. In Figure 4.6, it can be observed that column yielding mechanism occurs for Q values greater than 0.8 for 3-story frames with λ and ψ are equal to 1.0. The drift profiles in Figures 4.11 and 4.12 are consistent with this observation. When Q is increased from 0.2 to 0.6, maximum interstory drifts decreases and the location of MIDR moves to lower stories. However, when Q is increased from 0.6 to 0.8, MIDR increases because yielding occurs in the columns. Similar to 9-story and 20-story frames, MIDR profiles of Q=1.0 and Q=1.2 cases display the same trend.

Comparing Figures 4.7 and 4.8 and Figures 4.9 and 4.10, it is observed that frames with higher regular height are subjected to higher inelastic interstory drift ratios. The capacity ratio effect on inelastic drift ratio is investigated in the following sections with other factors.

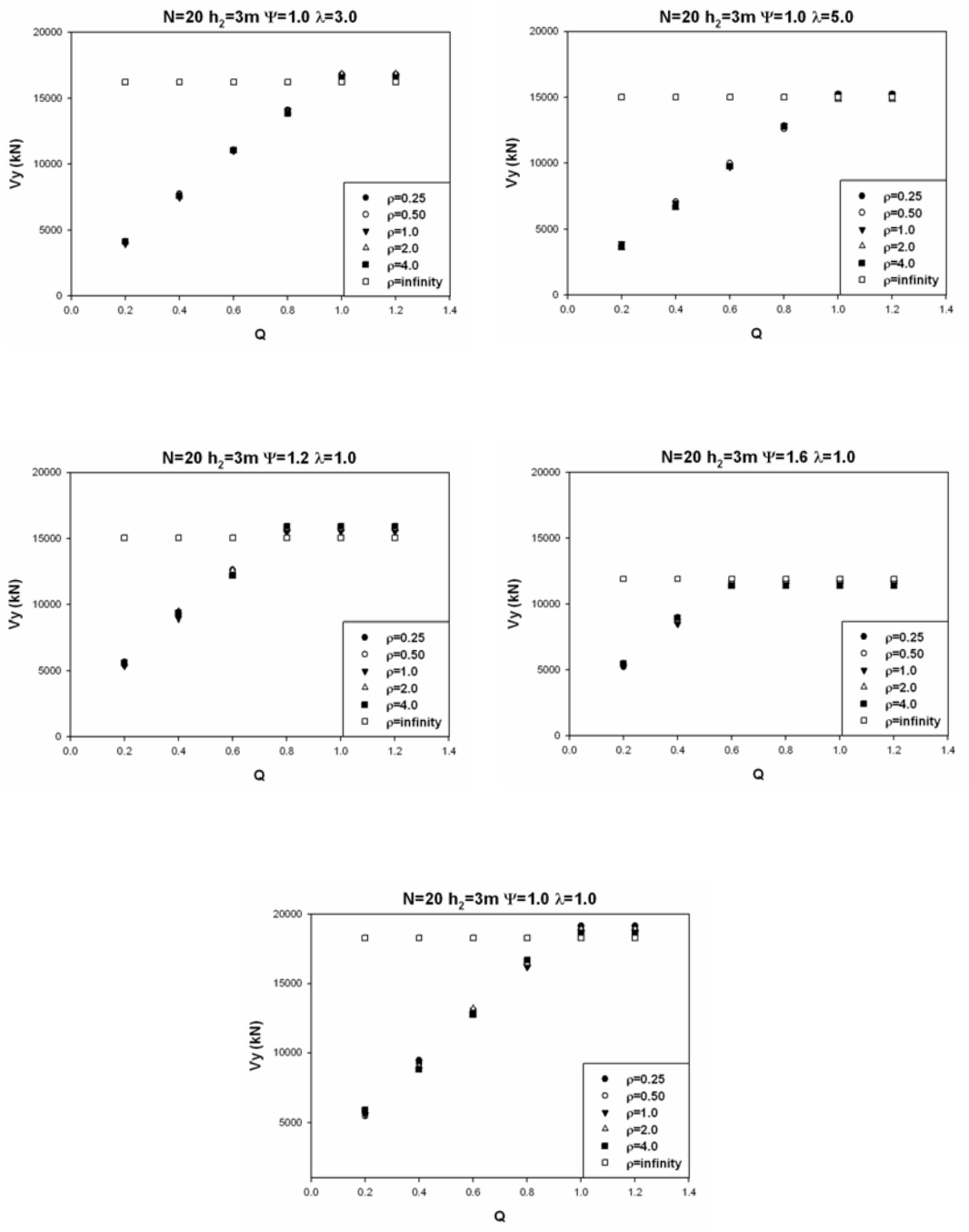

Figure 4.2: Effect of Q on base shear (N=20, h_2=3 m)

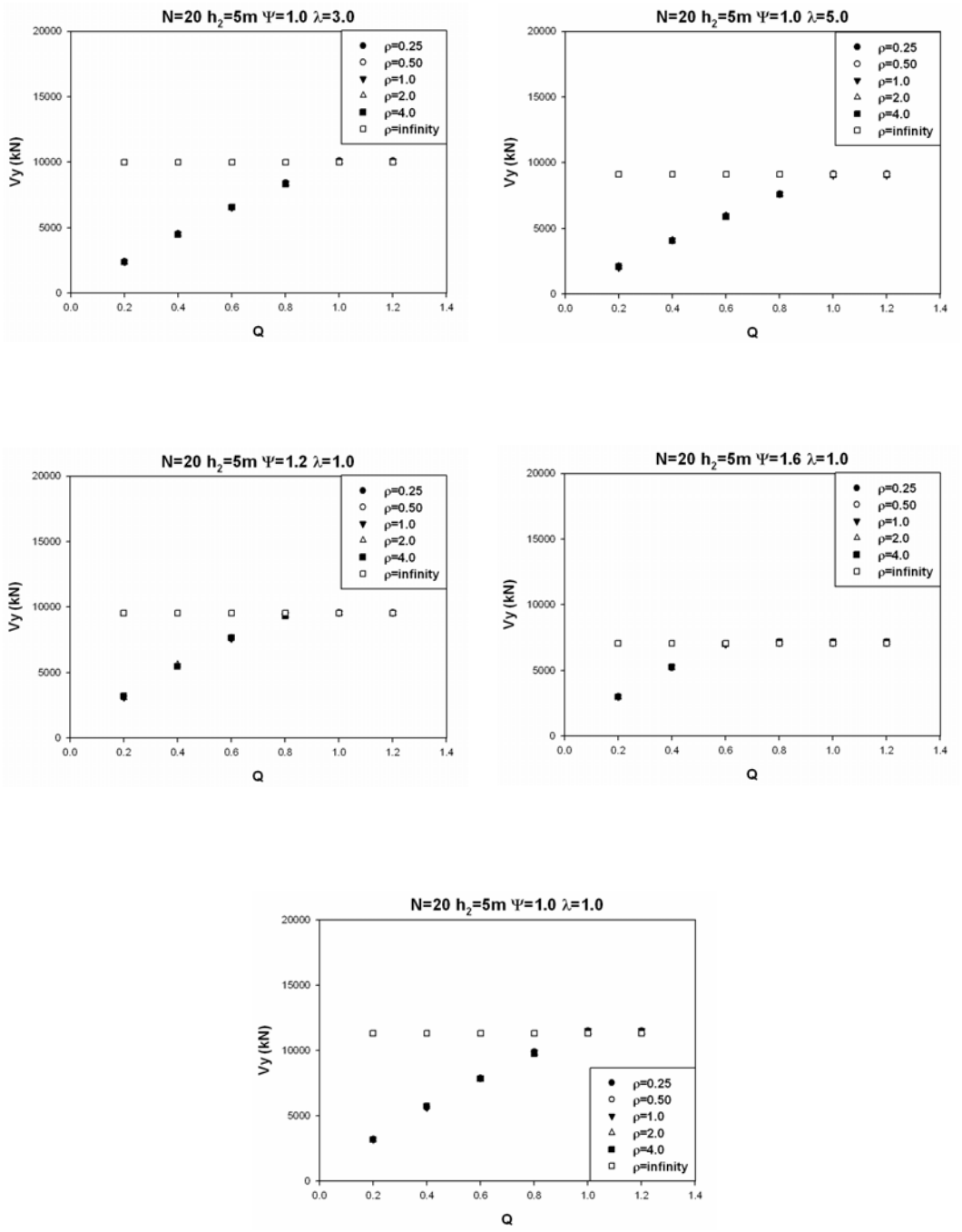

Figure 4.3: Effect of Q on base shear capacity (N=20, h_2=5 m)

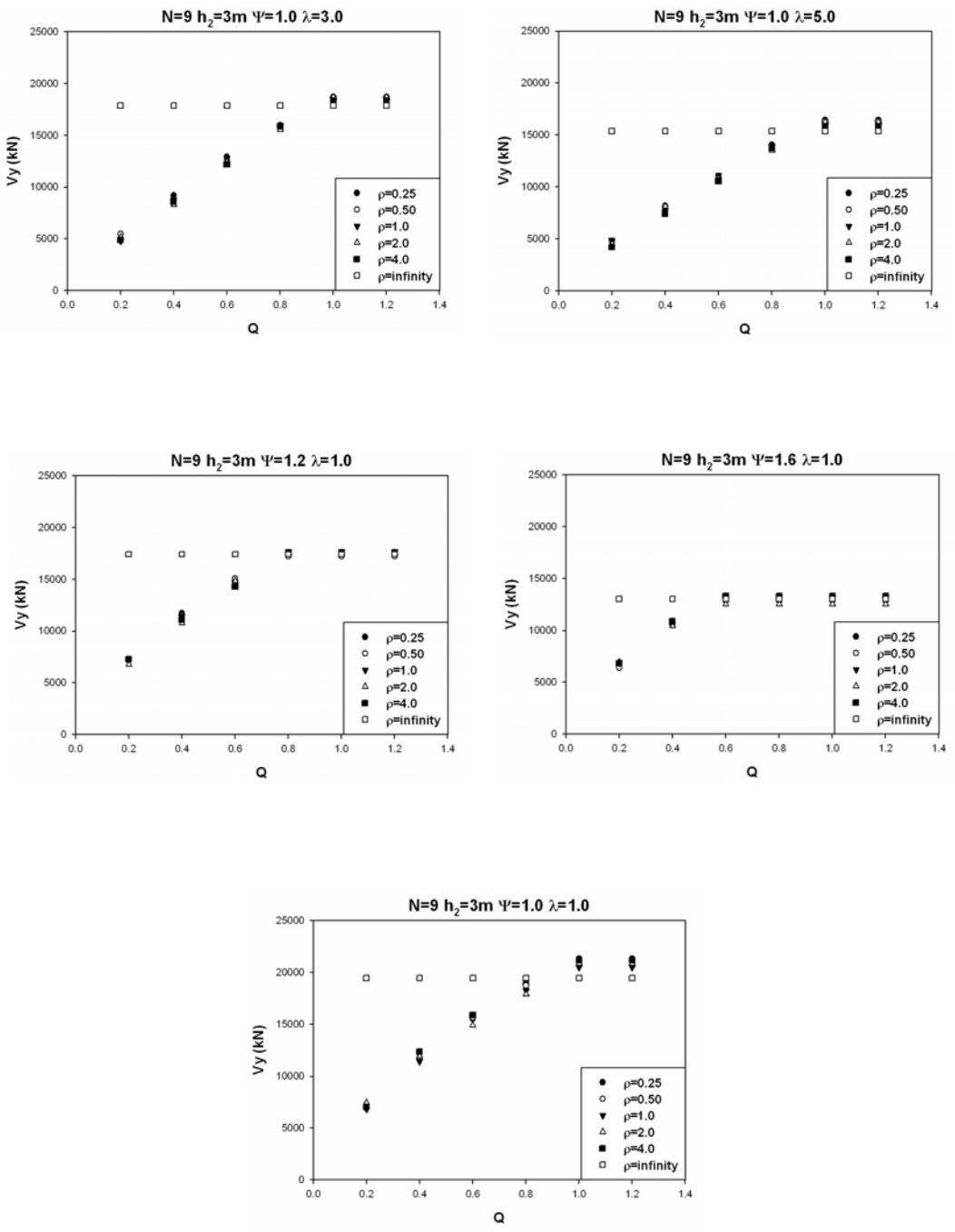

Figure 4.4: Effect of Q on base shear capacity (N=9, h_2=3 m)

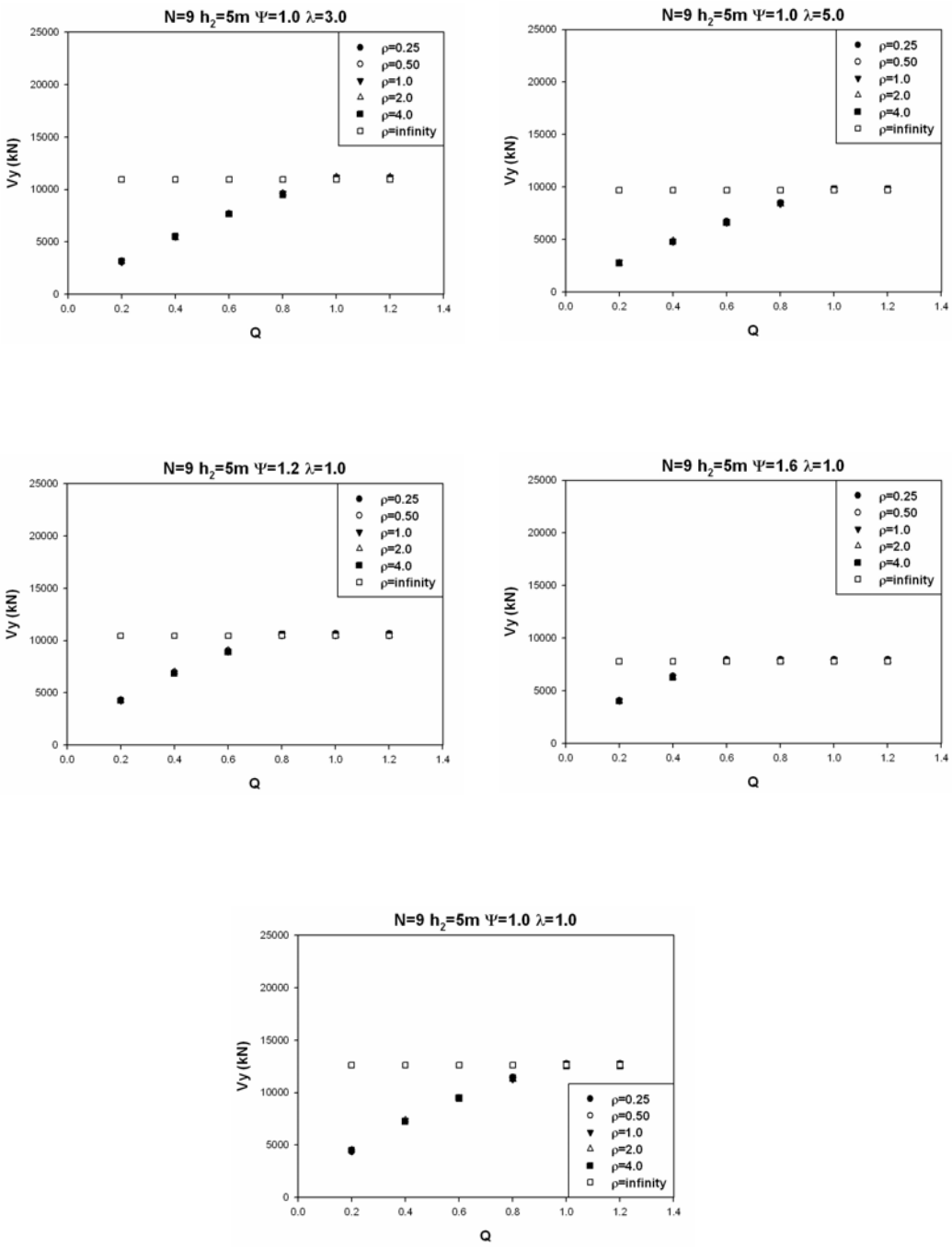

Figure 4.5: Effect of Q on base shear capacity (N=9, h_2=5 m)

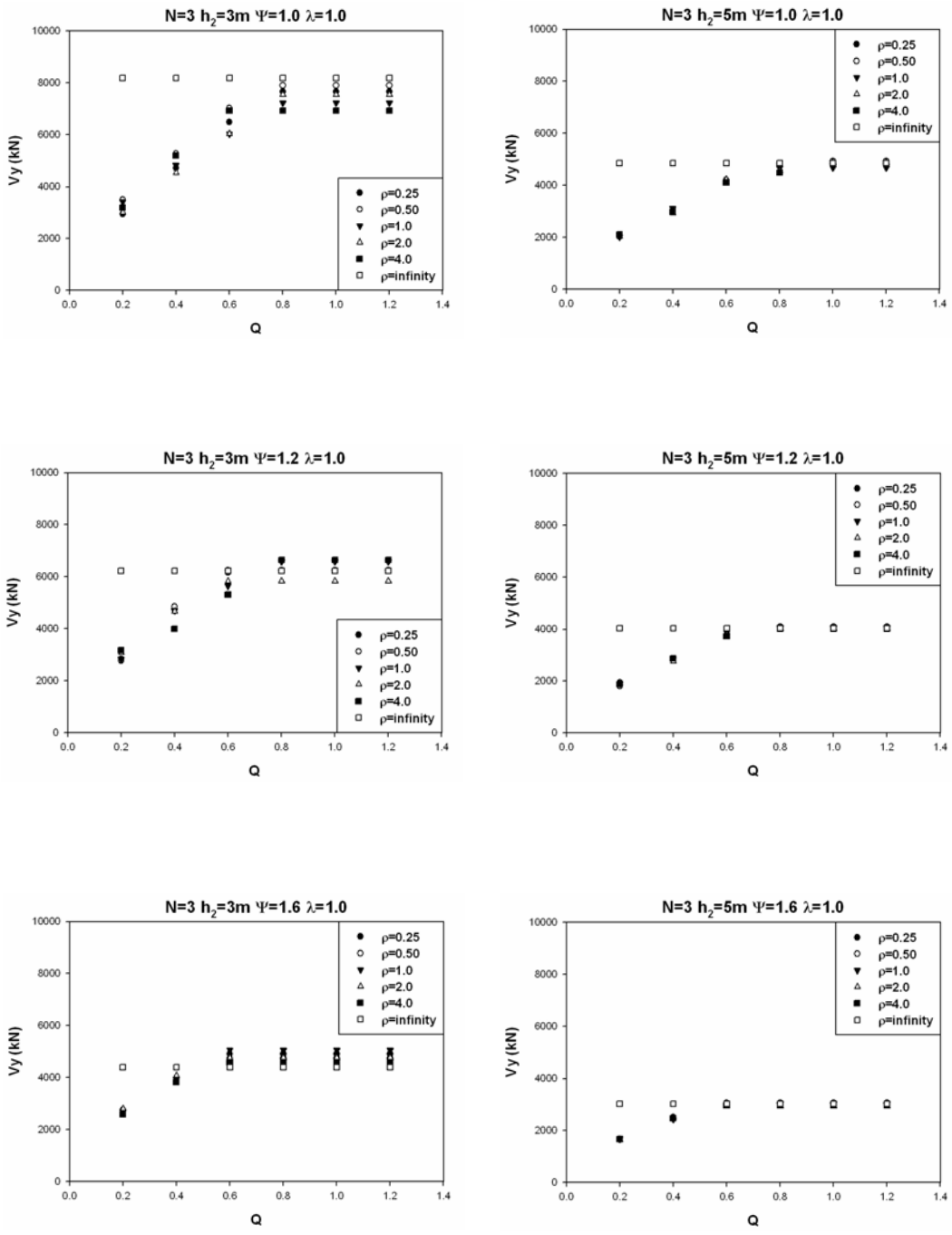

Figure 4.6: Effect of Q on base shear capacity (N=3, h_2=3 m and 5 m)

N=20 h_2=3 m ρ=0.50 ψ=1.0 λ=1.0

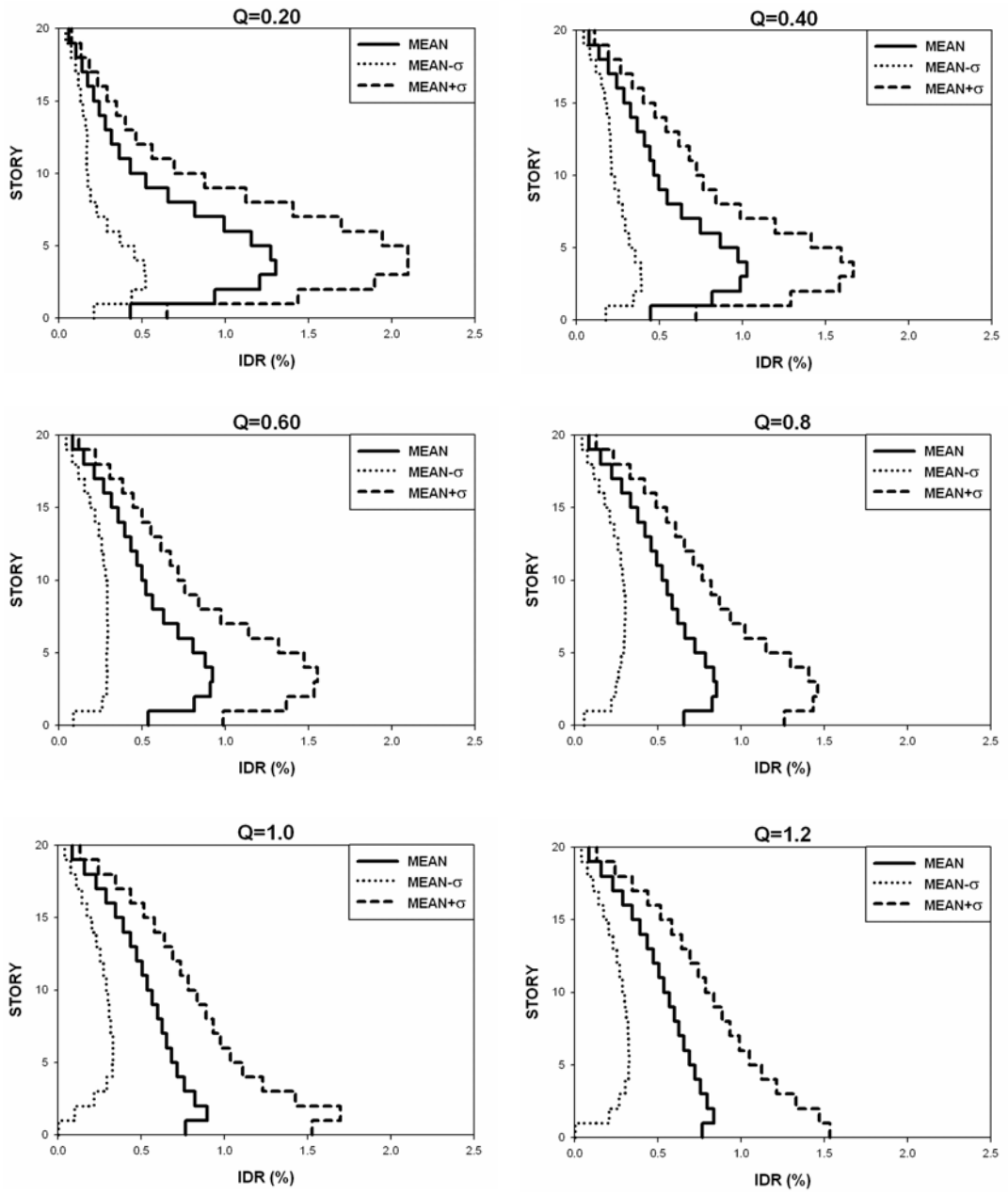

Figure 4.7: Effect of Q on IDR (N=20, h_2=3 m)

N=20 h_2=5 m ρ=0.50 ψ=1.0 λ=1.0

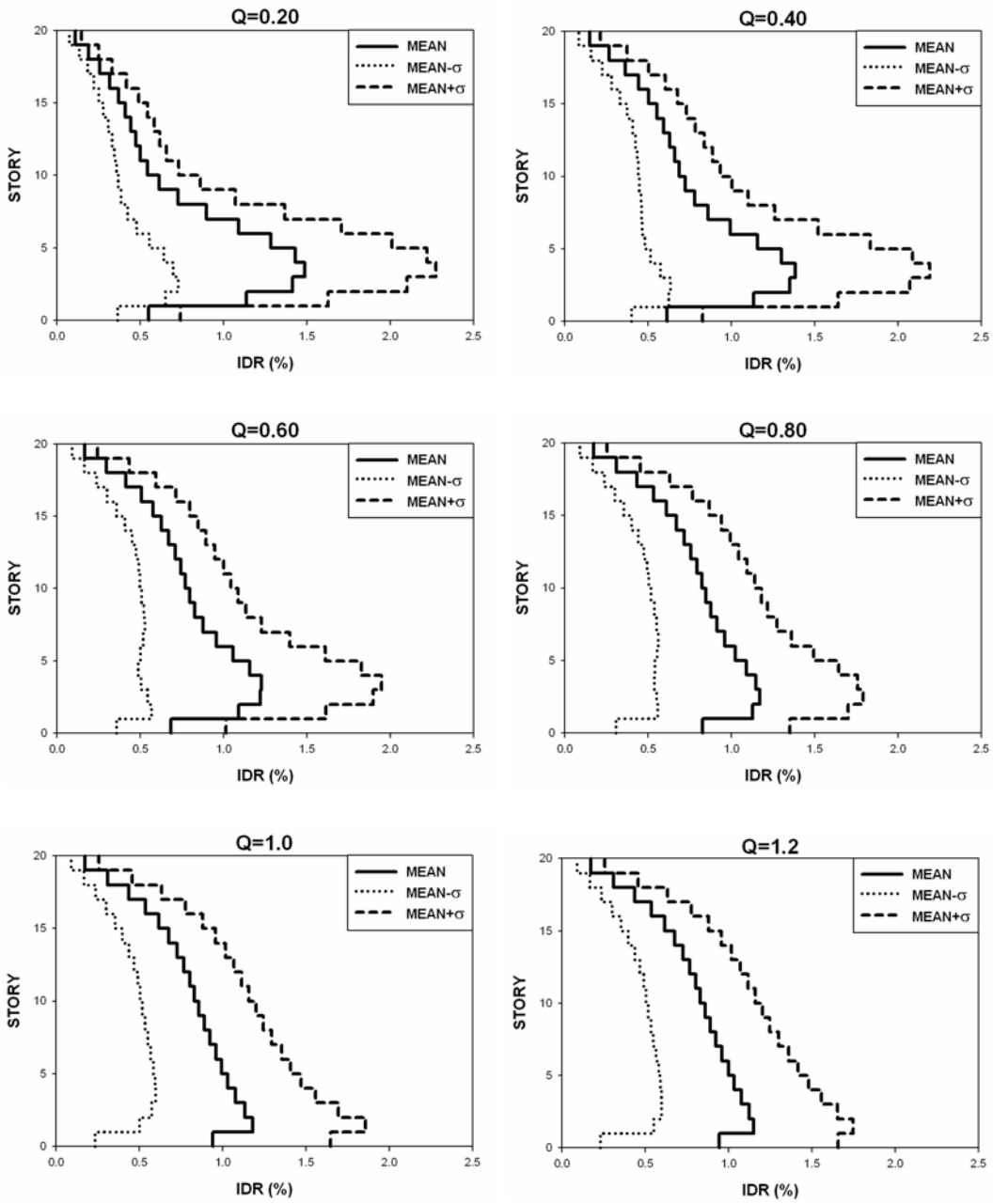

Figure 4.8: Effect of Q on IDR (N=20, h_2=5 m)

N=9 h_2=3 m ρ=0.50 ψ=1.0 λ=1.0

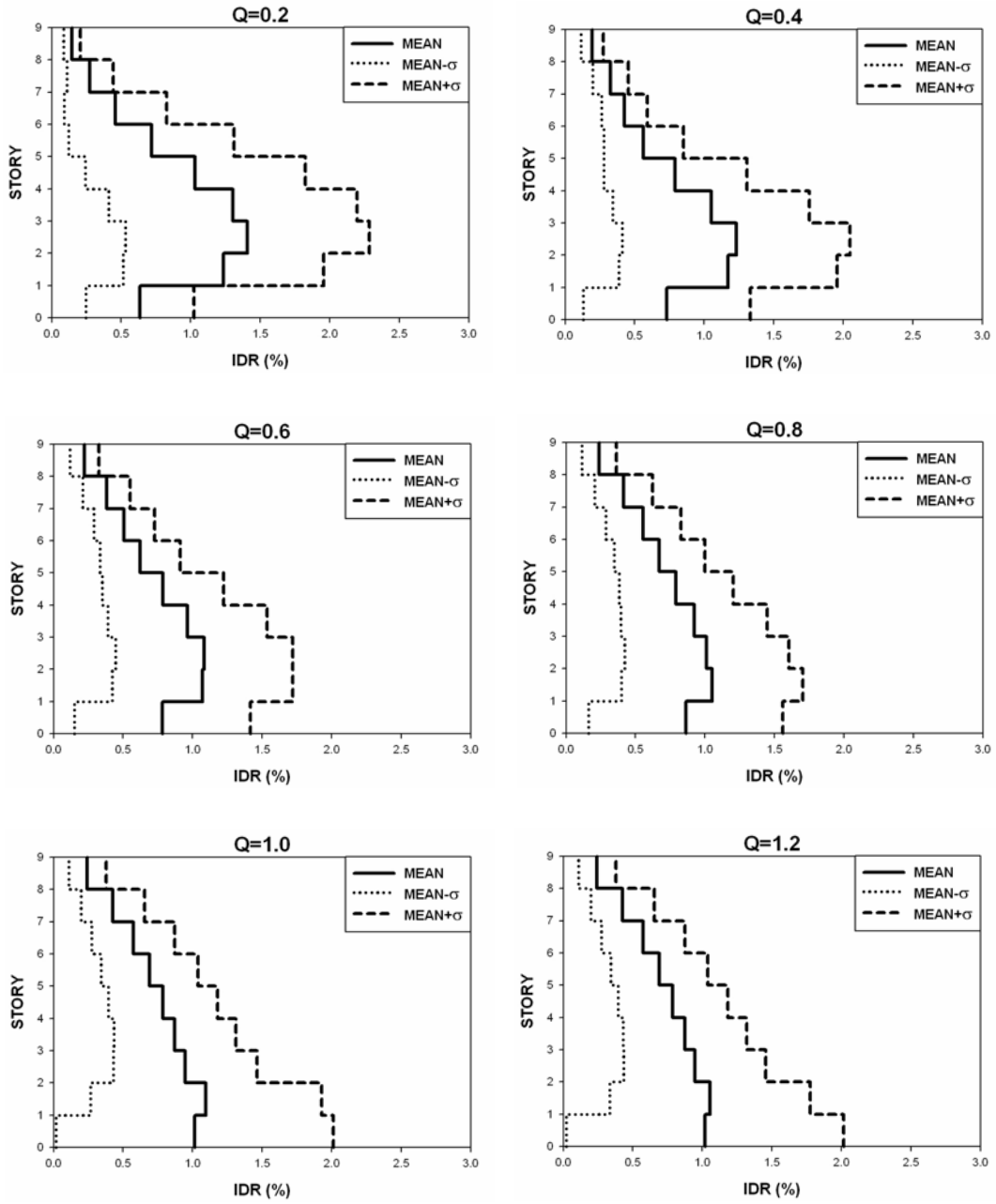

Figure 4.9: Effect of Q on IDR (N=9, h_2=3 m)

N=9 h_2=5 m ρ=0.50 ψ=1.0 λ=1.0

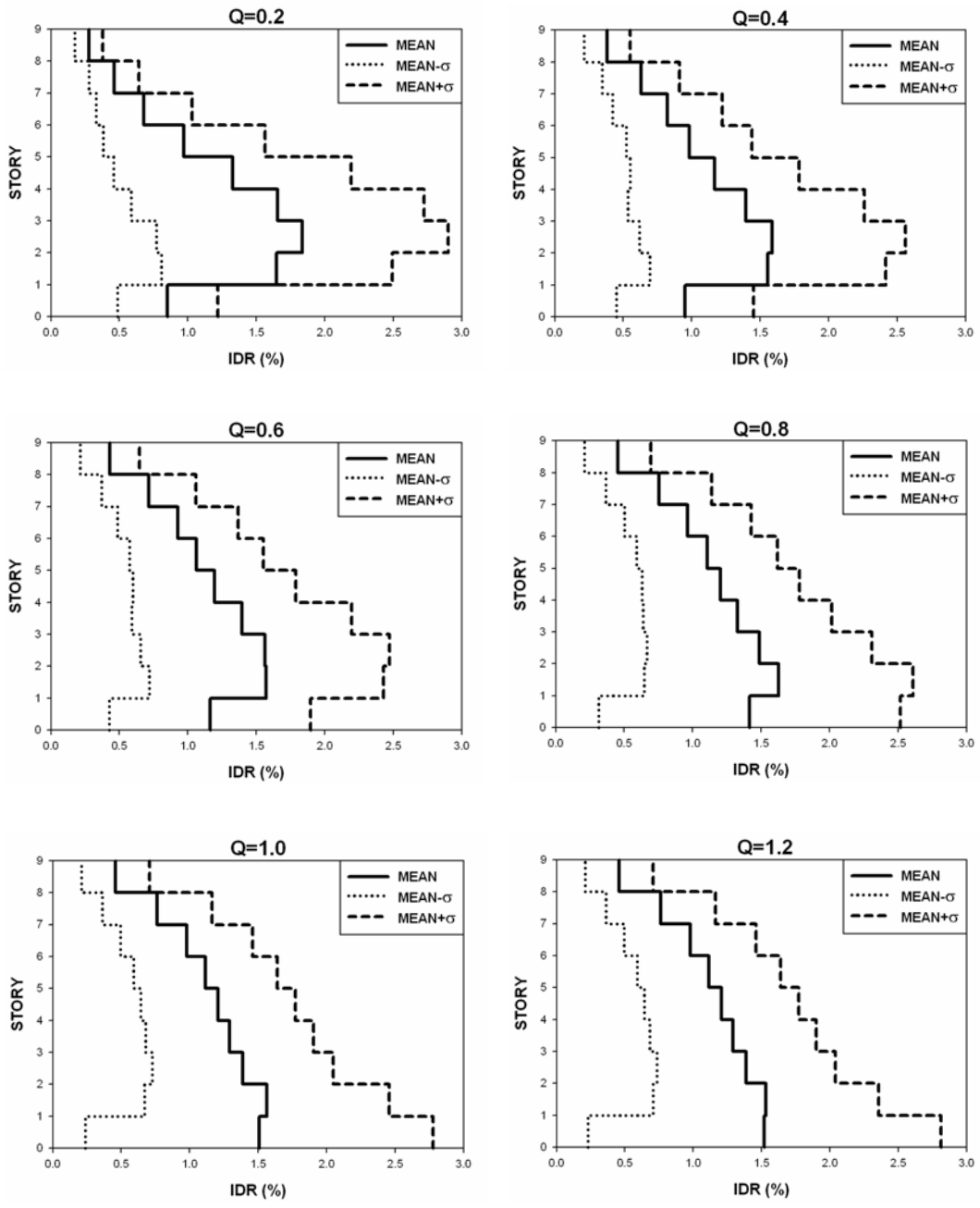

Figure 4.10: Effect of Q on IDR (N=9, h_2=5 m)

N=3 h_2=3 m ρ=0.50 ψ=1.0 λ=1.0

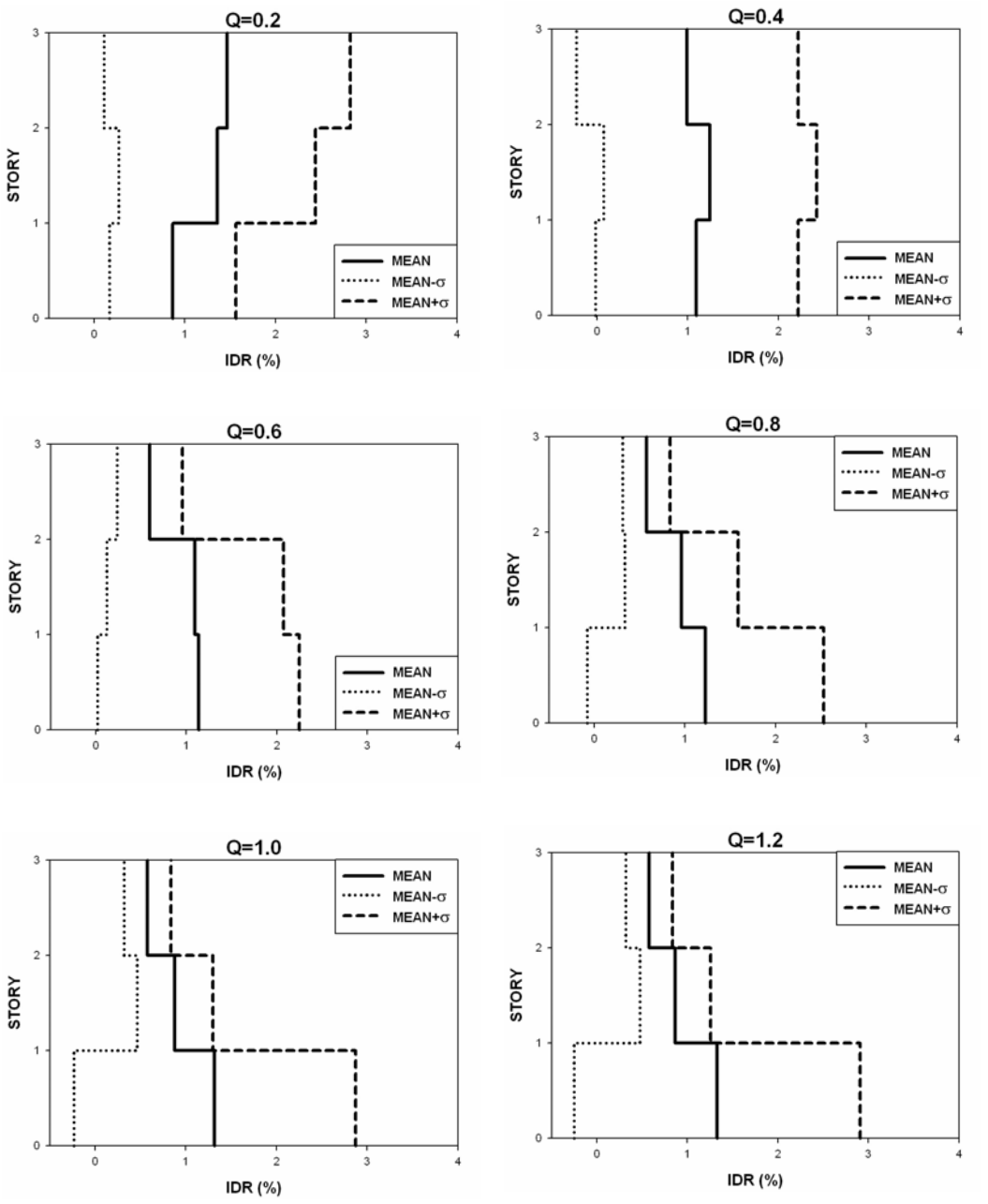

Figure 4.11: Effect of Q on IDR (N=3, h_2=3 m)

N=3 h_2=5 m ρ=0.50 ψ=1.0 λ=1.0

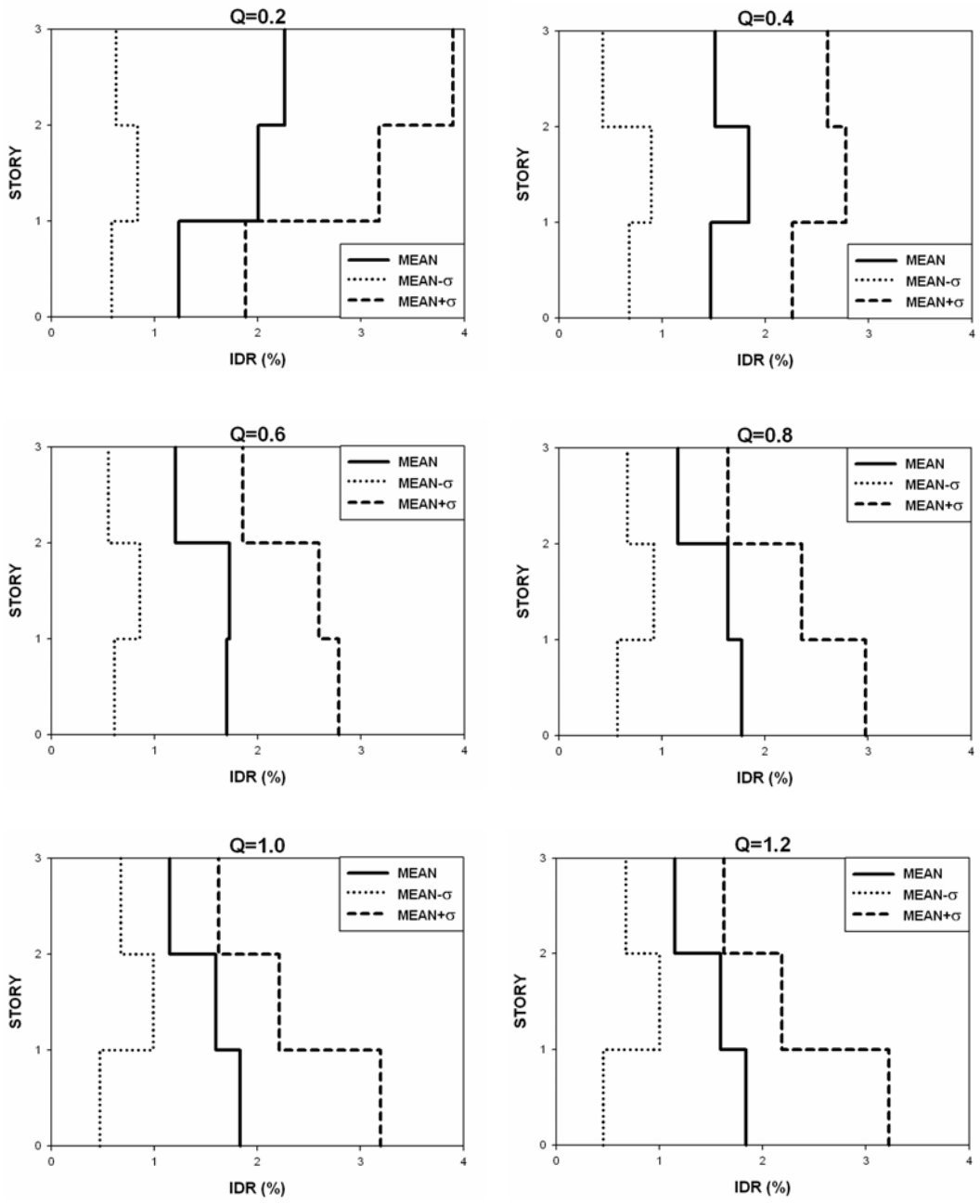

Figure 4.12: Effect of Q on IDR (N=3, h_2=5 m)

4.4.2 EFFECTS OF SEISMIC FORCE REDUCTION FACTOR (q)

The elastic force reduction factor (q) is defined as

$$q = \frac{W \times S_a(T_1, \xi)}{V_y} \tag{4.2}$$

where $S_a(T_1, \xi)$ is the spectral acceleration ordinate corresponding to the fundamental period (T_1) and the viscous damping ratio (ξ) of the system, V_y is the lateral yield strength of the system and W is the weight of the system. The numerator of the Equation 4.2 represents the elastic strength demand. It is obvious that when q is greater than 1.0, the system deforms inelastically. q is less than 1.0 for linear systems. The results corresponding to q values smaller than 1.0 are not utilized during the evaluation because inelastic drift ratio is equal to 1.0 for these cases.

Figure 4.13 shows the scatter plots of changes in the inelastic drift ratio (C_Δ) with respect to q. As a general trend, it is seen that inelastic maximum interstory drift ratio and C_Δ increase with q. For Q=0.20 and Q=0.40 cases, C_Δ values approach 1.0 for large q values. Moreover, it is observed that inelastic maximum interstory drift demands decrease with increasing girder capacities for Q values between 0.20 and 0.6. They start to increase between 0.60 and 1.20, the reason of which is explained in the previous section. Furthermore, increase in Q implies a decrease in the seismic force reduction factor. Frames with higher girder capacity have higher V_y, which reduce the value of q.

The inelastic maximum interstory drift ratio of shear frames shows an increasing trend with increasing q as illustrated in Figure 4.14. Q does not have any effects on maximum inelastic interstory drift ratio of shear frames as shown in Figure 4.14 because beam to column capacity ratio does not change base shear capacity of frame with $\rho=\infty$.

h_2=3 m ρ=0.50 ψ=1.0 λ=1.0

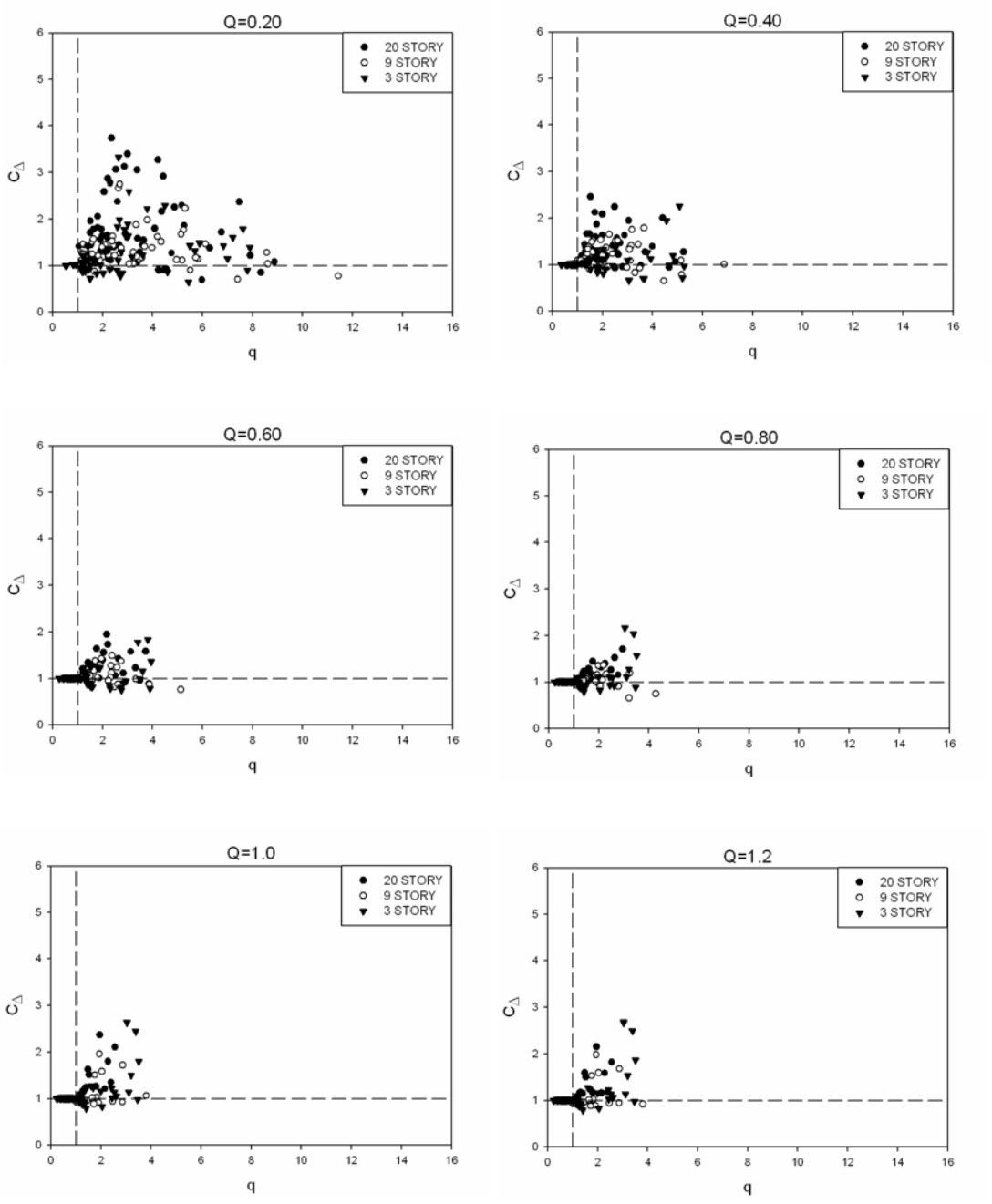

Figure 4.13: Relationship between C_Δ and q (ρ=0.50)

h_2=3 m ρ=∞ ψ=1.0 λ=1.0

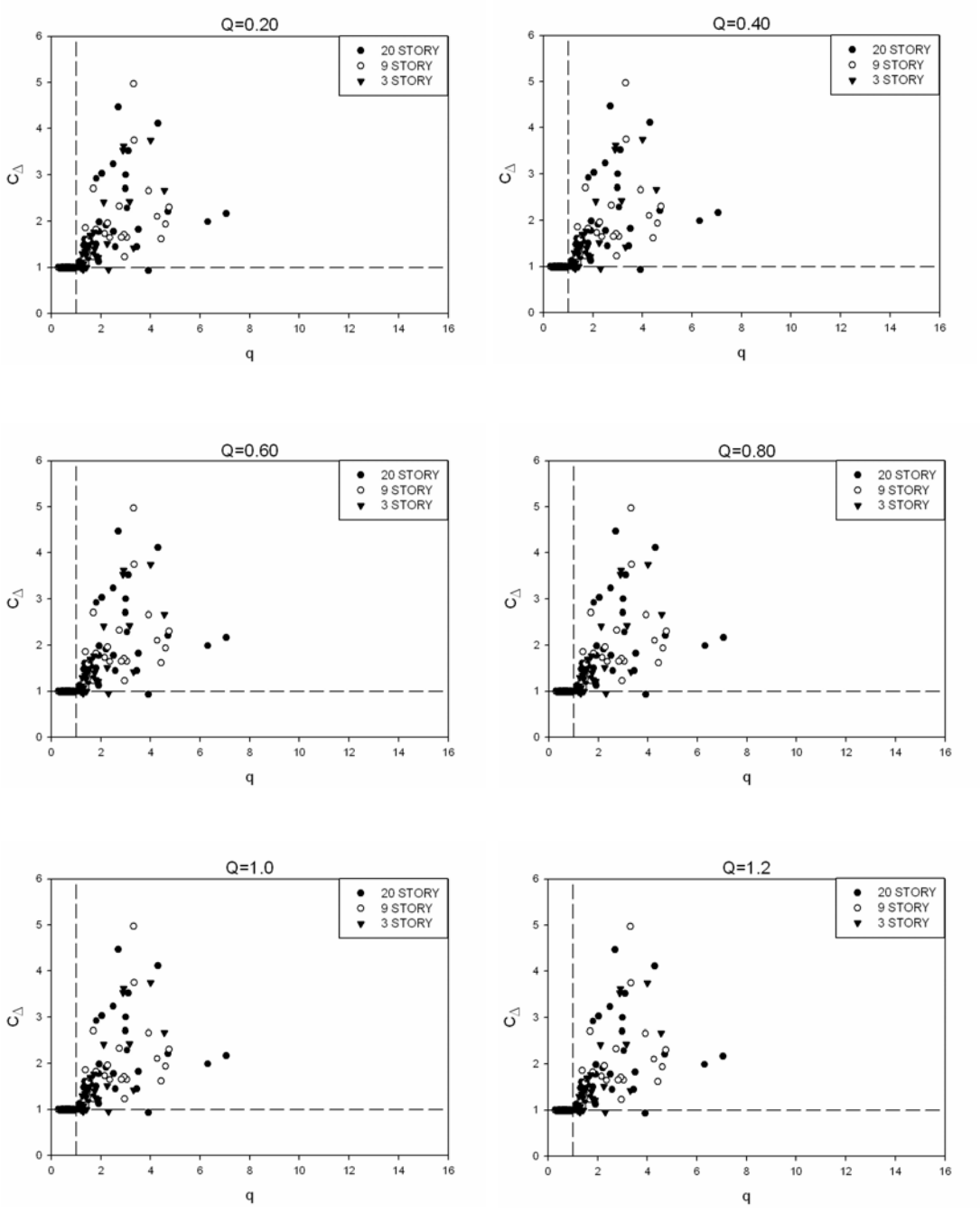

Figure 4.14: Relationship between C_Δ and q (ρ=infinity)

4.4.3 EFFECTS OF THE RATIO OF PULSE PERIOD TO FUNDAMENTAL PERIOD (T_p/T)

Several studies have shown that strong pulses observed in some near fault ground motions affect inelastic displacement demand significantly. Baez and Miranda [47] have found that the inelastic structural response is very sensitive to the presence of long duration acceleration pulses that lead to large inelastic demands.

In order to illustrate T_p/T effect on inelastic drift ratio, scatter diagrams have been plotted in Figure 4.15, 4.16 and 4.17. From these diagrams it is seen that inelastic drift ratio is controlled by the ratio of pulse period to natural period. Theoretically when q increases, degree of inelasticity increases, which increases the amount of period elongation. Therefore, T_p/T values corresponding to maximum inelastic drift ratio should increase as q increases. This trend is observed between $1.0<q<2.0$ and $2.0<q<3.0$ data. However, it is not clearly observable for larger q values since there is smaller amount of data for larger q values. Inelastic drift ratio approaches 1.0 for long period structures and even less depending on the lateral strength capacity. The amplitude of inelastic demand increases as the lateral strength capacity of the structures decreases as stated in previous section.

Inelastic demand of the short period structures (i.e. 3-story MRF) is not affected significantly by pulse signals as shown in Figure 4.17. Amplification factor to estimate inelastic drift demand is higher than 1.0 for 3-story MRFs with $q>3.0$.

20 Story h_2=3 m ρ=0.5 ψ=1.0 λ=1.0

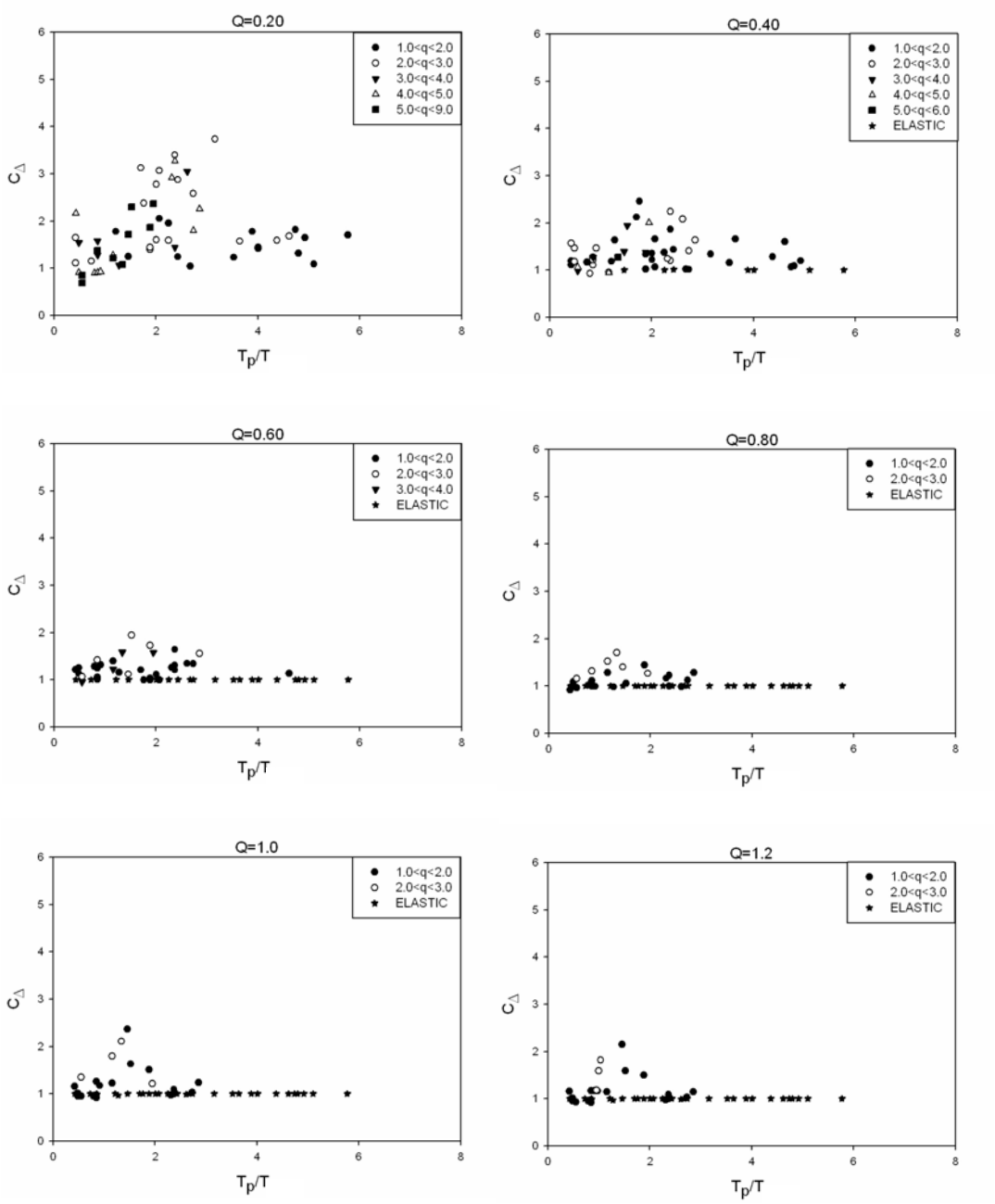

Figure 4.15: Effect of T_p/T on the inelastic drift demand (N=20)

9 Story h_2=3 m ρ=0.5 ψ=1.0 λ=1.0

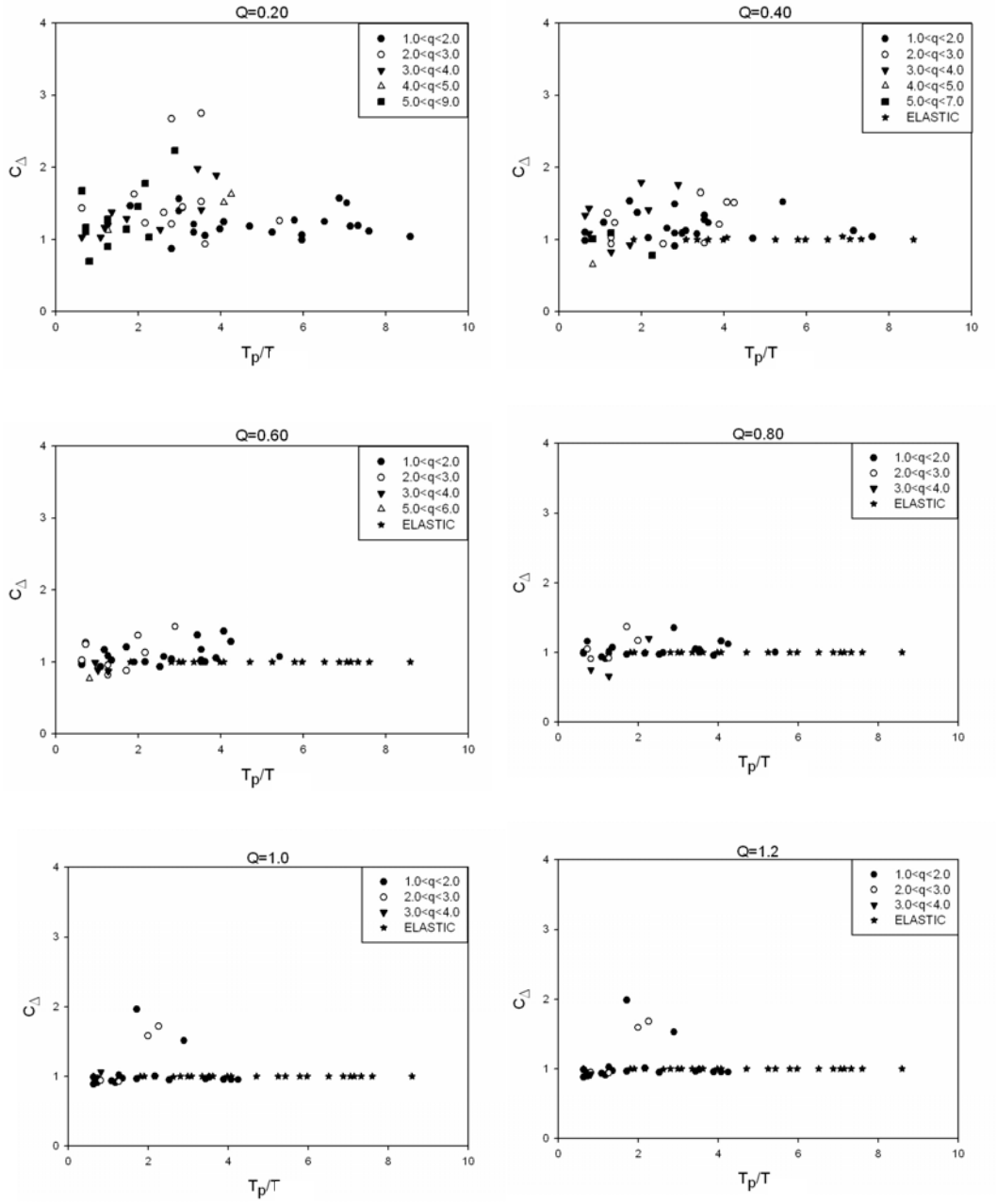

Figure 4.16: Effect of T_p/T on the inelastic drift demand (N=9)

3 Story h_2=3 m ρ=0.5 ψ=1.0 λ=1.0

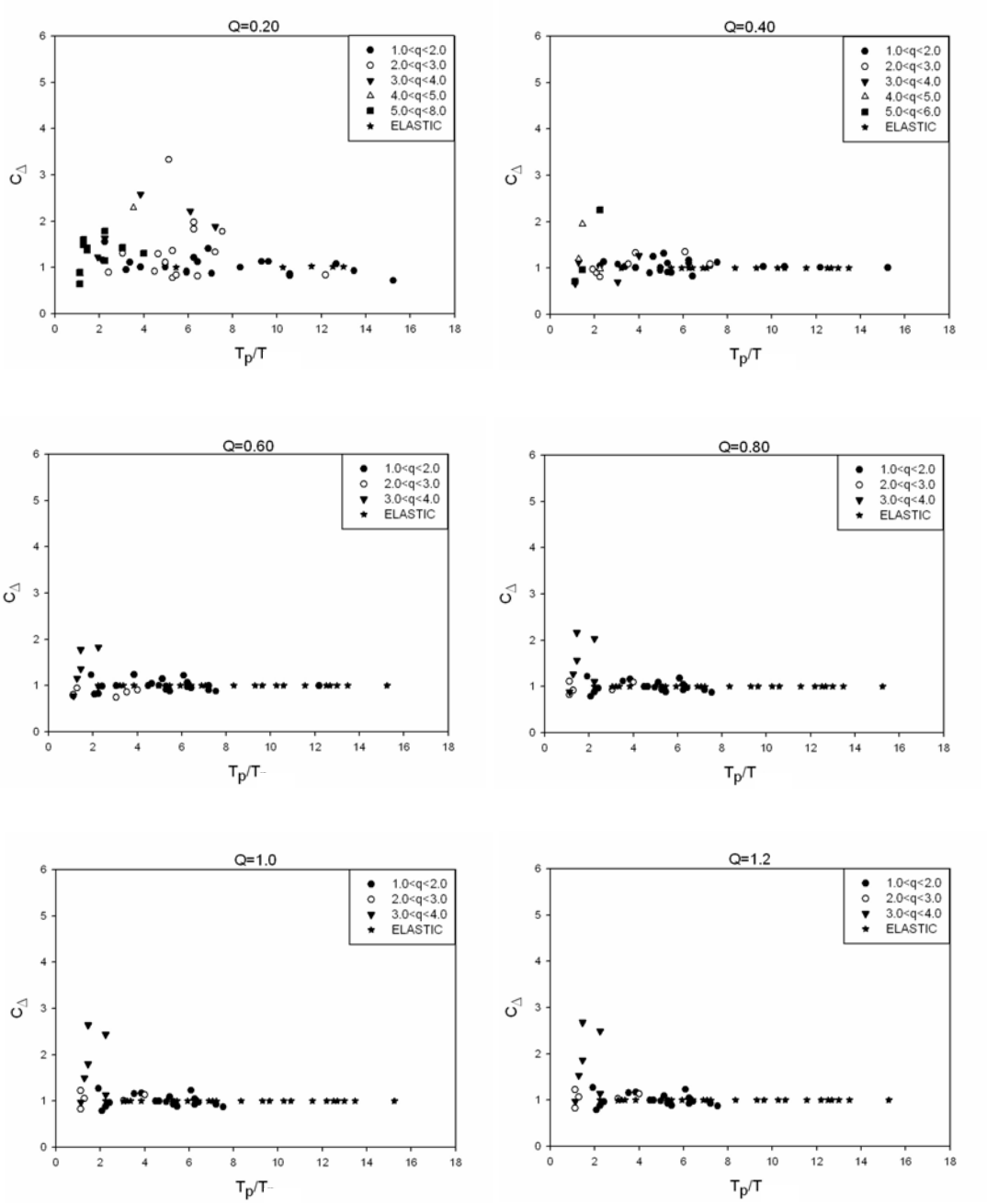

Figure 4.17: Effect of T_p/T on the inelastic drift demand (N=3)

4.4.4 EFFECTS OF BEAM TO COLUMN STIFFNESS RATIO (ρ)

Beam to column stiffness ratio (ρ) is the ratio of sum of beam stiffness to column stiffness at a story. Six different ρ values are utilized in the analyses (ρ=0.25, 0.50, 1.0, 2.0, 4.0 and ∞).

Mean values of maximum elastic and inelastic interstory drift ratio profiles obtained from 58 near fault ground motions are plotted in Figures 4.18, 4.19 and 4.20. Similar to maximum elastic interstory drift demand, inelastic MIDR decreases as beam to column stiffness ratio increases. However, it is observed that when ρ is increased to infinity, MIDR increases and location of MIDR moves to the ground story. Although maximum inelastic interstory drift ratio is higher than maximum elastic interstory drift ratio, inelastic drift demand is not greater than elastic drift demand in all stories.

Figure 4.21, 4.22, 4.23, 4.24 and 4.25 present mean inelastic drift ratios (C_Δ) of different frames. It can be seen that inelastic drift ratio reaches its maximum value when ρ is infinity for regular frames (ψ=1.0, λ=1.0). This phenomenon does not depend on number of stories and beam to column capacity ratio. Strong column–weak beam (e.g. Q=0.40) or weak column–strong beam (e.g. Q=1.2) frames with soft story also have maximum inelastic drift ratio when beam to column stiffness ratio equals to infinity. Inelastic drift ratios of weak column-strong beam frames with soft story show regular increase as ρ is increasing because yielding occurs at weak columns and increasing ρ values stiffens the girders with respect to columns. It can be stated that C_Δ values for strong column-weak beam frames do not show regular increase or decrease pattern as ρ increases. Moreover, changing ρ values of weak column-strong beam and strong column-weak beam frames with stiffness distribution does not significantly influence C_Δ. A very small regular increase in inelastic drift ratio is observed for these frames.

20 Story h_2=3 m Q=0.40 ψ=1.0 λ=1.0

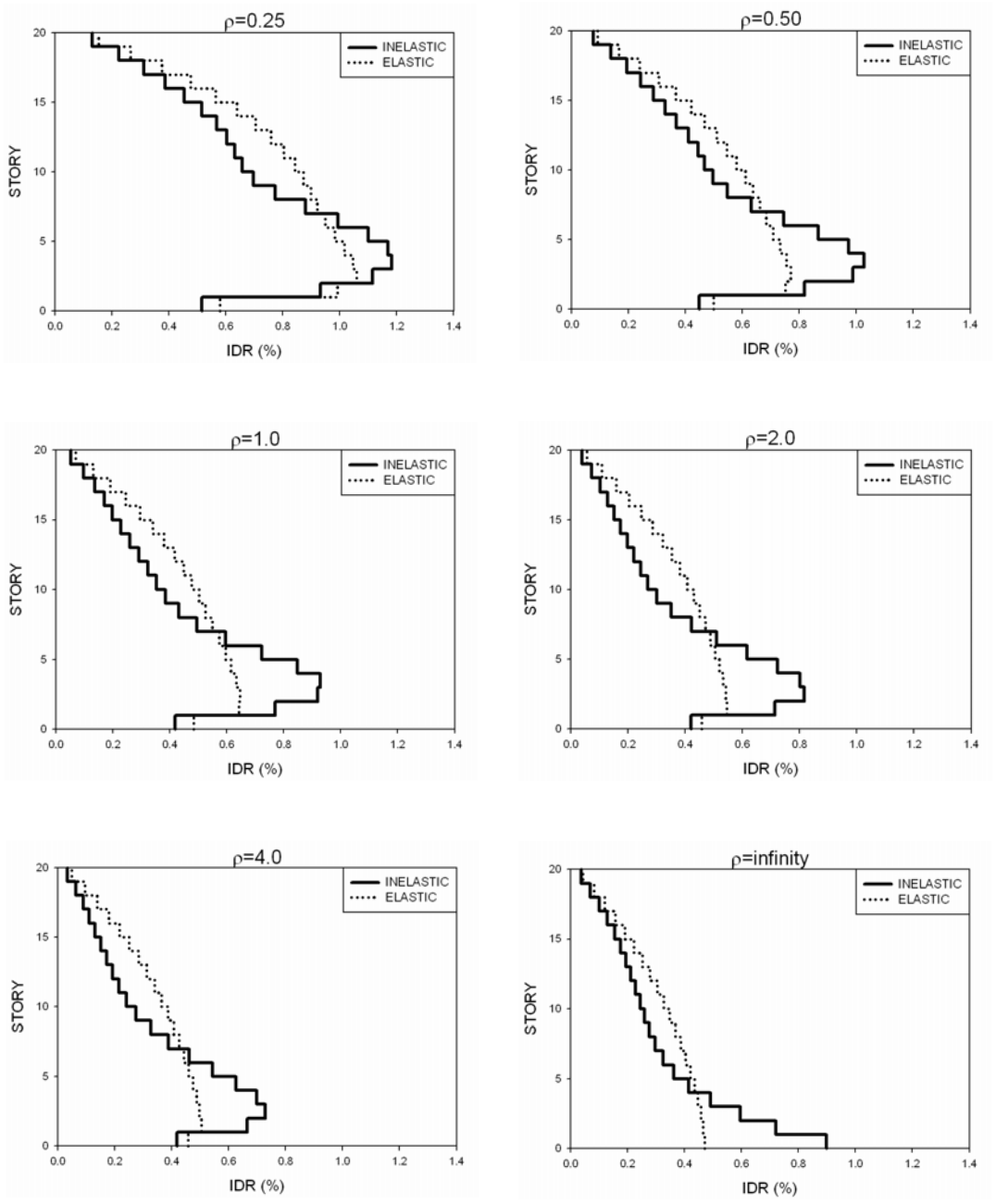

Figure 4.18: Comparison of ρ on the inelastic and elastic drift demands (N=20)

9 Story h_2=3 m Q=0.40 ψ=1.0 λ=1.0

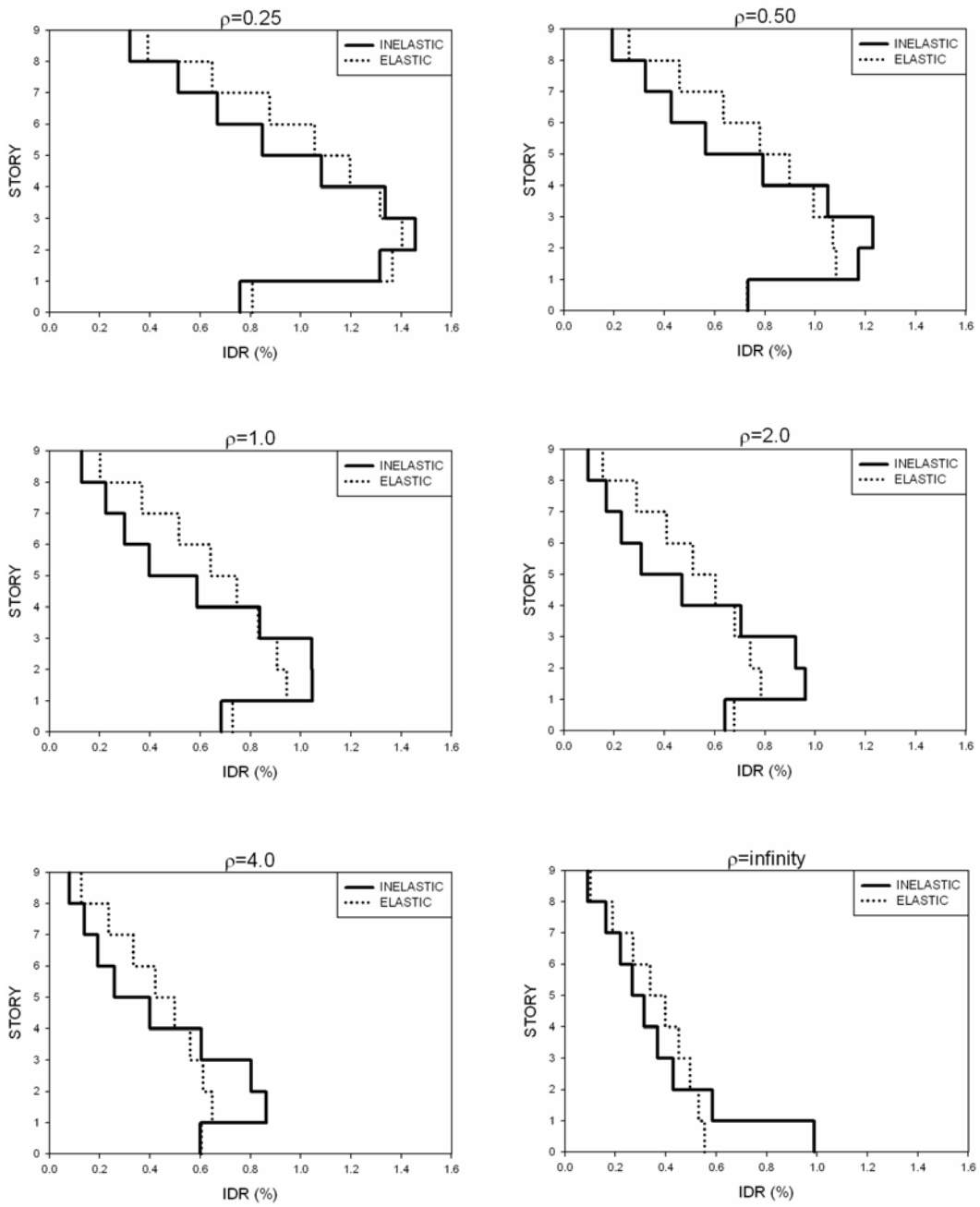

Figure 4.19: Comparison of ρ on the inelastic and elastic drift demands (N=9)

3 Story h_2=3 m Q=0.40 ψ=1.0 λ=1.0

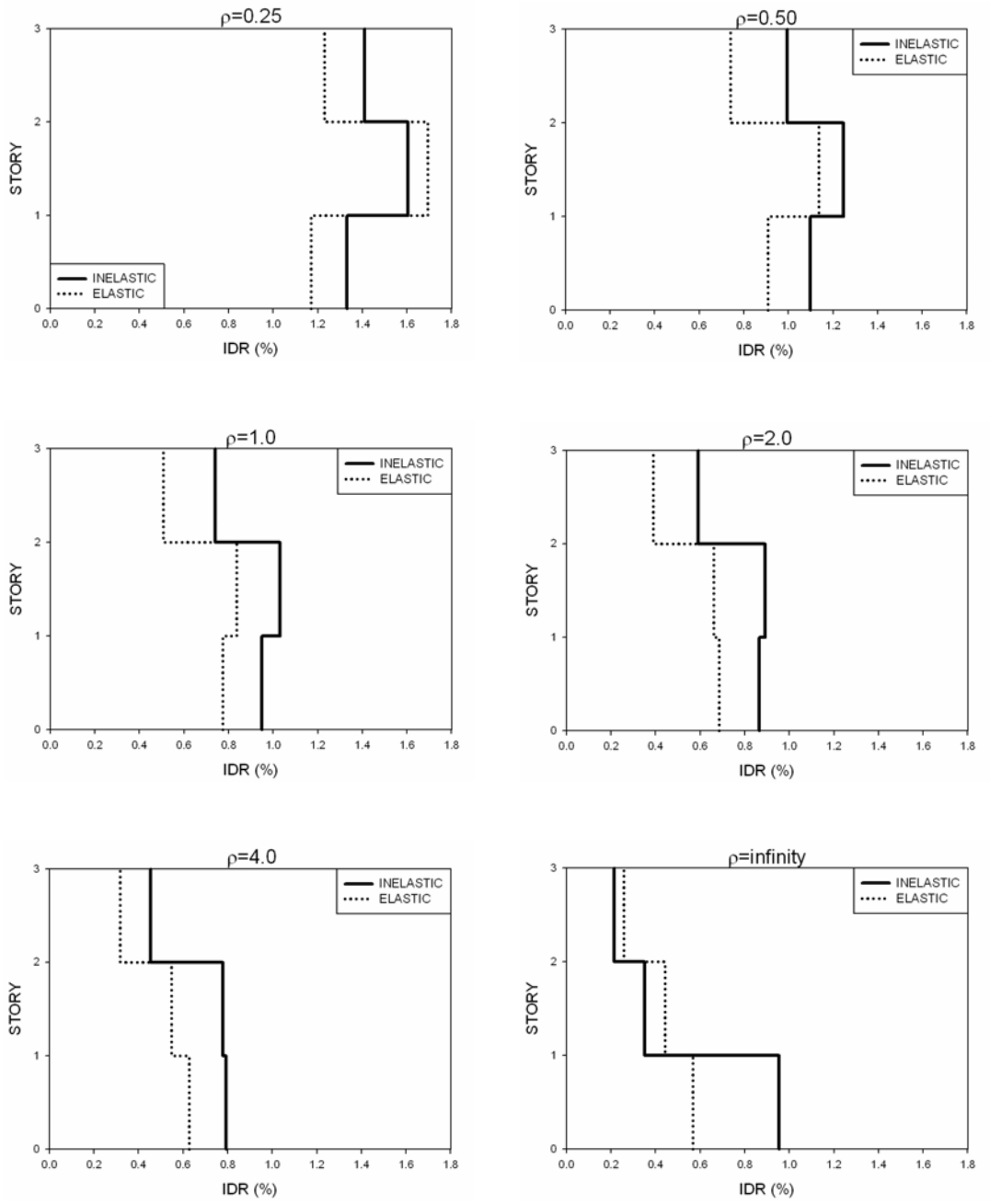

Figure 4.20: Comparison of ρ on the inelastic and elastic drift demands (N=3)

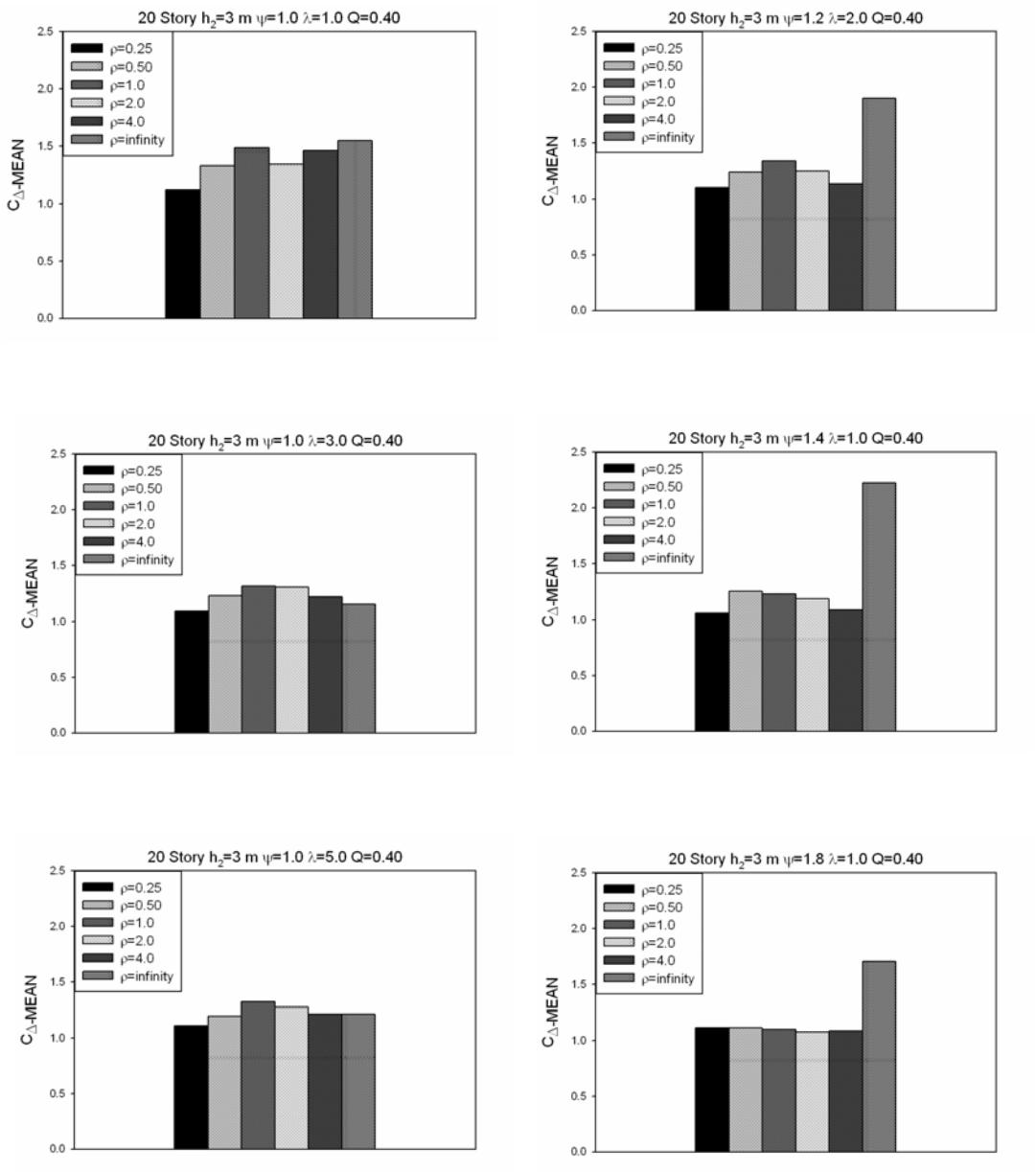

Figure 4.21: Effect of ρ on inelastic drift ratio (N=20, Q=0.40)

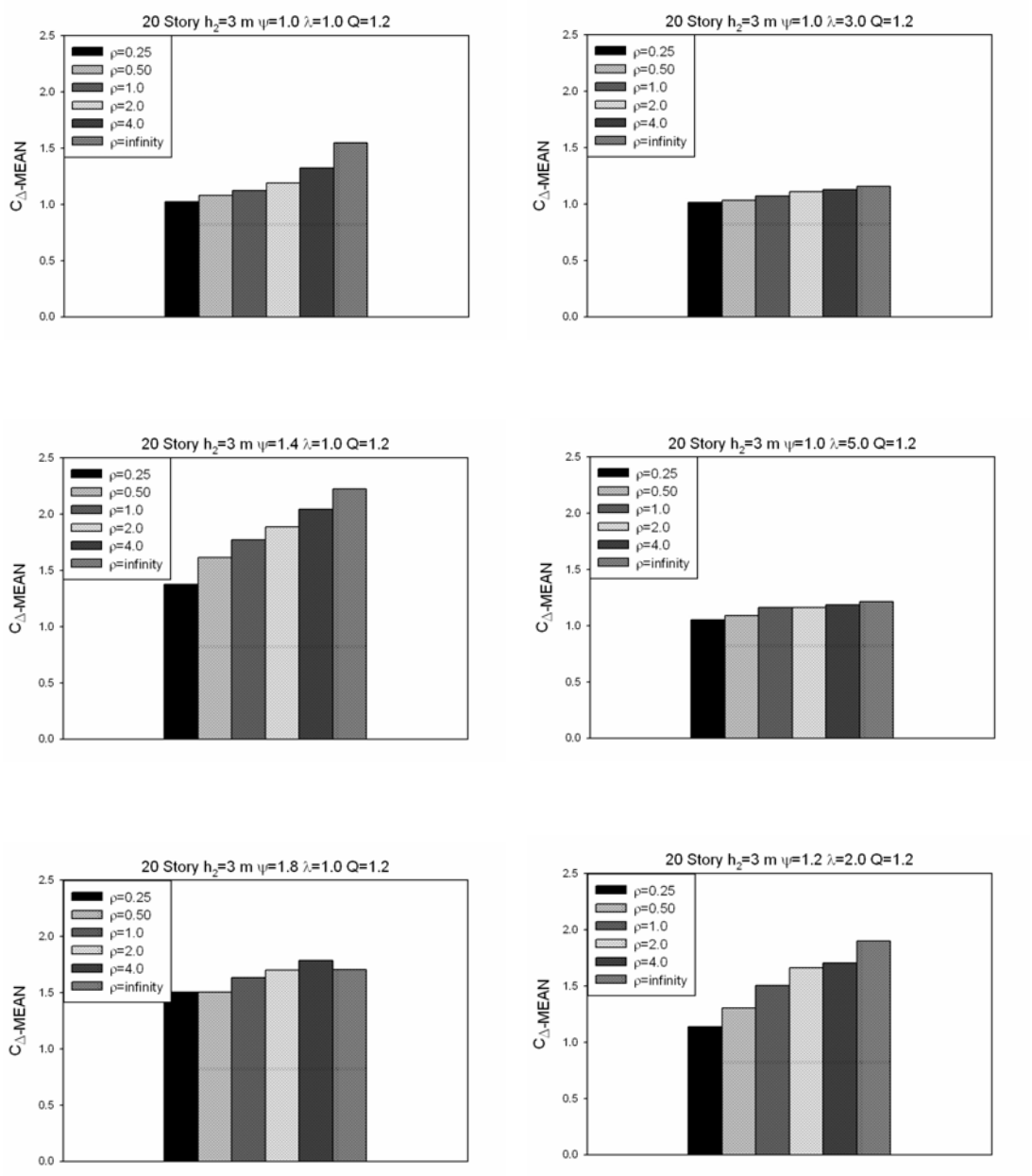

Figure 4.22: Effect of ρ on inelastic drift ratio (N=20, Q=1.2)

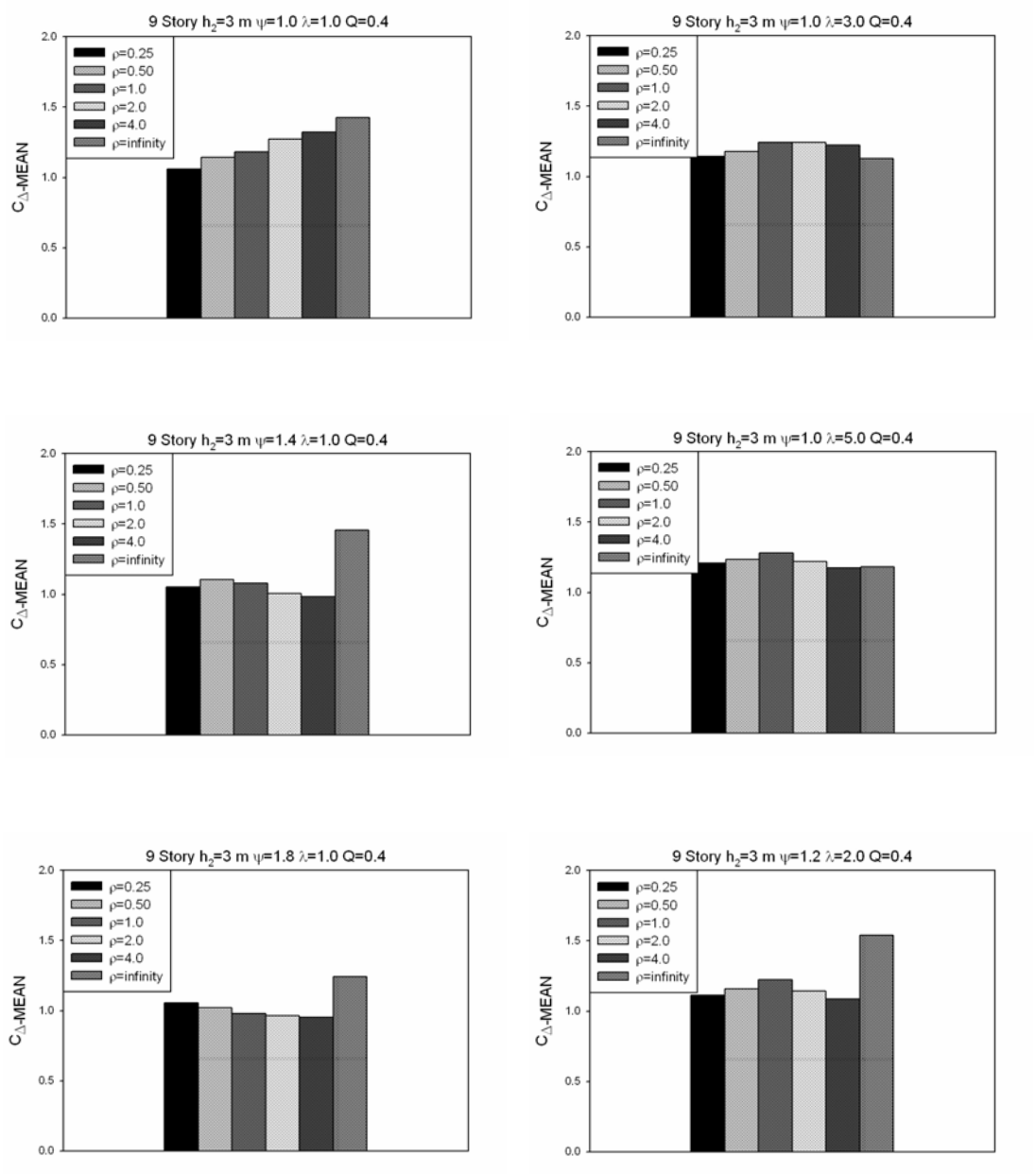

Figure 4.23: Effect of ρ on inelastic drift ratio (N=9, Q=0.40)

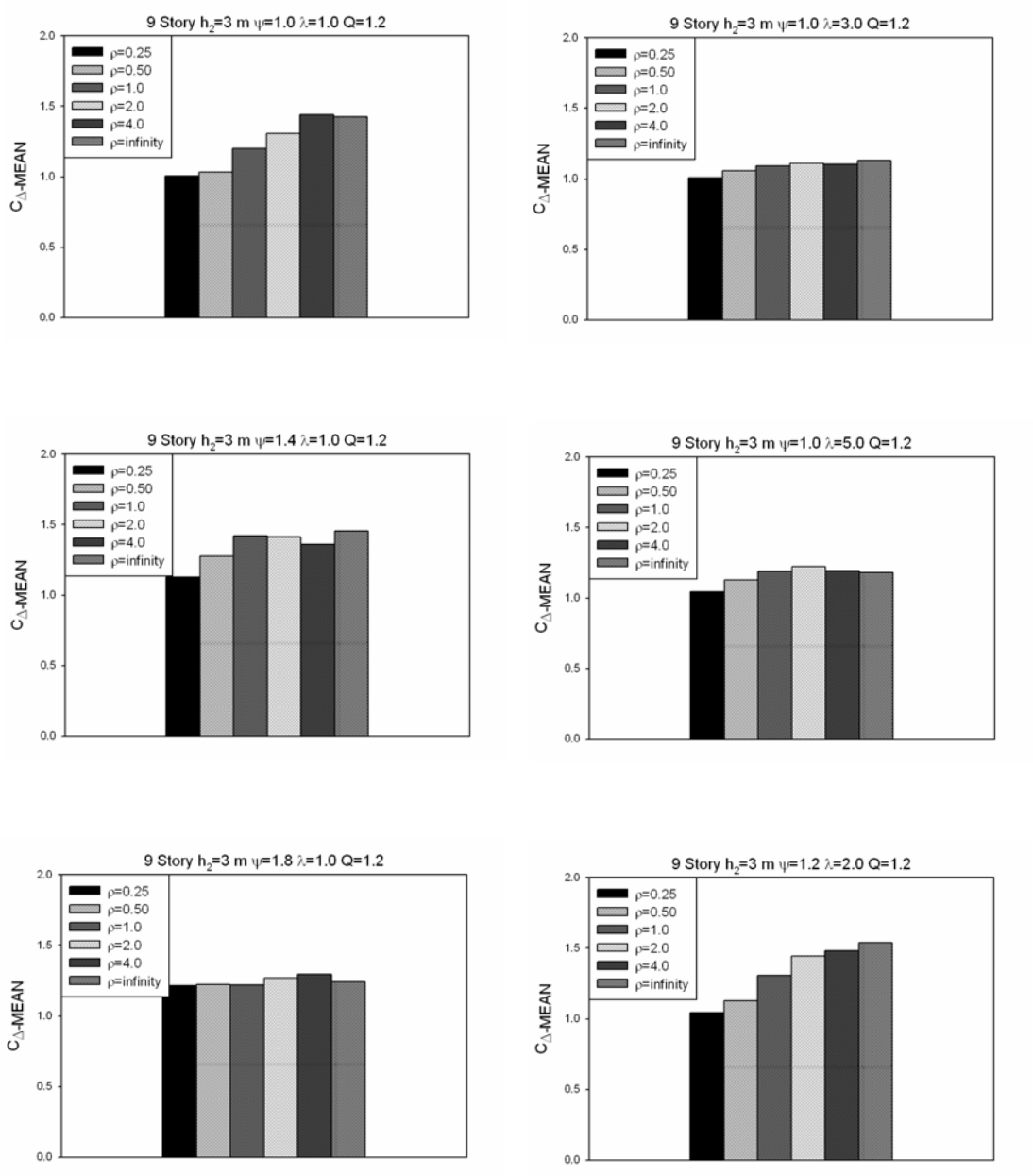

Figure 4.24: Effect of ρ on inelastic drift ratio (N=9, Q=1.2)

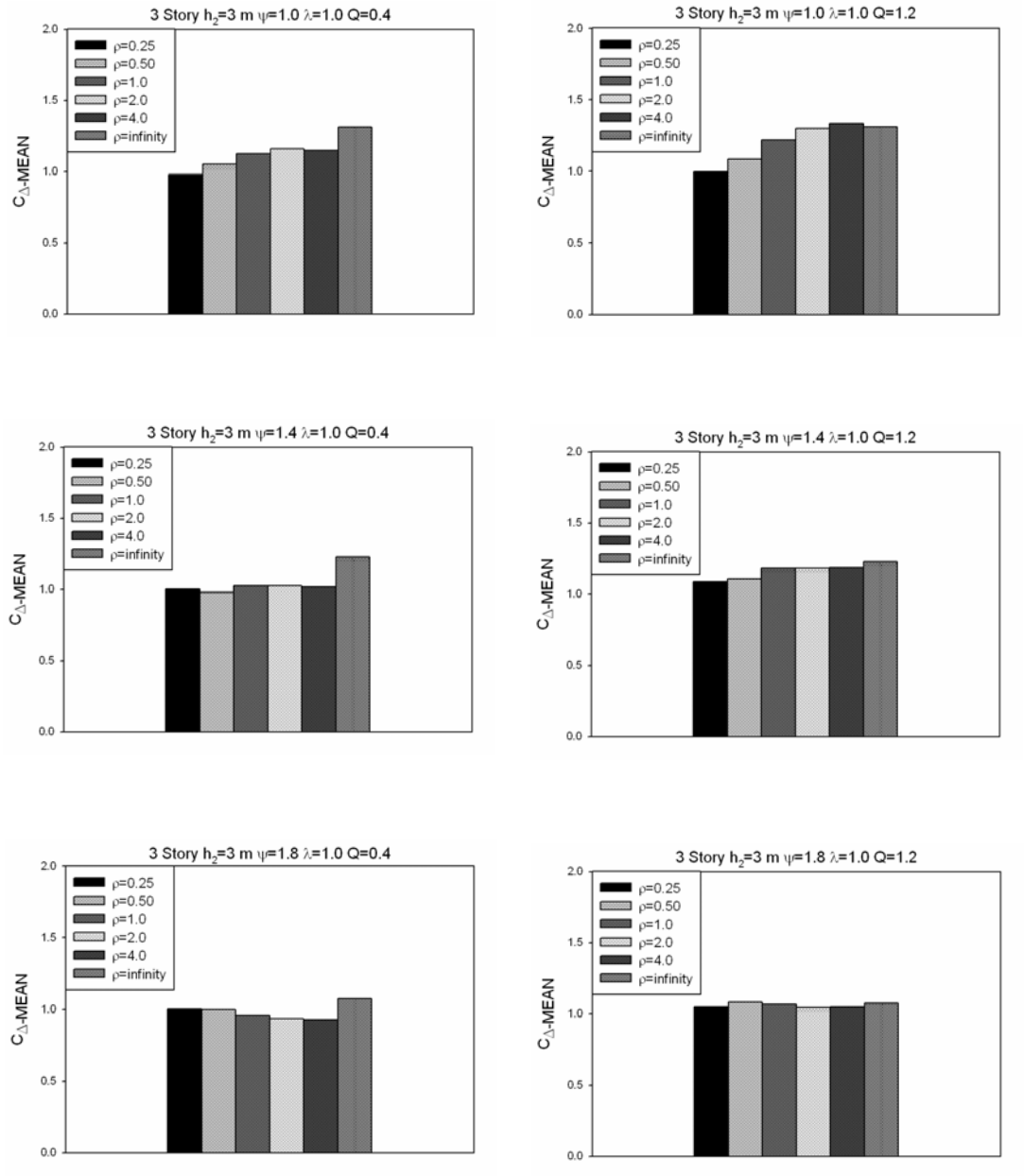

Figure 4.25: Effect of ρ on inelastic drift ratio (N=3)

4.4.5 EFFECTS OF SOFT STORY FACTOR (Ψ)

Soft story factor (defined by the symbol ψ=1.0, 1.2, 1.4, 1.6 and 1.8) is defined as the ratio of ground story height to regular story height.

Mean inelastic and elastic drift profiles obtained from 58 ground motions are plotted for frames with different soft story factors in Figures 4.26 to 4.31. It is observed that as the ratio of ground story height to regular story height increases, MIDR increases and location of MIDR shifts to the lower parts of the frame for both elastic and inelastic cases. Weak column-strong beam frames having soft story show more inelastic demand than strong column-weak beam frames. Moreover, if weak column-strong beam frames have soft story, maximum inelastic interstory drift ratio increases strongly. For example, MIDR of 20 story frame with ψ=1.4 possessing beam to column capacity ratio (Q) 0.40 and 1.20 are 1.1 % and 1.8 %, respectively as shown in Figures 4.26 and 4.27. It can be stated that MIDR of weak column-strong beam frame occurs at lower stories with respect to strong column-weak beam frames.

Figures 4.32 - 4.34 show mean inelastic drift ratios obtained from 58 ground motion for a range of moment resisting frames. It can be seen that inelastic drift ratios of strong column-weak beam frames decrease as ground story height increases. Both maximum inelastic drift ratio and maximum elastic drift ratio increase, but the ratio of inelastic MIDR to elastic MIDR decreases. It is observed that C_{Δ} values of weak column-strong beam frames do not increase or decrease regularly with increasing soft story factor.

20 Story h_2=3 m Q=0.40 ρ=0.5 λ=1.0

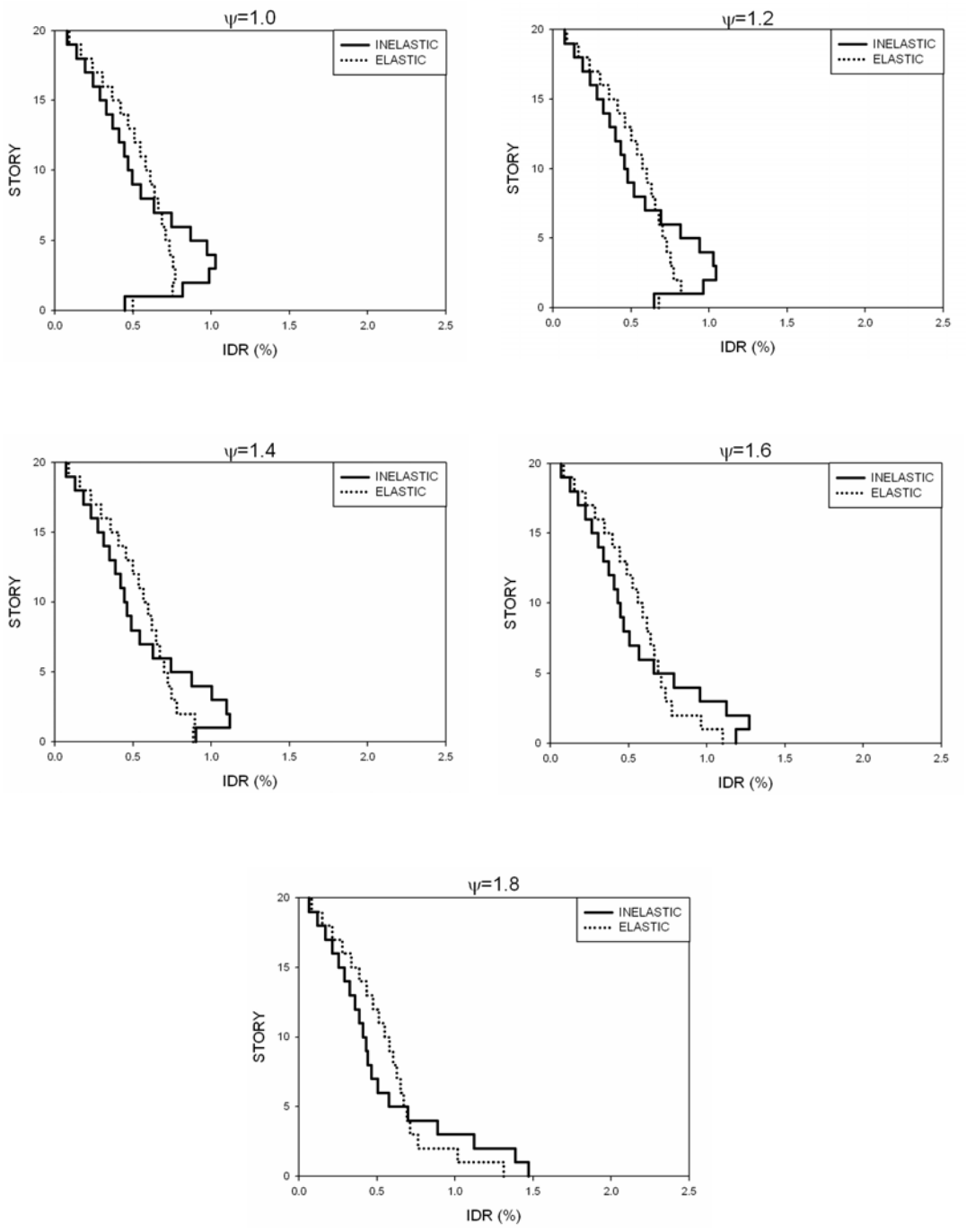

Figure 4.26: Comparison of soft story effect on the inelastic and elastic drift demand (N=20, Q=0.40)

20 Story h_2=3 m Q=1.2 ρ=0.5 λ=1.0

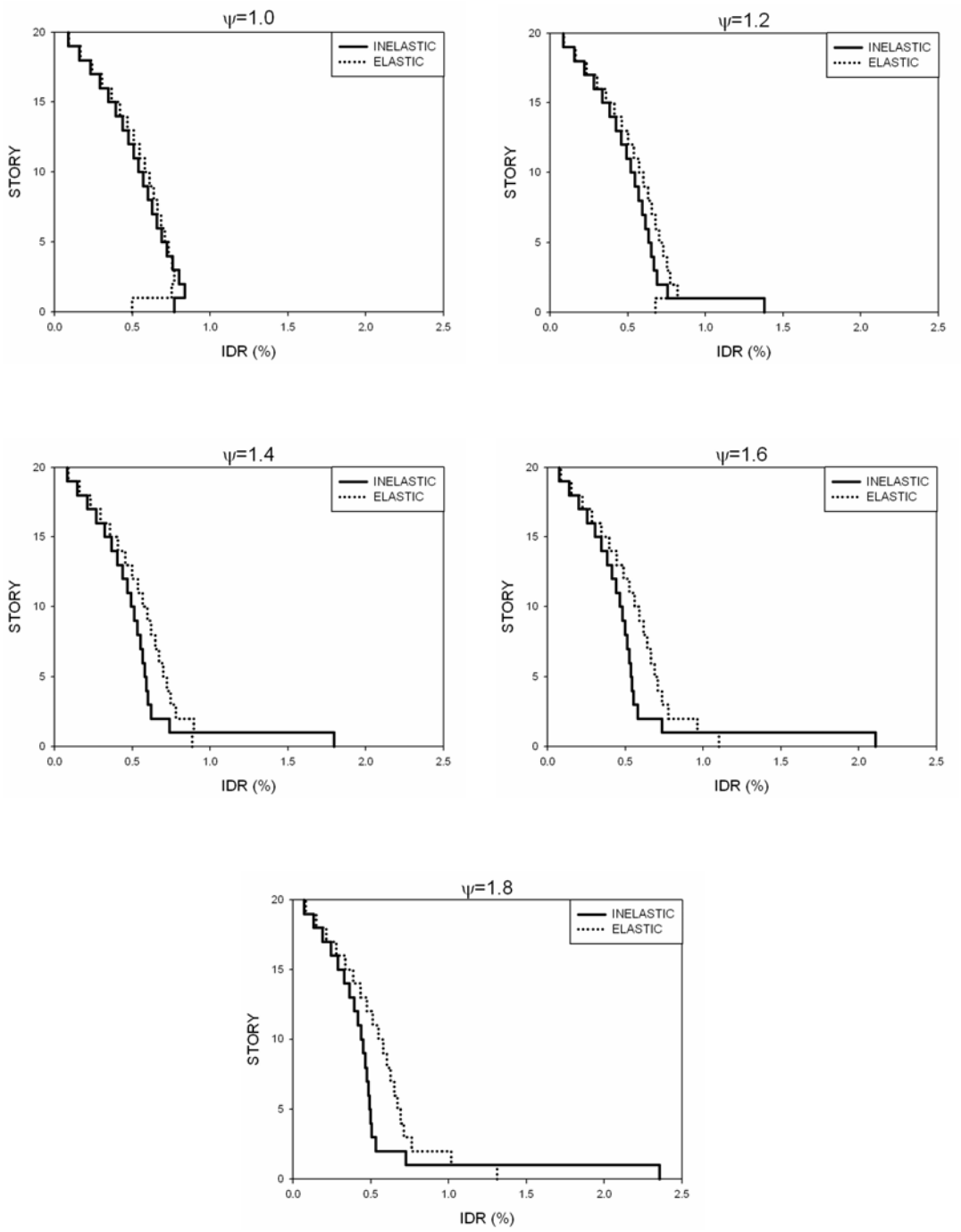

Figure 4.27: Comparison of soft story effect on the inelastic and elastic drift demand (N=20, Q=1.2)

9 Story h_2=3 m Q=0.40 ρ=0.5 λ=1.0

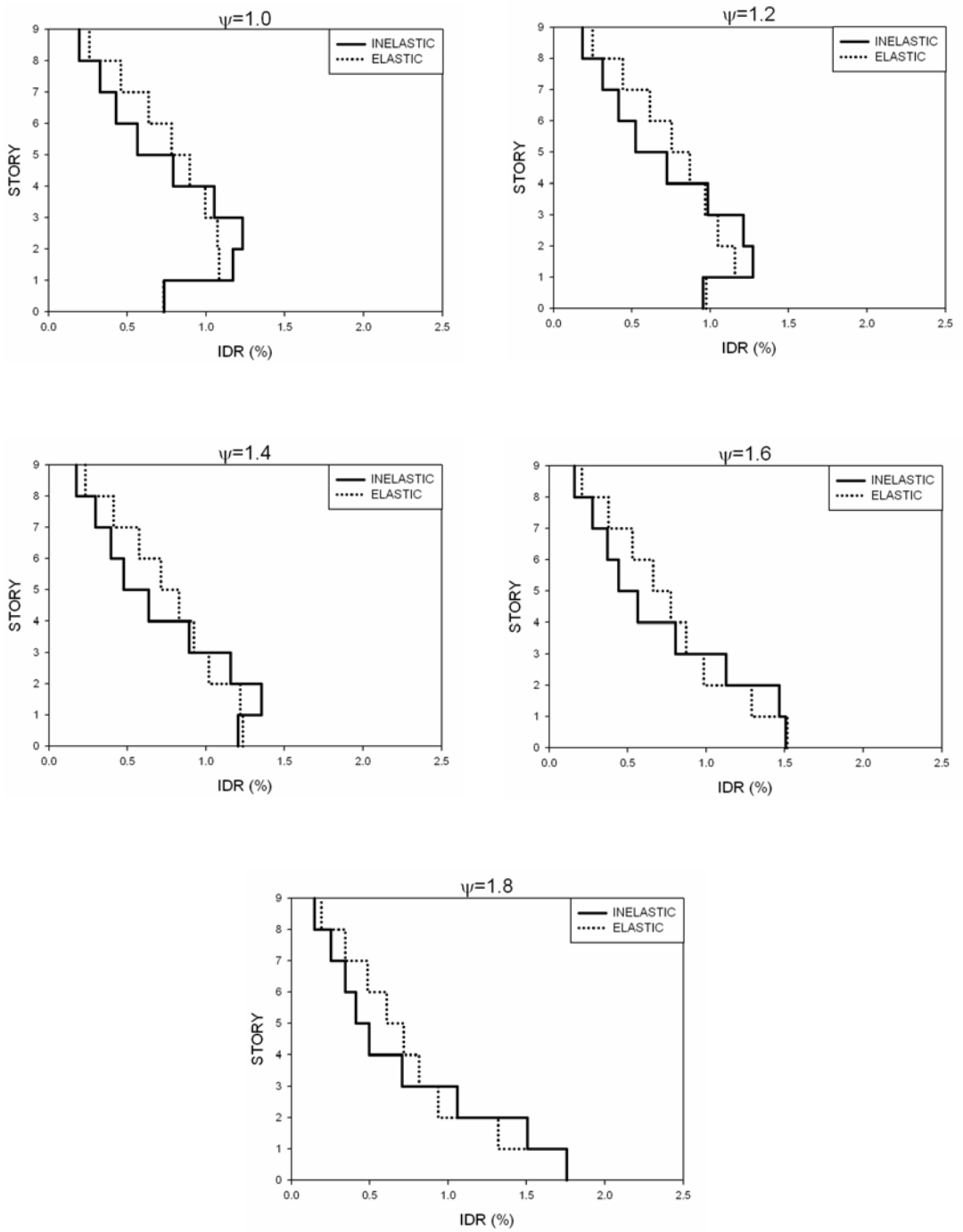

Figure 4.28: Comparison of soft story effect on the inelastic and elastic drift demand (N=9, Q=0.40)

9 Story h_2=3 m Q=1.2 ρ=0.5 λ=1.0

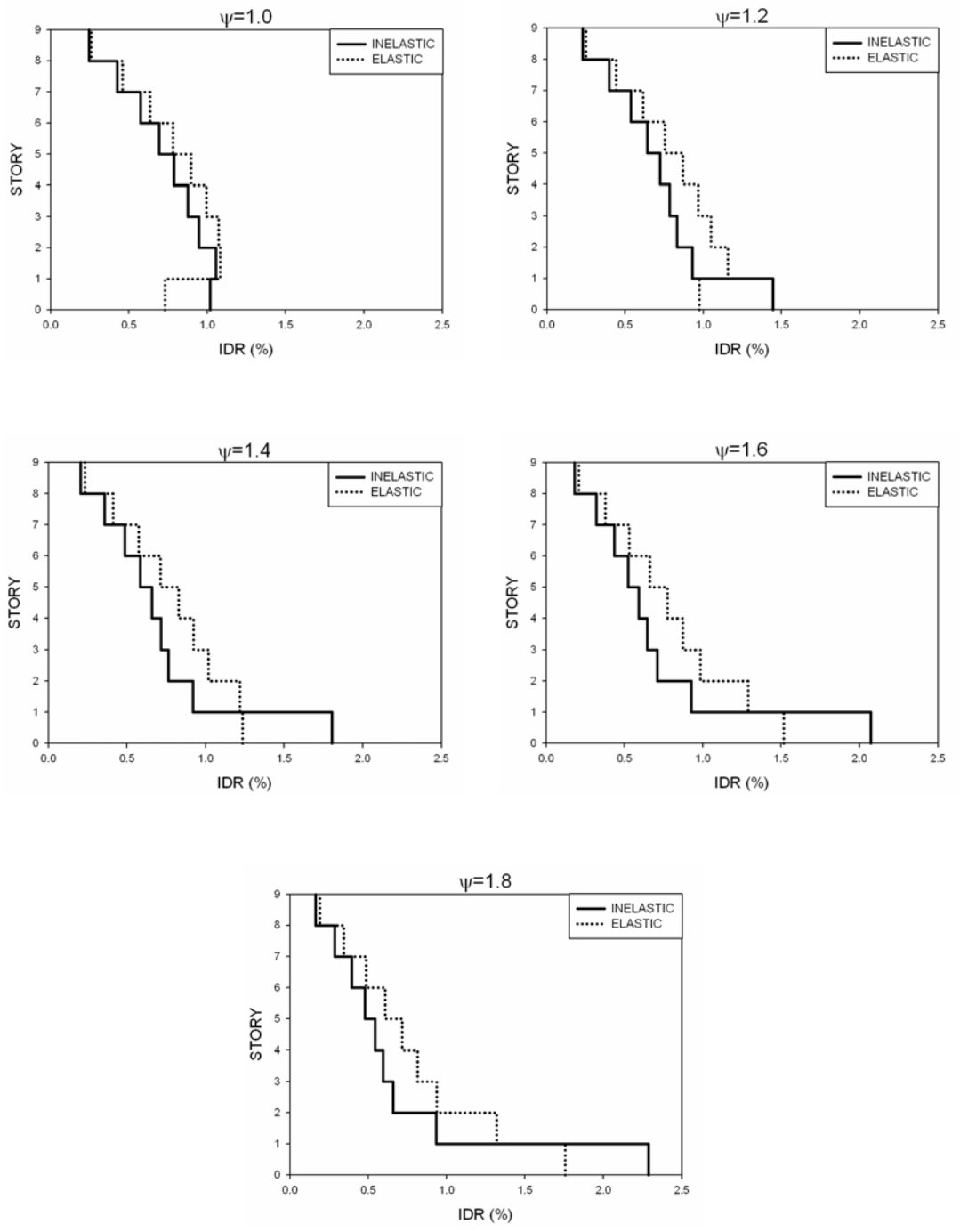

Figure 4.29: Comparison of soft story effect on the inelastic and elastic drift demand (N=9, Q=1.2)

3 Story h_2=3 m Q=0.40 ρ=0.5 λ=1.0

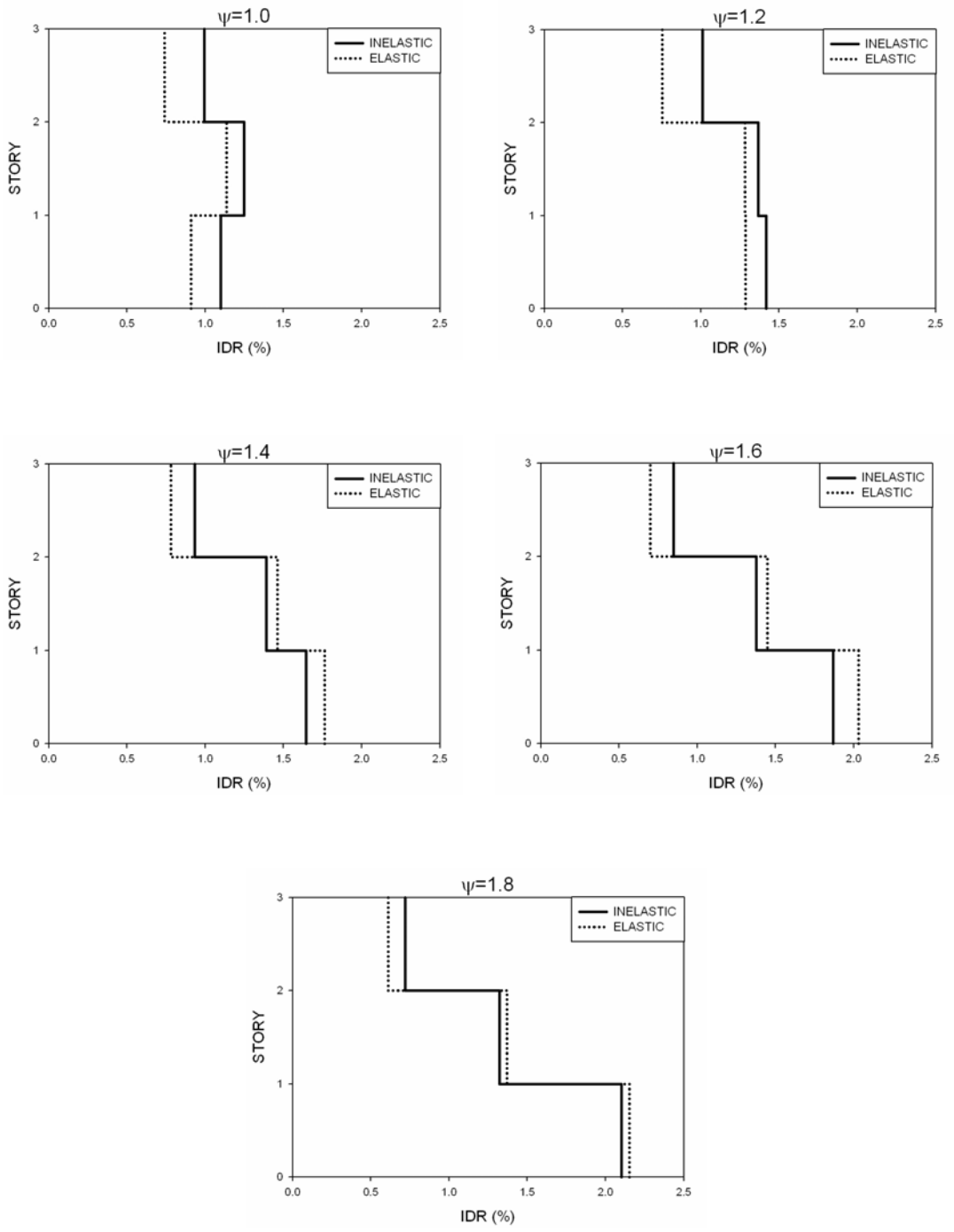

Figure 4.30: Comparison of soft story effect on the inelastic and elastic drift demand (N=3, Q=0.40)

3 Story h_2=3 m Q=1.2 ρ=0.5 λ=1.0

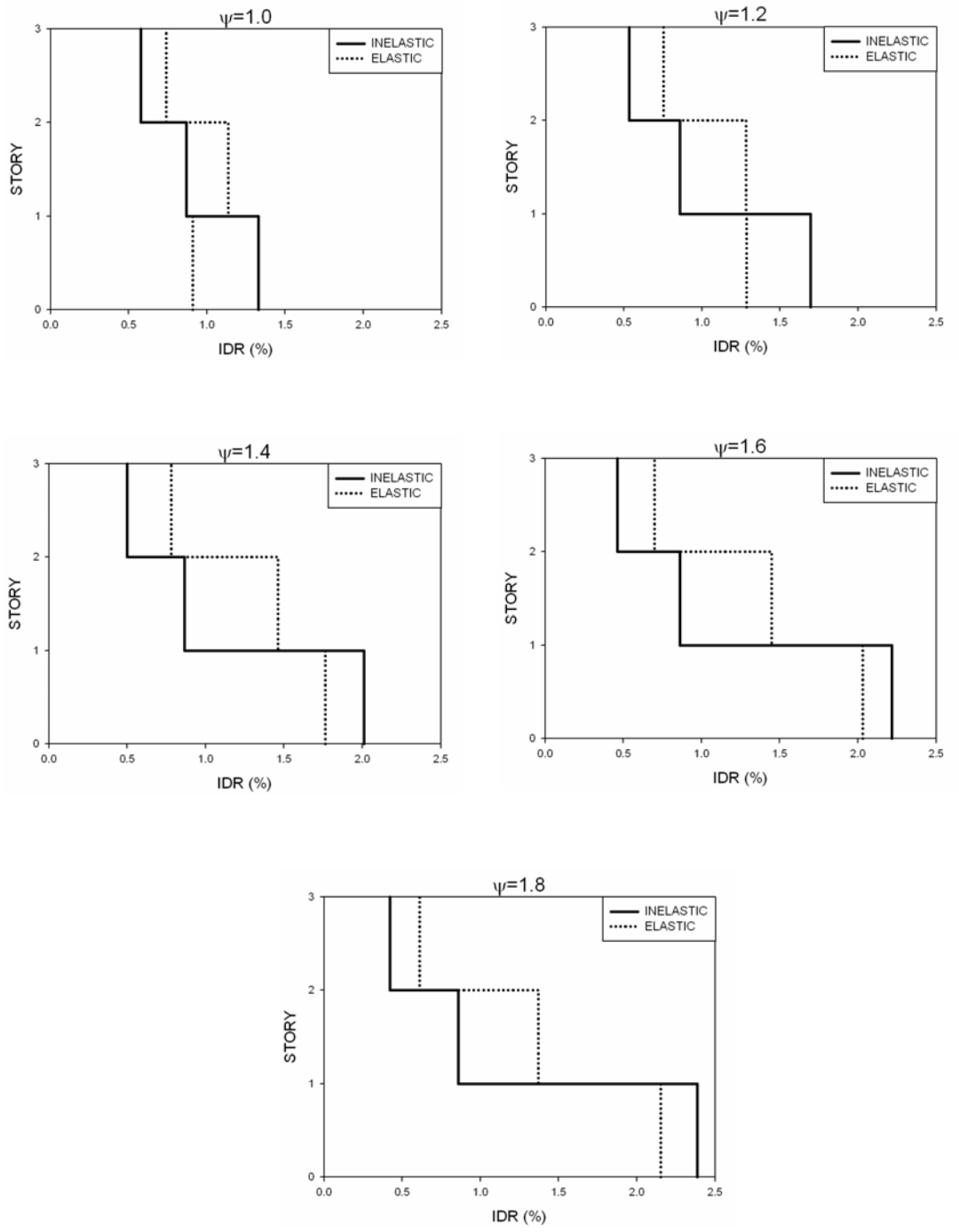

Figure 4.31: Comparison of soft story effect on the inelastic and elastic drift demand (N=3, Q=1.2)

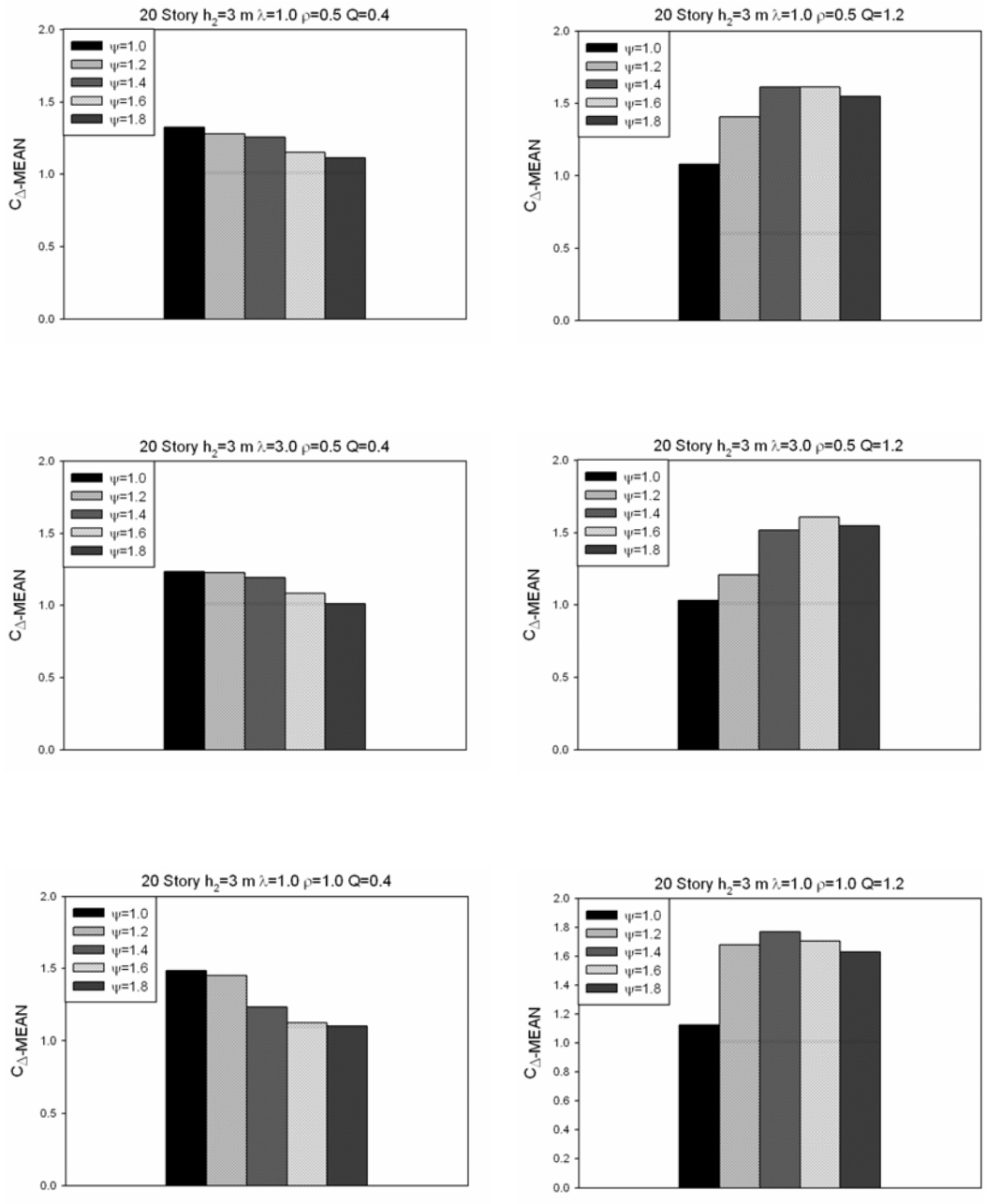

Figure 4.32: Effect of soft story on inelastic drift ratio (N=20)

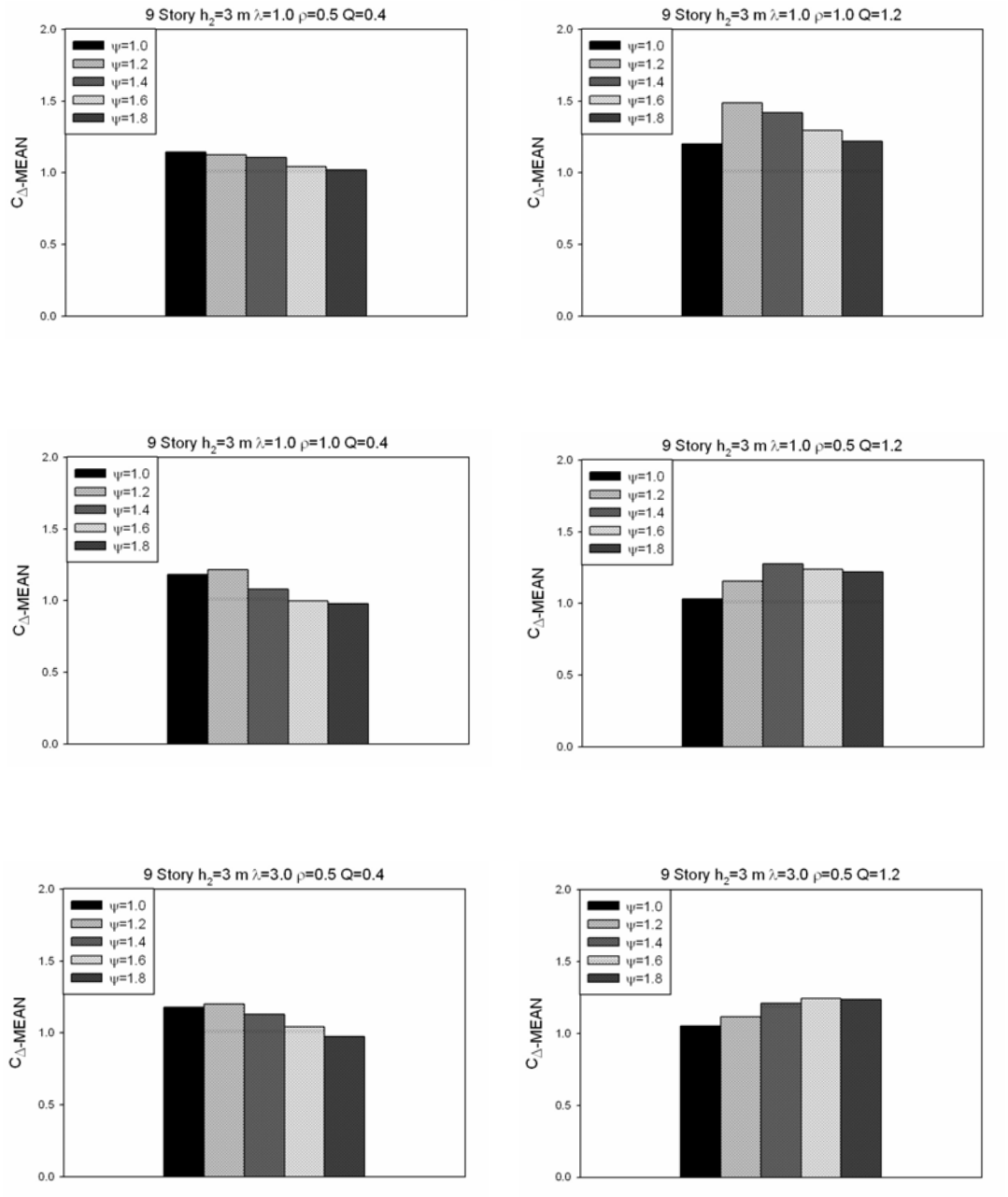

Figure 4.33: Effect of soft story on inelastic drift ratio (N=9)

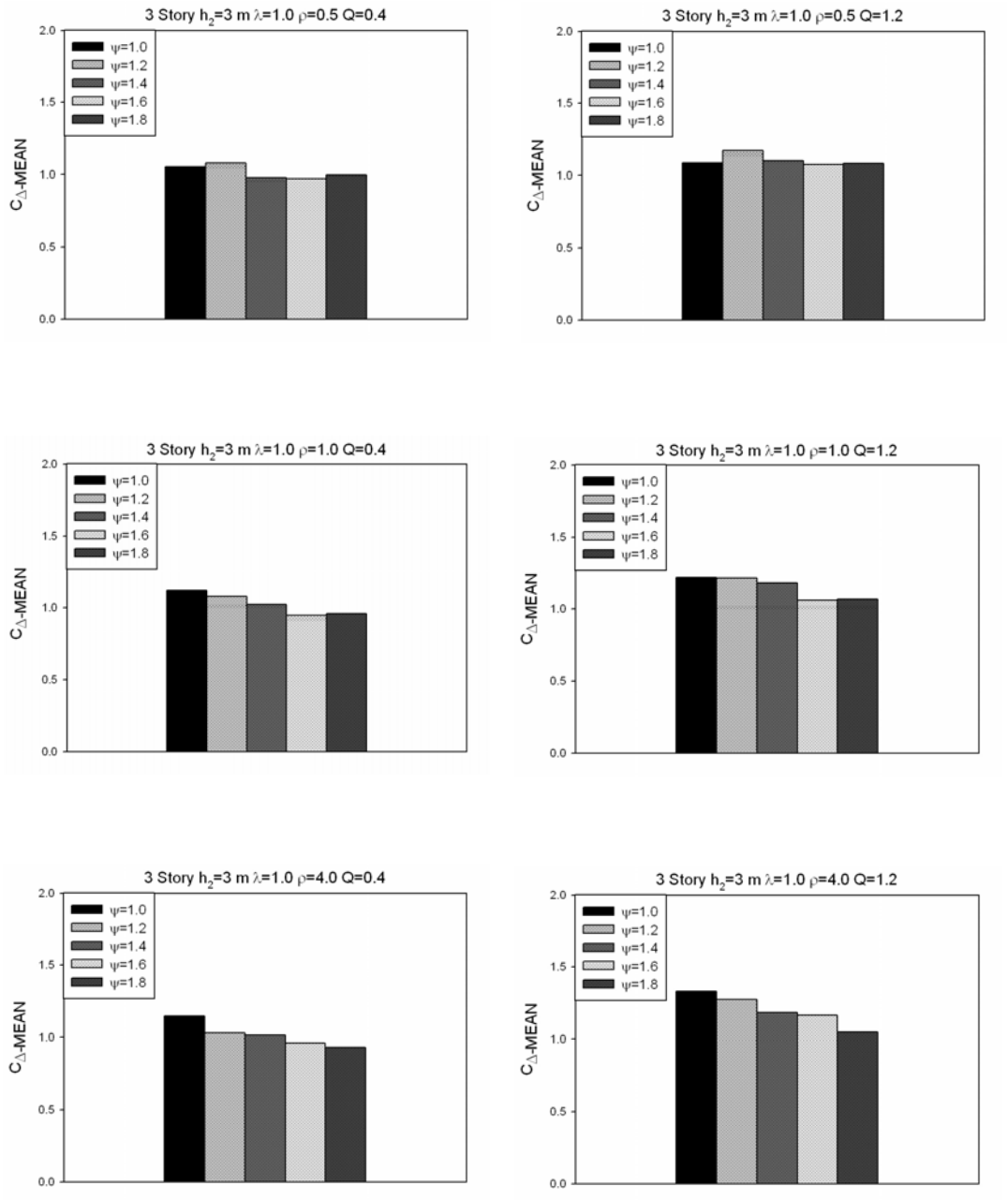

Figure 4.34: Effect of soft story on inelastic drift ratio (N=3)

4.4.6 EFFECTS OF STIFFNESS DISTRIBUTION FACTOR (λ)

The effect of stiffness irregularity on inelastic displacement demand and inelastic drift ratio is investigated in this section. Stiffness is reduced linearly from ground story to top story in order to create stiffness irregularity. The factor of λ is defined as the ratio of the lateral stiffness at the ground story of the building to the lateral stiffness at the top story of the building. 1.0, 2.0, 3.0, 4.0, 5.0 and 6.0 are used as λ ranges.

Elastic and inelastic mean interstory drift profiles obtained from 58 ground motions corresponding to different stiffness distribution factors are presented in Figure 4.35 - 4.38. In section 4.3.1, it was stated that base shear capacity of a frame decreases with increasing stiffness distribution factor. Therefore, it is expected that maximum inelastic interstory drift ratio increases with λ. Although inelastic MIDR of 20-story frame (Q=0.40) decreases while λ increases from 1.0 to 4.0 in Figure 4.35, inelastic MIDR of 20-story frame (Q=1.20) and MIDR of 9-story frames (Q=0.40 and Q=1.20) increase with λ as shown in Figure 4.36, 4.37 and 4.38, respectively. It is also observed that the location of inelastic MIDR moves to the upper stories with increasing λ.

Inelastic drift ratios of these frames are shown as histograms in Figure 4.39. It is observed that, similar to inelastic MIDR values, inelastic drift ratios of 20-story frame (Q=1.20) and 9-story frames (Q=0.40 and Q=1.20) increase with λ. Only the C_Δ of 20-story strong column-weak beam frame (Q=0.4) decreases regularly with λ.

4.4.7 EFFECTS OF REGULAR STORY HEIGHT (h_2)

Four different regular story heights are used in nonlinear analyses (h_2= 3 m, 4 m, 5 m and 6 m). In section 3.2.5, it was shown that story height does not have any effect on mode shapes, but linear interstory drift ratios increase with regular story height.

Figures 4.40 to 4.43 show elastic and inelastic average interstory drift ratios. In general inelastic maximum interstory drift ratio increases with regular story height. It is observed that interstory drift increases with regular story height. However, when interstory drift does not increase as much as regular story height, interstory drift ratio decreases for these cases as in Figure 4.40 between h_2=5 m and h_2=6 m. It is also seen that, when Q is increased from 0.4 to 1.2, inelastic MIDR decreases, which may not be expected, since the weak column-strong beam case is expected to undergo larger drifts. The reason for this unexpected behavior is the fact that base shear capacity is much larger in Q=1.2 case than Q=0.4 case.

Effect of regular story height on inelastic drift ratio is presented in Figure 4.44. It is observed that inelastic drift ratio decreases when regular story height increases, which means that the increase in elastic MIDR is greater than inelastic MIDR.

4.5 REPRESENTATIVE EQUATION FOR INELASTIC DRIFT RATIO

The maximum inelastic interstory drift ratio is defined as the product of the maximum drift ratio of a linear elastic moment resisting frame with the same initial lateral stiffness and same amount of damping as that of elastic system modified by a factor, C_Δ, as follows:

$$MIDR_{INELASTIC} = C_\Delta \times MIDR_{ELASTIC} \tag{4.3}$$

This type of method was first proposed, albeit in a more limited sense, by Veletsos and Newmark [68]. They studied the ratio of the maximum deformation of elasto-plastic systems to the maximum deformation of elastic systems with the same initial stiffness and same damping ratio. Many other studies in earthquake structural engineering have adopted a similar approach [19, 47, 59] For example, Miranda [47] conducted a statistical study of ratios of maximum inelastic to maximum elastic displacements computed from ground motions recorded on firm

soils for SDOF systems. These particular studies are valid for SDOF systems and for ground motions that are not influenced by forward directivity. Therefore, in this study a statistical study is performed in order to find a representative formula for inelastic drift ratio computed from near fault ground motions characterized by large, long-period velocity pulses.

Before proceeding further a sobering and cautionary note is in order. The inelastic deformation of plane frames is affected by many parameters. This study has examined what is believed to be the most significant ones among these. Yet, anyone who has dealt with structural dynamics and earthquake engineering can not escape expressing the truism that the idealizations we use in estimating response are always less than perfect, and the scatter in the seismic input will never be eliminated, but with further insight into the physics of the phenomena reduced. The seemingly complex expression for C_Δ is therefore confined to the limits of this dissertation, and is a crude distillation of many inter-related factors.

Since a large scatter of data exists when all the 542'880 inelastic drift ratios are compared, it was not possible to obtain a formula covering all the data. Therefore, a representative formula is generated for 20-story regular moment resisting frame with h_2=3 m and ρ=0.5. The following simplified expression is presented as.

$$C_\Delta = \max(\Omega,1) \tag{4.4}$$

where $$\Omega = \frac{0.29(T_p/T)^{-0.5Q} + 1.9 * q^{-0.005Q(T_p/T)} - 2}{0.15^{(T_p/T)} + 0.6q^{-16Q} + 0.17Q} + 0.5$$

Here T_p/T is the ratio of pulse period to fundamental period, Q is the beam to column capacity ratio and q is the elastic force reduction factor. Figure 4.45 shows the correlation between C_Δ calculated from Equation 4.4 and C_Δ obtained from time history analyses. Despite the fact that data contains scatter, the expression gives good estimates of inelastic drift ratio for representative frames. Average of $C_{\Delta\text{-ANALYSIS}}$ (exact values, E) and $C_{\Delta\text{-FORMULA}}$ (approximate values, A)

are 1.50 and 1.49, respectively. In addition, the average of the ratios of approximate values to exact values (A/E) is 1.00. Maximum and minimum values of A/E are 2.36 and 0.45, respectively. Although average of A/E values is good, Equation (4.4) may overestimate or underestimate the required values. However, it was not possible to obtain a uniformly good correlation between the inelastic drift ratios obtained from analysis and the generated Equation (4.4). The reason for this situation can be better understood by turning to Table 4.1 where it can be seen that inelastic drift ratios corresponding to similar values of input variables (Q, Tp/T, and q) can vary considerably among each other. Therefore, any summary equation would represent an error for such data. As a result, it can be stated that the main reason of obtaining poor correlation is the very nature of the considered problem.

Table 4.1: C_Δ values obtained from time history analyses

Q	T_p/T	q	C_Δ
0.2	3.65	2.33	1.58
0.2	3.16	2.36	3.74
0.2	2.01	2.99	1.60
0.2	2.37	3.00	3.39
0.4	1.76	1.53	2.46
0.4	1.88	1.57	1.33
0.4	0.85	2.65	1.22
0.4	0.91	2.69	1.47
0.6	0.85	1.47	1.26
0.6	0.85	1.43	1.64
0.6	2.31	2.33	1.58
0.6	2.37	2.36	3.74

20 Story h_2=3 m Q=0.40 ρ=0.5 ψ=1.0

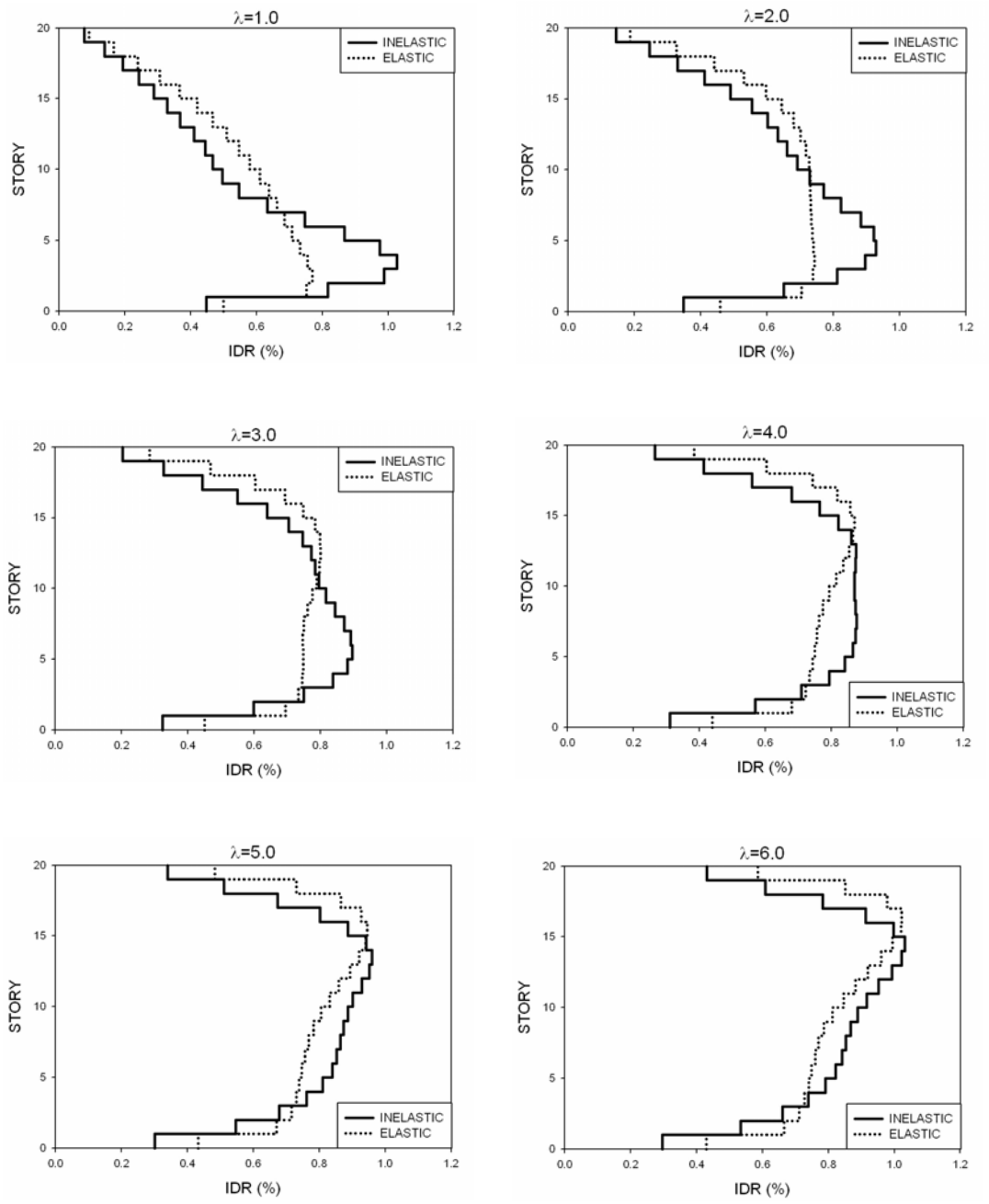

Figure 4.35: Comparison of stiffness distribution on the inelastic and elastic drift demand (N=20, Q=0.40)

20 Story h_2=3 m Q=1.2 ρ=0.5 ψ=1.0

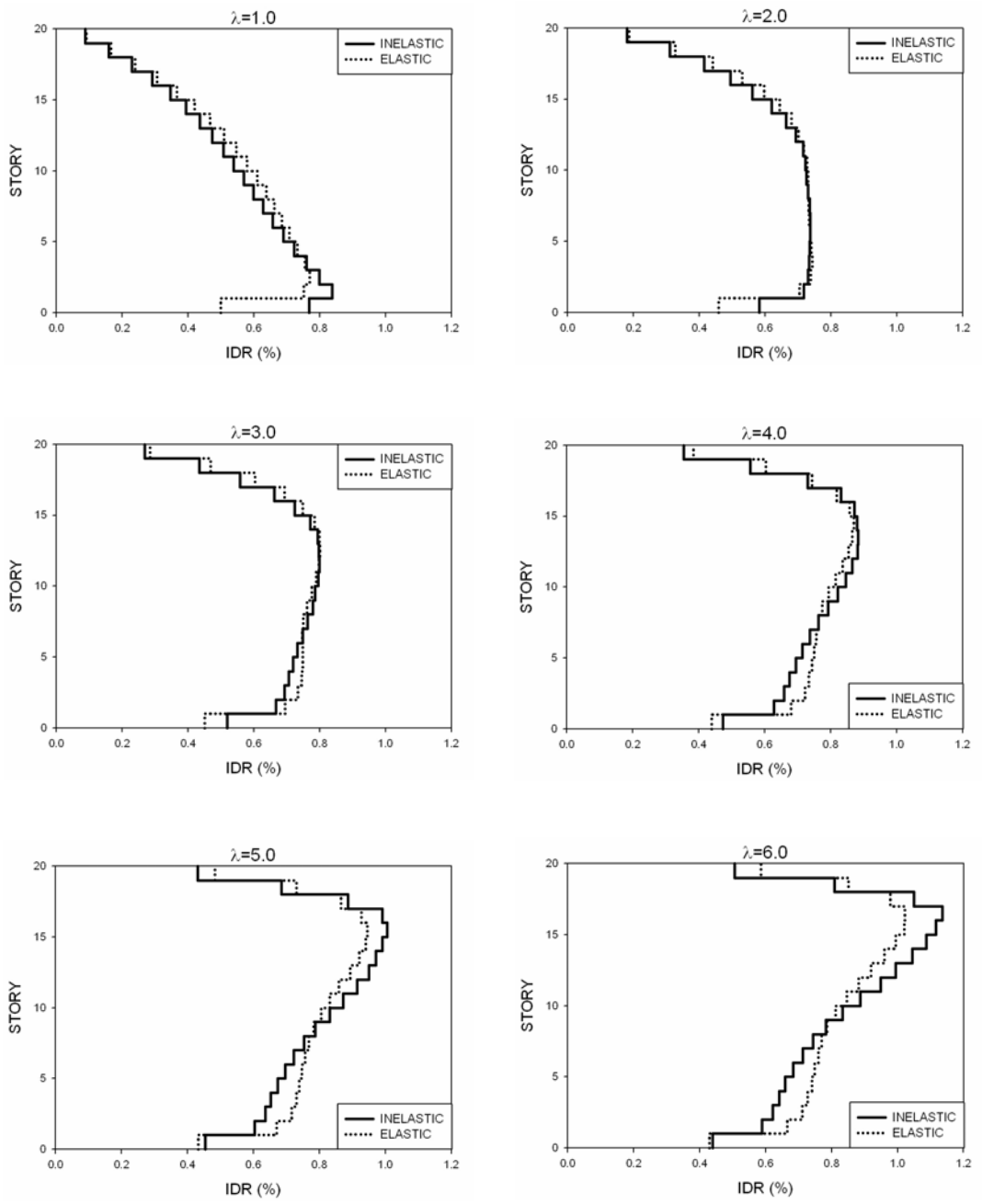

Figure 4.36: Comparison of stiffness distribution on the inelastic and elastic drift demand (N=20, Q=1.2)

9 Story h_2=3 m Q=0.40 ρ=0.5 ψ=1.0

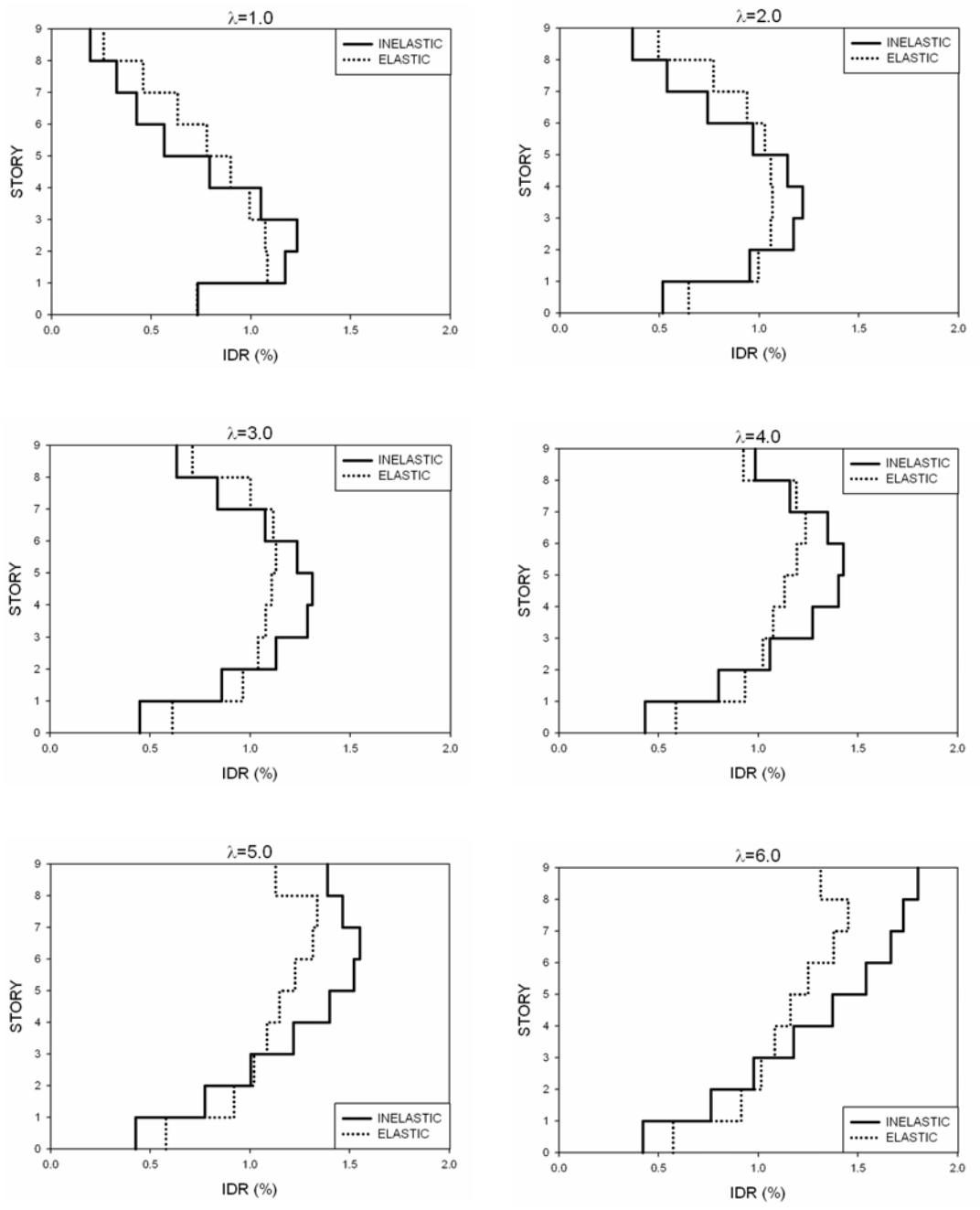

Figure 4.37: Comparison of stiffness distribution on the inelastic and elastic drift demand (N=9, Q=0.40)

9 Story h_2=3 m Q=1.2 ρ=0.5 ψ=1.0

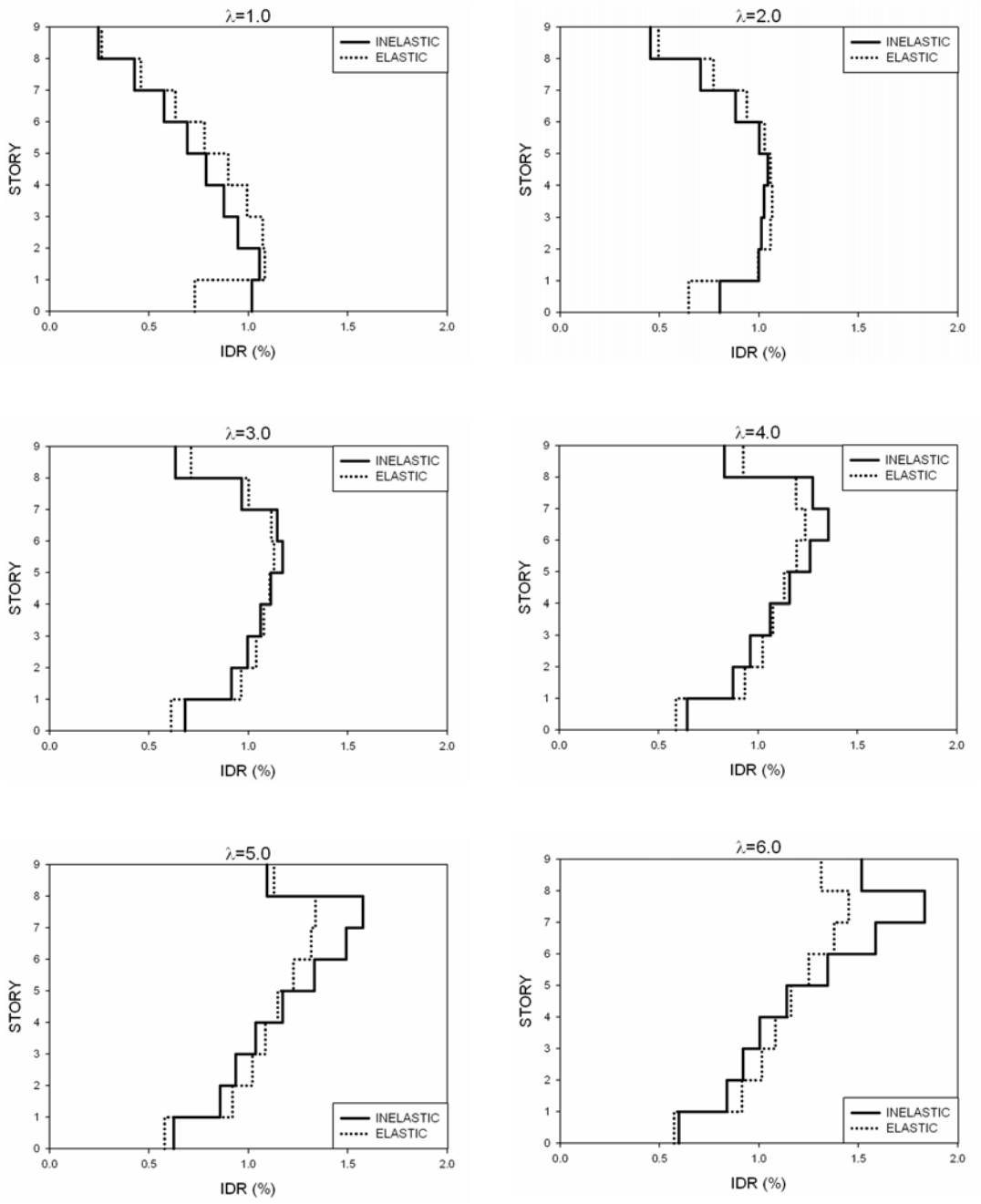

Figure 4.38: Comparison of stiffness distribution on the inelastic and elastic drift demand (N=9, Q=1.2)

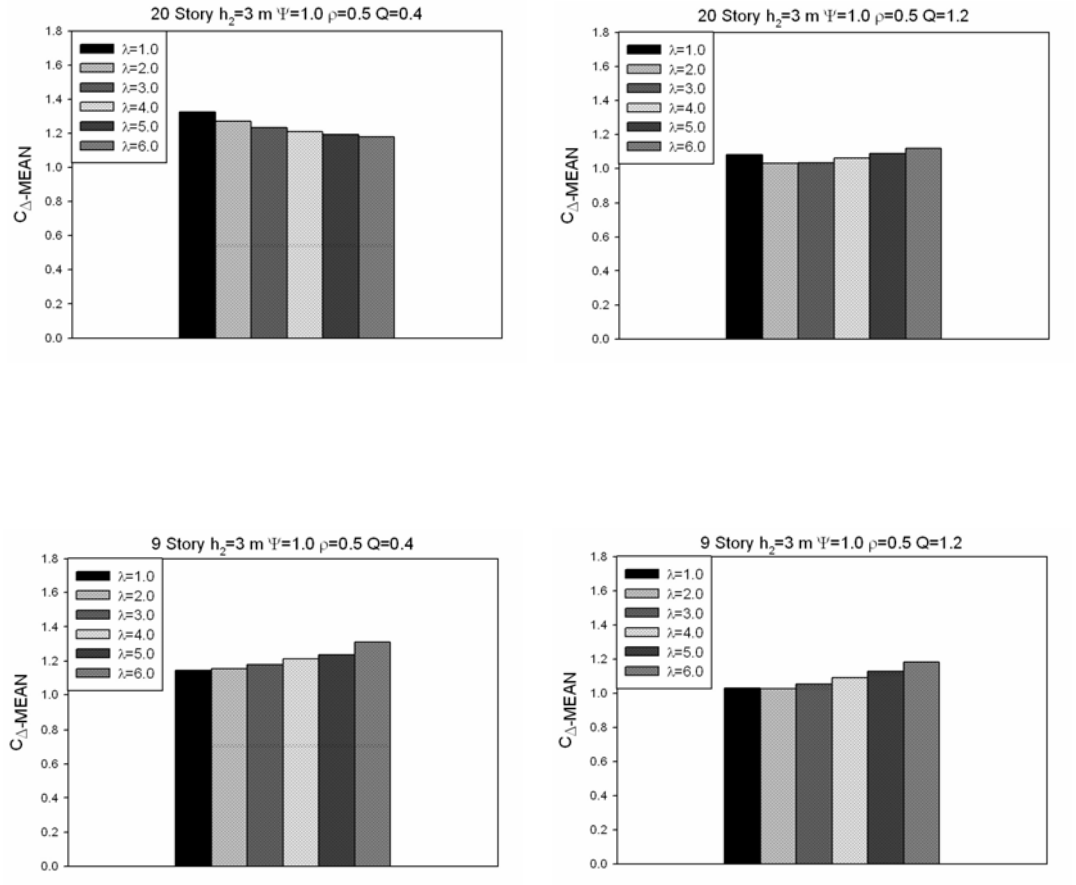

Figure 4.39: Effect of stiffness distribution on inelastic drift ratio (N=20 and 9, Q=0.40 and 1.2)

20 Story Q=0.40 ρ=0.5 ψ=1.0 λ=1.0

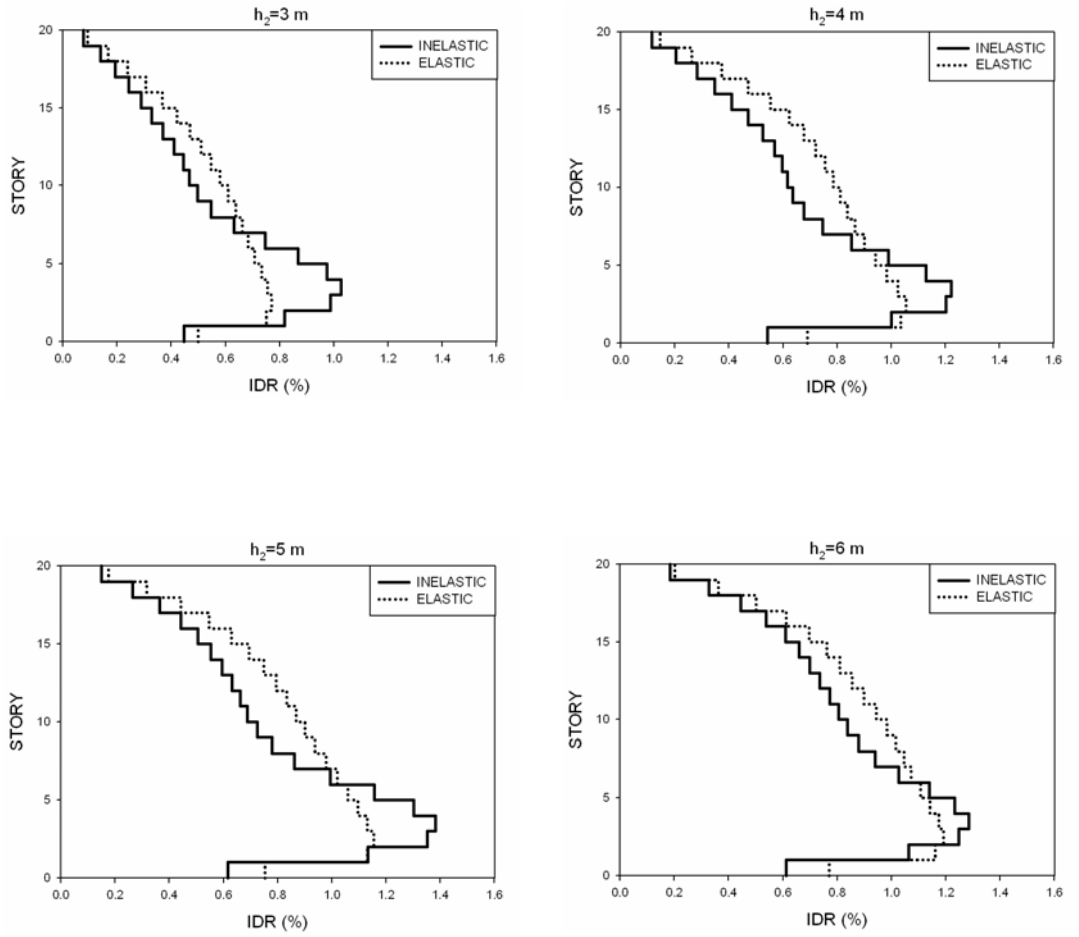

Figure 4.40: Comparison of regular story height effect on the inelastic and elastic drift demand (N=20, Q=0.40)

20 Story Q=1.2 ρ=0.5 ψ=1.0 λ=1.0

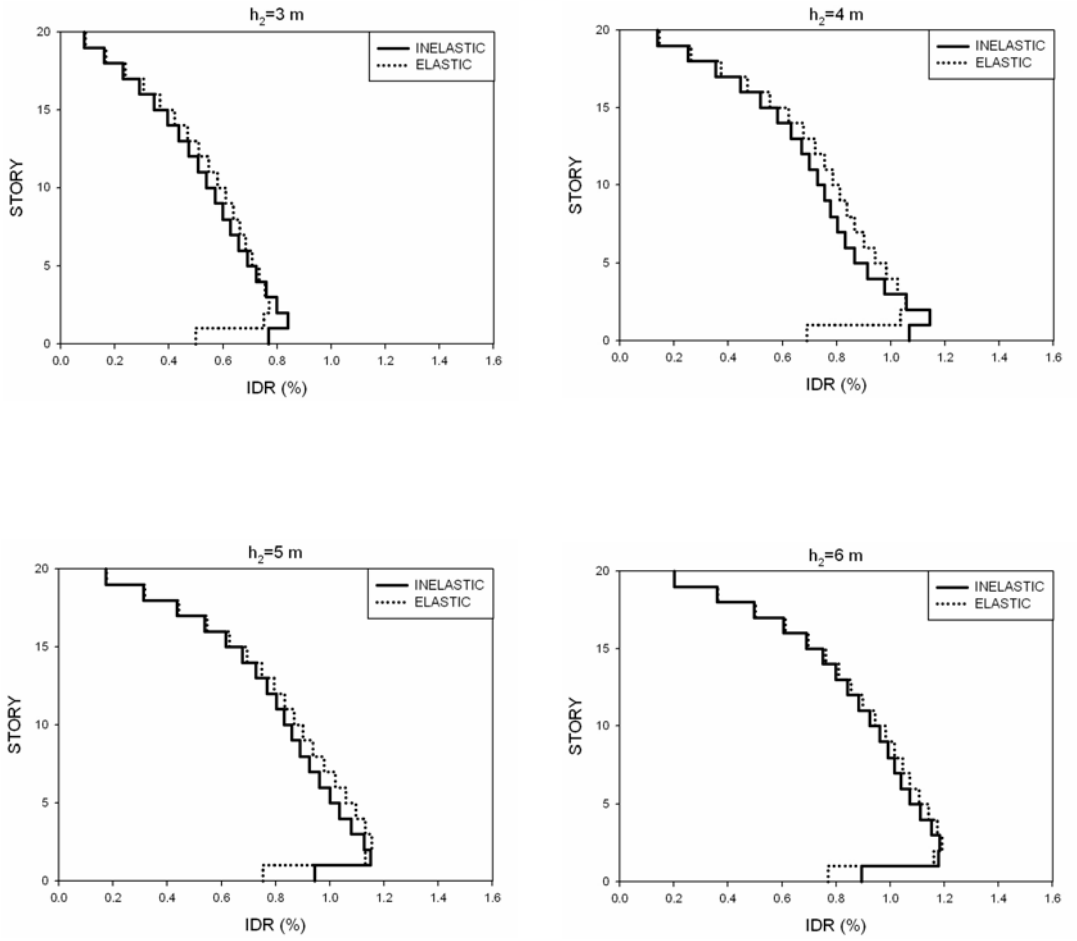

Figure 4.41: Comparison of regular story height effect on the inelastic and elastic drift demand (N=20, Q=1.2)

9 Story Q=0.40 ρ=0.5 ψ=1.0 λ=1.0

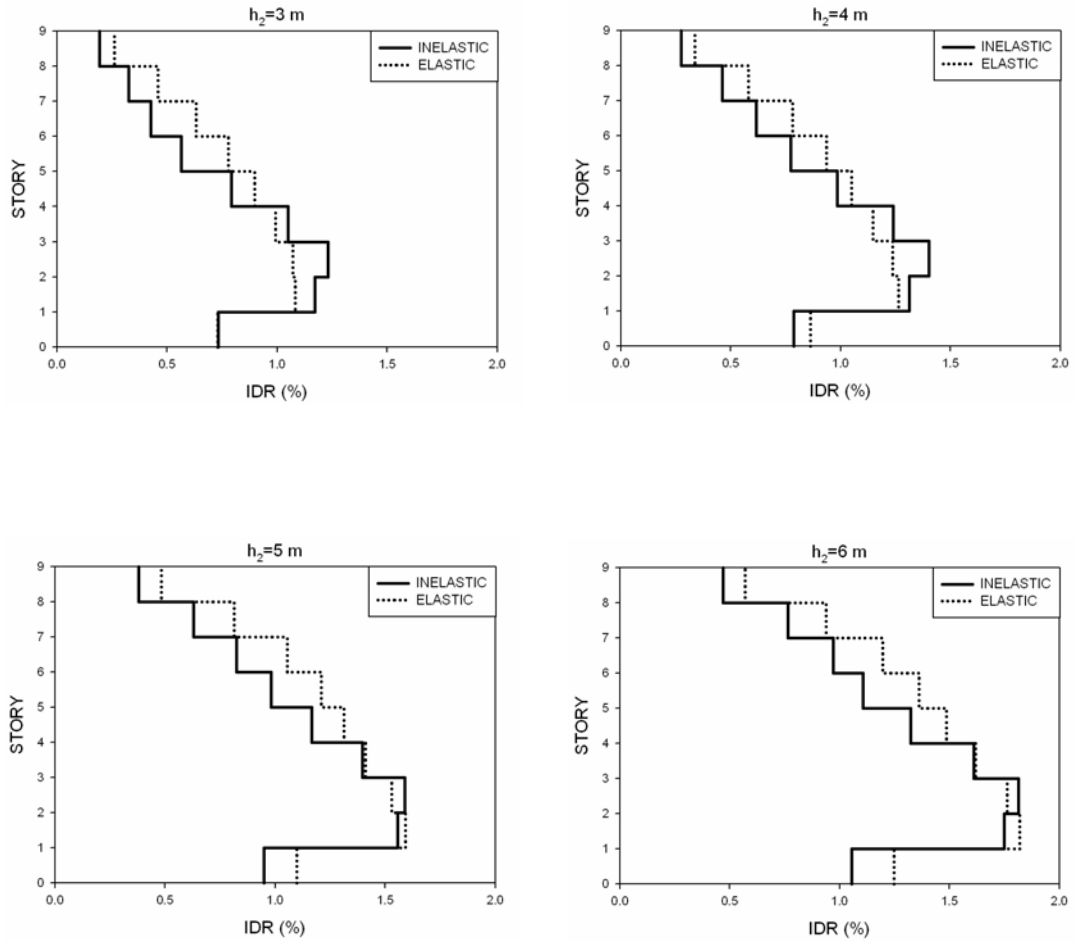

Figure 4.42: Comparison of regular story height effect on the inelastic and elastic drift demand (N=9, Q=0.40)

9 Story Q=1.2 ρ=4.0 ψ=1.0 λ=1.0

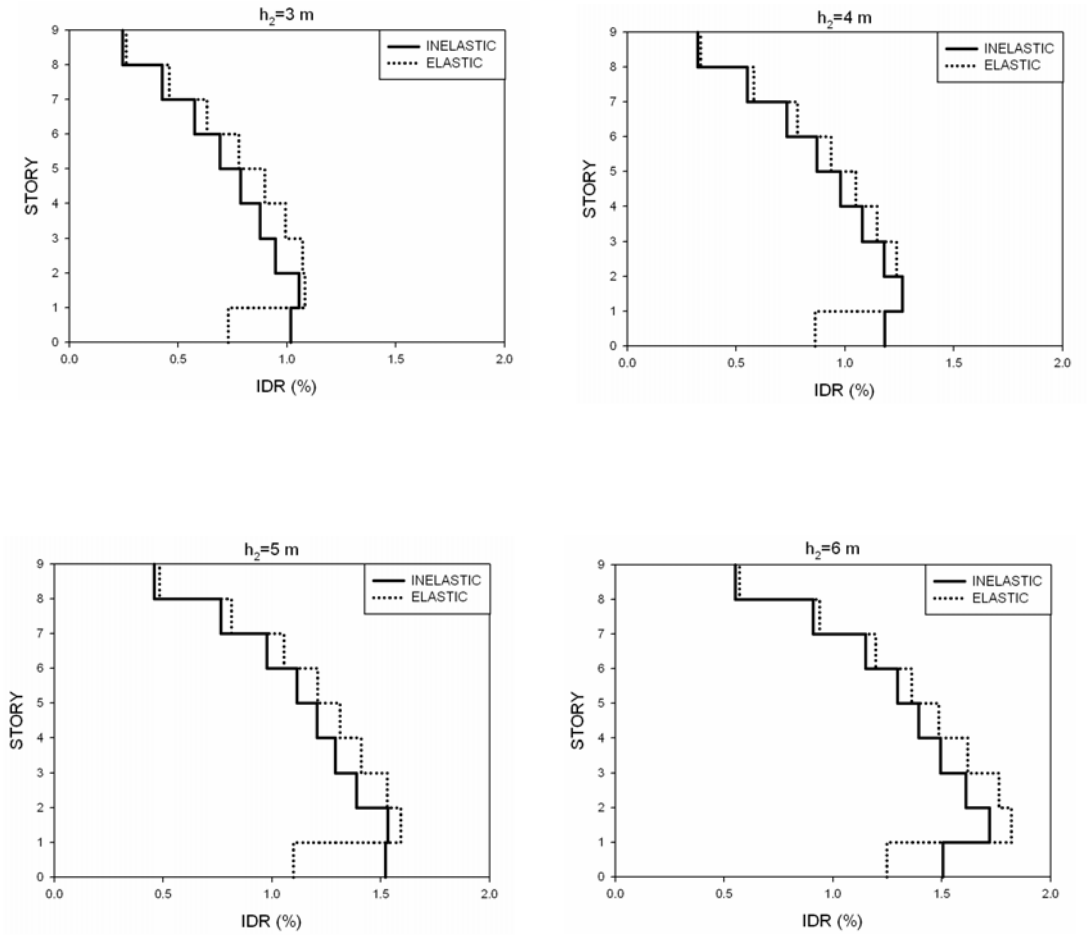

Figure 4.43: Comparison of regular story height effect on the inelastic and elastic drift demand (N=9, Q=1.2)

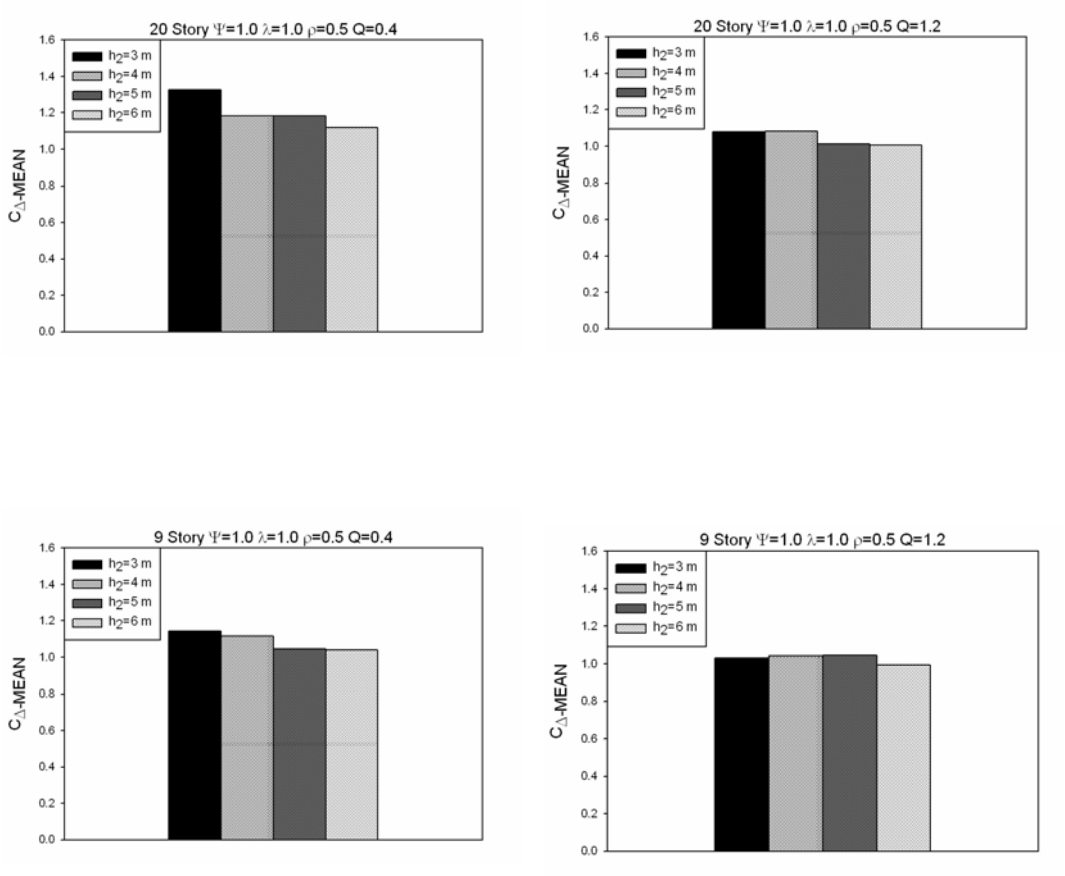

Figure 4.44: Effect of regular story height on inelastic drift ratio (N=20 and 9, Q=0.40 and 1.2)

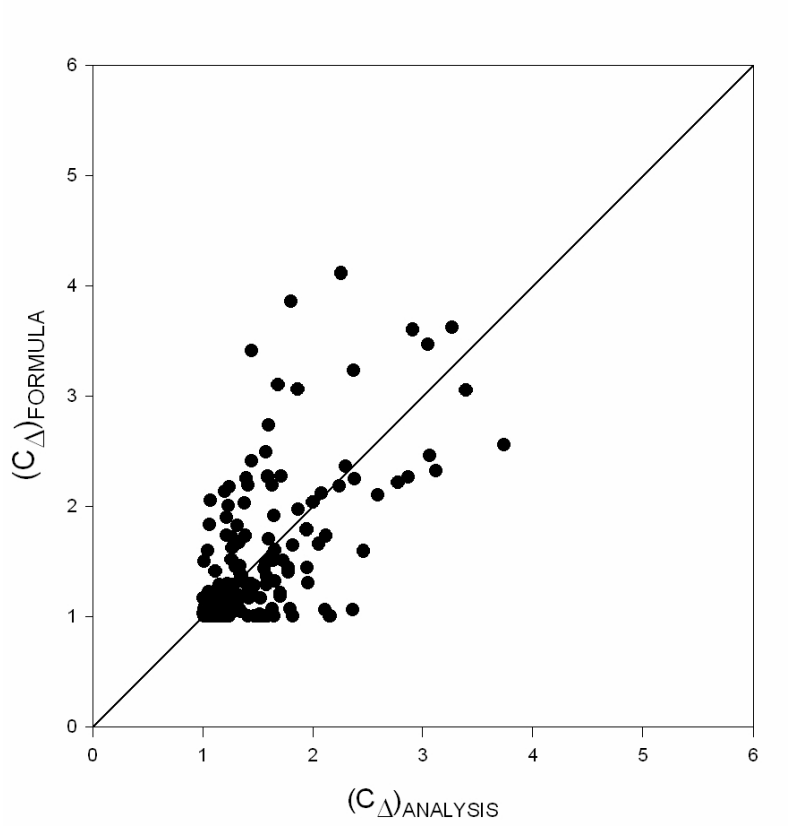

Figure 4.45: Correlation between $(C_\Delta)_{FORMULA}$ and $(C_\Delta)_{ANALYSIS}$

CHAPTER 5

VERIFICATION

5.1 VERIFICATION OF THE PROPOSED EQUATIONS FOR THE ELASTIC GSDR AND MIDR

The accuracy of the improved equations for the prediction of elastic ground story drift ratio and maximum inter-story drift ratio will be investigated in this chapter. In order to evaluate the validity of proposed equations on different frames with different structural properties, four moment resisting frames (N=5, 7, 12 and 15 stories tall) were generated by removing the upper stories of 20 story and 9 story SAC MRFs. These frames are represented by generic fishbone models. An extra 41’760 linear time history analyses were conducted to investigate the accuracy of the equations.

The approximate equations for GSDR of shear frame, GSDR and MIDR of moment resisting frame are given in Equations (3.3), (3.14) and (3.19), respectively. The values computed by using these equations are referred as “approximate” and the values found from linear time history analyses are referred as “exact” in the context of this chapter. In order to evaluate the accuracy of the equations, approximate values are plotted against the exact values and the mean and standard deviation values for the ratio of approximate result to exact (A/E) result are calculated.

The ground story drift ratios of shear frames computed by using Equation (3.3) are compared with time history analysis results for frames with different N (number of story), λ (stiffness distribution coefficient) and ψ (soft story factor) values in Figures 5.1-5.7. It is observed that the approximate equation captures the exact response very well for "high"-rise frames (N=20, 15 and 12). However, the equation overestimates the response for low-rise frames (N=3 and 5). Since the sinusoidal function used in this equation overestimates the amplitude of the first mode vector (ϕ) of low rise frames at the ground story, Equation (3.3) results in higher values with respect to time history analyses. The sinusoidal function results in approximately 10 percent higher values for also 9-story and 7-story MRFs. Mean and standard deviation values for A/E values related to $GSDR_{SH}$ obtained from 58 ground motions for different frame configurations are shown in Table 5.1. It is observed that the proposed equation provides acceptably accurate estimates. The average A/E values increase with stiffness distribution coefficient for low rise frames. The error is maximum for 3-story MRFs.

Figures 5.8 – 5.14 show the comparison of the approximate values for the ground story drift ratio of moment resisting frames ($GSDR_{MF}$) calculated by using Equation (3.14) and the exact values. Approximate equations for $GSDR_{SH}$ and $GSDR_{MF}$ show similar errors with respect to exact values, because the error caused by the sinusoidal function is also present in $GSDR_{MF}$. Similar to $GSDR_{SH}$, approximate equation for $GSDR_{MF}$ gives good results for high rise frames. Due to overestimation of the amplitude of the first mode vector (ϕ) at the ground story, approximate ground story drift ratio is higher than exact results for low rise frames. In addition, the expression slightly overestimates $GSDR_{MF}$ of 9-story and 7-story MRFs. Statistical information of these figures are given in Table 5.2. It is seen that for high rise frames with higher beam to column stiffness ratio, approximate equation generally results in better estimations. It is also observed that standard deviation decreases with increasing ρ values because higher mode effect is more pronounced for low ρ values which results in long period frames. Like $GSDR_{SH}$, maximum errors are observed at 3-story MRFs. Error of the equation increases with increasing soft story factor for 3-story frame.

The maximum inter-story drift ratio of moment resisting frames given in Equation (3.19) is calculated by multiplying $GSDR_{MF}$ with γ'_{MIDR} in Equation (3.18). The comparisons of approximate results with exact values for maximum inter-story drift ratio are shown in Figures 5.15 – 5.21. It is seen that for 20-story and 15 story frames with $\rho = 0.25$, the equation underestimates the response for some of the ground motion records. Spectral displacements corresponding to the second and third modes are higher than the spectral displacements corresponding to the first mode for these ground motions. Therefore the proposed equation underestimates the response, since only the fundamental mode response is taken into account during the generation of the proposed equation. It is observed that Equation (3.19) captures maximum inter-story drift ratio of 20, 15, 12, 9 and 7 story MRFs well. Furthermore, for 5-story and 3-story frames with low soft story factors, the values calculated by using the formula are good enough. However, deviations from the actual values increase for low rise frames with ψ values of 1.6 and 1.8. Mean and standard deviation of the ratio of approximate values to exact results are given in Table 5.3. In average of A/E values are around 1.0 for high- and mid-rise frames. The standard deviation decreases with increasing ρ values. It can be stated that the proposed procedure for maximum inter-story drift ratio gives sufficiently good results for frames except for 3-story MRFs.

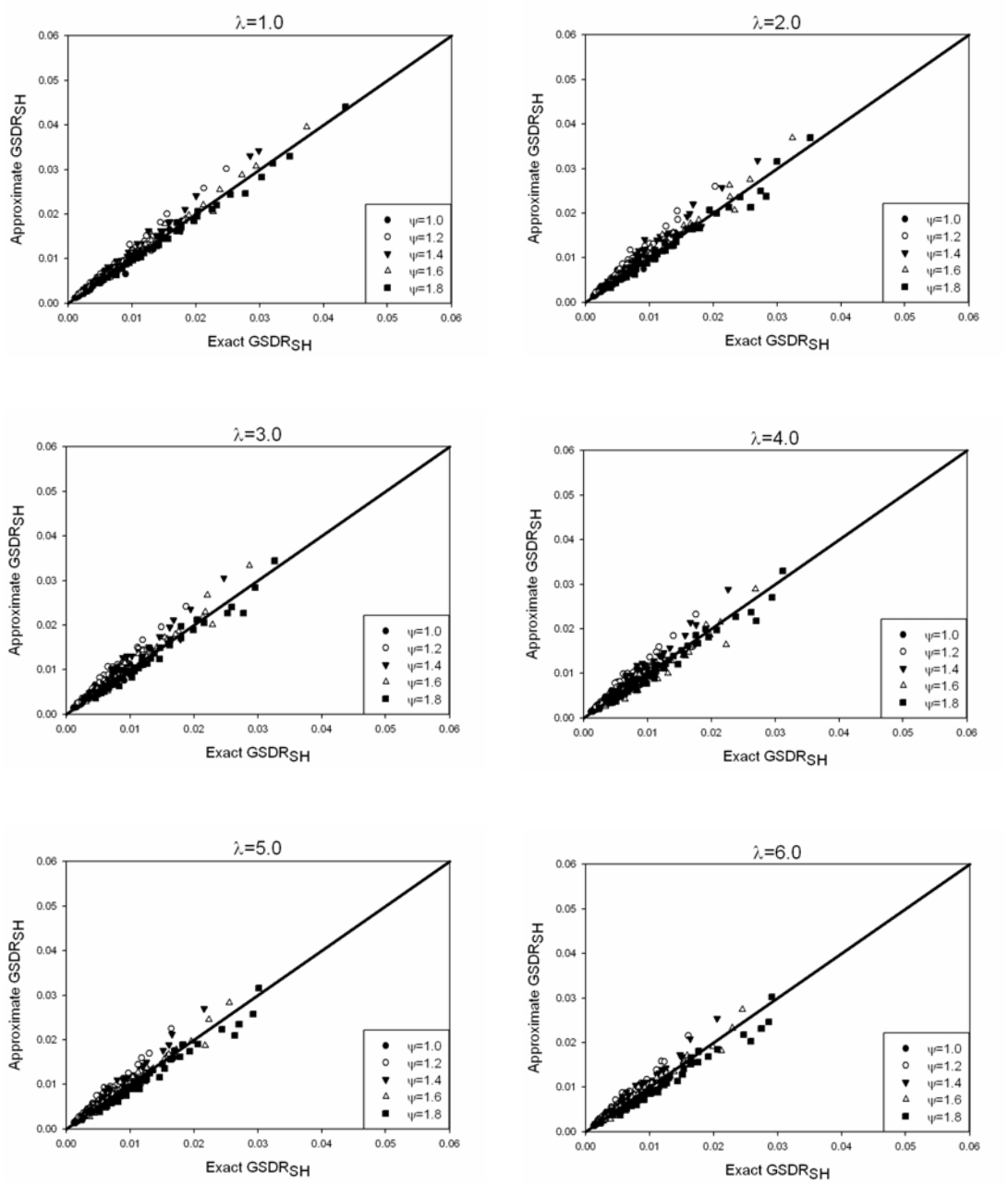

Figure 5.1: Comparison of approximate results with exact values of $GSDR_{SH}$ (N=20, h_2 =3 m)

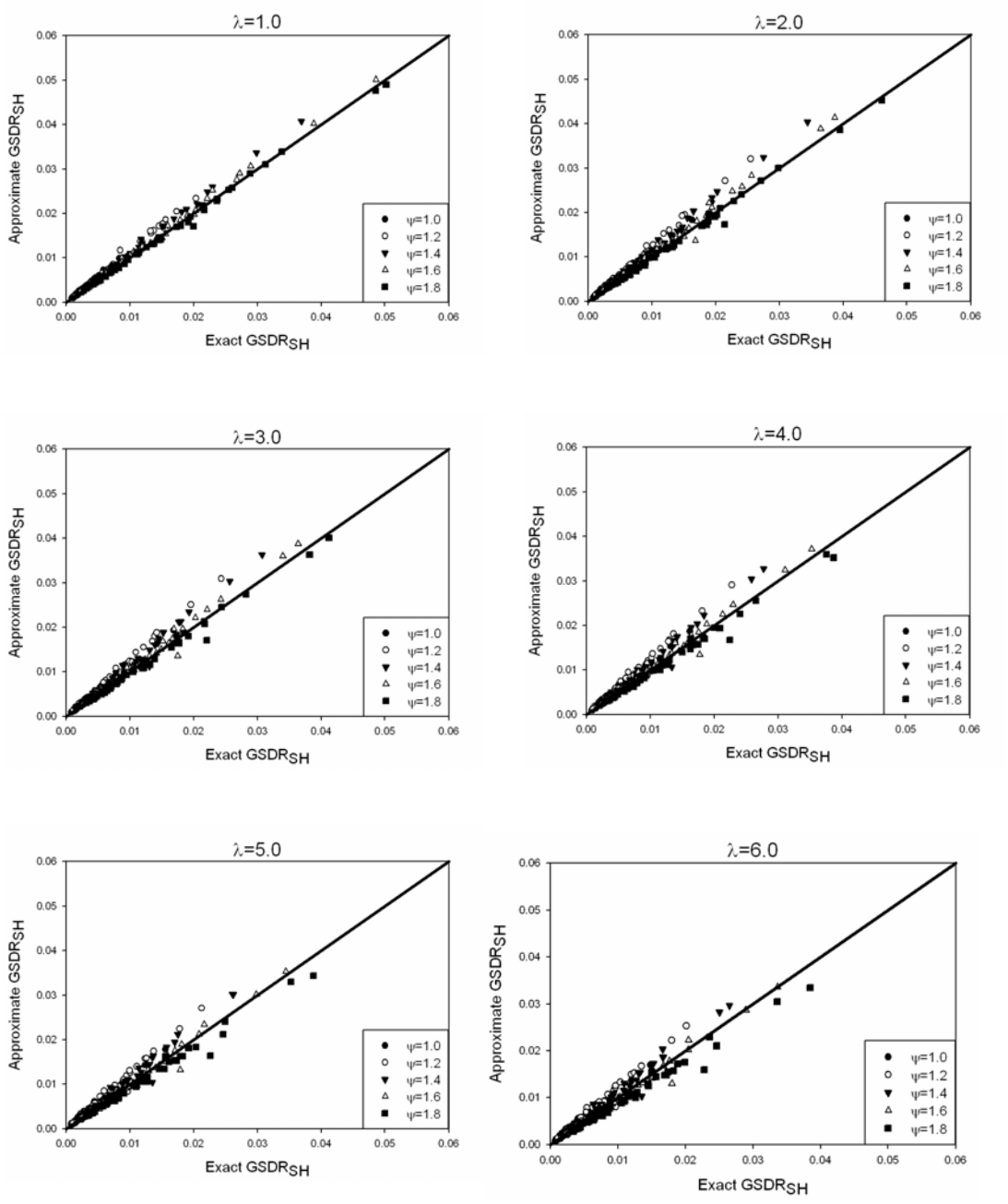

Figure 5.2: Comparison of approximate results with exact values of $GSDR_{SH}$ (N=15, h_2 =3 m)

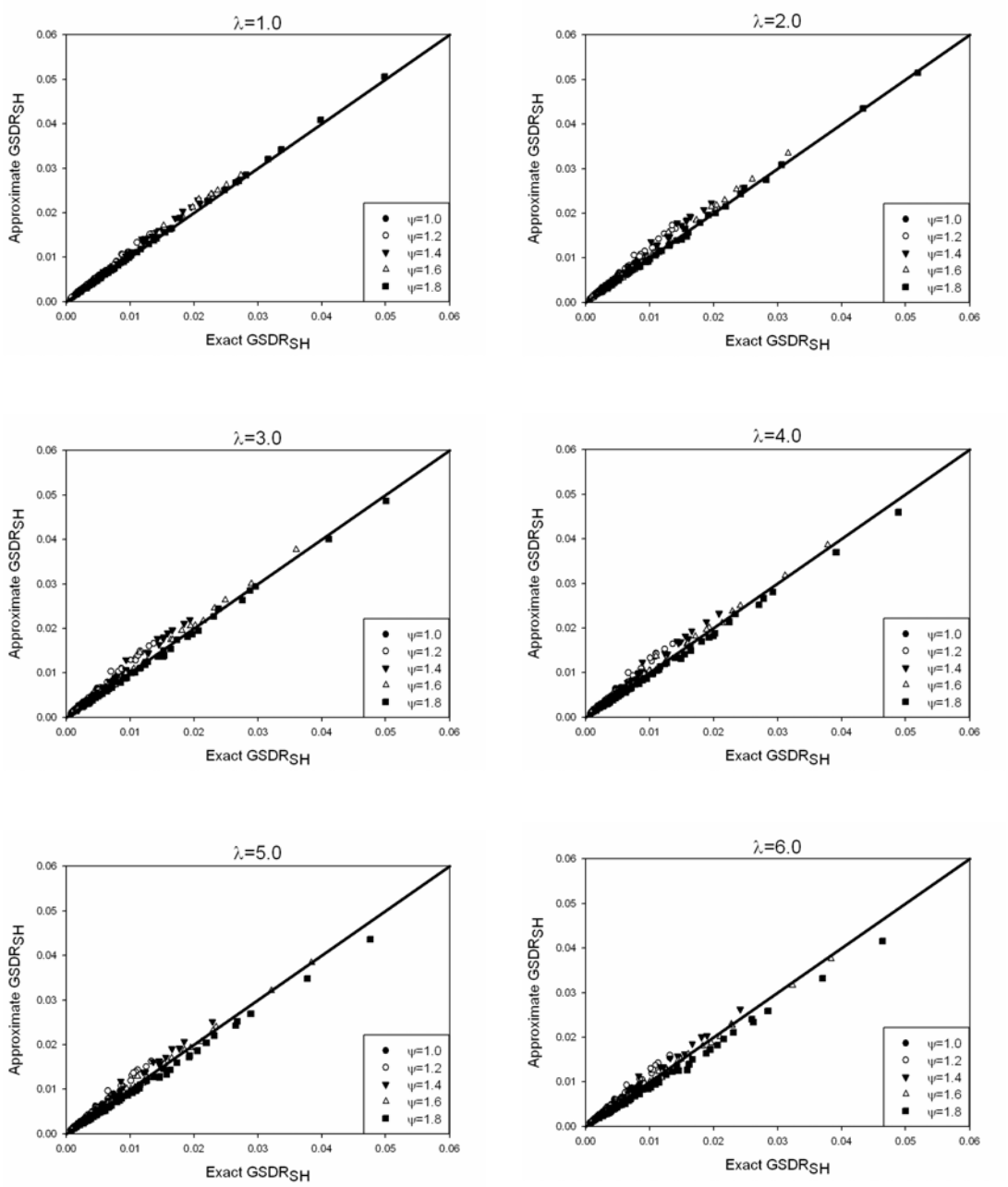

Figure 5.3: Comparison of approximate results with exact values of $GSDR_{SH}$ (N=12, h_2 =3 m)

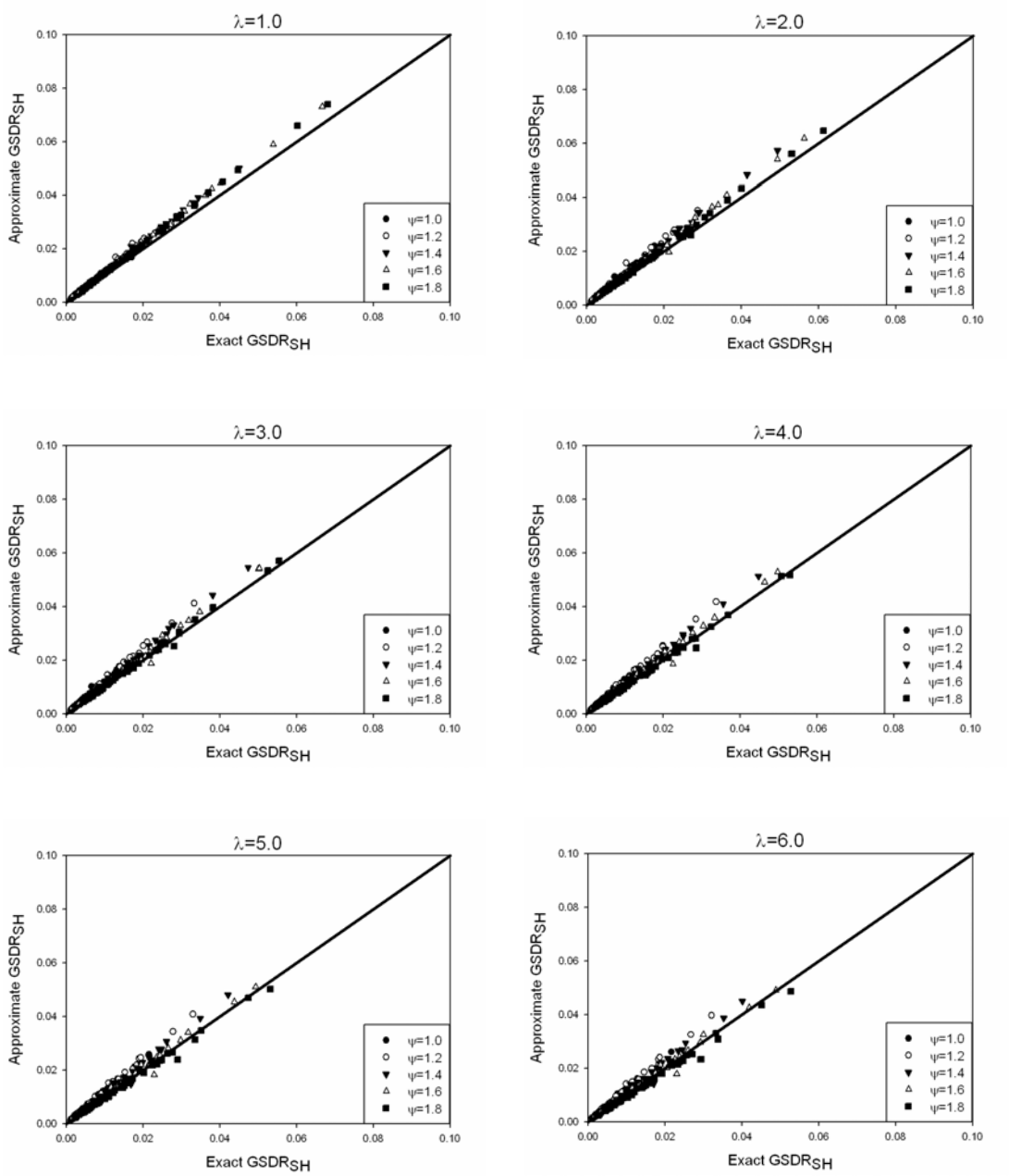

Figure 5.4: Comparison of approximate results with exact values of $GSDR_{SH}$ (N=9, h_2 =3 m)

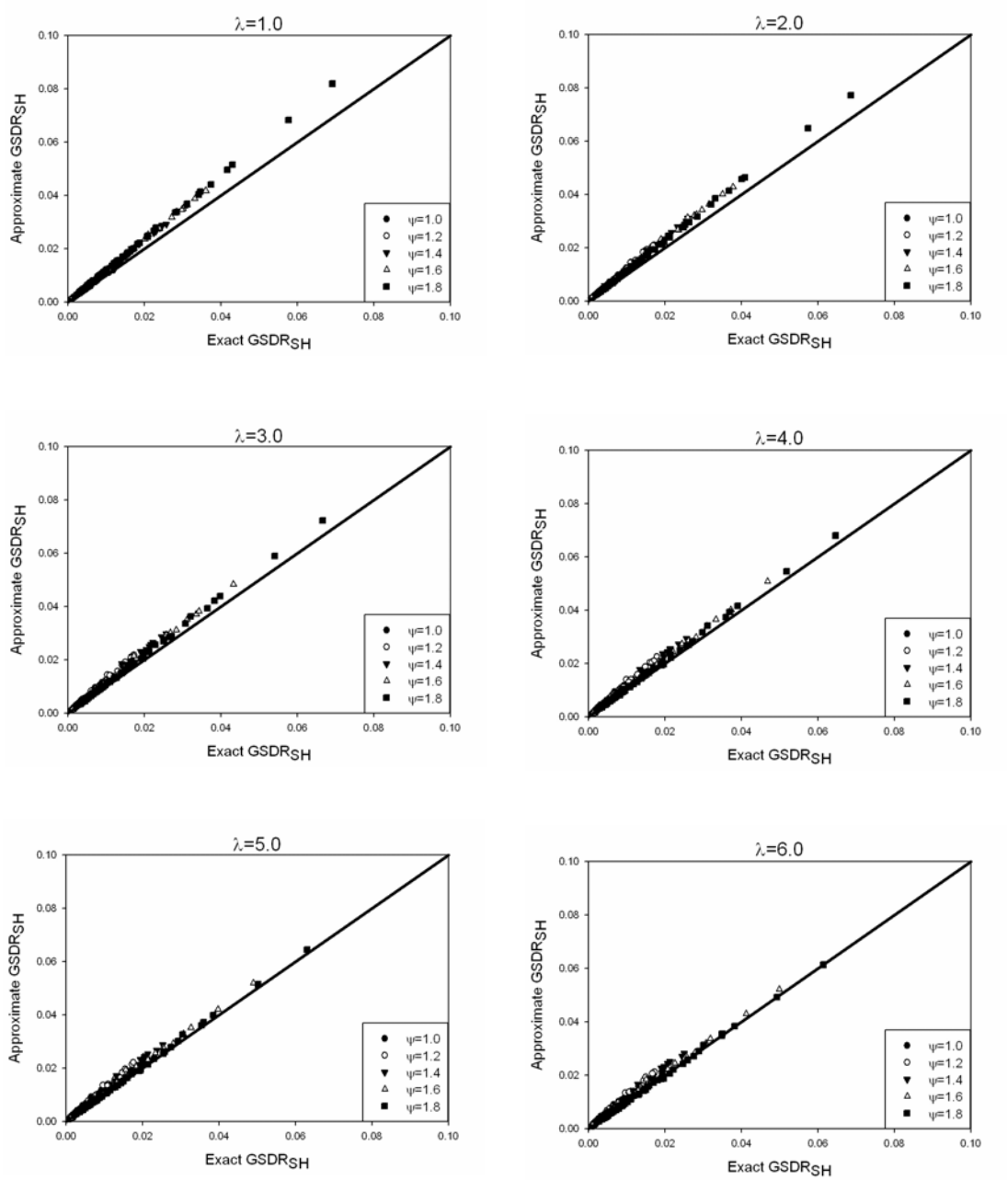

Figure 5.5: Comparison of approximate results with exact values of $GSDR_{SH}$ (N=7, h_2 =3 m)

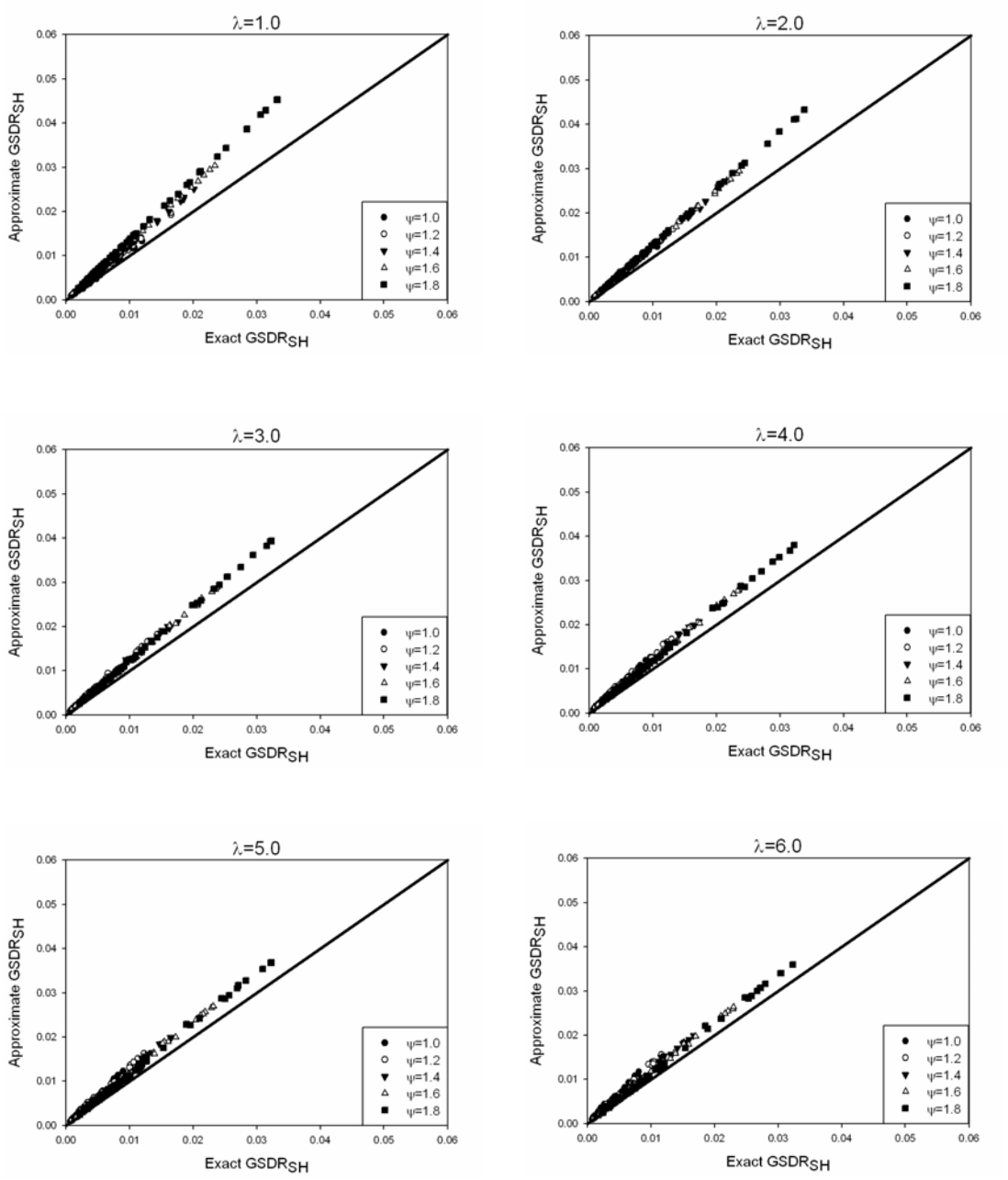

Figure 5.6: Comparison of approximate results with exact values of $GSDR_{SH}$ (N=5, h_2 =3 m)

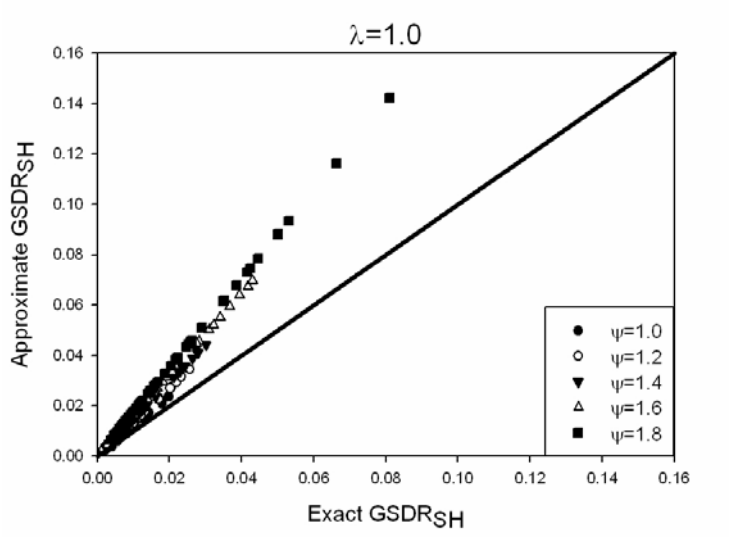

Figure 5.7: Comparison of approximate results with exact values of $GSDR_{SH}$ (N=3, h_2 =3 m)

Table 5.1: A/E statistics for $GSDR_{SH}$

	λ		ψ 1.0	1.2	1.4	1.6	1.8
20 STORY	1	MEAN	0.993	1.175	1.123	1.031	0.957
		STDEV	0.079	0.080	0.065	0.053	0.040
	2	MEAN	1.087	1.266	1.188	1.072	0.963
		STDEV	0.102	0.104	0.093	0.072	0.062
	3	MEAN	1.097	1.270	1.178	1.052	0.944
		STDEV	0.104	0.119	0.099	0.088	0.072
	4	MEAN	1.085	1.253	1.158	1.031	0.920
		STDEV	0.111	0.119	0.106	0.095	0.073
	5	MEAN	1.070	1.238	1.136	1.005	0.894
		STDEV	0.107	0.118	0.108	0.089	0.070
	6	MEAN	1.058	1.212	1.112	0.980	0.870
		STDEV	0.106	0.117	0.110	0.085	0.066
15 STORY	1	MEAN	0.999	1.137	1.091	1.023	0.974
		STDEV	0.067	0.063	0.048	0.034	0.032
	2	MEAN	1.076	1.214	1.136	1.039	0.964
		STDEV	0.084	0.075	0.066	0.060	0.041
	3	MEAN	1.090	1.217	1.137	1.028	0.944
		STDEV	0.075	0.084	0.076	0.061	0.046
	4	MEAN	1.093	1.223	1.125	1.011	0.920
		STDEV	0.091	0.097	0.087	0.066	0.046
	5	MEAN	1.094	1.211	1.108	0.990	0.895
		STDEV	0.103	0.107	0.092	0.065	0.050
	6	MEAN	1.084	1.196	1.091	0.971	0.874
		STDEV	0.104	0.109	0.094	0.066	0.053
12 STORY	1	MEAN	1.004	1.125	1.087	1.044	1.010
		STDEV	0.043	0.043	0.040	0.027	0.019
	2	MEAN	1.090	1.183	1.120	1.044	0.987
		STDEV	0.069	0.070	0.064	0.049	0.031
	3	MEAN	1.104	1.204	1.118	1.027	0.960
		STDEV	0.086	0.093	0.076	0.056	0.034
	4	MEAN	1.111	1.188	1.104	1.009	0.932
		STDEV	0.101	0.093	0.072	0.051	0.032
	5	MEAN	1.098	1.174	1.091	0.991	0.907
		STDEV	0.097	0.091	0.075	0.046	0.032
	6	MEAN	1.077	1.159	1.077	0.971	0.885
		STDEV	0.095	0.093	0.078	0.044	0.037

Table 5.1: A/E statistics for $GSDR_{SH}$ (Continued)

	λ		ψ 1.0	1.2	1.4	1.6	1.8
9 STORY	1	MEAN	1.024	1.131	1.111	1.095	1.092
		STDEV	0.057	0.049	0.037	0.022	0.016
	2	MEAN	1.113	1.192	1.138	1.079	1.049
		STDEV	0.089	0.084	0.053	0.042	0.029
	3	MEAN	1.144	1.204	1.130	1.057	1.015
		STDEV	0.091	0.071	0.052	0.048	0.035
	4	MEAN	1.152	1.206	1.122	1.036	0.983
		STDEV	0.095	0.073	0.066	0.052	0.033
	5	MEAN	1.160	1.197	1.109	1.015	0.955
		STDEV	0.097	0.091	0.074	0.056	0.036
	6	MEAN	1.160	1.188	1.098	0.996	0.931
		STDEV	0.099	0.097	0.076	0.056	0.039
7 STORY	1	MEAN	1.048	1.139	1.150	1.159	1.185
		STDEV	0.037	0.032	0.020	0.016	0.011
	2	MEAN	1.146	1.199	1.160	1.132	1.126
		STDEV	0.057	0.051	0.046	0.033	0.017
	3	MEAN	1.177	1.216	1.154	1.104	1.080
		STDEV	0.078	0.072	0.062	0.042	0.024
	4	MEAN	1.193	1.216	1.137	1.078	1.046
		STDEV	0.091	0.087	0.065	0.042	0.025
	5	MEAN	1.206	1.209	1.122	1.058	1.016
		STDEV	0.101	0.092	0.065	0.043	0.023
	6	MEAN	1.209	1.203	1.111	1.041	0.991
		STDEV	0.115	0.104	0.069	0.042	0.026
5 STORY	1	MEAN	1.077	1.179	1.234	1.297	1.363
		STDEV	0.046	0.029	0.011	0.009	0.006
	2	MEAN	1.180	1.244	1.237	1.244	1.275
		STDEV	0.046	0.037	0.023	0.016	0.012
	3	MEAN	1.254	1.269	1.232	1.210	1.217
		STDEV	0.064	0.054	0.032	0.025	0.015
	4	MEAN	1.299	1.293	1.232	1.187	1.174
		STDEV	0.072	0.059	0.051	0.031	0.021
	5	MEAN	1.331	1.306	1.222	1.164	1.141
		STDEV	0.083	0.069	0.057	0.031	0.025
	6	MEAN	1.355	1.309	1.213	1.145	1.115
		STDEV	0.114	0.083	0.048	0.041	0.030
3 STORY	1	MEAN	1.159	1.331	1.477	1.616	1.755
		STDEV	0.041	0.014	0.010	0.006	0.004

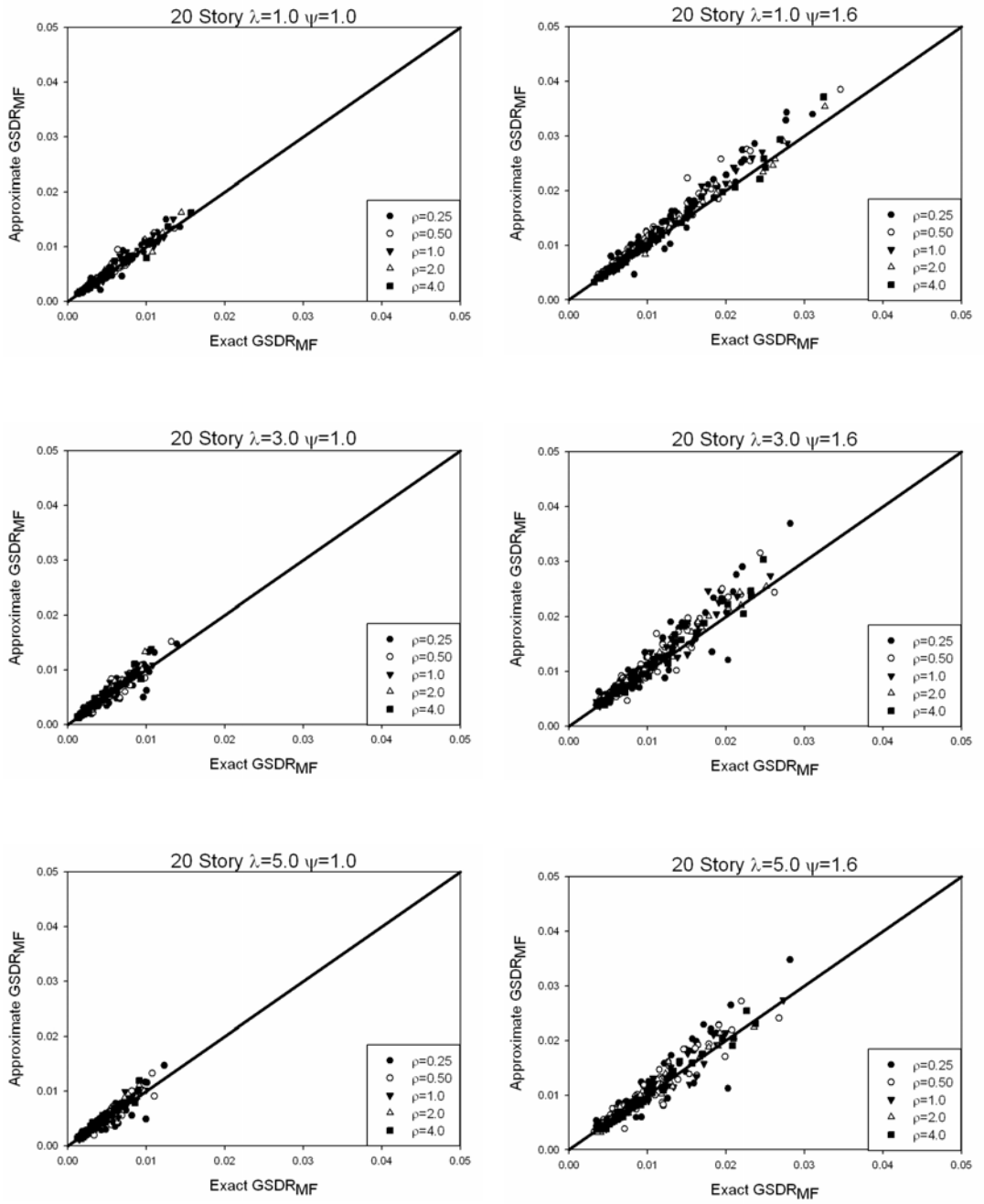

Figure 5.8: Comparison of approximate results with exact values of $GSDR_{MF}$ (N=20, h_2 =3 m)

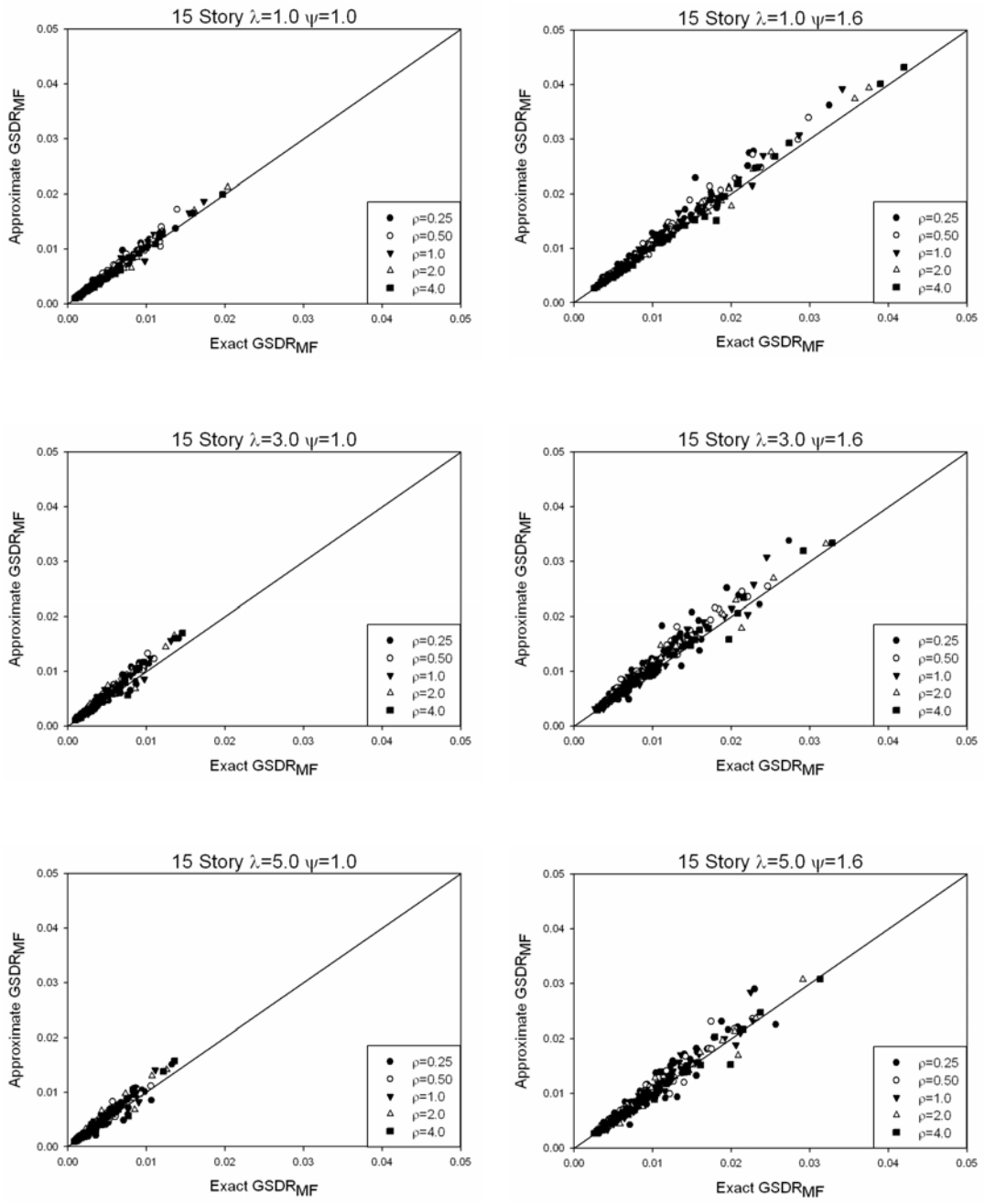

Figure 5.9: Comparison of approximate results with exact values of $GSDR_{MF}$ (N=15, h_2 =3 m)

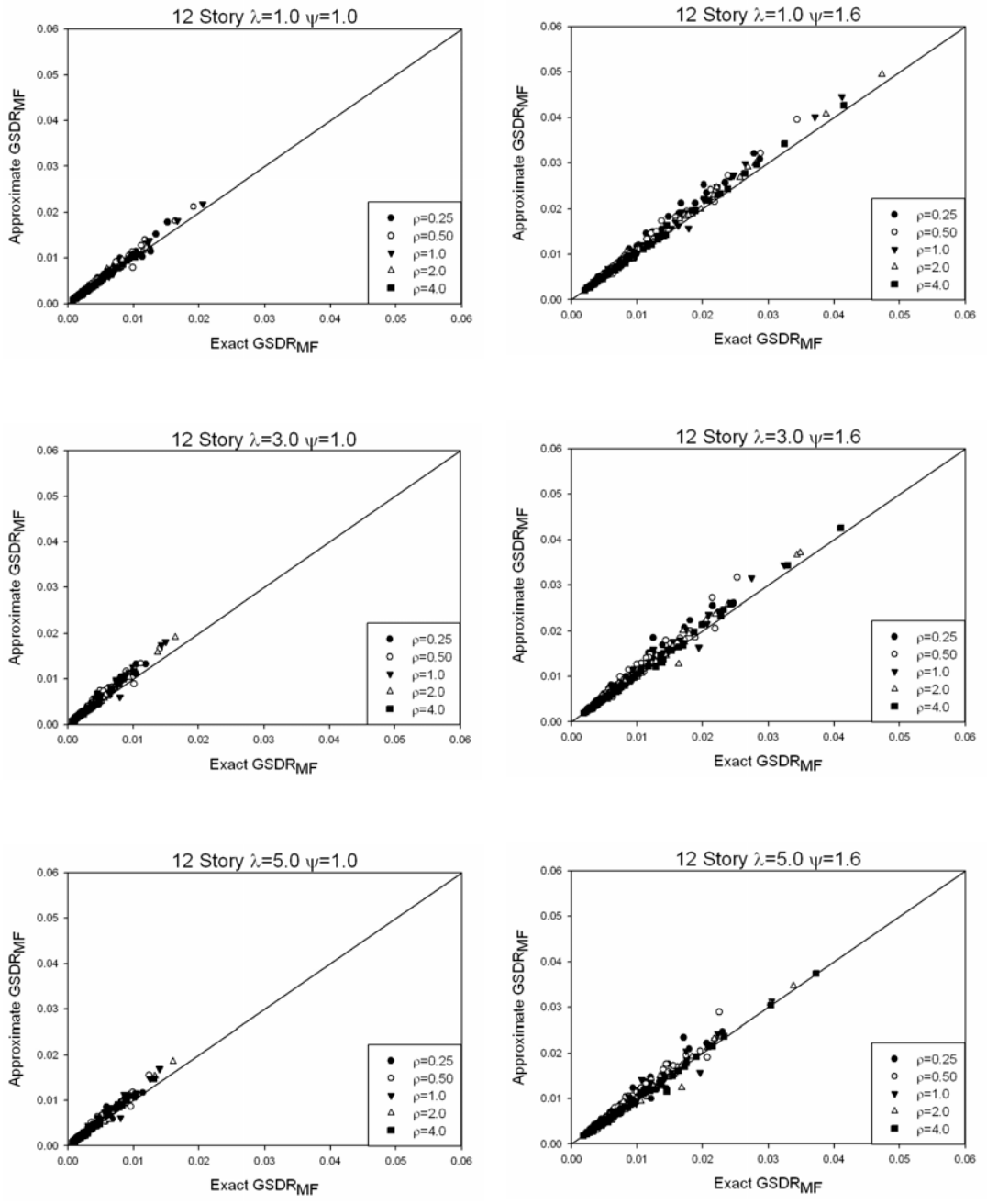

Figure 5.10: Comparison of approximate results with exact values of $GSDR_{MF}$ (N=12, h_2 =3 m)

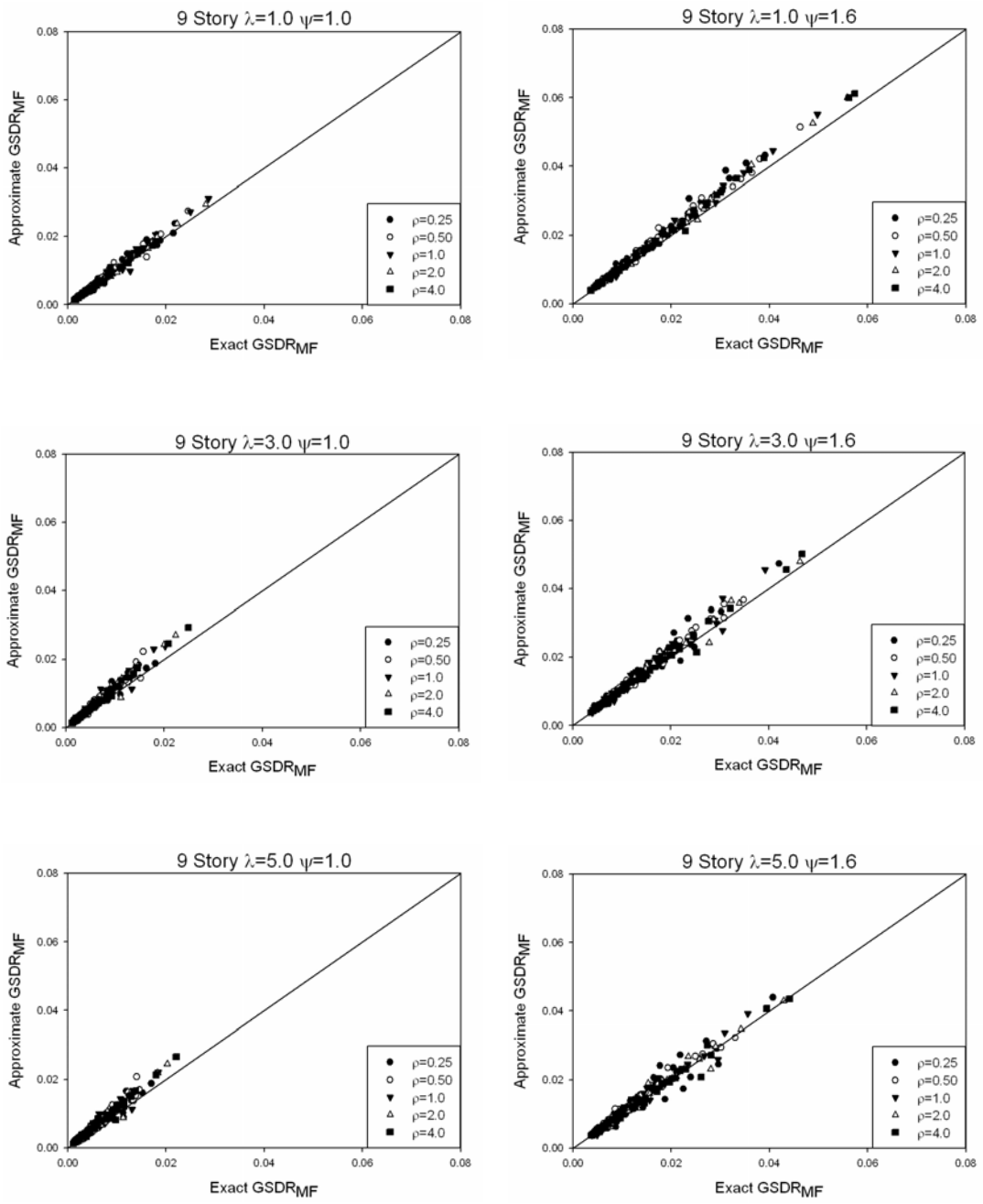

Figure 5.11: Comparison of approximate results with exact values of $GSDR_{MF}$ (N=9, h_2 =3 m)

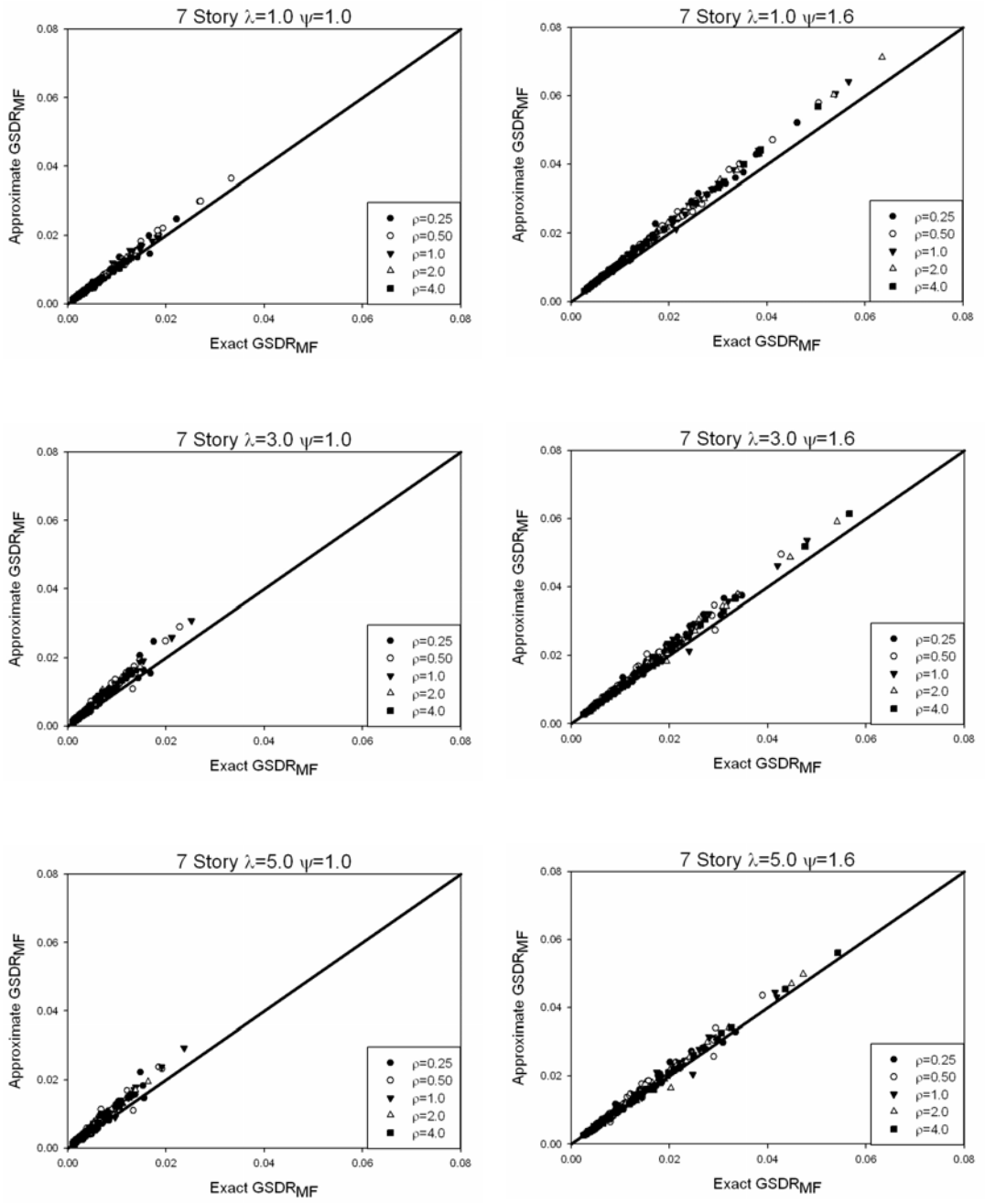

Figure 5.12: Comparison of approximate results with exact values of $GSDR_{MF}$ (N=7, h_2 =3 m)

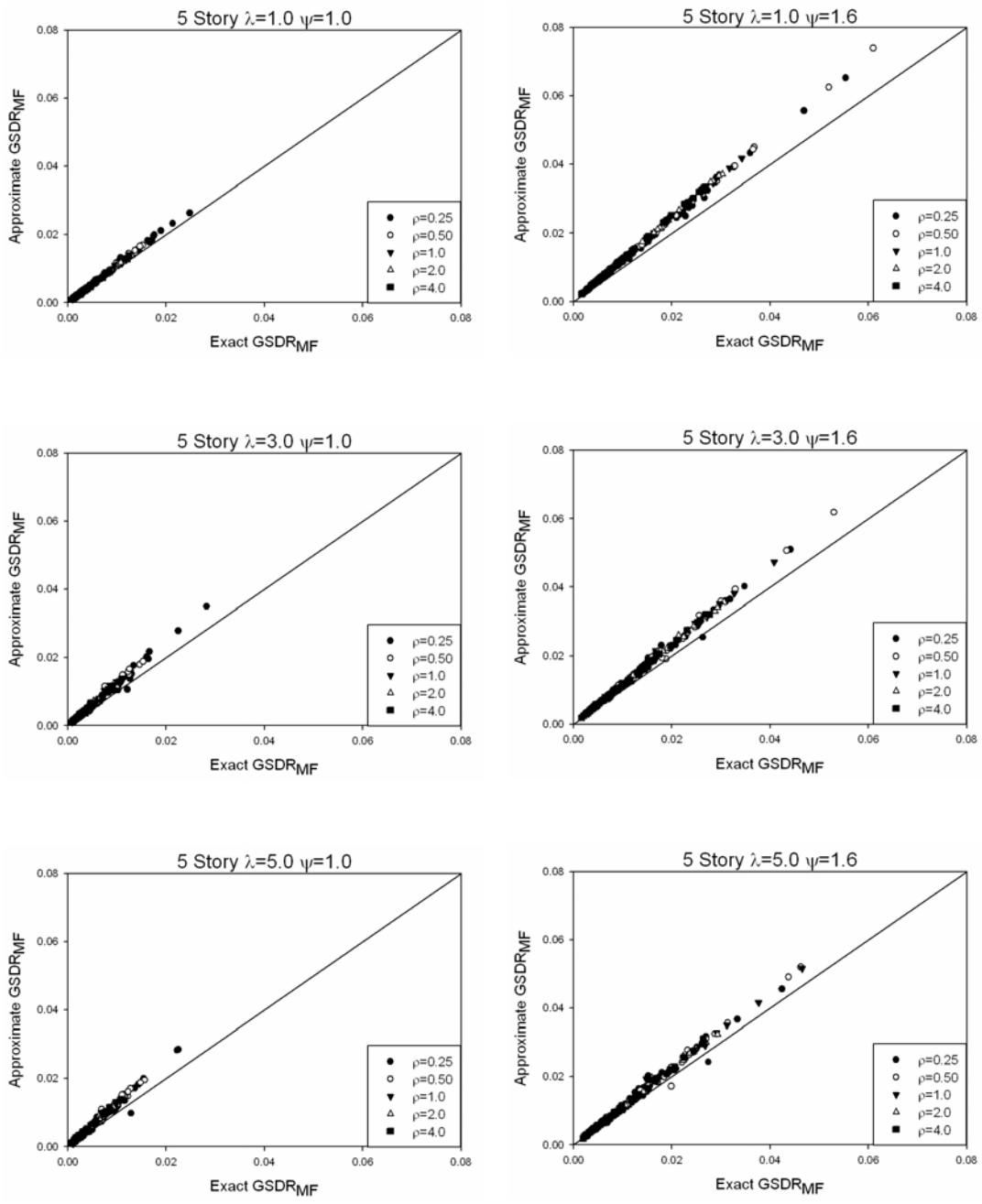

Figure 5.13: Comparison of approximate results with exact values of $GSDR_{MF}$ (N=5, h_2 =3 m)

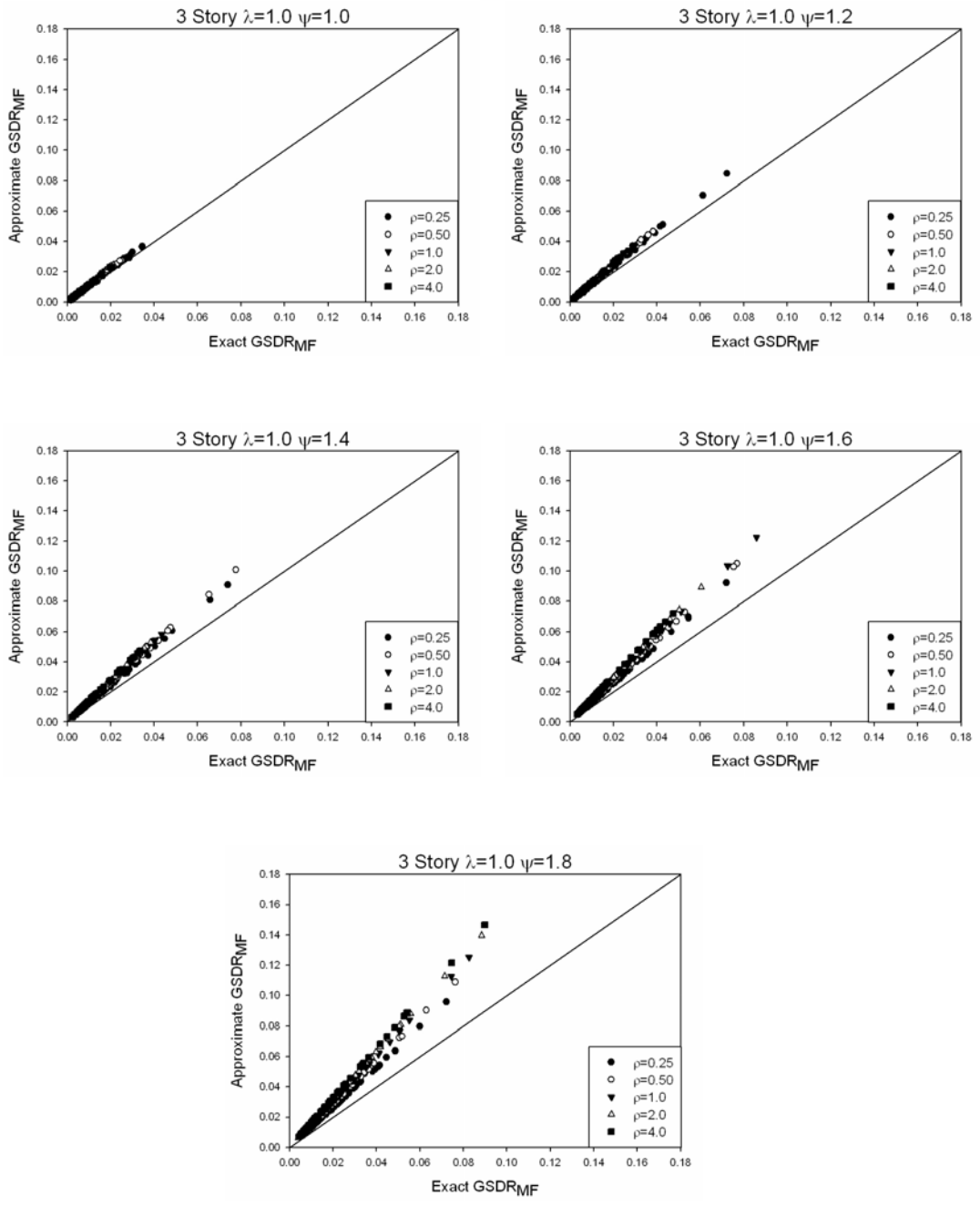

Figure 5.14: Comparison of approximate results with exact values of $GSDR_{MF}$ (N=3, h_2 =3 m)

Table 5.2: A/E statistics for $GSDR_{MF}$

	λ	ψ		ρ 0.25	0.50	1.00	2.00	4.00
20 STORY	1	1.00	MEAN	0.994	1.011	1.013	1.019	0.994
			STDEV	0.133	0.097	0.080	0.077	0.076
	1	1.60	MEAN	1.128	1.112	1.070	1.037	1.030
			STDEV	0.138	0.094	0.071	0.056	0.057
	3	1.00	MEAN	1.029	1.061	1.094	1.081	1.071
			STDEV	0.178	0.152	0.107	0.110	0.113
	3	1.60	MEAN	1.145	1.110	1.082	1.056	1.037
			STDEV	0.186	0.151	0.100	0.065	0.089
	5	1.00	MEAN	0.999	1.031	1.049	1.058	1.050
			STDEV	0.176	0.151	0.117	0.091	0.116
	5	1.60	MEAN	1.101	1.062	1.021	1.023	0.997
			STDEV	0.194	0.155	0.103	0.092	0.074
15 STORY	1	1.00	MEAN	1.029	1.066	1.035	1.006	0.990
			STDEV	0.099	0.082	0.076	0.074	0.059
	1	1.60	MEAN	1.127	1.101	1.074	1.033	1.016
			STDEV	0.087	0.067	0.054	0.046	0.054
	3	1.00	MEAN	1.085	1.125	1.129	1.114	1.087
			STDEV	0.125	0.105	0.108	0.105	0.101
	3	1.60	MEAN	1.128	1.123	1.080	1.048	1.022
			STDEV	0.159	0.092	0.093	0.079	0.065
	5	1.00	MEAN	1.040	1.109	1.096	1.097	1.080
			STDEV	0.161	0.104	0.116	0.120	0.103
	5	1.60	MEAN	1.075	1.073	1.030	1.003	0.987
			STDEV	0.146	0.096	0.094	0.083	0.076
12 STORY	1	1.00	MEAN	1.062	1.062	1.042	1.023	1.001
			STDEV	0.081	0.084	0.061	0.063	0.056
	1	1.60	MEAN	1.128	1.108	1.069	1.037	1.025
			STDEV	0.065	0.054	0.056	0.031	0.033
	3	1.00	MEAN	1.124	1.165	1.135	1.113	1.097
			STDEV	0.098	0.113	0.105	0.075	0.096
	3	1.60	MEAN	1.147	1.113	1.069	1.031	1.016
			STDEV	0.093	0.100	0.067	0.062	0.045
	5	1.00	MEAN	1.113	1.131	1.128	1.097	1.091
			STDEV	0.110	0.114	0.107	0.097	0.090
	5	1.60	MEAN	1.078	1.064	1.030	0.992	0.976
			STDEV	0.106	0.098	0.079	0.067	0.058
9 STORY	1	1.00	MEAN	1.039	1.070	1.041	1.025	1.019
			STDEV	0.084	0.082	0.079	0.062	0.066
	1	1.60	MEAN	1.089	1.095	1.084	1.068	1.062
			STDEV	0.074	0.050	0.039	0.037	0.035
	3	1.00	MEAN	1.114	1.155	1.163	1.136	1.114
			STDEV	0.102	0.123	0.116	0.102	0.082
	3	1.60	MEAN	1.097	1.084	1.072	1.048	1.038
			STDEV	0.097	0.060	0.077	0.053	0.051

Table 5.2: A/E statistics for $GSDR_{MF}$ (Continued)

	λ	ψ		ρ 0.25	0.50	1.00	2.00	4.00
9 STORY	5	1.00	MEAN	1.067	1.138	1.151	1.142	1.138
			STDEV	0.131	0.126	0.122	0.110	0.106
	5	1.60	MEAN	1.029	1.050	1.019	1.003	0.993
			STDEV	0.126	0.078	0.080	0.074	0.060
7 STORY	1	1.00	MEAN	1.062	1.067	1.068	1.049	1.036
			STDEV	0.079	0.064	0.063	0.049	0.038
	1	1.60	MEAN	1.117	1.130	1.124	1.123	1.121
			STDEV	0.052	0.039	0.033	0.023	0.018
	3	1.00	MEAN	1.155	1.180	1.173	1.155	1.151
			STDEV	0.120	0.107	0.078	0.097	0.090
	3	1.60	MEAN	1.100	1.117	1.087	1.074	1.075
			STDEV	0.064	0.064	0.052	0.039	0.038
	5	1.00	MEAN	1.141	1.185	1.181	1.177	1.162
			STDEV	0.136	0.123	0.108	0.101	0.104
	5	1.60	MEAN	1.063	1.059	1.042	1.027	1.026
			STDEV	0.070	0.079	0.059	0.053	0.037
5 STORY	1	1.00	MEAN	1.065	1.095	1.097	1.083	1.066
			STDEV	0.052	0.043	0.034	0.036	0.039
	1	1.60	MEAN	1.174	1.206	1.222	1.234	1.245
			STDEV	0.033	0.026	0.018	0.014	0.010
	3	1.00	MEAN	1.157	1.200	1.220	1.236	1.230
			STDEV	0.102	0.101	0.077	0.069	0.068
	3	1.60	MEAN	1.136	1.145	1.150	1.155	1.166
			STDEV	0.058	0.046	0.044	0.033	0.029
	5	1.00	MEAN	1.170	1.215	1.246	1.273	1.290
			STDEV	0.117	0.105	0.108	0.079	0.089
	5	1.60	MEAN	1.093	1.095	1.101	1.105	1.114
			STDEV	0.070	0.057	0.046	0.047	0.043
3 STORY	1	1.00	MEAN	1.039	1.092	1.122	1.137	1.137
			STDEV	0.043	0.033	0.031	0.028	0.037
	1	1.20	MEAN	1.161	1.223	1.252	1.273	1.285
			STDEV	0.044	0.028	0.021	0.021	0.017
	1	1.40	MEAN	1.222	1.295	1.344	1.377	1.402
			STDEV	0.031	0.024	0.019	0.014	0.011
	1	1.60	MEAN	1.269	1.357	1.429	1.478	1.518
			STDEV	0.020	0.019	0.012	0.008	0.007
	1	1.80	MEAN	1.312	1.425	1.511	1.579	1.630
			STDEV	0.014	0.011	0.011	0.007	0.006

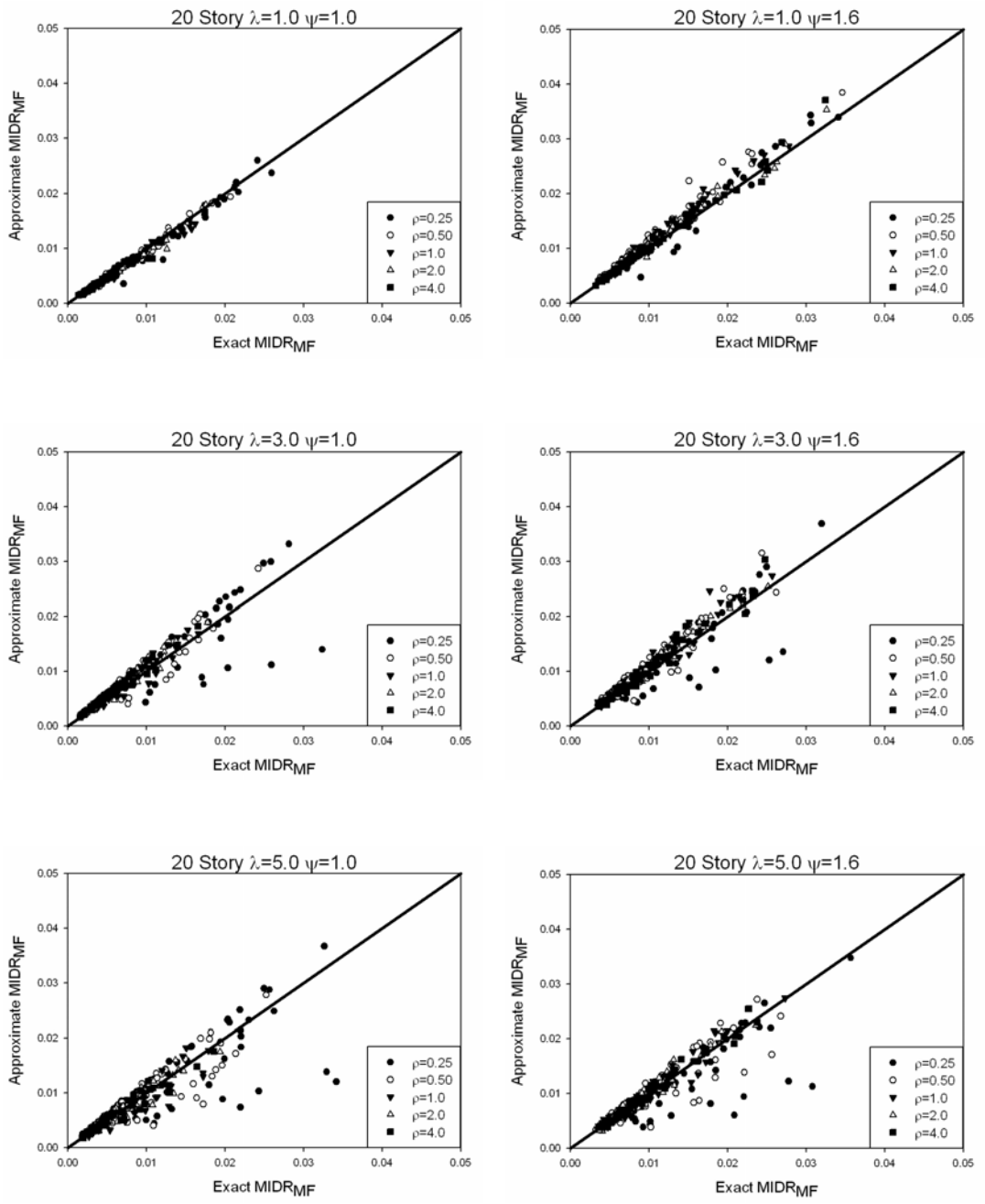

Figure 5.15: Comparison of approximate results with exact values of $MIDR_{MF}$ (N=20, h_2 =3 m)

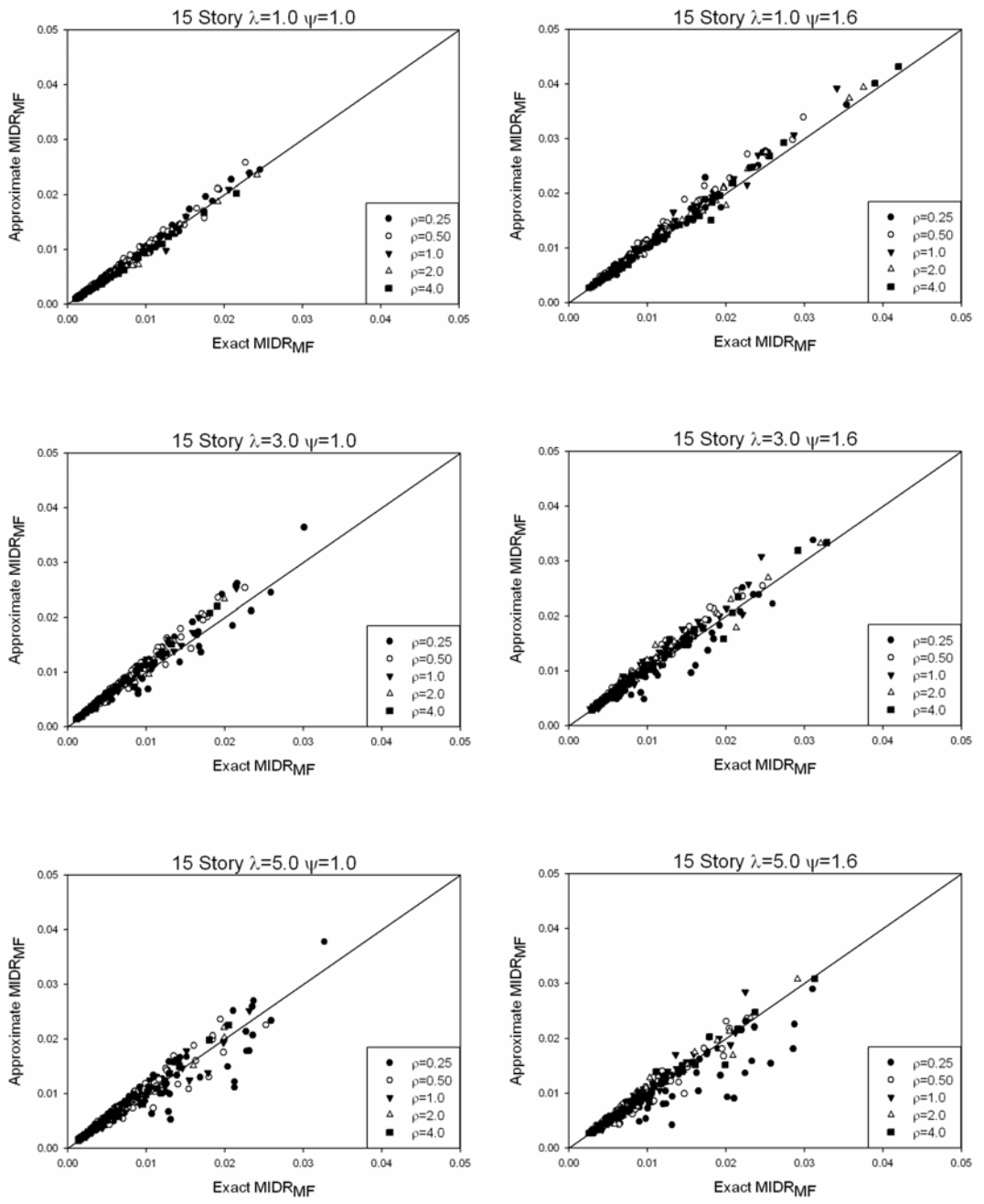

Figure 5.16: Comparison of approximate results with exact values of $MIDR_{MF}$ (N=15, h_2 =3 m)

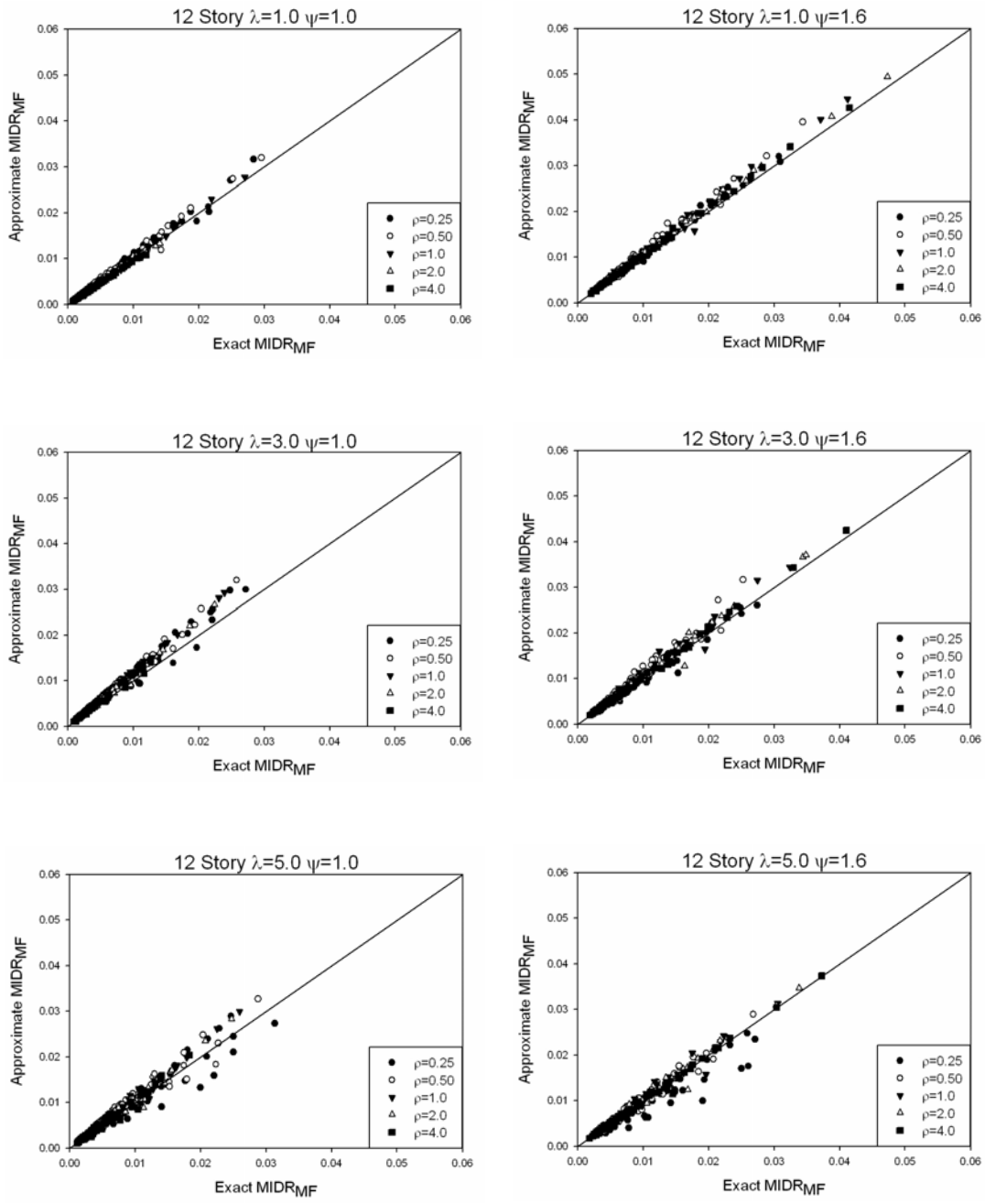

Figure 5.17: Comparison of approximate results with exact values of $MIDR_{MF}$ (N=12, h_2 =3 m)

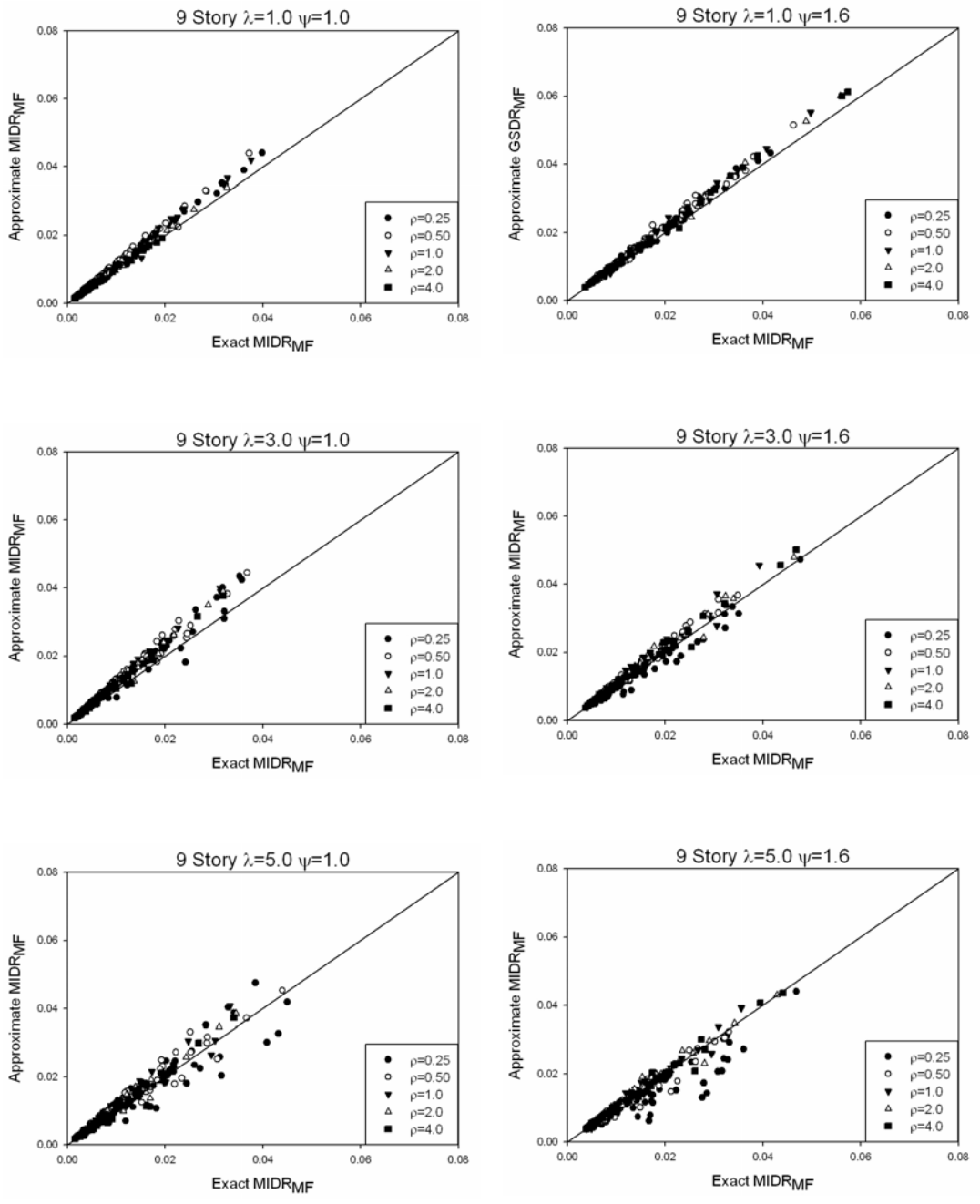

Figure 5.18: Comparison of approximate results with exact values of $MIDR_{MF}$ (N=9, h_2 =3 m)

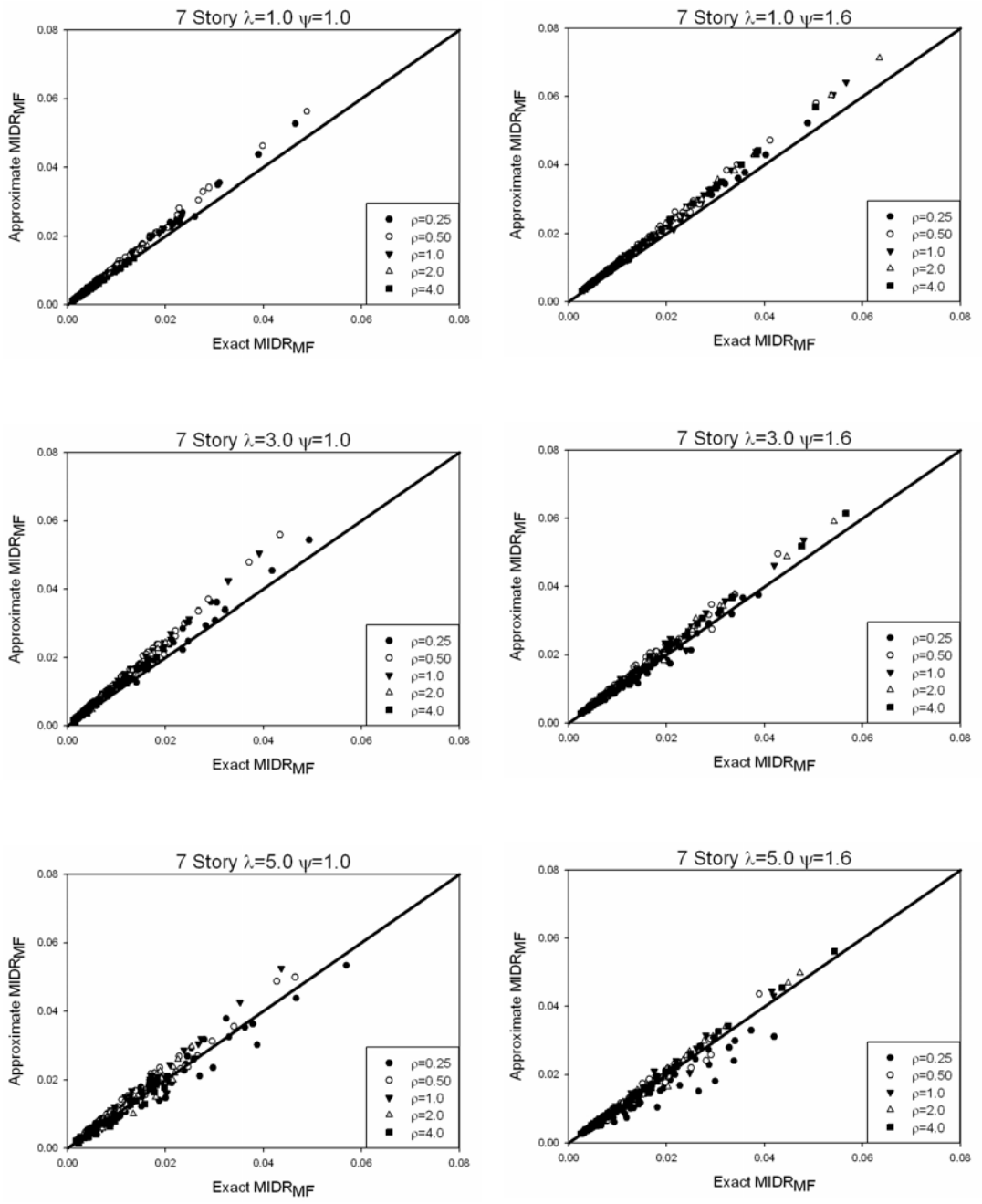

Figure 5.19: Comparison of approximate results with exact values of $MIDR_{MF}$ (N=7, h_2 =3 m)

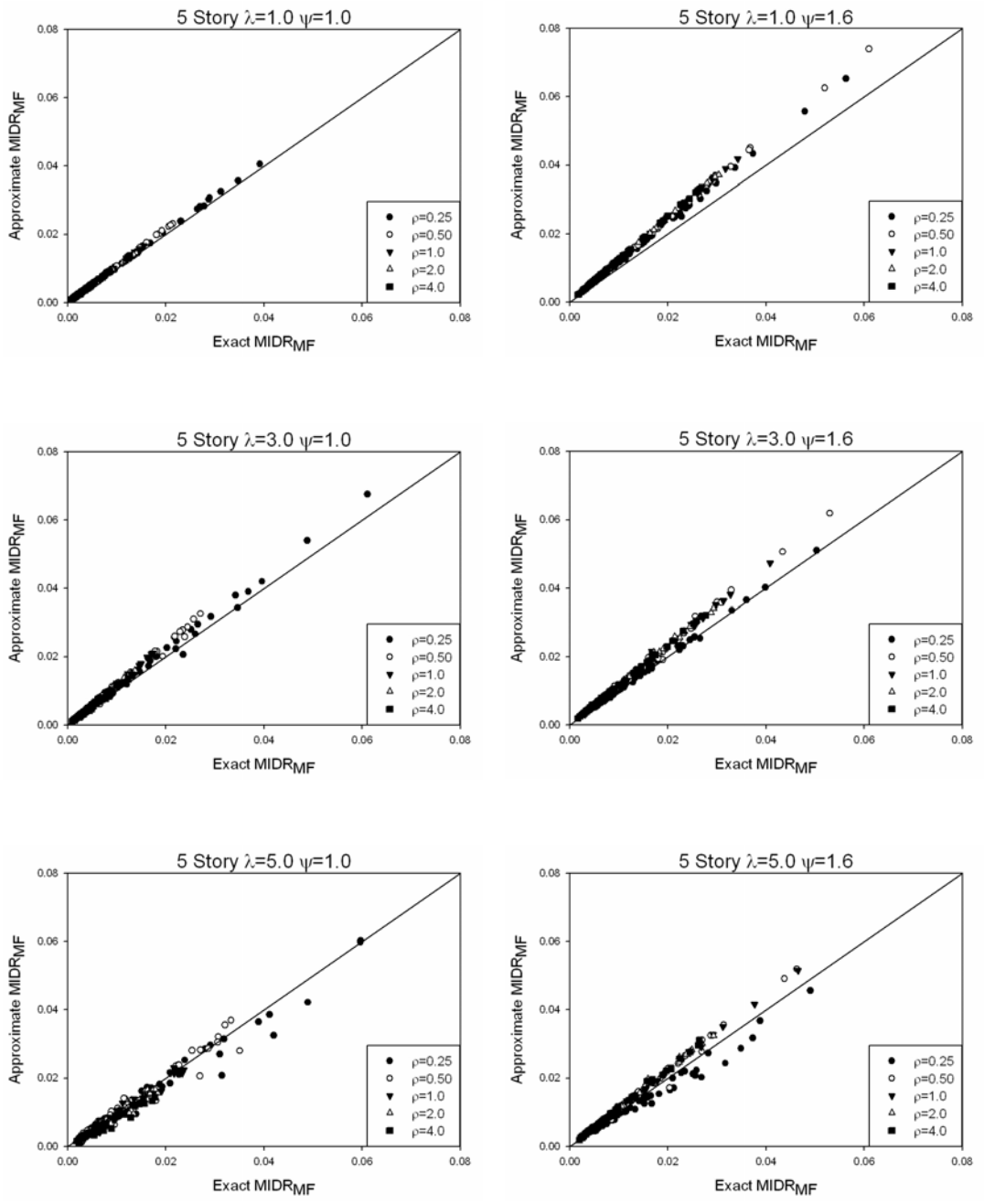

Figure 5.20: Comparison of approximate results with exact values of $MIDR_{MF}$ (N=5, h_2 =3 m)

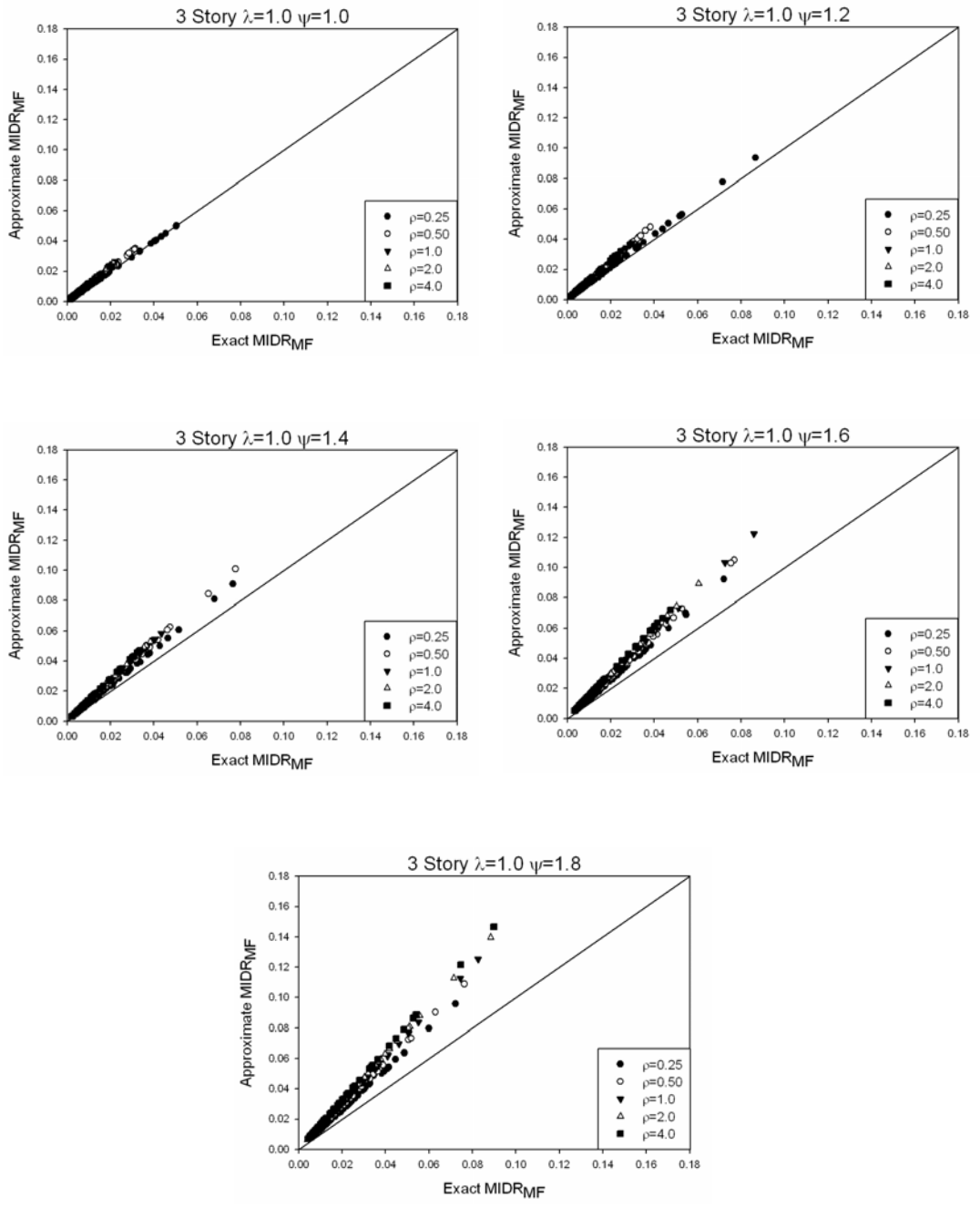

Figure 5.21: Comparison of approximate results with exact values of $MIDR_{MF}$ (N=3, h_2 =3 m)

Table 5.3: A/E statistics for $MIDR_{MF}$

	λ	ψ		ρ 0.25	0.50	1.00	2.00	4.00
20 STORY	1	1.00	MEAN	0.930	0.949	0.941	0.940	0.925
			STDEV	0.091	0.059	0.058	0.057	0.060
	1	1.60	MEAN	1.026	1.112	1.070	1.037	1.030
			STDEV	0.114	0.094	0.071	0.056	0.057
	3	1.00	MEAN	1.025	1.064	1.091	1.092	1.097
			STDEV	0.236	0.169	0.119	0.091	0.079
	3	1.60	MEAN	0.968	1.089	1.082	1.056	1.037
			STDEV	0.201	0.144	0.100	0.065	0.089
	5	1.00	MEAN	0.962	0.979	0.999	1.008	1.003
			STDEV	0.267	0.214	0.170	0.131	0.123
	5	1.60	MEAN	0.862	0.984	1.009	1.020	0.997
			STDEV	0.220	0.187	0.110	0.087	0.074
15 STORY	1	1.00	MEAN	0.998	1.039	0.989	0.942	0.922
			STDEV	0.058	0.055	0.058	0.057	0.048
	1	1.60	MEAN	1.033	1.101	1.074	1.033	1.016
			STDEV	0.072	0.067	0.054	0.046	0.054
	3	1.00	MEAN	1.089	1.158	1.161	1.139	1.127
			STDEV	0.156	0.100	0.063	0.051	0.056
	3	1.60	MEAN	0.962	1.110	1.080	1.048	1.022
			STDEV	0.135	0.082	0.093	0.079	0.065
	5	1.00	MEAN	0.989	1.065	1.062	1.067	1.056
			STDEV	0.204	0.152	0.121	0.080	0.081
	5	1.60	MEAN	0.837	1.024	1.024	1.003	0.987
			STDEV	0.170	0.126	0.092	0.083	0.076
12 STORY	1	1.00	MEAN	1.047	1.059	1.008	0.958	0.927
			STDEV	0.049	0.060	0.050	0.040	0.040
	1	1.60	MEAN	1.041	1.108	1.069	1.037	1.025
			STDEV	0.050	0.054	0.056	0.031	0.033
	3	1.00	MEAN	1.138	1.216	1.196	1.136	1.107
			STDEV	0.101	0.053	0.058	0.060	0.064
	3	1.60	MEAN	0.991	1.109	1.069	1.031	1.016
			STDEV	0.079	0.095	0.067	0.062	0.045
	5	1.00	MEAN	1.039	1.109	1.115	1.056	1.025
			STDEV	0.151	0.117	0.087	0.095	0.106
	5	1.60	MEAN	0.870	1.026	1.028	0.992	0.976
			STDEV	0.132	0.093	0.073	0.067	0.058
9 STORY	1	1.00	MEAN	1.106	1.144	1.087	1.023	0.984
			STDEV	0.046	0.059	0.058	0.047	0.039
	1	1.60	MEAN	1.023	1.095	1.084	1.068	1.062
			STDEV	0.049	0.050	0.039	0.037	0.035
	3	1.00	MEAN	1.152	1.233	1.242	1.192	1.133
			STDEV	0.125	0.090	0.058	0.062	0.062
	3	1.60	MEAN	0.939	1.080	1.072	1.048	1.038
			STDEV	0.090	0.061	0.077	0.053	0.051

Table5.3: A/E statistics for $MIDR_{MF}$ (Continued)

	λ	ψ		ρ 0.25	0.50	1.00	2.00	4.00
9 STORY	5	1.00	MEAN	1.019	1.091	1.118	1.078	1.022
			STDEV	0.189	0.145	0.113	0.098	0.103
	5	1.60	MEAN	0.814	0.996	1.012	1.003	0.993
			STDEV	0.146	0.102	0.075	0.074	0.060
7 STORY	1	1.00	MEAN	1.112	1.139	1.108	1.044	0.995
			STDEV	0.041	0.041	0.035	0.028	0.024
	1	1.60	MEAN	1.065	1.130	1.124	1.123	1.121
			STDEV	0.024	0.039	0.033	0.023	0.018
	3	1.00	MEAN	1.143	1.254	1.238	1.179	1.121
			STDEV	0.083	0.058	0.067	0.078	0.078
	3	1.60	MEAN	0.972	1.115	1.087	1.074	1.075
			STDEV	0.050	0.060	0.052	0.039	0.038
	5	1.00	MEAN	1.006	1.133	1.103	1.034	0.964
			STDEV	0.123	0.096	0.115	0.132	0.124
	5	1.60	MEAN	0.851	1.021	1.042	1.027	1.026
			STDEV	0.103	0.068	0.059	0.053	0.037
5 STORY	1	1.00	MEAN	1.025	1.075	1.070	1.031	1.059
			STDEV	0.022	0.021	0.013	0.013	0.031
	1	1.60	MEAN	1.154	1.206	1.222	1.234	1.245
			STDEV	0.018	0.026	0.018	0.014	0.010
	3	1.00	MEAN	1.070	1.168	1.168	1.140	1.084
			STDEV	0.054	0.071	0.079	0.054	0.055
	3	1.60	MEAN	1.010	1.145	1.150	1.155	1.166
			STDEV	0.022	0.046	0.044	0.033	0.029
	5	1.00	MEAN	0.932	0.992	0.939	0.880	0.810
			STDEV	0.095	0.138	0.124	0.107	0.099
	5	1.60	MEAN	0.895	1.084	1.095	1.105	1.114
			STDEV	0.057	0.056	0.041	0.047	0.043
3 STORY	1	1.00	MEAN	0.994	1.115	1.196	1.167	1.136
			STDEV	0.013	0.016	0.017	0.022	0.032
	1	1.20	MEAN	1.078	1.247	1.252	1.273	1.285
			STDEV	0.014	0.022	0.021	0.021	0.017
	1	1.40	MEAN	1.182	1.295	1.344	1.377	1.402
			STDEV	0.018	0.024	0.019	0.014	0.011
	1	1.60	MEAN	1.269	1.357	1.429	1.478	1.518
			STDEV	0.020	0.019	0.012	0.008	0.007
	1	1.80	MEAN	1.312	1.425	1.511	1.579	1.630
			STDEV	0.014	0.011	0.011	0.007	0.006

CHAPTER 6

SUMMARY, CONCLUSIONS AND RECOMMENDATIONS FOR FUTURE STUDIES

6.1 SUMMARY

Maximum interstory drift and the distribution of interstory drift along the height of the structure are the main causes of structural and nonstructural damage in buildings subjected to earthquake ground motions. Estimation of maximum interstory drift ratio is an important issue for the determination of local response of buildings.

The main objective of this study is to improve the simple equations that estimate maximum ground story displacement ratio of shear frames presented by Gülkan and Akkar (2002) and maximum ground story drift ratio and interstory drift ratio of regular moment resisting frames presented by Akkar et al. (2005). Another aim of the study is to provide knowledge on the response of regular and irregular, elastic and inelastic frame structures subjected to near fault ground motions. The effects of beam-to-column capacity ratio, seismic force reduction factor, ratio of pulse period to fundamental period, beam to column stiffness ratio, soft story factor, stiffness distribution coefficient, regular story height and number of stories on elastic and inelastic drift demands have been investigated in detail.

Important properties of near fault ground motions were summarized in Chapter 2. A set of 58 near-fault pulse-type ground motion records were downloaded from the PEER Strong Motion Database. 20-story, 9-story and 3-story steel moment resisting frame buildings designed as part of the SAC steel project were utilized. To avoid intrinsic complexity and additional computational effort required by detailed modeling, fishbone models were used in this research, which can be very useful for structural performance assessment and as well as design. Procedures to construct a generic frame model were described in Section 2.5. The validity of the proposed generic model was tested by comparing estimates of element deformation demands and modal characteristics obtained using the simple fishbone model to results obtained using full frame representations. One of the aims of this study is the investigation of the effects of different structural properties on structural response. Some of the utilized structural properties (beam to column stiffness ratio, stiffness distribution coefficient, and beam-to-column capacity ratio, soft story factor, regular story height and number of stories) were defined in Section 2.6.

In Chapter 3, elastic response of MDOF systems subjected to near-fault ground motions were analyzed. Effects of different structural properties on the structural response of linear MDOF systems were investigated. Nonlinear regression analyses were performed on the results obtained from the modal analyses of generic frame models. The approximate ground story drift expression proposed by Gülkan and Akkar (2002) for regular shear frames was modified by considering non-uniform variables. A modification factor was proposed in Equation 3.9. In order to calculate the maximum interstory drift ratio of an irregular moment resisting frame, the equation proposed by Akkar et al. (2005) was improved in Equation 3.19.

Chapter 4 presents the effects of different structural properties on inelastic response of MDOF systems. An equation for the ratio of maximum inelastic interstory drift ratio to maximum elastic interstory drift ratio developed for a representative case was presented at the end of this chapter.

The proposed linear equation was verified in Chapter 5.

6.2 CONCLUSIONS

The following conclusions are derived from an evaluation of the results obtained in this study. These conclusions are based on a combination of the numerical analyses and literature surveys performed in this study.

6.2.1 CONCLUSIONS CONCERNING EFFECTS OF NEAR SOURCE GROUND MOTIONS

- There exists a need to refine current design procedures to overcome the destructive effect of near source ground motions in the design process.
- It is observed that velocity spectra of near fault records typically have higher ordinates than far fault records. These peaks at periods matching the pulse periods.
- Large magnitude earthquakes have longer pulse periods. It is confirmed that dense instrument arrays will serve to glean information for unraveling the characteristics of ground motions nucleating from faults that threaten urban environments.

6.2.2 CONCLUSIONS CONCERNING ELASTIC RESPONSE OF MULTI STORY FRAMES

- When maximum interstory drift ratios and maximum roof drift ratios of original frame and generic frame are compared, perfect correlation is obtained for the modal properties and elastic deformation demands. The correctness of accepting roof translation as a global index of structural performance is confirmed.

- Ground story drift ratio and maximum interstory drift ratio are amplified as the pulse period approaches the fundamental period of the structure and highest displacement demands are observed near $T_p/T=1.0$. The maximum story demands are accumulated on the lower levels in the vicinity of $T_p/T = 1.0$, which indicates a primarily first mode response.
- For systems with $T_p/T < 1$, contributions of higher modes significantly affect the general response, while for systems with $T_p/T > 1$ fundamental mode is dominant in the overall response of structures. The relative weight of higher mode effects increases with decreasing T_p/T which indicates the importance of higher modes in high-rise frames and for T_p/T values less than about 0.8.
- Maximum inter-story drift occurs in the upper stories of MRFs with smaller beam to column stiffness ratio (ρ) values. When ρ goes to larger values (shear frame), maximum interstory drift occurs in the ground story.
- Deviations of linear analyses from the fundamental mode shape are more pronounced for smaller ρ values and high rise frames because fundamental periods for these frames are very long and other modes also contribute to the response.
- There are no noticeable deviations for the ratio of MIDR to GSDR between response history results and first mode response for all ρ values.
- Elastic maximum interstory drift ratio increases with stiffness distribution coefficient, defined as ratio of the lateral stiffness at the ground story of the building to the lateral stiffness at the top story of the building, and maximum drift location shifts to upper stories. Increase in stiffness distribution coefficient increases the period of the building and the contribution of higher modes.
- Presence of the soft story produces greater effects in high-rise frames than low-rise frames with respect to lateral elastic deformations. Interstory deformation profiles obtained from response history analyses match first mode shapes for all values of the soft story factor.

- Changing story heights does not lead to any differences in mode shapes. Changing the story height does not modify participation factors (Γ) and mode shapes because stiffness of all stories decrease or increase by the same ratio.
- Maximum interstory drift ratio increases with story height due to the increase in spectral displacement. Low rise frames are influenced by increase of story height more than high rise frames, because increase in spectral displacement corresponding to period increase is greater in low rise frames.
- The approximate equations proposed for estimating the elastic ground story displacement ratio of shear and moment resisting frames (Equation 3.3 and 3.14) and the elastic maximum interstory drift ratio of moment resisting frame (Equation 3.19) provide accurate estimates for high-rise frames.

6.2.3 CONCLUSIONS CONCERNING INELASTIC RESPONSE OF MULTI STORY FRAMES

- Varying beam-to-column capacity ratio (Q) does not affect base shear capacity of shear frames since beam capacities do not affect the response in shear frames. They serve only to prevent the rotation of joints. In addition, increasing the ground story height, stiffness distribution coefficient and regular story height reduce base shear capacity for both shear frames and moment resisting frames.
- Increase in the soft story factor, defined as the ratio of ground story height to regular story height, and the regular story height decreases the value of Q after which column yielding mechanism is initiated.
- Increase of girder capacities reduces maximum inelastic interstory drifts for beam yielding mechanisms, but the inelastic drifts increase when column yielding takes place.

- Inelastic interstory drift ratio and the ratio of maximum inelastic interstory drift ratio to the maximum elastic interstory drift ratio (C_Δ) generally increase with seismic force reduction factor.
- Inelastic MIDR decreases as beam-to-column stiffness ratio increases. The inelastic drift ratio reaches its maximum value when ρ is infinity for regular frames and frames with soft story. Changing ρ values of weak column-strong beam and strong column-weak beam frames with non-uniform stiffness distribution does not significantly influence C_Δ.
- As the ratio of ground story height to regular story height increases, MIDR increases and location of MIDR shifts to the lower parts of the frame for both elastic and inelastic frames. Weak column-strong beam frames having a soft story show more inelastic demand than strong column-weak beam frames with soft story.
- Similar to the elastic case, maximum drift location moves to upper stories with increasing stiffness distribution coefficient
- Maximum inelastic interstory drift ratio increases with story height.
- The representative formula of maximum inelastic interstory drift ratio (C_Δ) (Equation 4.4) generated for 20-story regular moment resisting frame with h_2=3 m and ρ=0.5 gives acceptably good estimates for these frames. In addition, in spite of the fact that average of the ratio of $C_{\Delta\text{-FORMULA}}$ to $C_{\Delta\text{-ANALYSIS}}$ is 1.0, Equation (4.4) may overestimate or underestimate the analysis results due to the nature of the considered problem.

6.3 SUGGESTED FUTURE RESEARCH

This study can be extended in the future as stated below:

- The higher mode effects on inelastic lateral displacement demand should be analyzed more quantitatively.

- P-delta effects on structures subjected to large displacement pulses of near-fault ground motions should be investigated. The expression proposed in this study may be improved with a modification factor for P-delta effects.
- A simplified equation may be derived using nonlinear regression analyses to estimate inelastic drift ratio by considering beam to column capacity ratio, seismic force reduction factor, ratio of pulse period to fundamental period, beam to column stiffness ratio, soft story factor, stiffness distribution coefficient, regular story height and number of stories.

REFERENCES

[1] Abrahamson N., 2001, “Incorporating Effects of Near Fault Tectonic Deformation into Design Ground Motions”, a presentation sponsored by the EERI Friedman Family Visiting Professional Program, hosted by the University at Buffalo.

[2] Akkar S. D., Gülkan P., 2002, “A Critical Examination of Near-Field Accelerograms from the Sea of Marmara Region Earthquakes”, Bulletin of the Seismological Society of America, v. 92, no. 1, pp. 428-447.

[3] Akkar S., Yazgan U., Gülkan P., 2005, ”Drift Estimates in Frame Buildings Subjected to Near-Fault Ground Motions”, Journal of Structural Engineering, ASCE, Vol. 131, Issue 7, pp. 1014-1024.

[4] Alavi B., Krawinkler H., 2001, “Effects of Near-Fault Ground Motions on Frame Structures”, The John A. Blume Earthquake Engineering Research Center, Report No. 138, Stanford University, California.

[5] Alavi B., Krawinkler H., 2004, “Behavior of Moment-Resisting Frame Structures Subjected to Near-Fault Ground Motions”, Earthquake Engineering and Structural Dynamics, Vol. 33, Issue 6, pp. 687-706.

[6] Anderson J., and Bertero V., 1987, “Uncertainties in Establishing Design Earthquakes,” ASCE Journal of Structural Engineering, Vol. 113, No. 8, pp. 1709-1724.

[7] Applied Technology Council (ATC), 1996, “Seismic Evaluation and Retrofit of Concrete Buildings”, Report ATC-40, Applied Technology Council, Redwood City, California.

[8] Baez J. I., Miranda E., 2000, “Amplification Factors to Estimate Inelastic Displacement Demands for the Design of Structures in the Near Field”, Proceeding 12th World Conference on Earthquake Engineering, New Zealand.

[9] Benioff H., 1955, “Mechanism and Strain Characteristics of the White Wolf Fault as Indicated by the Aftershock Sequence, Earthquakes in Kern County, California, During 1955 (G.B. Oakeshotte, ed.),” California Division of Mines Bulletin, No. 171, 199-202.

[10] Bertero V. V., Anderson J. C., Sasani M., 1999, “Impulse EQGMs: A Historical and Critical Review”, Proceeding, ASCE Structural Congress, ASCE, Reston, Va., 91-94

[11] Bertero V., Mahin S., Herrera R., 1978, “Aseismic Design Implications of Near-Fault San Fernando Earthquake Records,” Earthquake Engineering and Structural Dynamics, Vol. 6, pp. 31-42.

[12] Blume J. A., 1968, “Dynamic Characteristics of Multistory Buildings”, Journal of the Structural Division, ASCE, Vol.94 (ST2), pp. 377-402.

[13] Bray J. D., Rodriguez-Marek A., 2004, “Characterization of Forward-Directivity Ground Motions in the Near-Fault Region”, Soil Dynamics and Earthquake Engineering, Vol. 24, 815-828.

[14] Building Seismic Safety Council (BSSC), 1997, “NEHRP Guidelines for the Seismic Rehabilitation of Buildings”, Reports FEMA 273 (Guidelines) and FEMA 274 (Commentary), Federal Emergency Management Agency, Washington, D.C.

[15] Building Seismic Safety Council (BSSC), 2000, “Prestandard and Commentary for the Seismic Rehabilitation of Buildings”. Report FEMA-356, Federal Emergency Management Agency, Washington, D.C.

[16] Chopra A.K., 2001, “Dynamics of Structures, Theory and Applications to Earthquake Engineering”, 2nd Edition, University of California at Berkeley, Prentice Hall, Upper Saddle River, New Jersey 07458

[17] Chopra A. K., 2004, “Estimating Seismic Demands for Performance-Based Engineering of Buildings”, 13th World Conference on Earthquake Engineering, Canada, Paper No. 5007.

[18] Chopra A. K., Chinatanpakdee C., 2001, “Drift Spectrum vs. Modal Analysis of Structural Response to Near Fault Ground Motions”, Earthquake Spectra, Vol. 17, No. 2, pp. 221-234.

[19] Chopra A. K., Chinatanpakdee C., 2004, “Inelastic Deformation Ratios for Design and Evaluation of Structures: Single-Degree-of-Freedom Bilinear Systems”, Journal of Structural Engineering, Vol. 130, No. 9, pp. 1309-1319.

[20] Elnashai A.S., 2001. “Advanced Inelastic Static (Pushover) Analysis for Earthquake Applications”, Structural Engineering and Mechanics, Vol. 12, No. 1, pp. 51-69.

[21] Fajfar P., Fischinger M., 1988, “N2-A Method for Non-Linear Seismic Analysis of Regular Buildings”, Proceedings of 9th World Conference on Earthquake Engineering, Tokyo, Japan, Vol. V, pp. 111-116

[22] Fajfar P., Strojnik S., 1981, “Simplified Method for Computation of Earthquake Induced Shears and Overturning Moments in Regular Multistorey Structures”, Proceedings of the 7th World Conference on Earthquake Engineering, Vol. 7, Turkish Society for Earthquake Engineering, Istanbul, Turkey.

[23] Federal Emergency Management Agency, 2000, “State of the Art Report on Systems Performance of Steel Moment Frames Subject to Earthquake Ground Shaking”, FEMA-355C, September.

[24] Ghobarah A., 2004, “On Drift Limits Associated with Different Damage Levels”, Performance-Based Seismic Design Concepts and Implementation, Bled, Slovenia, PEER Report, 2004/05, pp. 321-332.

[25] Gupta, A., Krawinkler H., 2000, “Dynamic P-delta Effects for Flexible Inelastic Steel Structures,” ASCE Journal of Structural Engineering, Vol. 126, No. 1, pp. 145-154.

[26] Gülkan P., Akkar S., 2002, “A Simple Replacement for the Drift Spectrum”, Engineering Structures, Vol. 24, pp. 1477-1484.

[27] Gülkan P., Sözen M., 1974, “Inelastic Response of Reinforced Concrete Structures to Earthquakes Motions”, ACI Journal, Vol. 71, pp. 604-610.

[28] Hall J. F., Heaton T. H., Halling M. W., Wald D. W., 1995, “Near-Source Ground Motion and its Effects on Flexible Buildings”, Earthquake Spectra, Vol. 11, No. 4, pp. 569-605.

[29] Heidebrecht A. C., Stafford Smith B., 1973, “Approximate Analysis of Tall Wall-Frame Structures”, Journal of Structural Divisions, ASCE, Vol. 99, No. 2, pp. 199-221.

[30] Hong L., Hwang W., 2000, “Emprical formula for fundamental vibration periods of reinforced concrete buildings in Taiwan”, Earthquake Engineering and structural Dynamics, Vol. 29, Issue 3, pp. 327-337

[31] Iwan W. D., 1997, “Drift Spectrum: Measure of Demand for Earthquake Ground Motion”, Journal of structural Engineering, Vol. 123, No. 4, pp. 397-404.

[32] Iwan W. D., 1999, “Implications of Near-Fault Ground Motion for Structural Design”, US-Japan Workshop on Performance Based Earthquake Engineering Methodology for RC Building Structures”, Maui, Hawaii (available from PEER, UC Berkeley).

[33] Iwan W. D., 1980, “Estimating Inelastic Spectra from Elastic Spectra”, Earthquake Engineering Structural Dynamics, Vol. 8, No. 4, pp. 375–388.

[34] Iwan W. D., Guyader A. C., 2002, “A Study of the Accuracy of the Capacity Spectrum Method in Engineering Analysis.” Proc., 3rd U.S.-Japan Workshop on Performance-Based Earthquake Engineering Methodology for Reinforced Concrete Building Structures, Pacific Earthquake Engineering Research Center, 16–18 August 2001, Seattle, Washington, 86–102.

[35] Iwan W. D., Huang C. T., Guyader A. C., 2000, “Important Features of the Response of Inelastic Structures to Near-Field Ground Motion”, Proceedings of 12th World Conference on Earthquake Engineering, Paper No. 1740.

[36] Jennings R.L., Newmark N.M., 1960, “Elastic Response of Multi-Story Shear Beam Type Structures Subjected to Strong Ground Motion”, Proceedings of the 2nd World Conference on Earthquake Engineering, Science Council of Japan, Tokyo, Japan, Vol. II, pp. 699-717

[37] Kalkan E., Kunnath S. K., 2006, “Effects of Fling Step and Forward Directivity on Seismic Response of Buildings”, Earthquake Spectra, Vol. 22, No. 2, pp. 367-390.

[38] Khan F. R., Sbarounis J. A., 1964, “Interaction of Shear Walls and Frames”, Journal of Structural Divisions, ASCE, Vol. 90, No. 3, pp. 285-335.

[39] Kim J., Collins K. R., 1999, “Uniform Hazard Drift Demand Spectra”, Proceedings, First International Conference on Advanced in Structural Engineering and Mechanics, Seoul, Korea.

[40] Kim J., Collins K. R., 2002, “Closer Look at the Drift Demand Spectrum”, Journal of Structural Engineering, Vol. 128, No. 7, pp. 942-945.

[41] Krawinkler H., Alavi B., 1998, “Development of Improved Design Procedures for Near Fault Ground Motions,” SMIP98, Proceedings, Seminar on Utilization of Strong-Motion Data, Oakland, CA, September 15, California Division of Mines and Geology, Sacramento, CA, pp. 21-41.

[42] Krawinkler H., Seneviratna G.D.P.K, 1998, “Pros and Cons of a Pushover Analysis of Seismic Performance Evaluation”, Journal of Structural Engineering, Vol. 20, pp. 452-464.

[43] Lin Y., Chang K., Tsai M., Wang T., 2002, “Displacement-Based Seismic Design for Building”. Journal of the Chinese Institute of Engineers, Vol. 25, No. 1, pp. 89-98

[44] Mahin S., Bertero V., Chopra A., Collins R., 1976, “Response of the Olive View Hospital Main Building during the San Fernando Earthquake,” Earthquake Engineering Research Center, University of California, Berkeley, Report No.UCB/EERC-76/22, Oct. 1976.

[45] Malhotra P. K., 1999, “Response of Buildings to Near-Field Pulse-Like Ground Motions” Earthquake Engineering and Structural Dynamics, Vol. 28, pp. 1309-1326.

[46] Miranda E., 1999, “Approximate Seismic Lateral Deformation Demands in Multistory Buildings, Journal of Structural Engineering, ASCE, Vol. 125, No. 4, pp. 417-425.

[47] Miranda E., 2000, “Inelastic Displacement Ratios for Structures on Firm Sites”, Journal of Structural Engineering, Vol. 126, pp. 1150-1159.

[48] Miranda E., Akkar S.D., 2006, “Generalized Interstory Drift Spectrum, Journal of Structural Engineering, ASCE, Vol. 132, No. 6, pp. 840-852.

[49] Miranda E., Reyes C.J., 2002, “Approximate Lateral Drift Demands in Multi-Story Buildings with Nonuniform Stiffness, Journal of Structural Engineering, Vol. 128, No. 7, pp. 840-849.

[50] Moehle J. P., 1992, “Displacement-Based Design of RC Structures Subjected to Earthquake”, Earthquake Spectra, Vol. 8, Issue 3, pp. 403-428.

[51] Montes R., and Rosenblueth E., 1968. “Shears and Overturning Moments in Chimneys”, Proceedings of the 2nd Mexican Conference on Earthquake Engineering, Mexican Society of Earthquake Engineering, Veracruz, Mexico

[52] Nakashima M., Ogawa K., Inoue K., 2002, “Generic Frame Model for Simulation of Earthquake Responses of Steel Moment Frames”, Earthquake Engineering and Structural Dynamics, Vol. 31, pp. 671-692.

[53] Potzta G., Kollár L. P., 2003, “Analysis of Building Structures by Replacement Sandwich Beams”, International Journal of Solids and Structures, Vol. 40, No. 3, pp. 535-553.

[54] Prakash V., Powell G. H., Cambell S., 1993, “DRAIN-2DX Base Program Description User Guide”, Version 1.10. Report No. UCB/SEMM-93/17, University of California at Berkeley, Department of Civil Engineering.

[55] Qi X, Moehle J. P., 1991, “Displacement Design Approach for Reinforced Concrete Structures Subjected to Earthquakes”, Report No. UCB/EERC-91/02, Earthquake Engineering Research Center, University of California: Berkeley, CA.

[56] Rodrigez-Marek A., 2000, “Near-Fault Seismic Site Response”, Ph.D. Dissertation, Department of Civil Engineering, University of California Berkeley.

[57] Rosenblueth E., Herrera I., 1964, “On a Kind of Hysteretic Damping”, Journal of Engineering Mechanics, Vol. 90, No. 4, pp. 37–48.

[58] Rosman R., 1967, “Laterally Loaded Systems Consisting of Walls and Frames”, Tall Buildings, Pergamon Press, New York.

[59] Ruiz-Garcia J., Miranda E., 2003. “Inelastic displacement ratios for evaluation of existing structures”, Earthquake Engineering and Structural Dynamics, Vol. 32, pp. 1237-1258.

[60] Saiidi M., Sozen M. A., 1981, “Simple Nonlinear Seismic Analysis of R/C Structures”, Journal of the Structural Division, Vol. 107, No. 5, pp. 937-953.

[61] Seneviratna G. D. P. K., Krawinkler, H, 1997, “Evaluation of Inelastic MDOF Effects for Seismic Design”, John A. Blume Earthquake Engineering Center Report No. 120, Department of Civil Engineering, Stanford University.

[62] Singh J. P., 1985, “Earthquake Ground Motions: Implications for designing structures and reconciling structural damage”, Earthquake Spectra, Vol. 1, No.2, pp. 239-270.

[63] Somerville P. G., Smith N. F., Graves R. W., Abrahamson N. A., 1997, “Modification of Empirical Strong Ground Motion Attenuation Relations to Include the Amplitude and Duration Effects of Rupture Directivity”, Seismological Research Letters, Volume 68, 199-222.

[64] Somerville, P. G., 1998, “Development of an Improved Representation of Near-Fault Ground Motions”, SMIP98 Proceedings, Seminar on Utilization of Strong-Motion Data, Oakland, CA, September 15, California Division of Mines and Geology, Sacramento, CA, pp. 1-20.

[65] SPSS, 2006, “SPSS 15.0 for Windows Evaluation Version”, SPSS Inc.

[66] Stewart J.P., Chiou S., Bray J. D., Graves R. W., Sommerville P. G., Abrahamson N. A., 2001, “Ground Motion Evaluation Procedures for Performance-Based Design”, Report No PEER 2001/09, Pacific Earthquake Research Center, University of California, Berkeley

[67] Turkish Earthquake Code, 1998, Specification for Structures to be built in Disaster Areas

[68] Veletsos A.S, Newmark N. M., 1960, “Effect of Inelastic Behavior on the Response of Simple Systems to Earthquake Motions”, Proceedings of the World Conference on Earthquake Engineering, Japan, Vol. 2, pp. 895-912.

[69] Wald D. J., 1995, “A Preliminary Dislocation Model for the 1995 Kobe (Hyogo-Ken Nanbu), Japan, Earthquake Determined from Strong Motion and Teleseismic Waveforms”, Seismological Research Letters, Vol. 66, pp. 22-28.

[70] Westergaard H. M., 1933, “Earthquake Shock Transmission in Tall Buildings”, Engineering News Record, Vol. 111, No. 22, pp. 654-656.

[71] Wilkinson S. M., Hiley R. A., 2006, “A Non-Linear Response History Model for the Seismic Analysis of High-Rise Framed Buildings”, Computer and Structures, Vol. 84, pp. 318-329.

[72] Yazgan U., 2003, “A Methodology for Determination of Performance Based Design Parameters”, M.S. Thesis, Department of Civil Engineering, Middle East Technical University, September, 119 pp.

[73] Zalka K. A., 2000, “Stress Analysis of Buildings Under Horizontal Load, Part1: Basic Behavior-Deformations”, Proceedings of the Institution of Civil Engineers, Structures and Buildings, Vol. 140, No. 2, pp. 179-186.